厚生労働科学研究費補助金
化学物質リスク研究事業

個体の成長期における毒性メカニズムに基づく新規 in vitro 発達神経毒性評価法に関する研究
(H25-化学--一般-002)

平成 27 年度総括・分担研究報告書

研究代表者　諫田 泰成

平成 28（2016）年 3 月

目　　次

化学物質リスク研究事業　課題番号 H25-化学-一般-002

研究成果概要

個体の成長期における毒性メカニズムに基づく新規 in vitro 発達神経毒性評価法に関する研究

研究代表者　　国立医薬品食品衛生研究所　薬理部第二室
諫田　泰成

＜全体要旨＞
近年、自閉症など発達障害が急速に増加し社会問題となっている。その原因の一つは発達期における化学物質の曝露とされる。発達期の神経系は成体より化学物質に対する感受性が高く、健康被害が長期間あるいは遅発性に生じることが考えられるため、子どもの影響評価法の確立が強く望まれる。
現在、OECDやEPAによって、妊娠ラットを用いる発達神経毒性試験ガイドラインが制定されているが、試験方法が複雑で、試験期間は1年以上、動物数は720にも及び経費も膨大である。さらに、日本ではこのようなガイドラインは未整備である。そこで我々は、現行ガイドラインの欠点を克服し、簡便かつ低コストのin vitro評価系として、各発達期における神経系の毒性評価法、遅発性の神経回路異常による毒性評価法の基盤を開発している。
昨年度までに、遅発性神経毒性が懸念されるバルプロ酸および発生毒性が懸念される内分泌かく乱物質トリブチルスズを研究班で共通の化合物として用いて、各発達段階における神経毒性を明らかにした。本年度は、発達神経毒性を有する有機リン系農薬クロルピリホスを共通の化合物として新たに検証した。その結果、幹細胞から生後神経回路にいたるまで様々な毒性を明らかにした。これらの結果から、我々の手法は幹細胞から生後・幼若期までの各発達段階において神経毒性を評価できることが示唆された。また、発生過程で毒性発現メカニズムが異なることが考えられた。
今後は、国際的な検証チームと連携を図りながら、再現性・予測性を検証し、新規試験法としての確立を目指す。

＜研究分担者一覧＞

宇佐見誠（国立衛研）
「神経堤細胞の機能解析による評価法の開発」

佐藤薫（国立衛研）
「発達成長期神経系細胞新生への化学物質の影響評価」

関野祐子（国立衛研）
「生後神経回路の機能的影響評価指標に関する研究」

上野晋（産業医大）
「幼若期の神経回路機能に対する化学物質の影響評価」

A. 研究目的

発達期の中枢神経系は成体組織より化学物質に対する感受性が高く、健康被害が長期間あるいは遅発性に生じることが懸念される。

すでに我々は平成 22～24 年度の化学物質リスク事業「個体の成長期における神経系および肝臓系細胞の機能解析による化学物質の健康影響評価法に関する研究」において、各発達段階における評価系を構築した。

そこで、本年度は、遅発性の神経毒性が懸念されるバルプロ酸、および発生毒性が懸念される内分泌かく乱物質トリブチルスズに加えて、有機リン系農薬クロルピリホスを研究班共通の化学物質として使用し、当初の計画に従って、我々が独自に構築した各発達段階における in vitro 神経毒性評価を行った。

B. 研究方法

詳細は各分担報告書を参照のこと。

C. 研究結果

以下に示すように、幹細胞から生後・幼若期までの各発達段階において、陽性対照化合物クロルピリホスの神経毒性作用が検出できることを明らかにした。

【①ヒト未分化細胞の代謝】

クロルピリホスによりヒト幹細胞のエネルギー代謝異常を見出した。とくに、化学物質によりミトコンドリア形態制御機構が阻害され ATP 産生が抑制されることにより増殖が抑制される新規の毒性発現メカニズムを明らかにした。

【②神経堤細胞の遊走】

ラット神経堤細胞遊走実験法により、培養 48 時間までは 50μM までは神経堤細胞の遊走促進傾向が認められた。培養 48 から 72 時間では、最低濃度の 6.25μM 以上で抑制傾向が認められた。従って、クロルピリホスは神経堤細胞の遊走に対して複数のメカニズムを介して影響を及ぼすと考えられた。

【③発達成長期神経系細胞新生】

前脳矢状切片の脳室下帯に存在する神経幹細胞および前駆細胞を蛍光標識し切片培養を行い、評価化合物を適用し定量的な評価を行った。クロルピリホスは、新生神経系細胞数減少、新生オリゴデンドロサイト数の減少を引き起こすことを明らかにした。

【④生後神経回路】

バルプロ酸は伝達物質の放出異常と神経発達の異常を示し、行動異常は早期に出現した。クロルピリホスも同様な変化が観察され、過剰な脳回の形成も認められた。

【⑤幼若期神経回路】

有機リン系農薬クロルピリホス（CP）を VPA や TBT と同様に胎生期曝露ラットを用いた生後早期の海馬神経回路機能を評価したところ、VPA 胎生期曝露の場合に認められた興奮性神経回路の発達が亢進する傾向が認められた。

D. 考察

本研究において、陽性対照化合物であるバルプロ酸およびトリブチルスズに加えて、クロルピリホスを用いて、幹細胞から生後・幼若期までの毒性を統合的に評価した。

バルプロ酸およびトリブチルスズと同様に、クロルピリホスはすでに幹細胞に対して毒性が認められた。妊娠動物の投与により生後早期の海馬の興奮性神経回路の亢進、小脳の突起伸展の異常をきたすことから、我々が開発した各発達期における毒性評価系の有用性を示すことができた。

今後は、試験法の確立に向けて、本評価法の再現性、予測性などを検証する予定である。とくに、2015 年より開始された HESI の NeuroTOX と連携を図りながら、プロトコルの整備を進め、国際的な評価系へと発展させることを目指し、国内外のグルーバルな化学物質の管理などに役立てたい。

E. 結論

我々が構築した各発達期の神経毒性評価により、バルプロ酸およびトリブチルスズの各発達段階における神経毒性を明らかにした。

F. 研究発表

分担研究者の報告書に示すように、多数の論文発表および学会発表を行った。

厚生労働科学研究費補助金（化学物質リスク研究事業）
分担研究報告書

ヒト未分化細胞を用いた化学物質の影響

研究代表者　　国立医薬品食品衛生研究所薬理部第二室長
諫田　泰成

要旨
ヒト未分化細胞およびヒト iPS 細胞を用いて、発達神経が懸念される化学物質の影響を検討した。その結果、遅発性神経毒性が懸念される有機スズ化合物トリブチルスズおよび有機リン系農薬クロルピリホスの曝露により両細胞株の増殖抑制が認められた。この毒性メカニズムとしてミトコンドリアの形態異常による ATP 産生の低下を見いだした。以上の結果から、ヒト未分化/幹細胞におけるミトコンドリア機能を指標にして、成長期における化学物質の発達神経毒性を評価できる可能性が示唆された

A. 研究目的

近年、子供の学習障害や自閉症などの発達障害が増加しているが、その原因の一つとして環境中の化学物質の関与が指摘されている。ヒト iPS 細胞などの未分化細胞はヒト発生過程を in vitro で模倣できることから、化学物質の神経毒性を検出できる可能性があり期待は大きい。しかしながら、評価系としての手法はいまだ確立されていない。

そこで本研究では、化学物質の発達期における毒性を評価するために、複数のヒト未分化細胞を用いて発達神経毒性を評価できるのか検討を行った。評価系の構築には発達毒性が懸念される陽性対象物質が必要となる。昨年度までに、研究班で共通のバルプロ酸を用いることにより、ヒト未分化細胞のエネルギー代謝が重要であることを見出した。

そこで、本年度は、研究班共通の化学物質として内分泌撹乱作用を有し発達神経毒性が懸念される環境汚染物質トリブチルスズ（TBT）を引き続き検討を行った。さらに、発達神経神経毒性を有する化合物として有機リン系農薬クロルピリホス（CPF）を追加して、毒性メカニズムの検討を行った。本研究により、ヒト未分化細胞のミトコンドリア機能による毒性評価の有用性を検証した。

B. 研究方法

1. 細胞培養

ヒト未分化細胞株 NT2/D1 は 10%FBS を含む DMEM 培地を用いた。また、ヒト iPS 細胞株 253G1 は、TeSR-E8 培地（Stem Cell Technologies）にてフィーダーフリーの条件で培養した。

2. ミトコンドリアの形態

細胞を 4%FFA で固定後、ミトコンドリアを 50 nM の MitoTracker Red CMXRos (Cell Signaling Technology) および DAPI により染色し、confocal 顕微鏡（Nikon A1）で観察した。Dot 状のミトコンドリアが 10%未満の細胞数を数えた。

3. qPCR

TRIzol 試薬（Life Technologies）を用いて RNA を単離した。QuantiTect SYBR Green RT-PCR Kit (QIAGEN)、ABI PRISM 7900HT を用いて qPCR を行った。

4. ATP 量

ATP 量は、ルシフェラーゼ法により計測した。

5. MTT アッセイ

MTT アッセイは CellTiter 96 AQueous One Solution Cell Proliferation Assay (Promega)を用いて行った。

6. ミトコンドリア膜電位

ミトコンドリア膜電位の測定は細胞をJC10 (Life technologies)で染色したのちFACS ARIAII (BD Biosciences)を用いて行った。

7. shRNA を用いたノックダウン

shRNA 導入はレンチウイルス(SIGMA)を用いた。ヒト iPS 細胞にウイルスを moi 1 で感染させた。さらに 24 時間後にピューロマイシンを添加して感染細胞のセレクションを行った。

C. 研究結果

1. ヒト iPS 細胞に対する TBT の作用

前年度にヒト未分化株細胞を用いて、TBT によりエネルギー代謝異常が誘導されることを見出した。本年度は他の未分化細胞においても同様であるのか明らかにするために、ヒト iPS 細胞を用いてその毒性メカニズムを検討した。図 1A, B に示すように、TBT 曝露により濃度依存的に増殖の低下が認められた。一方、毒性の低い酢酸スズ（TA）では影響は認められなかった。また 50nM TBT 曝露では未分化状態に影響はなかったが、ATP 量の低下が認められた（図 1C, D）。

ATP 量が低下したので、ミトコンドリア機能に着目した。まず主要な機能であるミトコンドリア膜電位について調べた結果、TBT 曝露により膜電位の低下が認められた (図 2A)。さらにミトコンドリアの形態異常が引き起こされることも見出した (図 2B, C)。一方、TA ではこうした影響は認められなかった。したがって TBT によりミトコンドリア機能低下が引き起こされることが示唆された。

次に、ミトコンドリアの形態制御因子の発現について検討した。qPCR により、分裂因子（Drp1, Fis1）および融合因子（Mfn1, Mfn2, Opa1）の遺伝子発現には影響が認められなかった（図 3A）。非常に興味深いことに、TBT の暴露によって Mfn1 のタンパク分解が誘導されることが示唆された（図 3B, C）。さらに Mfn1 の関与を調べるため shRNA を用いてノックダウンを行った結果、ミトコンドリア形態異常が観察された (図 3D, E, F)。したがって、TBT によるミトコンドリア機能の低下はミトコンドリア融合タンパク質の分解によって誘導されることが示唆された。

Mfn1 を特異的に分解するユビキチンリガーゼとして MARCH5 が報告されている（Park et al., Cell Death Dis., 2014）。そこで、TBT のミトコンドリアに対する作用が MARCH5 を介しているのか検討するためにノックダウンを行った（図 4A）。その結果、TBT の Mfn1 分解は阻害された（図 4B, C）。したがって、TBT のミトコンドリアに対する作用は MARCH5 を介することが示唆された。

以上の iPS 細胞の結果から、TBT の曝露によりミトコンドリアの形態異常が起きて ATP 産生が低下し、その結果、細胞増殖が抑制されることが示唆された。

2. ヒト NT2/D1 細胞に対する CPF の作用

TBT 曝露により観察された現象が他の化学物質でも引き起こされるのか明らかにするために、発達神経毒性が懸念されるクロルピリホス（CPF）を用いて NT2/D1 細胞で検討を行った。図 5 に示すように、CPF 曝露により濃度依存的に増殖の低下が認められた。また ATP 量についても濃度依存的な低下が認められた（図 6）。さらにミトコンドリアを観察した結果、30μM CPF 曝露によりミトコンドリアの形態異常が引き起こされることも見出した (図 7)。既報では、CPF 曝露したラット皮質ニューロンにおいて、ミトコンドリア軸索輸送の阻害や膜電位の低下が引き起こされる一方で、ATP 産生量へは影響しないという報告がある（Middlemore-Risher et al., J. Pharmacol. Exp. Ther., 2011）。本研究では既報と同程度の濃度で、ミトコンドリアの分裂促進に伴い ATP 量の低下が認められたため、既報と異なる結果となった。この違いは、未分化細胞の方が成熟神経細胞よりも化学物質に対する感受性が高いことが要因にあると考えられる。

以上の結果から、NT2/D1 細胞において TBT と同様に、CPF はミトコンドリア機能異常を介した細胞毒性を引き起こすことが明らかになった。また、未分化株細胞で ATP 量やミトコンドリア形態といった指標を用いることにより、発達神経毒性を評価できる可能性が示唆された。

D. 考察

本研究において、ヒト未分化株細胞およびヒト iPS 細胞を用いて、前年度の研究で見出した指標により発達神経が懸念される化学物質の影響を評価できることを明らかにし

た。特に、ヒト iPS 細胞で使用した TBT は 50nM で血中に存在しうる濃度であり、本アッセイ系は非常に好感度であると考えられた。

今回、ヒト iPS 細胞を用いて TBT の毒性作用点として、MARCH5-Mfn1 分解を介したミトコンドリアの分裂による ATP 産生の低下を見出した。現在、ATP は Tox21 でも肝臓細胞を用いてミトコンドリア毒性の大規模なバリデーション試験が進行中である。今後、神経などの前駆細胞をもちいて、他の化学物質の曝露によってミトコンドリアの機能異常が認められるのか検討を加えることにより、化学物質の毒性評価に幅広く応用できるのか明らかになると期待される。

また、本研究では、ヒト NT2/D1 細胞を用いて発達神経毒性が懸念される化学物質である CPF の毒性発現機構についても調べた。その結果、TBT と同様にミトコンドリア毒性を示すことが明らかとなった。したがって、発達神経毒性を示す化学物質の毒性評価においてミトコンドリアの機能異常は有効であり幅広く応用できる可能性が期待される。最近、メチル水銀の毒性をヒト iPS/ES 細胞で評価できる試みが報告されているが（He et al., Toxicol Lett, 2012）、どこまで動物実験の代替できるのか、ヒトにおける毒性を予測できるのかはほとんど明らかになっていない。今後も被験物質を増やし iPS 細胞をはじめとした未分化細胞を用いることで、ミトコンドリアを指標とした毒性マーカーの探索や評価法の検討を行う。特にスループット性の高い手法を開発し、簡便で再現性のある評価法の確立を目指したい。

E. 結論

ヒト未分化細胞およびヒト iPS 細胞のミトコンドリア機能を指標とすることにより、成長期における化学物質の発達神経毒性を評価できる可能性が示唆された。

F. 研究発表

1. 論文発表

論文

英文

[1] Ishida K., Kotake Y., Miyara M., Aoki K., Sanoh S., Kanda Y., Ohta S. Involvement of GluR2 decrease in lead-induced neuronal cell death. *J. Toxicol. Sci.* 38:513-21 (2013). （**日本毒性学会田邊賞受賞論文**）

[2] Yamada S., Kotake Y., Sekino Y. and Kanda Y.*, AMP-activated protein kinase-mediated glucose transport as a novel target of tributyltin in human embryonic carcinoma cells. *Metallomics* 5:484-91 (2013). *C.A. （**第 3 回メタロミクス研究フォーラム若手奨励賞受賞論文**）

[3] Kanda Y. Cancer Stem Cells - Fact or Fiction? (Chapter1). Role of Cancer Stem Cells in Cancer Biology and Therapy. CRC Press (2013).

[4] Nakamura Y., Matsuo J., Miyamoto N., Ojima A., Ando K., Kanda Y., Sawada K., Sugiyama A., Sekino Y. Standardization of testing methods with iPS derived cardiomyocytes for evaluating drug-induced repolarization delay. *Journal of Pharmaceutical Sciences* 124:494-501 (2014).

[5] Yamada S., Kotake Y., Demizu Y., Kurihara M., Sekino Y. and Kanda Y. “Isocitrate dehydrogenase 3 as a novel target of tributyltin in human embryonic carcinoma cells.” *Sci. Rep.* (2014) 4: 5952

[6] Nagakubo T., Demizu Y., Kanda Y., Misawa T., Shoda T., Okuhira K., Sekino Y., Naito M., Kurihara M.. Development of cell-penetrating R7 fragment-conjugated helical peptides as inhibitors of estrogen receptor-mediated transcription. *Bioconjugate Chemistry* 25, 1921−1924 (2014).

[7] Hirata N., Yamada S., Shoda T. ,Kurihara M., Sekino Y., Kanda Y. “Sphingosine-1-phosphate promotes expansion of cancer stem cells via S1PR3 by a ligand-independent Notch activation” *Nature Commun.* (2014) 5:4806

[8] Hayakawa T., Kunihiro T., Ando T., Kobayashi S., Matsui E., Yada H., Kanda Y., Kurokawa J., Furukawa T.

"Image-based evaluation of contraction-relaxation kinetics of human-induced pluripotent stem cell-derived cardiomyocytes: correlation and complementarity with extracellular electrophysiology." *J. Mol. Cell. Cardiol.* (2014) 77:178-91

[9] Hiyoshi H., Goto N., Tsuchiya M., Iida K., Nakajima Y., Hirata N., Kanda Y., Nagasawa K., Yanagisawa J. "YL-109 is a novel antitumor agent suppressing triple-negative breast cancer progression by inducing ubiquitin ligase CHIP." *Sci. Rep.* (2014) 4:7095.

[10] Tsuchiya M, Nakajima Y, Hirata N, Morishita T, Kishimoto H, Kanda Y, Kimura K. Ubiquitin ligase CHIP suppresses cancer stem cell properties in a population of breast cancer cells. *Biochemical and Biophysical Research Communications* 452:928-32 (2014).

[11] Kanda Y. Assessment of cigarette smoking toxicity using cancer stem cells. Nova Science Publishers (2014).

[12] Yosuke Demizu, Takashi Misawa, Takaya Nagakubo, Yasunari Kanda, Keiichiro Okuhira, Yuko Sekino, Mikihiko Naito, Masaaki Kurihara. Structural development of stabilized helical peptides as inhibitors of estrogen receptor (ER)-mediated transcription. *Bioorg.Med.Chem.* 23:4132-8 (2015).

[13] Asakura K, Hayashi S, Ojima A, Taniguchi T, Miyamoto N, Nakamori C, Nagasawa C, Kitamura T, Osada T, Honnda Y, Kasai C, Ando H, Kanda Y, Sekino Y, Sawada K. Improvement of acquisition and analysis methods in multi-electrode array experiments with iPS cell-derived cardiomyocyte. *Journal of Pharmacological and Toxicological Methods* (2015)

[14] Yamada S., Kotake Y., Nakano M., Sekino Y. and Kanda Y.* Tributyltin induces mitochondrial fission through NAD-IDH dependent mitofusin degradation in human embryonic carcinoma cells. *Metallomics* 7:1240-6 (2015). *C.A.

[15] Hirata N., Yamada S., Asanagi M., Sekino Y. and Kanda Y.* Nicotine induces mitochondrial fission through mitofusin degradation in human multipotent embryonic carcinoma cells. *Biochemical and Biophysical Research Communications*, 470:300-5 (2016).

[16] Asanagi M., Yamada S., Hirata N, Itagaki H., Kotake Y., Sekino Y. Kanda Y.* Tributyltin induces G2/M cell cycle arrest via NAD^+-dependent isocitrate dehydrogenase in human embryonic carcinoma cells. *J. Toxicol. Sci.* (in press). *C.A.

和文

[1] 関野祐子、佐藤薫、諫田泰成、石田誠一：ヒト iPS 分化細胞を利用した医薬品のヒト特異的有害反応評価系の開発・標準化、国立医薬品食品衛生研究所報告. 131: 25-34. (2013)

[2] 諫田泰成、再生心筋細胞を用いた安全性薬理評価系の開発、再生医療における臨床研究と製品開発、p572-576、技術情報協会 (2013).

[3] 諫田泰成、ヒト iPS 細胞から心筋細胞への分化誘導法、日本薬理学雑誌、141: 32-36 (2013).

[4] 諫田泰成、ヒト iPS 細胞を用いた心毒性試験の現状と課題、谷本学校毒性質問箱 16: p91-94 (2014).

[5] 諫田泰成、ヒト iPS 細胞を用いた成熟心筋細胞の開発、心電図, 34, 306-309 (2014)

[6] 澤田光平、松尾純子、長田智治、吉田善紀、白尾智明、佐藤薫、諫田泰成、関野祐子：霧島会議 Stem Cell Safety Pharmacology Working Group まとめ－ヒト ES/iPS 細胞由来心筋細胞を用いた催不整脈作用検出とその課題－、心電図 34:306-9 (2014).

[7] 諫田泰成、癌幹細胞の受容体を標的とした創薬の可能性、日本薬理学雑誌 144:17-21 (2014).

[8] 平田尚也、諫田泰成：癌幹細胞の解析モデルと創薬への応用、CBI 学会誌

(2015).

[9] 芦原貴司、黒川洵子、諫田泰成、原口亮、稲田慎、中沢一雄、堀江稔. ヒト iPS 細胞由来心筋細胞シートの不整脈研究への応用可能性： in silico 不整脈学の観点から. 生体医工学, 53(3), 100-105. 2015.

[10] 山田茂、諫田泰成、幹細胞と発達神経毒性、日本薬理学雑誌 146:171-3 (2015).

[11] 諫田泰成：癌幹細胞の創薬応用、技術情報協会 (in press).

[12] 諫田泰成、芦原貴司、黒川洵子：ヒト iPS 細胞から成熟した心筋細胞の開発と安全性評価への応用、日本薬理学雑誌 (in press)

2. 学会発表

[1] 諫田泰成：リゾリン脂質による乳癌幹細胞の増殖制御と創薬応用、第 136 回日本薬学会シンポジウム、20160328

[2] 諫田泰成：ヒト iPS 細胞技術を用いた次世代心臓安全性評価: JiCSA の取り組み. 第 89 回日本薬理学会年会, バシフィコ横浜, 東京, 20160310

[3] 諫田泰成：ヒト iPS 細胞由来の成熟心筋細胞の作製と標準化に向けた次世代評価法の開発、第 3 回霧島会議、東京、20160218

[4] 諫田泰成：ヒト iPS 細胞由来心筋細胞による新しい安全性評価法の大規模検証実験：JiCSA の取り組み. 第 1 回 AMED RS シンポジウム, 読売大手町ホール, 東京, 20150201

[5] 諫田泰成：GPCR によるリガンド非依存的な Notch シグナルの活性化機構、BMB2015 ワークショップ、横浜、20151202

[6] 諫田泰成：ヒト未分化細胞のエネルギー代謝に基づく環境ホルモンの毒性評価、第 18 回環境ホルモン学会シンポジウム、栃木、20151210

[7] 諫田泰成：ヒト iPS 細胞を利用した医薬品の心臓安全性評価系の開発と国際標準化、安全性評価研究会・夏のフォーラム 2015、八ヶ岳、20150911

[8] 関野祐子、諫田泰成：ヒト iPS 心筋細胞を利用した催不整脈性リスク評価と ICHS7B 改訂に関する国際動向について、第 42 回 日本毒性学会学術年会、金沢、201507

[9] Naoya Hirata, Yosuke Demizu, Masaaki Kurihara, Yuko Sekino, Yasunari Kanda. Estrogen induces proliferation of breast cancer stem cells via NO/sGC/cGMP signaling pathway. 第 13 回幹細胞シンポジウム、東京、201505

[10] 出水庸介、三澤隆史、長久保貴哉、諫田泰成、奥平桂一郎、関野祐子、内藤幹彦、栗原正明：エストロゲン受容体転写活性化阻害能を有するヘリカルペプチドの開発 、第 10 回ケミカルバイオロジー学会、仙台、201506

[11] 諫田泰成：エストロゲンによる NO シグナルを介した乳癌幹細胞の増殖機構、第 14 回生命科学研究会、三浦市、201506

[12] 山田茂、古武 弥一郎、中野瑞穂、関野祐子、諫田泰成：ミトコンドリア品質管理に対するトリブチルスズの影響、第 42 回 日本毒性学会学術年会、金沢、201507

[13] 石田慶士、古武弥一郎、青木香織、瀧下智子、木村朋紀, 諫田泰成、太田茂：有機スズ神経毒性に関与する核呼吸因子-1(NRF-1)阻害機構の解明、第 42 回 日本毒性学会学術年会、金沢、201507

[14] 平田尚也、山田茂、出水庸介、栗原正明、関野祐子、諫田泰成：エストロゲンによる NO を介した乳癌幹細胞の増殖機構、第 132 回日本薬理学会関東部会、20150704

[15] 諫田泰成：化学物質の in vitro 発達神経毒性評価に向けた取り組み、第 34 回生体と金属・化学物質に関する研究会（チョークトーク 2015）、滋賀、20150821

[16] 黒川洵子、諫田泰成、古川哲史：ヒトが創った心臓：iPS 細胞から大人の心筋細胞を創る秘蔵のレシピ公開、生体機能と創薬シンポジウム 201508

[17] 児玉昌美、李敏、芦原貴司、諫田泰成、関野祐子、古川哲史、黒川洵子：ヒトカリウムチャネル遺伝子導入によるヒト iPS 細胞由来心筋細胞の成熟化のメカニズムー発現レベルからの考察ー、生体機能と創薬シンポジウム 2015、

20150827

[18] 石田慶士，古武弥一郎，青木香織，瀧下智子，木村朋紀，諫田泰成，太田 茂：低濃度トリブチルスズによるニューロン脆弱化機構の解明、第 10 回メタルバイオサイエンス研究会、名古屋、20150828

[19] 山田茂、古武弥一郎、関野祐子、諫田泰成：ミトコンドリア品質管理に対するトリブチルスズの新たな毒性作用、日本神経化学会、大宮、2015 年 9 月

[20] 平田尚也、諫田泰成：前立腺癌幹細胞に対するスフィンゴシン 1 リン酸の機能、日本癌学会、名古屋、2015 年 9 月

[21] 麻薙美紀、山田茂、古武弥一郎、板垣宏、関野祐子、諫田泰成「ヒト未分化細胞を用いた化学物質の毒性評価」、フォーラム 2015 衛生薬学・環境トキシコロジー、神戸、2015 年 9 月 17-18 日

[22] 田中克哉、三澤隆史、出水庸介、諫田泰成、槇島誠、関野祐子，内藤幹彦，栗原正明：ジフェニルメタンを基本骨格とするエストロゲン受容体アンタゴニストの創製、第 59 回日本薬学会関東支部大会、201509

[23] 平田尚也、関野祐子、諫田泰成：スフィンゴシン 1 リン酸による Notch3 を介したグリオーマ幹細胞の増殖、第 133 回日本薬理学会関東部会、201510

[24] DEVELOPMENT OF HELICAL PEPTIDES AS INHIBITORS OF ESTROGEN RECEPTOR-MEDIATED TRANSCRIPTION. Yosuke Demizu, Takashi Misawa, Yasunari Kanda, Nobumichi Ohoka, Yuko Sekino, Mikihiko Naito, and Masaaki Kurihara 第 52 回ペプチド討論会、201511

[25] 出水庸介，三澤隆史，諫田泰成，大岡伸道，関野祐子，内藤幹彦，栗原正明：エストロゲン受容体を標的とした転写活性化阻害および分解誘導ペプチドの創製、第 33 回メディシナルケミストリーシンポジウム、201511

[26] 山田茂、関野祐子、諫田泰成：ミトコンドリア品質低下を介した有機スズの新規毒性メカニズム、BMB2015、神戸、2015 年 12 月

[27] 山崎大樹，安藤博之，吉永貴史，山本渉，朝倉圭一，谷口智彦，宇田宗晃，諫田泰成，長田智治，林誠治，宮本憲優，葛西智恵子，田渋弘行，犬塚隆志，杉山篤，澤田光平，関野祐子．ヒト iPS 細胞由来分化心筋細胞を用いた TdP リスク評価 - JiCSA60 化合物を用いて - . 第 89 回日本薬理学会年会，バシフィコ横浜，神奈川，20160310

[28] 山田茂，麻薙美紀，山崎大樹，諫田泰成，関野祐子．ヒト iPS 細胞のミトコンドリアダイナミクスを用いた細胞毒性評価. 第 89 回日本薬理学会年会，バシフィコ横浜，神奈川，20160309-11

[29] 麻薙美紀、山田茂、平田尚也、板垣宏、関野祐子、諫田泰成：ヒト未分化細胞を用いた発達神経毒性評価の試み、第 89 回日本薬理学会年会，バシフィコ横浜，神奈川，20160309-11

[30] 平田尚也、関野祐子、諫田泰成：リゾフォスファチジン酸はトリプルネガティブ乳癌幹細胞の増殖を誘導する、第 89 回日本薬理学会年会，バシフィコ横浜，神奈川，20160309-11

[31] Reiko Kimura, Masami Kodama, Kazuharu Furutani, Yasunari Kanda, Yoshihisa Kurachi , Yuko Sekino , Tetsushi Furukawa,Junko Kurokawa ヒト iPS 細胞由来心筋の活動電位形成に関連する遺伝子の定量的発現解析におけるリファレンス遺伝子の選定、第 89 回日本薬理学会年会，バシフィコ横浜，神奈川，20160309-11

[32] Erina Hayashi, Reiko Kimura, Min Li, Tomoko Ando, Takashi Ashihara, Yuko Sekino, Tetsushi Furukawa, Yasunari Kanda , Junko Kurokawa. 内向き整流性カリウムチャネルを過剰発現させたヒト iPS 由来心筋細胞を用いた薬理作用解析、第 89 回日本薬理学会年会，バシフィコ横浜，神奈川，20160309-11

[33] 井出吉紀，小林真里子，平田尚也，板垣宏，関野祐子，諫田泰成．ヒト iPS 細胞由来心筋細胞を用いた新しい安全性薬理試験法：膜電位感受性色素イメージング（VSO）と多点電極（MEA）の同時計測による検証実験．第 89 回日本薬理学会年会，バシフィコ横浜，神奈川，20160309-11

[34] 久保祐亮，山田茂，犬塚隆志，諫田泰成，

関野祐子. 創薬応用を目指したヒト iPS 細胞から GABA 作動性神経細胞への効率的な分化誘導法の確立. 第 15 回日本再生医療学会総会, 大阪国際会議場, 大阪, 2015 年 3 月 17~19 日

[35] Yoshinori Ide , Michinori Ichikawa , Mariko Kobayashi, Kenji Tsubokura, Daiju Yamazaki, Yasunari Kanda, Yuko Sekino. Development of non-staining imaging technique for evaluating safety using human iPSC-derived cardiomyocytes. 第 93 回日本生理学会大会, 札幌コンベンションセンター, 北海道, 2015 年 3 月 22~24 日

[国際学会]

[1] Ashihara T, Kurokawa J, Kanda Y, Haraguchi R, Nakazawa K, Horie M: Spiral wave behaviors and antiarrhythmic drug efficacy in human induced pluripotent stem cell-derived myocardial sheet are different from those in original heart: A simulation study. Heart Rhythm 2015 Scientific Sessions, 2015.05.14, Poster, Boston.

[2] Yasunari Kanda: S1P induces proliferation of cancer stem cells via a ligand-independent Notch activation. FASEB, Banff 2015.08.25

[3] Yosuke Demizu, Takashi Misawa, Yasunari Kanda, Yuko Sekino, Masaaki Kurihara. Development of Cell-penetrating Fragment Conjugated Helical Peptides as Inhibitors of Estrogen Receptor-Mediated Transcription. 11th Australian Peptide Conference 2015, 25th October 2015

[4] Kanda Y, Li M, Ashihara T, Yuko S, Furukawa T, Kurokawa J. Assessment of drug-induced QT prolongation using human iPS cell-derived mature cardiomyocytes, Prague, Czech Republic, Sep 30, 2015.

[5] Yasunari Kanda, Shigeru Yamada, Yuko Sekino. Toxicity Assessment by Mitochondrial Dynamics in Human iPS Cells. 55th Annual Meeting of the Society of Toxicology, New Orleans, 2016.03

H. 知的財産の出願・登録状況

［特許］

1. 特許出願番号 : 2013-116243 （PCT/JP2014/002888）

「正常な内向きのカリウム電流特性を有する iPS 細胞由来心筋モデル細胞」

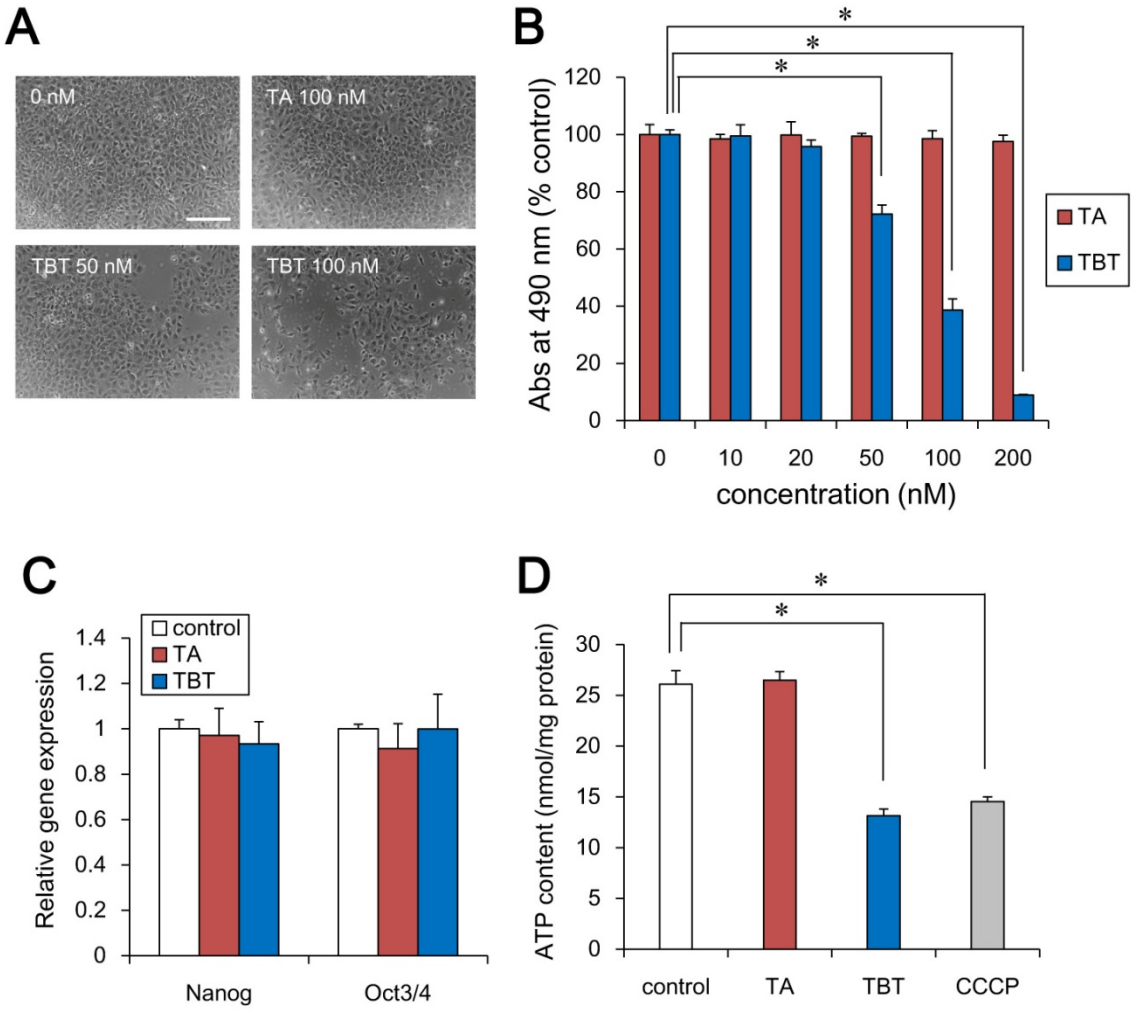

図 1 トリブチルスズによるヒト iPS 細胞の毒性作用

A) iPS 細胞に異なる濃度の有機スズ TBT を曝露させ、72 時間後に位相差画像を取得した。
B)A)において MTT assay を行った。濃度依存的な増殖の低下が認められた。一方、無機スズ TA は効果がなかった。
C)iPS 細胞に 50nM の TBT を曝露させ、72 時間後に RNA を回収した。Nanog, Oct3/4 の qPCR を行った。
D) iPS 細胞に 50nM の TBT を曝露させ、72 時間後に ATP を測定した。TBT および脱共役剤 CCCP で ATP が低下した。TA は効果がなかった。

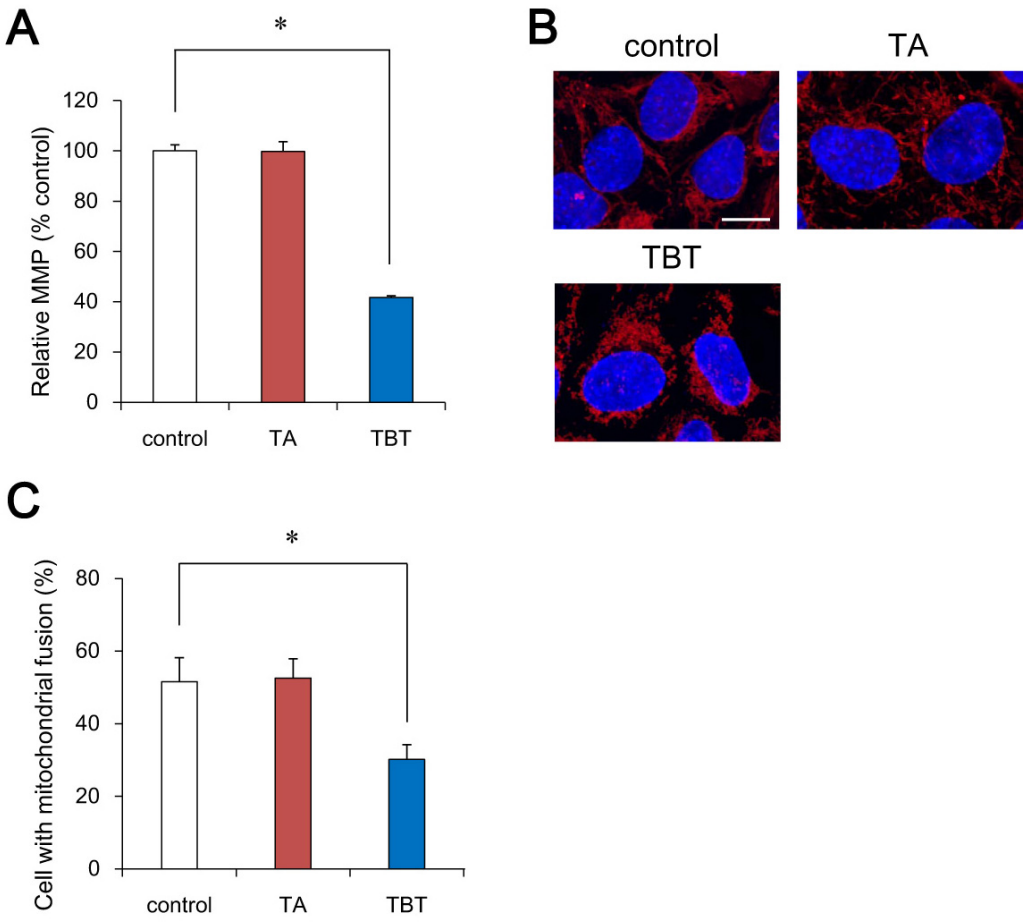

図２　トリブチルスズによるミトコンドリア機能阻害

A) iPS 細胞に 50nM の TBT を曝露させ、1 時間後にミトコンドリア膜電位を測定した。TBT で膜電位が低下した。TA は効果がなかった。

B) iPS 細胞に 50nM の TBT を曝露させ、72 時間後にミトコンドリア形態を共焦点顕微鏡で観察した。

C)B)の結果を定量的に評価した。TBT でミトコンドリア分裂低下が認められた。TA は変化がなかった。

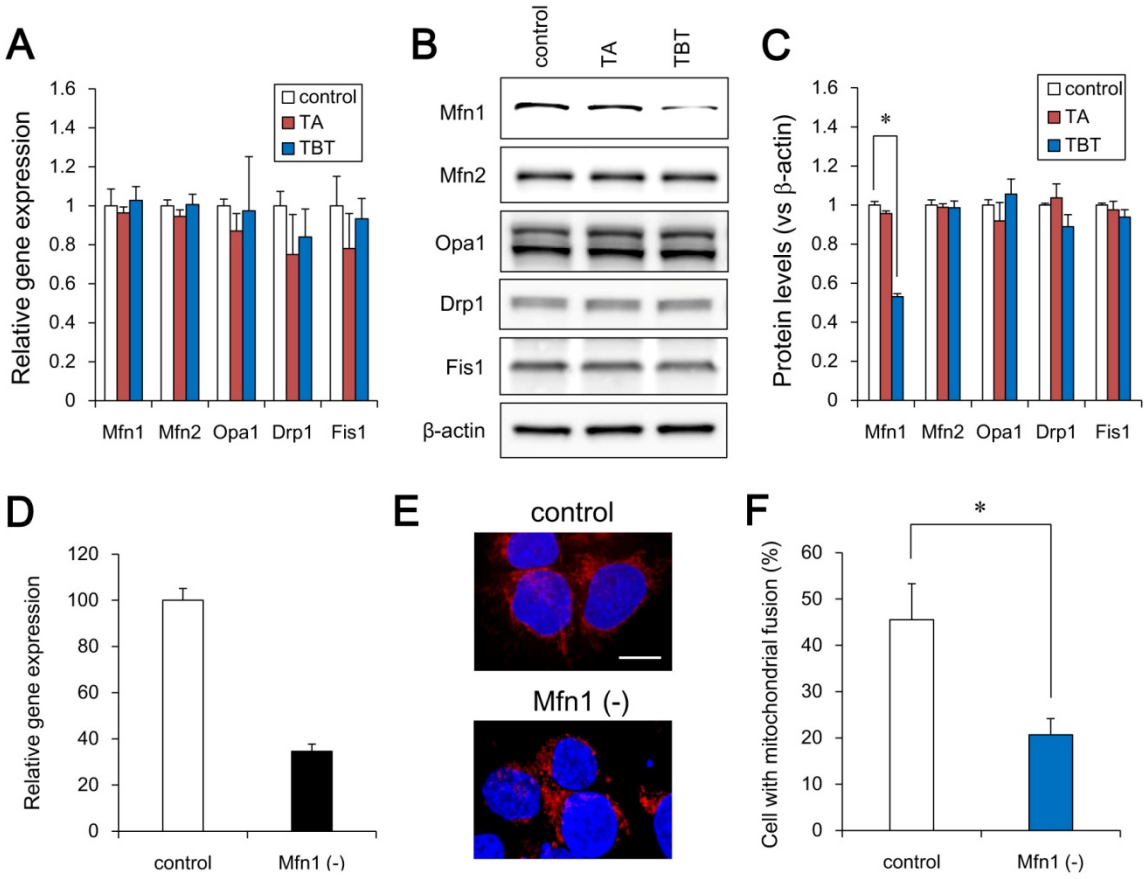

図３　トリブチルスズによる Mfn の分解

A) iPS 細胞に 50nM の TBT を曝露させ、72 時間後に RNA を回収した。Mfn1, Mfn2, Opa1, Drp1, Fis1 の qPCR を行った。

B) iPS 細胞に 50nM の TBT を曝露させ、72 時間後に蛋白質を回収した。Mfn1, Mfn2, Opa1, Drp1, Fis1 のウェスタンブロットを行った。

C)B)の結果を定量的に評価した。TBT で Mfn1 が分解した。

D)レンチウイルスを用いて iPS 細胞に Mfn1 shRNA を導入した後、RNA を回収した。Mfn1 ノックダウン効率を qPCR にて調べた。

E) Mfn1 ノックダウン細胞のミトコンドリア形態を共焦点顕微鏡で観察した。

F)E)の結果を定量的に評価した。Mfn1 ノックダウンによりミトコンドリア分裂低下が認められた。

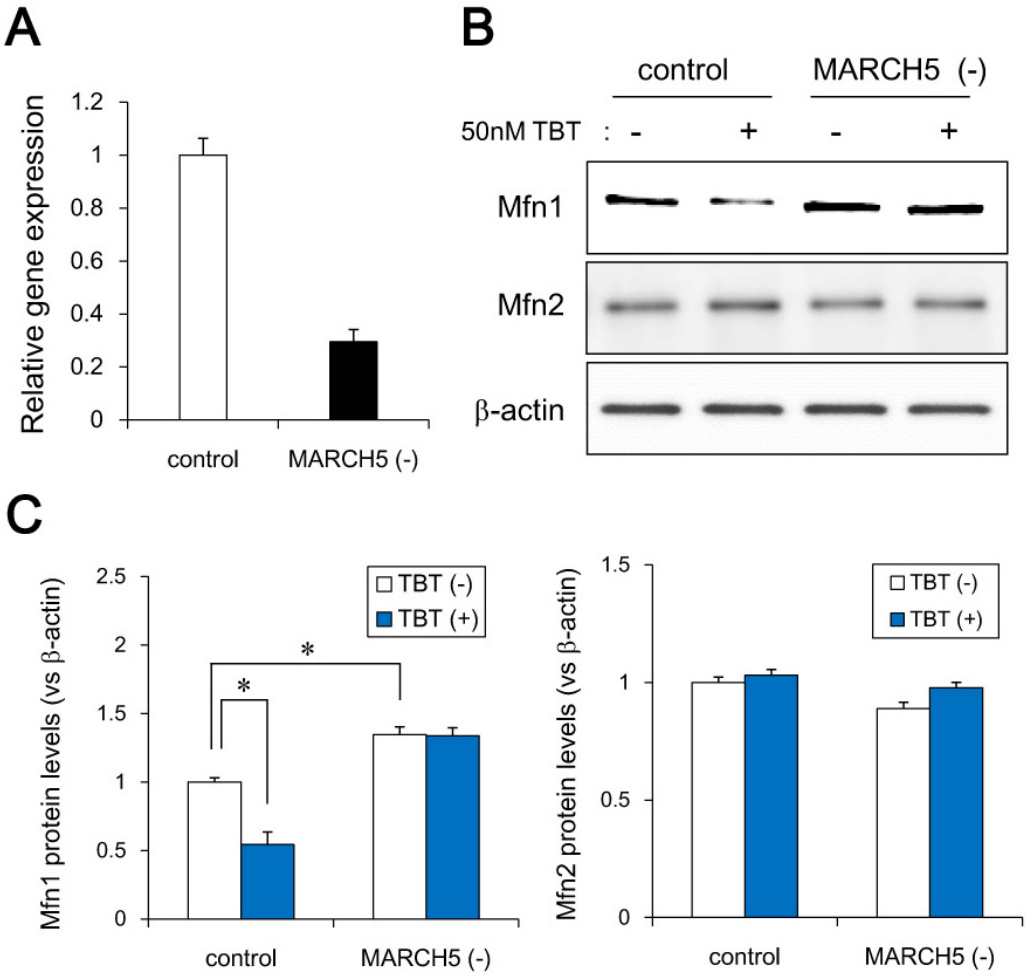

図４　トリブチルスズの Mfn1 分解における MARCH5 の関与

A) iPS 細胞に MARCH5 siRNA を導入した後、RNA を回収した。MARCH5 ノックダウン効率を qPCR にて調べた。

B) MARCH5 ノックダウン細胞に 50nM の TBT を曝露させ、72 時間後に蛋白質を回収した。Mfn1, Mfn2 のウェスタンブロットを行った。

C)B)の結果を定量的に評価した。MARCH5 ノックダウンにより TBT の Mfn1 分解が阻害された。

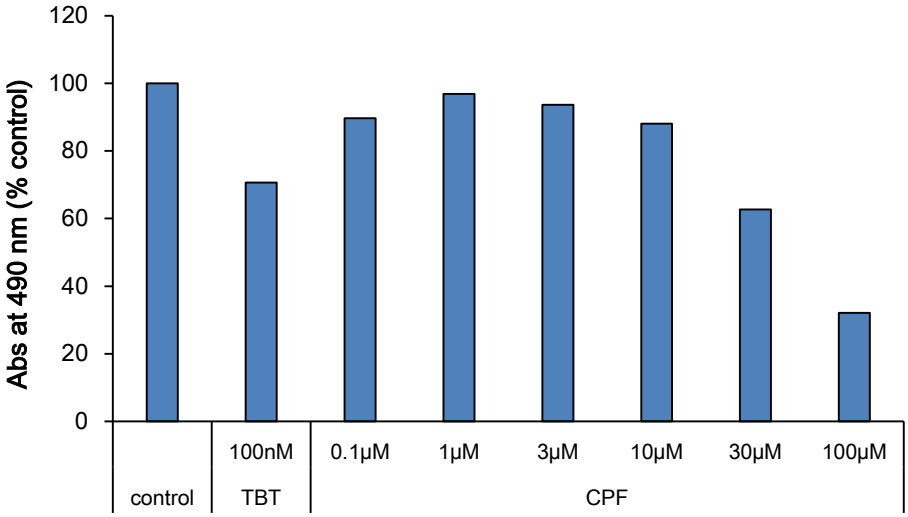

図５　クロルピリホスによる **NT2/D1** 細胞の増殖抑制
NT2/D1 細胞において、クロルピリホスの暴露による濃度依存的な増殖低下が認められた。

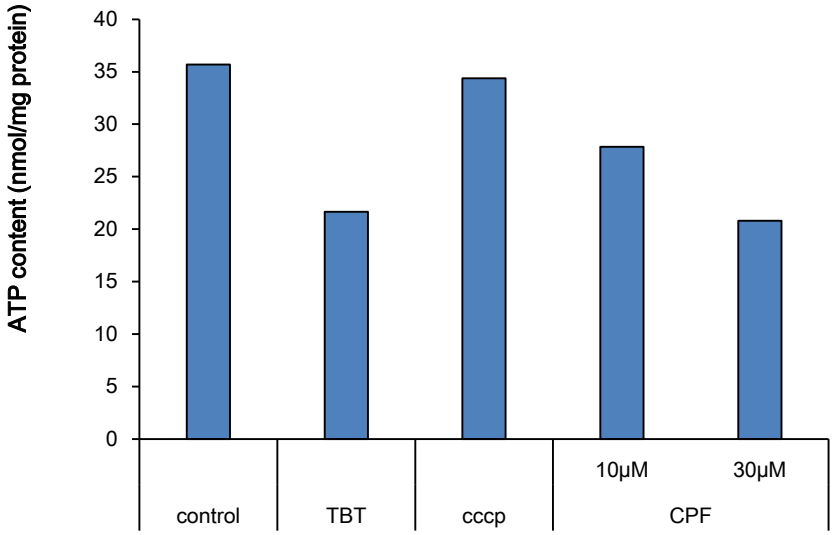

図６　クロルピリホスによる NT2/D1 細胞の ATP 産生抑制

NT2/D1 細胞において、クロルピリホスの暴露による濃度依存的な ATP 産生抑制が認められた。

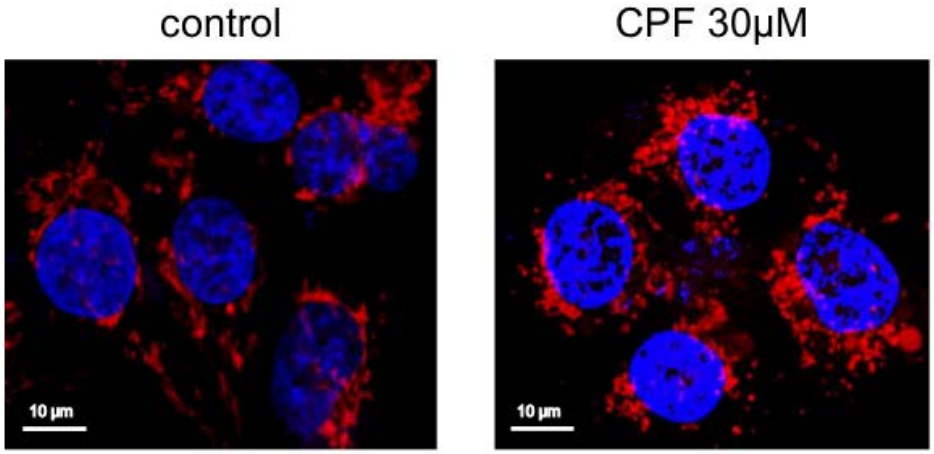

図７　クロルピリホスによるミトコンドリア分裂促進
NT2/D1 細胞において、30μM クロルピリホスの暴露によりミトコンドリア分裂促進が認められた。

厚生労働科学研究費補助金（化学物質リスク研究事業）
分担研究報告書

神経堤細胞の機能解析による評価法の開発

研究分担者　国立医薬品食品衛生研究所　薬理部第四室長
宇佐見　誠
研究協力者　宮島　敦子
研究協力者　入江　智彦

要旨
ラット神経堤細胞遊走実験法を用いて、発達神経毒性を有すると考えられる化学物質として、クロルピリホスの神経堤細胞に及ぼす影響を調べた。ラット 10.5 日胚から菱脳部の神経管を摘出して培養し、培養 24 時間目にクロルピリホスを培養液に添加した。培養期間中に神経管から遊出する神経堤細胞の広がりを測定し、神経堤細胞の遊走を調べた。その結果、25 μM 以上のクロルピリホスにより、形態変化を示す細胞が散見され、細胞毒性によると考えられた。神経堤細胞の遊走に及ぼす影響として、培養 48 時間までは 50μM までは促進傾向が認められ、100μM では抑制傾向が認められた。培養 48 から 72 時間では、最低濃度の 6.25μM 以上で抑制傾向が認められ、25 μM 以上で有意差が認められた。神経堤細胞の遊走促進をより高感度に調べることができる方法として、培養 18 時間で神経管を除去すると、クロルピリホス (100 μM) は神経堤細胞の遊走を促進する場合もあったが、72 時間では遊走の抑制傾向が認められた。これらのことから、クロルピリホスは、神経堤細胞の遊走に対して複数のメカニズムを介して影響を及ぼすと考えられた。以上のように、ラット神経堤細胞遊走実験法により、発達神経毒性を有する化学物質の神経堤細胞に及ぼす影響を明らかにすることが出来た。本実験法は、毒性発現メカニズムに基づいた化学物質の発達神経毒性評価法として有用であると考えられた。

A. 研究目的

近年、子供の学習障害や自閉症などの発達障害が増加しているが、その原因として化学物質の関与が指摘されている。神経提細胞は、脊椎動物における個体発生の限られた時期に存在し、胚の隅々に遊走した後に末梢神経、グリア細胞などの神経系細胞を含む様々な細胞に分化することにより、個体の機能発育および形態形成に重要な役割を果たす。そのため、発生過程における神経提細胞の誘導、遊走、分化などにおける異常は、神経提症と総称される神経芽細胞腫などの神経系の異常を含むさまざまな疾患を引き起こす。

また、神経提細胞のうち、頭部神経管に由来する頭部神経提細胞の異常では、顔面の奇形などの形態形成に及ぼす影響も認められる。神経提症による顔面奇形と同様の奇形は、胚のレチノイン酸への過剰暴露においても生じることから、神経提細胞は化学物質による毒性の標的組織となり得ると考えられている。しかし、適切な実験法が確立されていないため、化学物質の神経提細胞機能に及ぼす影響は、ほとんど調べられていない。

本研究では、神経提細胞の特徴的な機能である細胞遊走を主な指標とする、形態形成期に重要な役割を果たす神経堤細胞の機能に及ぼす化学物質の影響を調べる方法を確立し、個体の成長期における化学物質の健康影響評価法の一つとして用いることを目的とする。神経提細胞実験法としては、初期着床胚をまるごと培養するラット全胚培養法との比較実験が可能であり、解析が容易な、ラット神経提細胞を用いた実験法の確立を目指した。

本実験法を利用することにより、神経堤細胞遊走に影響する化学物質とそのメカニズムを同定し、ヒトにおける当該化学物質に対する高暴露集団およびメカニズムに関与す

る遺伝子疾患等を有する集団などの、ハイリスク集団について、疫学的調査の基盤的情報を提供すると共に、健康影響の予防のための方策となる情報を得られることが期待される。

初年度は、神経系の発生に影響を及ぼすことが知られているバルプロ酸をモデル化学物質として用いて、ラット神経堤細胞遊走実験法の発達神経毒性評価法としての有用性について検討した。次年度は、内分泌撹乱作用を有する環境汚染物質であるトリブチルスズをモデル化学物質として用いた。最終年度である今年度は、神経発達毒性が報告されている農薬であるクロルピリホスをモデル化学物質として用いた。

B. 研究方法

1. 動物

ウィスターラット（Crlj:WI, 日本チャールスリバー）を用いた。発情前期の雌ラットを雄と終夜同居させ、妊娠ラットを得た。同居中の深夜を妊娠 0 日として起算した。妊娠 10.5 日に、妊娠ラットから初期着床胚を摘出して実験に用いた。

2. ラット神経堤細胞の培養

摘出したラット初期着床胚から、電解研磨したタングステン針を用いて、菱脳部を切り出し、物理的に神経管を取り出した。体幹神経堤細胞を用いる場合は、前肢芽の部位から神経管を同様の方法で取り出した。取り出した神経管を、培養シャーレ（Becton, Dickinson and Company）に培養液(10% Fetal Bovine Serum を含む Dulbecco's Modified Eagle Medium, GIBCO)と共に入れ、炭酸ガスインキュベーター内で、5% CO_2、37℃にて培養した。培養 24 時間目にクロルピリホスを含む培養液に交換して、48 時間まで培養した。クロルピリホスは、ジメチルスルホキシドに溶解して用いた。

3. ラット神経堤細胞の観察

培養 24 時間及び 48 時間に、神経管から遊走した細胞すべてを含む領域を、位相差顕微鏡（BZ-900、株式会社キーエンス）で撮影し、神経管の培養容器底面への付着及び遊走細胞の広がりを観察した。

4. データの解析

細胞の撮影画像ファイルを画像解析ソフト ImageJ (Rasband, W.S. ImageJ, U. S. National Institutes of Health, Bethesda, Maryland, USA, http://rsb.info.nih.gov/ij/, 1997-2009) で開き、最外側の神経提細胞をポリゴンツールでつないでできる図形を円とみなして、そのピクセル数で表される面積から計算した半径を神経堤細胞の遊走距離として解析した。

（倫理面への配慮）

動物の使用にあたっては国立医薬品食品衛生研究所の「動物実験に関する指針」を遵守した。

C. 研究結果

1. クロルピリホスのラット神経堤細胞遊走に及ぼす影響

クロルピリホス (6.25, 12.5, 25, 50 および 100 μM) を培養 24 時間目に添加して、ラット神経堤細胞に及ぼす影響を調べた。その結果、25 μM 以上のクロルピリホスにより、形態変化を示す細胞が散見され、細胞毒性によると考えられた(図 1)。

神経堤細胞の遊走に及ぼす影響として、培養 48 時間までは 50 μM までは促進傾向が認められ、100 μM では抑制傾向が認められた。培養 48 から 72 時間では、最低濃度の 6.25 μM 以上で抑制傾向が認められ、25 μM 以上で有意差が認められた (図 2)。

一方、神経堤細胞の遊走促進をより高感度に調べることができる方法として、培養 18 時間で神経管を除去すると、クロルピリホス (100 μM) は神経堤細胞の遊走を有意に促進した (図 3)。

遊走促進作用の確認および神経管の部位の違いによる神経堤細胞への影響を調べるために、頭部および腹部神経管を培養し、培養 18 時間で神経管を除去して、24 時間目にクロルピリホスを添加し 72 時間まで培養した。その結果、培養 48 時間では、クロルピリホスの影響は殆ど認められなかったが、培養 48 時間では、頭部神経堤細胞には遊走の抑制傾向が認められたが、腹部神経堤細胞には遊走の促進傾向が認められ、神経管の部位の違いによる影響が示された (図 4)。

D. 考察

ラット神経堤細胞遊走実験法により、発達神経毒性を有するクロルピリホスの神経堤

細胞ら及ぼす影響を調べた。その結果、クロルピリホスは、神経堤細胞の遊走に相反する作用を示したが、長時間の暴露では、細胞毒性によると考えられる遊走抑制作用が認められた。また、神経管の部位による影響の違いが認められた。これらのことから、クロルピリホスは、神経堤細胞の遊走に対して複数のメカニズムを介して影響を及ぼすと考えられる。

以上の結果から、発達神経毒性評価法として、本実験法は、化学物質の神経堤細胞機能阻害が関与する影響の評価法として有用であると考えられる。

E. 結論

ラット神経堤細胞遊走実験法により、発達神経毒性を有するクロルピリホスの神経堤細胞に及ぼす影響を調べた。クロルピリホスは、神経堤細胞の遊走に、促進と抑制の相反する作用を示したが、長時間の暴露では、細胞毒性によると考えられる遊走抑制作用が認められた。クロルピリホスは、神経堤細胞の遊走に対して複数のメカニズムを介して影響を及ぼすと考えられた。本実験法は、化学物質の神経堤細胞機能阻害が関与する発達神経毒性評価法として有用であると考えられた。

F. 研究発表

1. 論文発表

[1] Usami M., Mitsunaga K., Irie T., Miyajima A. and Doi O. Proteomic analysis of ethanol-induced embryotoxicity in cultured post-implantation rat embryos. *The Journal of Toxicological Sciences* 39: 285–292 (2014).

[2] Usami M., Mitsunaga K., Irie T. and Nakajima M. Various definitions of reproductive indices: a proposal for combined use of brief definitions. *Congenital Anomalies* 54: 67–68 (2014).

[3] Kim S.-R., Kubo T., Kuroda Y., Hojyo M., Matsuo T., Miyajima A., Usami M., Sekino Y., Matsushita T. and Ishida S. Comparative metabolome analysis of cultured fetal and adult hepatocytes in humans. *The Journal of Toxicological Sciences* 39: 717–23 (2014).

[4] Usami M., Mitsunaga K., Irie T., Miyajima A. and Doi O. Simple in vitro migration assay for neural crest cells and the opposite effects of all-trans-retinoic acid on cephalic- and trunk-derived cells. *Congenital Anomalies* 54: 184–8 (2014).

[5] Usami M., Mitsunaga K., Miyajima A., Takamatu M., Kazama S., Irie T., Doi O., and Takizawa T. Effects of 13 developmentally toxic chemicals on the migration of rat cephalic neural crest cels in vitro. Congenital Anomalies (2015).

[6] Irie T., Kikura-Hanajiri R., Usami M., Uchiyama N., Goda Y., and Sekino Y. MAM-2201, a synthetic cannabinoid drug of abuse, suppresses the synaptic input to cerebellar Purkinje cells via activation of presynaptic CB1 receptors. Neuropharmacology 95: 479–491 (2015).

2. 学会発表

[1] 宇佐見 誠, 高松 美奈, 風間 崇吾, 満長 克祥, 入江 智彦, 宮島 敦子, 土井 守,滝沢 達也. 化学物質が培養ラット神経堤細胞の増殖に及ぼす影響に関する研究. 第55 回日本先天異常学会学術集会. 横浜 (2015).

H. 知的財産の出願・登録状況

1. 特許取得

なし。

2. 実用新案登録

なし。

3. その他

なし。

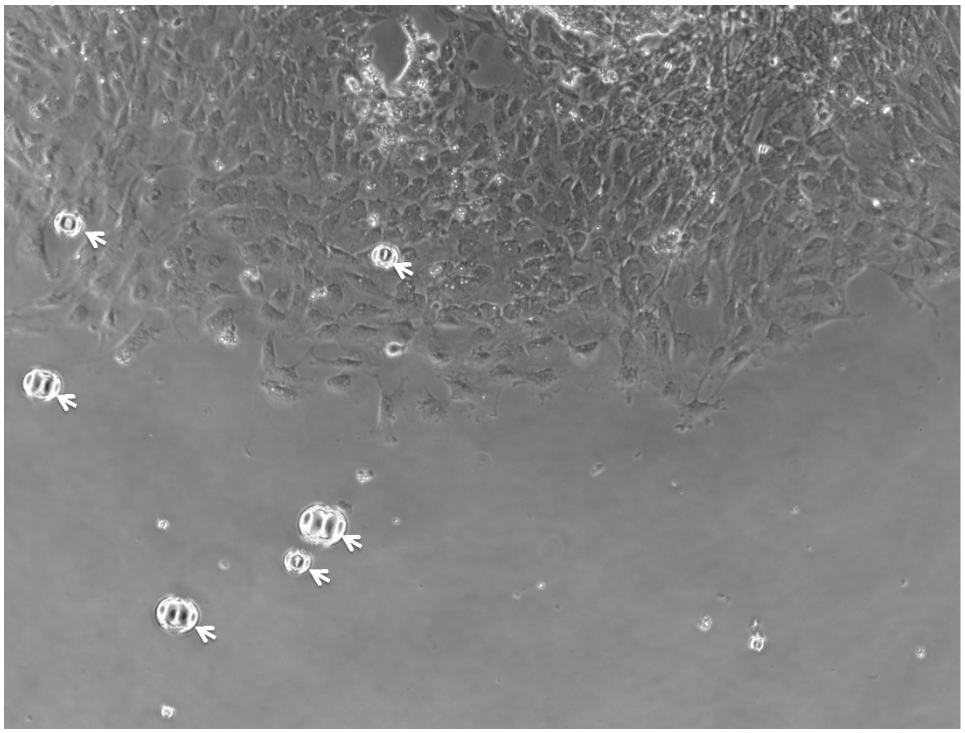

図 1. ラット神経堤細胞の形態に及ぼすクロルピリホスの影響
ラット 10.5 日の神経管から遊走する神経堤細胞を 48 時間培養した。培養 24 時間目からクロルピリホス (100 μM) を培養液に添加した。矢印は形態異常を起こした細胞を示す。

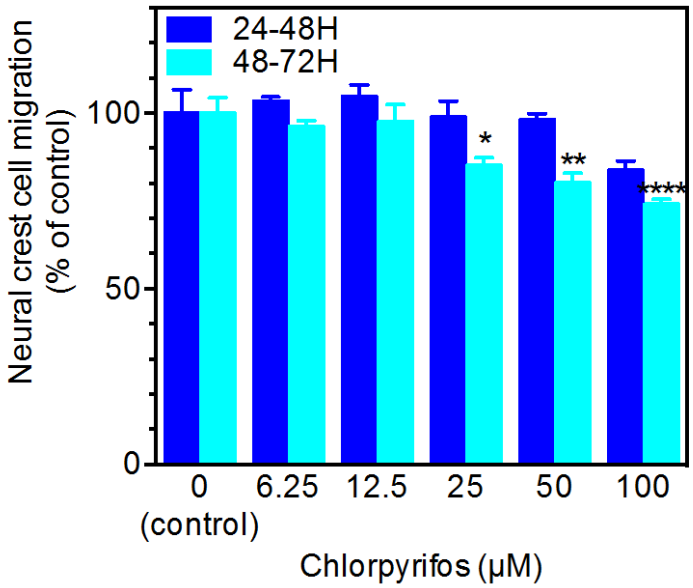

図 2. ラット神経堤細胞の遊走に及ぼすクロルピリホス (chlorpyrifos) の影響
ラット 10.5 日の神経管から遊走する神経堤細胞を 72 時間培養した。培養 24 時間目からクロルピリホスを培養液に添加した。平均値と標準誤差を示す。「*」は対照群と比較して統計学的な有意差があることを示す (* $p < 0.05$, ** $p < 0.01$, **** $p < 0.0001$,)。

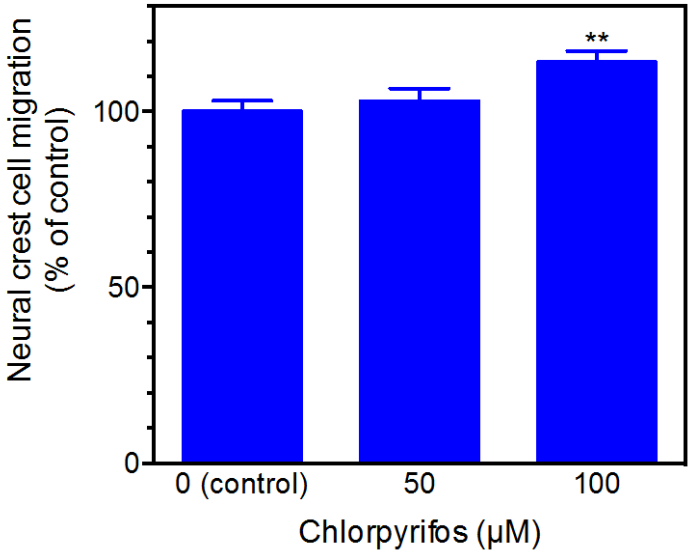

図 3. ラット神経堤細胞の遊走に及ぼすクロルピリホス (chlorpyrifos) の影響
ラット 10.5 日の神経管から遊走する神経堤細胞を 48 時間培養した。培養 24 時間目からクロルピリホスを培養液に添加した。平均値と標準誤差を示す。「*」は対照群と比較して統計学的な有意差があることを示す (** $p < 0.01$)。神経管を培養 18 時間目に除去した。

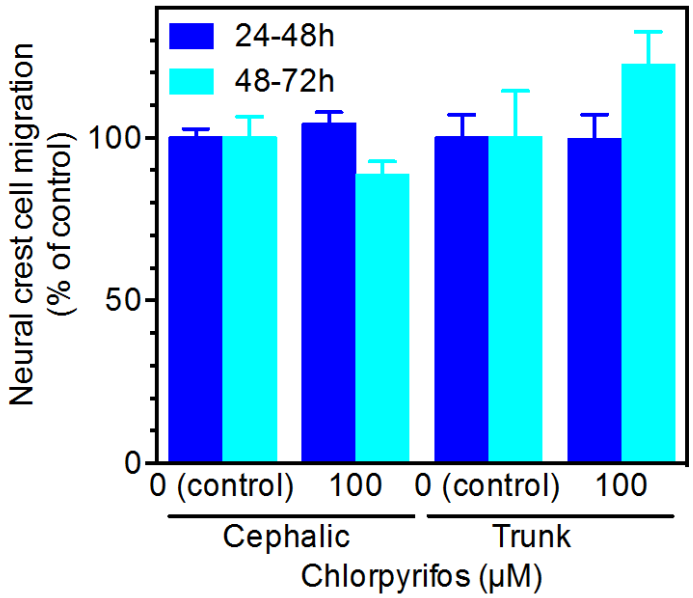

図 4. ラット頭部 (cephalic) および腹部 (trunk) 神経堤細胞の遊走に及ぼすクロルピリホス (chlorpyrifos) の影響
ラット 10.5 日の神経管から遊走する神経堤細胞を 72 時間培養した。培養 24 時間目からクロルピリホスを培養液に添加した。平均値と標準誤差を示す。神経管を培養 18 時間目に除去した。

厚生労働科学研究費補助金（化学物質リスク研究事業）
分担研究報告書

発達成長期神経系細胞新生への化学物質の影響評価

研究分担者　国立医薬品食品衛生研究所　薬理部第一室長
佐藤　薫

要旨
前脳矢状切片の側脳室下帯に存在する神経幹細胞および前駆細胞を蛍光標識し切片培養を行った。評価化合物クロルピリホスを適用し神経系細胞新生およびオリゴデンドロサイト新生に対する影響について定量的評価を行った。クロルピリホスは新生細胞数を濃度依存的に減少させる傾向を示した。新生オリゴデンドロサイト数も減少の傾向を示したが、新生細胞全体の減少よりも小さな変化であった。新生細胞中の新生オリゴデンドロサイトの割合を算出したところ、クロルピリホス 10 μM までは何ら影響がないが、100 μM　において新生細胞中の新生オリゴデンドロサイトの割合は増加の傾向を示した。従って、クロルピリホスはオリゴデンドロサイト以外の細胞に対して新生抑制影響がある可能性が示された。

A.目的

幼児期の側脳室下帯（subventricular zone: SVZ）からは神経系細胞（オリゴデンドロサイト、神経細胞、アストロサイト）新生が活発に起こっており、この時期にこれらの細胞に異常が起こると重篤な高次機能影響を引き起こす可能性が高い。実際に、幼児期の抗がん剤使用は知能障害を引き起こすことが知られており禁忌となっている。我々はこれまでに生後 2-3 日齢ラットの前脳矢状面切片培養系の SVZ に含まれる 神経幹細胞および前駆細胞を緑色蛍光蛋白質 (enhanced Green Fluorescent Protein: eGFP) によりピンポイントで標識し、免疫組織化学的検討と組み合わせることにより神経系細胞（特にオリゴデンドロサイト）の新生や遊走に対する化学物質の影響評価系を確立した。本研究では有機リン酸系農薬であるクロルピリホスの神経系細胞新生およびオリゴデンドロサイト新生に対する影響評価を行った。

B. 研究方法

1. 前脳矢状面切片培養系

生後 2-3 日齢ラットの前脳矢状面切片標本（150 μm）を作成しトランスメンブレン（Millipore）　上に静置し、eGFP tag を組み込んだ改変型レトロウィルスを SVZ に 30 nl ピンポイントで滴下することにより、局所的に神経幹細胞および前駆細胞を標識した。その後、切片培養用培地で 3 日間培養した。

2. 前脳矢状面培養切片の免疫組織化学的検討

eGFP 標識細胞の O1（オリゴデンドロサイト前駆細胞マーカー）発現について免疫組織化学的に検討した。ブロッキング液で 1 時間処理した後、4°C で抗 O1 抗体（IgM）（Millipore [Chemicon]　MAB344）により 2 日間処理し、PBS で 3 回洗浄した後、蛍光標識された二次抗体で 2 日間処理し（4°C）、PBS で洗浄した。eGFP(+) 細胞数、eGFP(+)O1(+) 細胞数、新生細胞遊走面積を算出した。

3. eGFP 標識細胞を含む前脳矢状面切片培養系を用いたクロルピリホスの評価

クロルピリホス（TRC, Canada）は 200 mM の DMSO ストックソルーションを作成し、培地にて用時希釈した。ピンポイントで eGFP で標識された神経幹細胞および神経系前駆細胞を SVZ に持つ前脳矢状面切片を クロルピリホス（1-100 μM）存在下で 3 日間培養し、新生細胞の増殖と遊走、オリゴデンドロサイト前駆細胞の増殖と遊走に対する作用を検討した。

C. 研究結果

1. 被験化合物の神経系新生細胞およびオリゴデンドロサイト新生に対する影響

クロルピリホスは DMSO に溶解したため、まず DMSO の影響について検討した。eGFP 標識された新生細胞群（神経幹細胞および前駆細胞）を SVZ に含む培養前脳矢状面切片をクロルピリホス適用時に想定される最高濃度の DMSO（0.05%）を含む培地で 3 日間培養したところ、eGFP(+) 細胞（神経幹細胞および前駆細胞）数、eGFP(+)O1(+) 細胞（新生オリゴデンドロサイト）数、新生細胞中の新生オリゴデンドロサイトの割合、これらの細胞の遊走に何ら影響はなかった（データ示さず）。

次に上記パラメーターに対するクロルピリホスの影響について検討した（図 1）。培養前脳切片をクロルピリホス入りの培地（final conc: 1-100 μM）で 3 日間培養したところ、100 μM クロルピリホス適用群では、培養前脳切片の膨潤がおこり切片の厚みが増していた。1-10 μM においてはこのような変化は観察されなかった。クロルピリホス（1-100 μM）は eGFP(+) 細胞（神経幹細胞および前駆細胞）数を濃度依存的に減少させる傾向があった（図 1B, 黄土色カラム）。eGFP(+)O1(+) 細胞（オリゴデンドロサイト前駆細胞）数も減少の傾向を示したが、新生細胞全体の減少よりも小さな変化であった（図 1B, 黄色カラム）。新生細胞中の新生オリゴデンドロサイトの割合（eGFP(+)O1(+) cell No. /eGFP(+) cell No. *100%）を算出し、クロルピリホスの作用を確認したところ、クロルピリホス 10 μM まではほとんど影響がなかったが、100 μM において新生細胞中のオリゴデンドロサイト前駆細胞の割合が増加の傾向を示した（図 1C）。新生細胞の遊走範囲もクロルピリホスによって濃度依存的に減少した。これは、上記に示す新生細胞数の減少に矛盾しない結果となっている。

D. 考察

クロルピリホスは有機リン酸系の殺虫剤であり、害虫の神経系アセチルコリンエステラーゼを阻害することにより作用を発揮するとされている。しかし、アセチルコリンエステラーゼ阻害作用よりも低い濃度で注意や記憶を損なうことが、ヒト、動物でともに報告されている（Brown and Brix, J Appl Toxicol 1998, 18, 393-408; Ray and Richards, Toxicol Lett 2001, 120, 343-351; Johnson et al., Toxicol Sci 2009, 109(1) 132-42）。このようにクロルピリホスは多岐にわたる作用メカニズムを持ち、その作用も多岐にわたることが予想されるが神経発達に対する影響はあまり知見がない。本研究では生後初期の神経系細胞新生およびオリゴデンドロサイト新生に対する影響評価を前脳切片培養系を用いて行った。

クロルピリホス（1-100 μM）は eGFP(+) 細胞（神経幹細胞および前駆細胞）数を濃度依存的に減少させる傾向があった。また、新生細胞中のオリゴデンドロサイト前駆細胞の場合は 100 μM において新生細胞中の新生オリゴデンドロサイトの割合が増加の傾向を示した。従って、クロルピリホスはオリゴデンドロサイト以外の細胞に対して新生抑制を引き起こす可能性が示された。脳神経系は主に神経細胞、アストロサイト、オリゴデンドロサイト、ミクログリア、血管系細胞で構成されているが、胎生期から生後にかけてクロルピリホスに暴露されたマウスは海馬の神経新生が低下することも報告されている（Wang et al., Reprod Toxicol 2013, 38, 25-36）。培養ヒトアストロサイト培養を用いた実験では、クロルピリホスがアストロサイトの炎症性活性化を引き起こすことが示されている（Mense et al., Toxicol Sci, 2006, 93(1) 125-35）。また、胎生期もしくは生後のクロルピリホスの in vivo 適用においては、グリア細胞新生時期に適用したときに最も発達阻害が誘発された（Garcia et al., Environ Toxicol Pharmacol 2005, 19(3), 455-61）。また、胎生期暴露はアストロサイト活性化マーカーである GFAP 発現レベルを上昇させた（Carcia et al., Brain Res Dev Brain Res 2002, 133(2), 151-61）。しかし、一方でオリゴデンドロサイト前駆細胞に対しても毒性が報告されている（Saulsbury et al., Toxicology 2009, 259(1-2), 1-9）。細胞種によりクロルピリホスへの感受性が違っており、アストロサイトはその中でも感受性の高い細胞であることが考えられるが、細胞種による感受性の違いについては細胞種特異的なマーカーを用いて確認する必要がある。このような細胞毒性のメカニズにとして細胞骨格への影響が考え

られる。クロルピリホスの長期的な投与により、軸索内輸送に影響があることが報告されている（Hernandez et al., Neurotoxicology 2015, 47, 17-26）。キネシンによる輸送（Gearhart et al., Toxicol Appl Pharmacol 2007, 218, 20-29）、tubulin　の修飾（Grigoryan et al., 2008, Chem Biol Interact 175, 180-186）、微小管形成阻害作用なども明らかとなっている（Prendergast, et al., Neuroscience 2007, 146, 330-339）。さらに、胎児新皮質において細胞分裂面が垂直から水平に移行する作用も報告されており、このような分裂面の角度が細胞の運命決定に影響を及ぼす可能性も示唆されている（Chen et al., PLoS One 2014, 9 (4) e95343）。さらに、ヒト胎生幹細胞由来神経幹細胞においてはクロルピリホスによって NF-kB 活性化を介したアポトーシスが誘導されること（Lee et al., Neurotoxicology 2014 42, 58-70）、ミトコンドリア長が増加するとともにその数が減ることも報告されており（Middlemore-Risher et al., 2011, J Pharamacol Exp Ther, 399(2) 341-9）、直接的なアポトーシス誘導作用を持つ可能性も考えられる。

クロルピリホスは高濃度領域（100 μM）において培養前脳切片の膨潤を引き起こした。これまでこのような報告はなく、新たなメカニズムを考慮に入れながら今後の検討を進める必要がある。

E. 結論

クロルピリホスは新生細胞数、新生オリゴデンドロサイト数、遊走面積ともに濃度依存的に減少させたが、その作用はオリゴデンドロサイト以外の細胞が標的となっている可能性が示された。さらに、高濃度クロルピリホス（＞100 μM）が浮腫を引き起こす可能性が示された。

F. 研究発表

1. 論文発表

[1] Ohara, Y., Koganezawa, N., Yamazaki, H., Roppongi, R. T., Sato, K., Sekino, Y., Shirao, T. (2015) Early-stage development of human induced pluripotent stem cell (hiPSC)-derived neurons. J Neurosci Res 93(12): 1804-13.

[2] 佐藤　薫. (2015) ミクログリアの発生と分化. Clinical Neuroscience 32(12) 1338-1341.

[3] Sato, K. (2015) Microglia effects on neuronal development. GLIA 63(8): 1394-495.

[4] Fujimori, K., Takaki, J., Miura, M., Shigemoto-Mogami, Y., Sekino, Y., Suzuki, T., Sato, K. (2015) Paroxetine prevented the down-regulation of astrocytic L-Glu transporters in neuroinflammation. J Pharmacol Sci, 127(1) 145-9.

[5] Shigemoto-Mogami, Y., Hoshikawa, K., Goldman, J.E., Sekino, Y. and Sato, K. (2014) Microglia enhances neurogenesis and oligodendrogenesis in the early postnatal subventricular zone. J Neurosci 34(5): 2231-2243.

[6] Shigemoto-Mogami, Y., Fujimori, K., Ikarashi, Y., Hirose, A., Sekino, Y. and Sato, K. (2014) Residual metals in carbon nanotubes suppress the proliferation of neural stem cells. Fundam Toxcol Sci, 1(3): 87-94.

[7] Takahashi K., Ishii-Nozawa R., Takeuchi K., Nakazawa K., Sekino Y. and Sato K. Niflumic acid activates additional currents of the human glial L-glutamate transporter EAAT1 in a substrate-dependent manner. Biol Pharm Bull 36(12): 1996-2004 (2013).

[8] Oguchi-Katayama A., Monma A., Sekino Y., Moriguchi T. and Sato K. Comparative gene expression analysis of the amygdalae of juvenile rats exposed to valproic acid at prenatal and postnatal stages. J Toxicol Sci 38(3): 381-402 (2013).

[9] Kinoshita M., Nasu-Tada K., Fujishita K., Sato K. and Koizumi S. Secretion of matrix metalloproteinase-9 from astrocytes by inhibition of Tonic P2Y14-receptor-mediated signal(s). Cell Mol Neurobiol 33 (1): 47-58 (2013).

2. 学会発表

[1] 高橋華奈子、最上(重本)由香里、清水英雄、中條かおり、干川和枝、岡田洋平、岡野栄之、関野祐子、佐藤　薫:ヒトiPS細胞由来神経細胞標本の機能的NMDA受容体発現とグルタミン酸興奮毒性発現の株間比較、日本薬学会第136年会(2016, 3,

横浜）
[2] 重本―最上　由香里、片倉　明日美、長谷川　陽介、関野　祐子、田辺　光男、佐藤　薫：神経幹細胞塊から機能的神経細胞を効率的に分化誘導するプロトコルの検討と分化に伴う機能的受容体分布変化、日本薬学会第 136 年会（2016, 3, 横浜）
[3] 佐藤　薫：ミクログリアの中枢神経系発達機能とその創薬・治療への応用、第 89 回日本薬理学会年会シンポジウム「創薬・治療のターゲットとしての細胞分化」（オーガナイザー）（2016, 3, 横浜）
[4] 清水英雄、小針彩奈、須知由未子、花村健次、白尾智明、田辺光男、関野祐子、佐藤　薫：シナプスイメージングに基づく中枢神経系有害反応の in vitro 評価のための新規パラメータ確立の試み、第 89 回日本薬理学会年会（2016, 3, 横浜）
[5] 重本―最上由香里、干川和枝、関野祐子、佐藤　薫：活性化型ミクログリアが引き起こす血液脳関門のバリア崩壊過程におけるサイトカイン・ケモカイン動態の解析、第 89 回　日本薬理学会年会（2016, 3, 横浜）
[6] 高橋華奈子、笠原のぞみ、小原悠、高瀬将弘、中條かおり、関野祐子、田辺光男、佐藤　薫：Neurosphere 維持期間が神経分化に及ぼす影響、第 89 回　日本薬理学会年会（2016, 3, 横浜）
[7] Takahashi, K., Shigemoto-Mogami, Y., Shimizu, H., Chujo, K., Hoshikawa, K., Okada, Y., Okano, H., Sekino, Y., Sato, K.: Comparison of the NMDA receptor expression and the extent of excitotoxicity in human induced pluripotent stem cell (hiPSC)-derived neurons. CBI 学会 2015 年大会（2015, 10, 東京）
[8] Shigemoto-Mogami, Y., Sato, K., Hoshikawa, K., Kikura-Hanajiri, R., Hakamatsuka, T., Sekino, Y.: Evaluation of drug-induced CB2 cannabinoid receptor activity in the CNS using the ERK1/2 phosphorylation pathway of microglial cells, CBI 学会 2015 年大会（2015, 10, 東京）
[9] 佐藤　薫, 清水英雄, 小針彩奈, 花村健次, 白尾智明, 田辺光男, 関野祐子：神経細胞の微細構造イメージングに基づく中枢神経系有害反応 in vitro 評価系の開発. 第 24 回日本バイオイメージング学会学術集会（2015,9, 東京）
[10] 佐藤　薫. ：非臨床薬理試験においてヒト iPS 細胞由来神経細胞を活用するために必要なこと. 千里ライフサイエンスセミナー J3（講演）,（2015, 9, 大阪）
[11] Hoshikawa, K., Takahashi, K., Irie, T., Sekino, Y., Sato, K.: Study about the mechanisms of DHA-induced enhancement of glial excitatory amino-acid transporter EAAT2 function. 第 58 回日本神経化学会大会（2015, 9, さいたま市）
[12] Shigemoto-Mogami, Y., Hoshikawa, K., Sekino, Y., Sato, K.: Microglia regulate the cytokine/chemokine dynamics in the brain and enhance the functional maturation of blood-brain barrier. 第 58 回日本神経化学会大会（2015, 9, さいたま市）
[13] Takahashi, K., Irie, T., Sekino, Y., Sato, K. Study about the mechanisms for the regulation of glial excitatory amino-acid transporter EAAT2 function by docosahexanoic acid. 第 38 回日本神経科学大会（2015, 7, 神戸市）
[14] Shigemoto-Mogami, Y., Hoshikawa, K., Sekino, Y., Sato, K.: Microglia affect blood-brain barrier function via cytokines and chemokines release. 第 38 回日本神経科学大会（2015, 7, 神戸市）
[15] Sato, K., Shigemoto-Mogami, Y., Hoshikawa, K., Sekino, Y.: Microglia affect functional maturation and inflammation-induced breakdown of the blood brain barrier by modulating the dynamics of cytokines and chemokines. Society for Neuroscience 2015 (2015, 10, Chicago, USA)
[16] Sato, K., Shigemoto-Mogami, Y., Hoshikawa, K., Sekino, Y.: Microglia have roles in both of maturation and break down of the barrier function of blood brain barrier. XII European Meeting on Glial Cells in Health and Disease (2015, 7, Bilbao, Spain)

A.

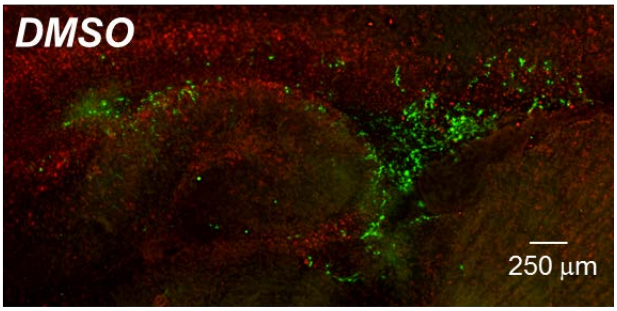

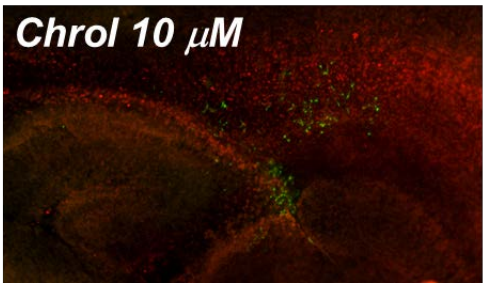

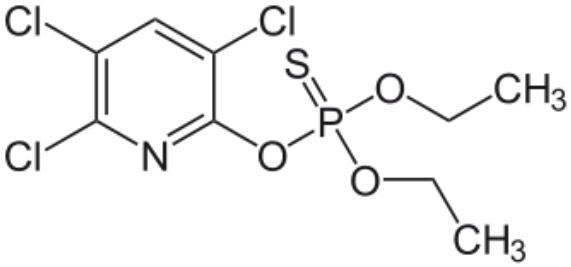

B.

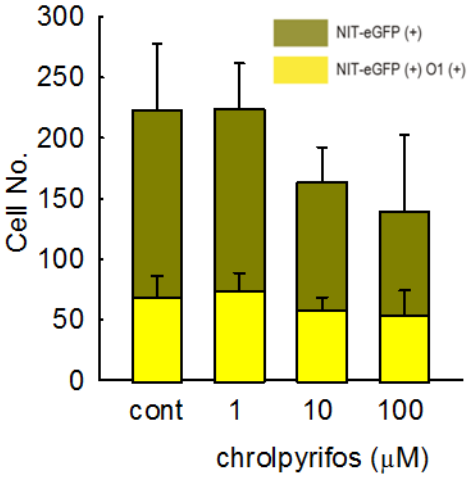

C.

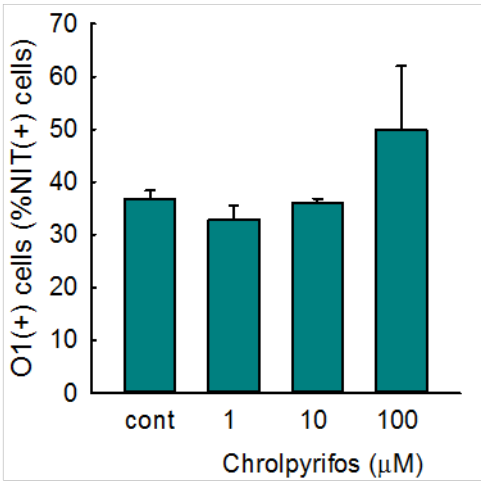

図 1. 前脳矢状面切片培養系における神経系細胞新生およびオリゴデンドロサイト新生に対するクロルピリホス の影響

SVZ 中、ピンポイントに eGFP 標識された新生細胞群（神経幹細胞および前駆細胞）を含む培養前脳矢状面切片を クロルピリホス (1-100 µM) 処理した（3 日間）。A: eGFP(+) 新生細胞（緑色）O1(+) オリゴデンドロサイト前駆細胞（赤）。B: 培養切片中 eGFP(+) 細胞数および eGFP(+)O1(+) 細胞数。クロルピリホスは新生細胞数を濃度依存的に減少させる傾向を示した（黄土色カラム）。C: eGFP(+) 細胞中の eGFP(+)O1(+) 細胞の割合。eGFP(+) 細胞中の eGFP(+)O1(+) 細胞の割合は クロルピリホスで増加の傾向があり、その作用はオリゴデンドロサイト以外の細胞が標的となっている可能性が示された。*: $p<0.05$, Tukey's test following ANOVA, N=4.

厚生労働科学研究費補助金（化学物質リスク研究事業）
分担研究報告書

生後神経回路の機能的影響評価指標に関する研究

研究分担者　国立医薬品食品衛生研究所　薬理部長
関野　祐子
研究協力者　豊橋技術科学大学　環境・生命工学系
吉田　祥子

要旨
昨年までに研究班共通の化学物質であるバルプロ酸を用いて、生後の神経回路発達の変化を伝達物質放出分布の変化として捉えることに成功した。この作用の機序を確認するために、化学構造の異なる各種のヒストン脱アセチル化酵素阻害剤の生後神経回路発達に及ぼす効果を検討した。その結果、ヒストン脱アセチル化酵素阻害剤は、神経発達の早期によって行動や脳の高次機能に影響することを明らかにした。一方、有機スズ化合物であるトリブチルスズは個体の行動に大きな影響現れるが神経構造への影響は小さいことが示唆された。さらに、反応機序の異なる発達神経毒性を有する有機リン系農薬であるクロルピリホスを追加して検討したところ、バルプロ酸と同様の影響が表れることを確認した。以上の結果、小脳の形態及び細胞機能の観察により、胎生期神経毒性を示す化学物質のスクリーニングが可能であることを示唆した。

A. 研究目的

バルプロ酸(VPA)、スベロイルアニリドヒドロキサム酸(SAHA)、MS-275 の３種のヒストン脱アセチル化酵素(HDAC)阻害剤、およびトリブチルスズ(TBT)投与による神経回路発達の変化を、発達期小脳を用いて検討するために、酵素を利用した測定法によって ATP の放出変化を観察した。同時に免疫組織化学的手法により、神経の形態的変化を観察した。さらに個体の行動に及ぼす変化を確認するために、発達期個体の行動観察を行った。

B. 研究方法

研究試料として発達期小脳を用いた（図１）。2013 から 2014 年にかけて、自閉症の特発脳部位が小脳であると報告されてきた。本研究では、小脳で、VPA が神経発達の早期化を引き起こすことが示唆され、また化学構造の異なる HDAC 阻害剤、および異なる作用機序で神経発達に影響すると考えられる TBT を妊娠動物に投与し、その効果を観察した。妊娠 16 日のラットに、600 ㎎/㎏の VPA(経口)、50mg/kg の SAHA(腹腔内)、4mg/kg の MS-275(経口)、20mg/kg の TBT(経口)でそれぞれ投与した。また、VPA と同様に自閉症の誘発が考えられているクロルピリホス（CPF）10mg/kg を経口投与しその効果を観察した。

投与動物は、各投与動物の任意に選んだ 3 匹について、生後 4 日から 10 日にかけて、温度維持した明環境下での３分間の自由行動の観察を行った。

シナプス形成のシグナルとされる ATP の放出量の変化を、酵素を用いた手法により測定した。各投与動物から、生後 6 日から 12 日の小脳スライスを調整し、ATP 放出量を測定した。

神経回路に対する影響を観察するために、神経刺激に対する GABA の放出量の変化を，生後７日から１８日にかけて観察した。

神経細胞の発達を免疫組織化学により観察するために、各投与動物から生後 10 日から１８日の小脳スライスを調整し、抗カルビンジン抗体による蛍光染色を行った。

さらに小脳全体への影響、長期にわたる影響を見るため、各時期の小脳スライスの HE 染色を行い、小脳各層の変化を観察した。顆粒細胞の増殖時期を確認するため、ブロモデオキシウリジン(BrdU)の 2 時間投与を行い、採取した小脳を抗 BrdU 抗体で染色して観察

した。

C. 研究結果

図2に示すように、行動観察の結果、VPA投与動物では,P4で多くの不随意運動を確認したが、成長するにつれて減少する傾向にあった。SAHA投与動物では,対照動物やVPA投与動物と比較して多くの不随意運動を確認し、且つP4～P8にかけ増加する傾向が見られた。MS-275投与動物では対照動物より若干の不随意運動の増加が確認された。TBT投与動物では,対照動物と比較して当初明らかに行動が減少していたが、成長につれて差は確認されなくなった。CPF投与動物ではVPA投与動物と同じような傾向を示したが、より程度が軽度だった。これは投与量が少なかった可能性がある。

VPA、SAHA投与動物では、対照動物に比べ早期から小脳皮質でATPが放出されることが確認されたが、TBTは早期からの放出は顕著でなく、かつ放出量は対照動物よりむしろ少ないことが観察された（図3)。

AMPA刺激に対するGABA放出量変化は、対照動物では一過性の上昇を示した後に速やかに減少するのに対し、VPA投与動物では繰り返し、長くGABA放出が続く傾向が示された（図4)。

さらに、SAHA 投与動物では,プルキンエ細胞に異常がみられ,細胞が不規則な多重構造を形成していることが観察された。樹状突起伸長は対照動物より早く、神経発達の早期化が伺われた。MS-275 投与動物では,P10 でのみ,プルキンエ細胞が不規則な多重構造を形成していることが観察されたが、P13 ではそのような分化異常は確認されなかった。さらに. TBT 投与動物では,プルキンエ細胞の層構造、樹状突起伸長のいずれにも異常はみられなかった（図 5)。

VPA 投与動物では、生後１２日以降に、V～VI 葉の一部に過剰な脳回の形成が観察された（図 6, 7)。いくつかの小脳では VIII 葉にみられるものもあった。拡大すると、分子層上部に顆粒細胞が蓄積し、また分子層中にも分布することが観察された。これらの変化は CPF 投与動物でも観察された。

生後３５日以降、これらの過剰な脳回部位を含め、小脳皮質の各所でプルキンエ細胞の死滅が観察された。これは、ヒトの自閉症において、小脳の萎縮・プルキンエ細胞死が見られるという報告と一致している。

過剰な脳回と分子層上部の顆粒細胞の蓄積は、これらの薬物投与によって顆粒細胞が過剰に増殖していることが示唆されたことから、顆粒細胞の増殖を確認するため、ブロモデオキシウリジン(BrdU)の 2 時間投与を行い、採取した小脳を抗 BrdU 抗体で染色して観察した。BrdU 投与による顆粒細胞増殖の確認からは、VPA 投与動物、CPF 投与動物の顆粒細胞増殖は、対照動物よりも早期に停止していることが示された（図 8)。過剰な脳回や蓄積した顆粒細胞は、増殖が延長されたのではなく、移動や選択的細胞死の抑制などによるものと考えられた。

D. 考察

発達期神経毒性が疑われる薬物の投与により、動物においても発達の一時期に行動異常が見られることを示した。より早い時期の行動異常は小脳の神経発達の変化と強い相関がみられたが、やや後期の行動異常は、もっと脳の別の部位、海馬や大脳の異常による変化との相関を伺わせた。また、伝達物質 ATP 量の変化から、発達期神経毒性の機序には早すぎる神経発達と、遅滞型の神経発達があることが伺われた。GABA 放出反応の異常は、早期（生後 2 週間）から神経回路の異常が始まっていることを示唆している。

さらに小脳の層に大きな変化が見られ、これが細胞死に至ることは、自閉症の発症機序に関わっていると考えられる。今後、薬物を追加して同様の現象が観察されるか検討する予定である。

E. 結論

本研究において、研究班共通の化学物質であるバルプロ酸、トリブチルスズ、クロルピリホスを用いて、生後の神経回路発達の変化を動物の行動、伝達物質放出量の変化、神経分化の変化として捉えることに成功した。従って、化学物質により神経発達の早期化および遅滞化により脳の高次機能に影響を与える可能性が示唆された。

F. 研究発表

1. 論文発表

1. ○Mabuchi H, Ong HY, Watanabe K, Yoshida S, Hozumi N. Visualization of Spatially Distributed Bioactive Molecules Using Enzyme-Linked Photo Assay. IEEJ Transactions (in press).
2. ○Watanabe K, Takahashi N, Hozumi N, Yoshida S. Improvements in Enzyme-Linked Photoassay Systems for Spatiotemporal Observation of Neurotransmitter Release. Sensors and Materials 27:1035-1044 (2015).
3. ○Gunawan AI, Hozumi N, Yoshida S, Saijo Y, Kobayashi K, Yamamoto S. Numerical analysis of acoustic impedance microscope utilizing acoustic lens transducer to examine cultured cells. Ultrasonics 63:102-110 (2015).
4. Gunawan AI, Hozumi N, Yoshida S, Saijo Y, Kobayashi K, Yamamoto S. Numerical analysis of ultrasound propagation and reflection intensity for biological acoustic impedance microscope. Ultrasonics 61:79–87 (2015).
5. ○Wang T, Kumada T, Morishima T, Iwata S, Kaneko S, Yanagawa Y, Yoshida S, Fukuda A. Accumulation of GABAergic Neurons, Causing a Focal Ambient GABA Gradient, and Downregulation of KCC2 Are Induced During Microgyrus Formation in a Mouse Model of Polymicrogyria. Cereb Cortex. 24:1088-101. (2014)
6. Kobayashi K, Yoshida S, Saijo Y, Hozumi N. Acoustic impedance microscopy for biological tissue characterization. Ultrasonics 54:1922-8 (2014).
7. ○吉田祥子、穂積直裕、発達期小脳アストロサイトの機能と秩序形成、日本神経回路学会誌 Vol. 20, p.14-18 (2013)
8. ○Yoshida S , Yamada H, Shioki Y, Hozumi N, Yagihashi M, Kobayashi K, Yamamoto S. Visualization of cancer distribution for living tissues using acoustic impedance microscope. Ultrasonics Symposium (IUS), 2013 IEEE International、Doi:10.1109/ULTSYM.2013.0514 (2013)
9. Hozumi N, Gunawan AI, Kajima S, Yoshida S, Saijo Y, Kobayashi K, Yamamoto S. Sound field analysis for biological acoustic impedance microscope for its precise calibration. Ultrasonics Symposium (IUS), 2013 IEEE International, 10.1109/ULTSYM. 2013. 0310 (2013)

2. 学会発表

[1] 中嶋さりい，勝股大樹，阿部巧，穂積直裕，笛田由紀子、上野晋、関野祐子、吉田祥子, Alteration of neuronal development and behavioral anomaly in autistic-like anomalous developing cerebellum. 第 38 回日本神経科学大会 神戸 2015

[2] 高橋信人，渡邊一徳，穂積直裕，吉田祥子，Improvements of enzyme-Linked photo assay systems for rapid spatio-temporal observation of neurotransmitter release. 第 38 回日本神経科学大会 神戸 2015

[3] 冨田達朗，穂積直裕，笛田由紀子、上野晋、関野祐子、吉田祥子, The effects of HDAC inhibitors to developing cerebellar astrocytes. 第 38 回日本神経科学大会 神戸 2015

[4] Y. Fueta, Y. Sekino, S. Yoshida, S. Ueno, Gabaergic involvement in the hippocampal development of the basic excitability and feedback inhibition in juvenile rats prenatally exposed to valproic acid. Society of Toxicology 54th Annual Meeting San Diego 2015

[5] S. Yoshida, Y. Fueta, S. Ueno, Y. Sekino, Prenatal administration of valproic acid or SAHA alters the development of Purkinje cell dendrites and network formation in rat cerebellum. 第 58 回日本神経化学会大会 さいたま市 2015

[6] N. Takahashi, H. Mabuchi, Y. Shigemoto - Mogami, K. Sato, Y. Sekino, N. Hozumi, S. Yoshida, Visualization of neurotransmitter release in the rat - derived neuroshere cells using enzyme - linked photo - assay. 8th FAOPS Congress Bangkok 2015

[7] S. Iwamoto, D. Katsumata, Y. Fueta, S. Ueno, Y. Sekino, N. Hozumi, S. Yoshida, Developmental alteration with administration of valproate enhanced neuronal activities in the juvenile cerebellar cortex. AP-IRC2015 Tahara 2015

[8] T. Mikami, S. Nakajima, Y. Fueta, S. Ueno, Y.

Sekino, N. Hozumi, S. Yoshida, Observation of the alteration of neuronal activities in Valproate-administrated rat cerebellum using the enzyme-linked photo-assay. AP-IRC2015 Tahara 2015
[9] 馬渕 光・渡辺一徳・吉田祥子・穂積直裕, 神経伝達物質の可視化システムの開発. 平成 27 年電気学会全国大会 東京 2015

H. 知的財産の出願・登録状況

特許

1. 吉田祥子：特許出願番号 2011-176342、2015.12.10 特許査定「細胞放出物質検出装置、細胞放出物質検出方法及び細胞放出物質検出用固定化酵素基板」
2. 吉田祥子、穂積直裕、氏家雅彦、須山洋行：特許出願番号 2013-258731「光学観察装置、光学観察方法、標本観察画像の画像処理プログラム」
3. 吉田祥子、穂積直裕、氏家雅彦：特許出願番号 2015-223557「光学観察装置」

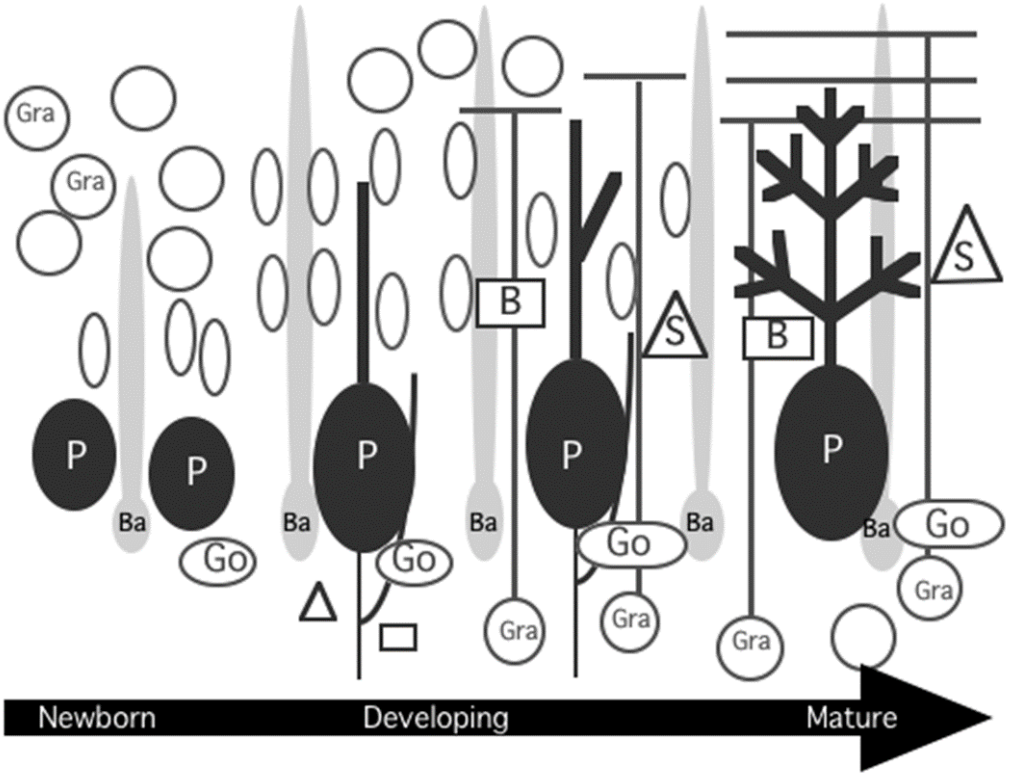

図１　ラット・マウスの小脳の発達様式

出生時のラット・マウスの小脳は、外顆粒層と未発達のプルキンエ細胞層(Purkinje cell layer; PL)から構成されるが、生後約２週間かけて顆粒細胞が分裂・分化しプルキンエ細胞下に遊走して内顆粒層（internal granular layer; IGL）を形成、同時にプルキンエ細胞は樹状突起を伸長させ、顆粒細胞および脳室帯から遊走してくるゴルジ細胞、バスケット細胞、星状細胞と神経回路を構成して皮質表面に分子層(molecular layer; ML)を形成し、成熟した小脳の 3 層構造をかたち作る。
(P:プルキンエ細胞、Gra:顆粒細胞、B:バスケット細胞、S:星状細胞、Go:ゴルジ細胞、Ba:バーグマングリア)。

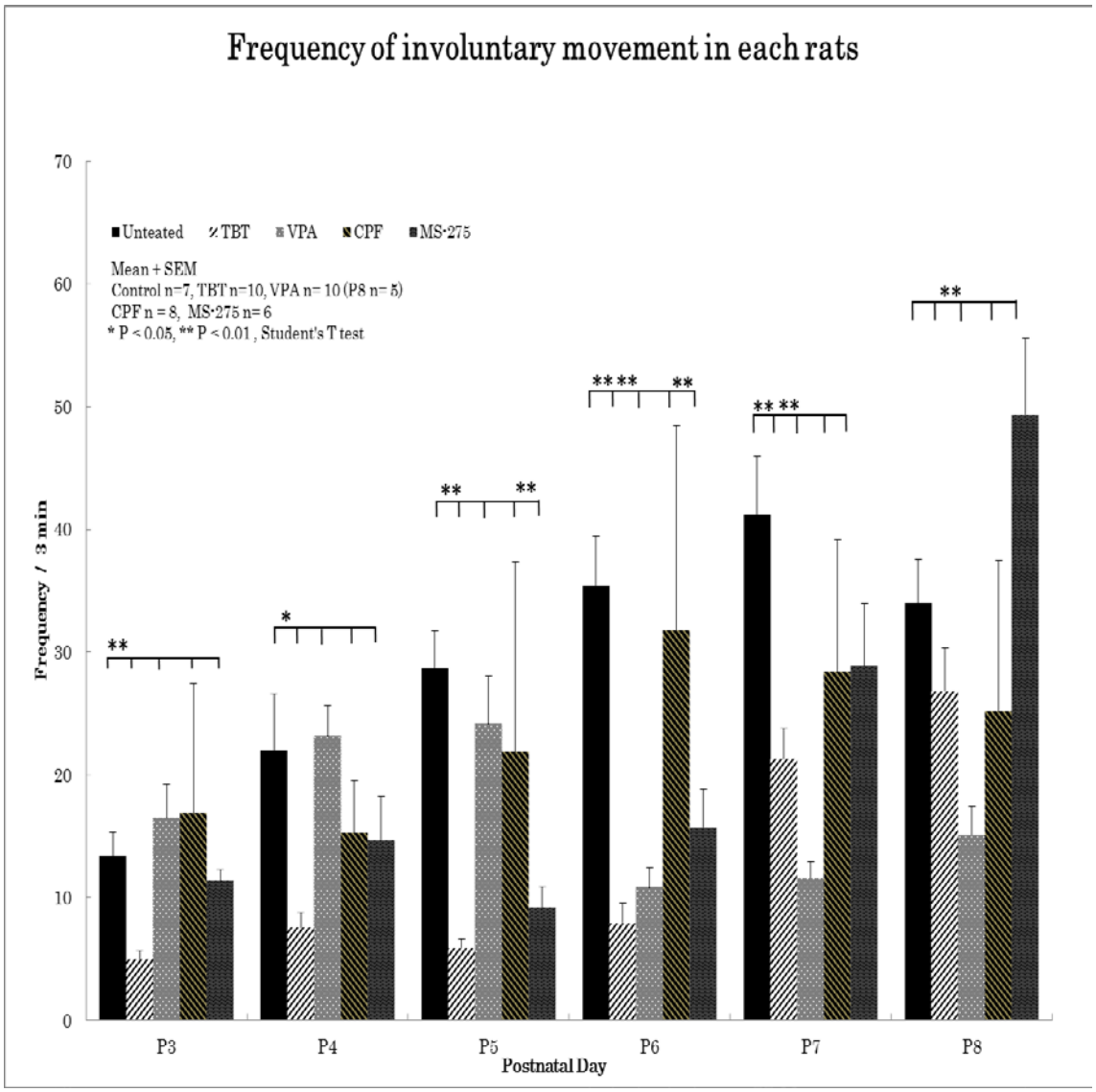

図 2　各投与動物の発達期の自由行動観察。

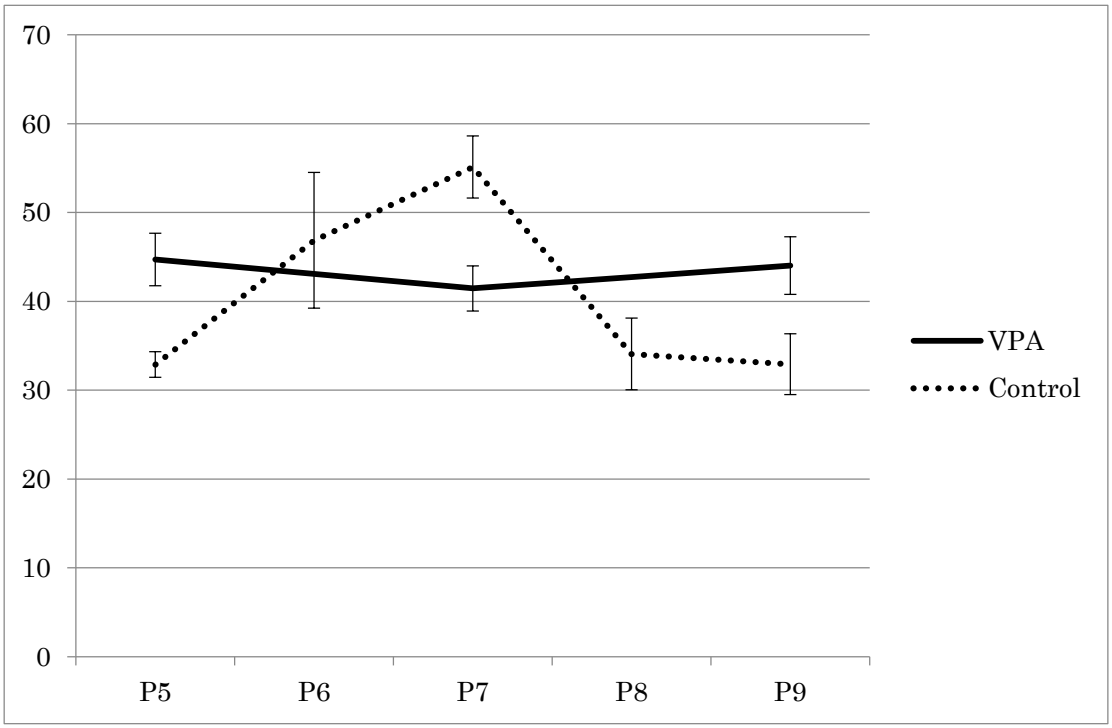

図 3　発達期小脳皮質分子層からの GABA 放出量。発蛍光光量を相対値で示している。対照動物が一過性の GABA 放出量の増加を示すのに対し、VPA 投与動物では一定の放出量で変化を示さない。

A

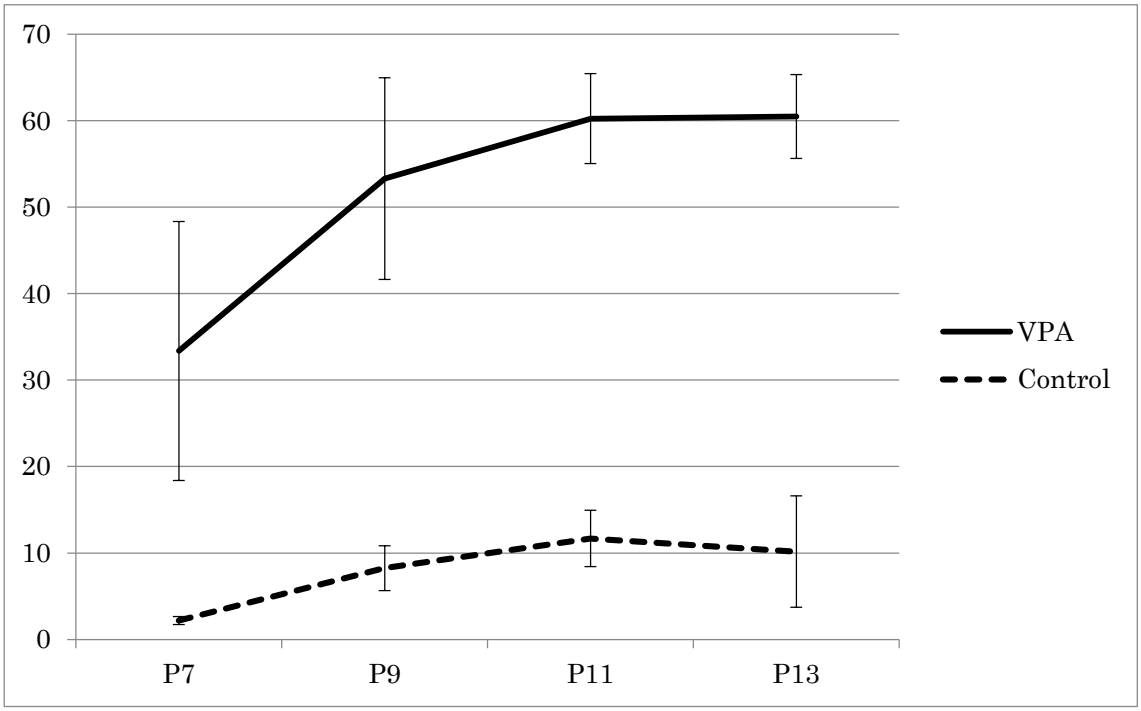

B

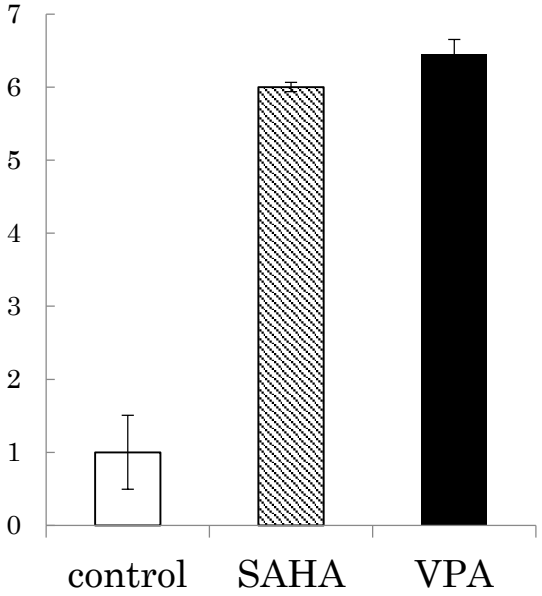

図 4　発達期小脳皮質分子層からの 100μM グルタミン酸刺激による ATP 放出量。A, 発蛍光光量を相対値で示している。対照群に対し、発生初期から著しい増加を示す。B, 対照動物を 1 とした、P9 での ATP 放出量。SAHA 投与群の放出量は、VPA 投与群よりやや少ない。

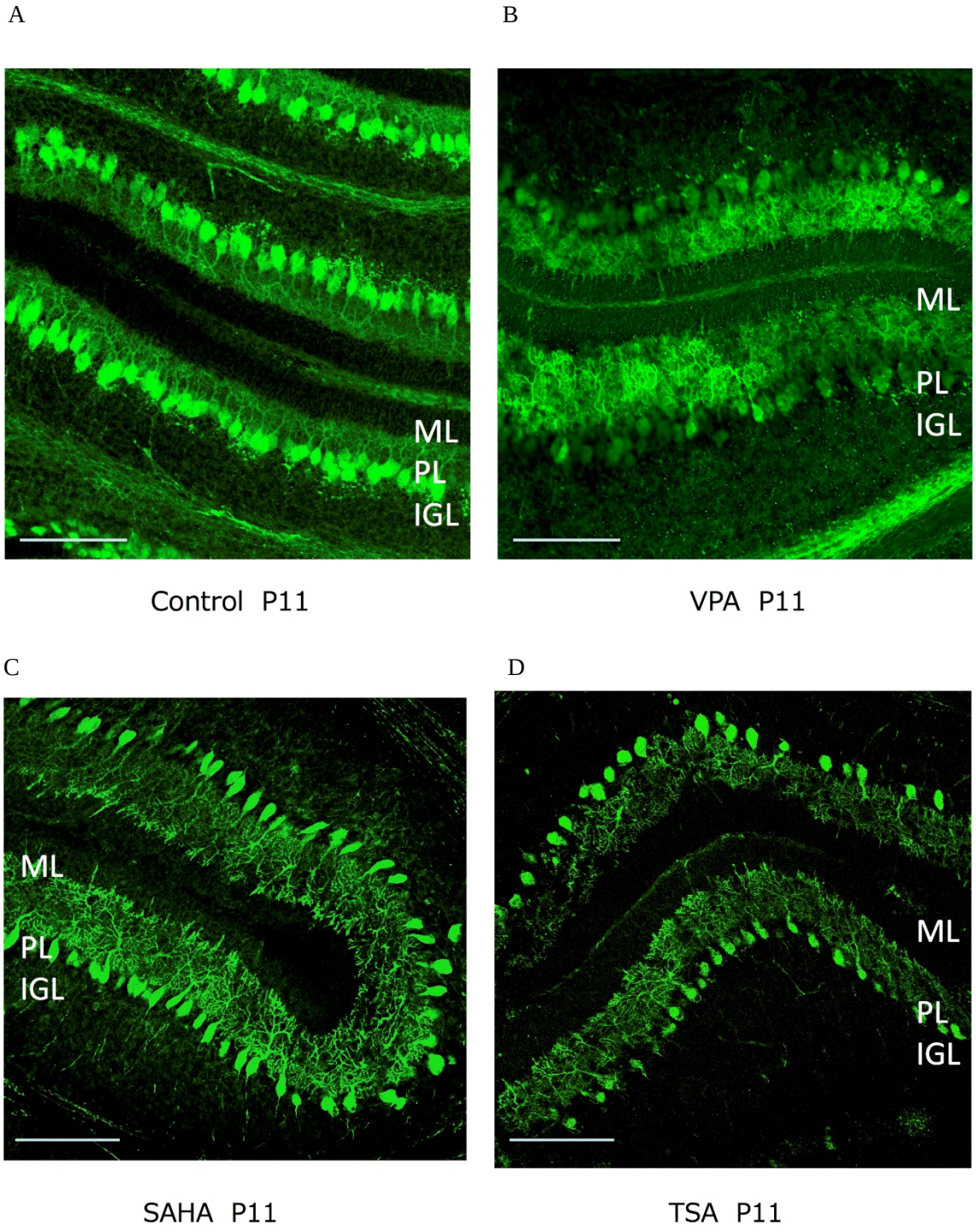

図 5　抗カルビンジン D-28k 抗体によるプルキンエ細胞染色。対照動物(A)に比べ、VPA 投与動物(B)、SAHA 投与動物(C)で網目状にプルキンエ細胞の樹状突起が伸長している。トリコスタチン投与動物(D)では大きな変化はない。

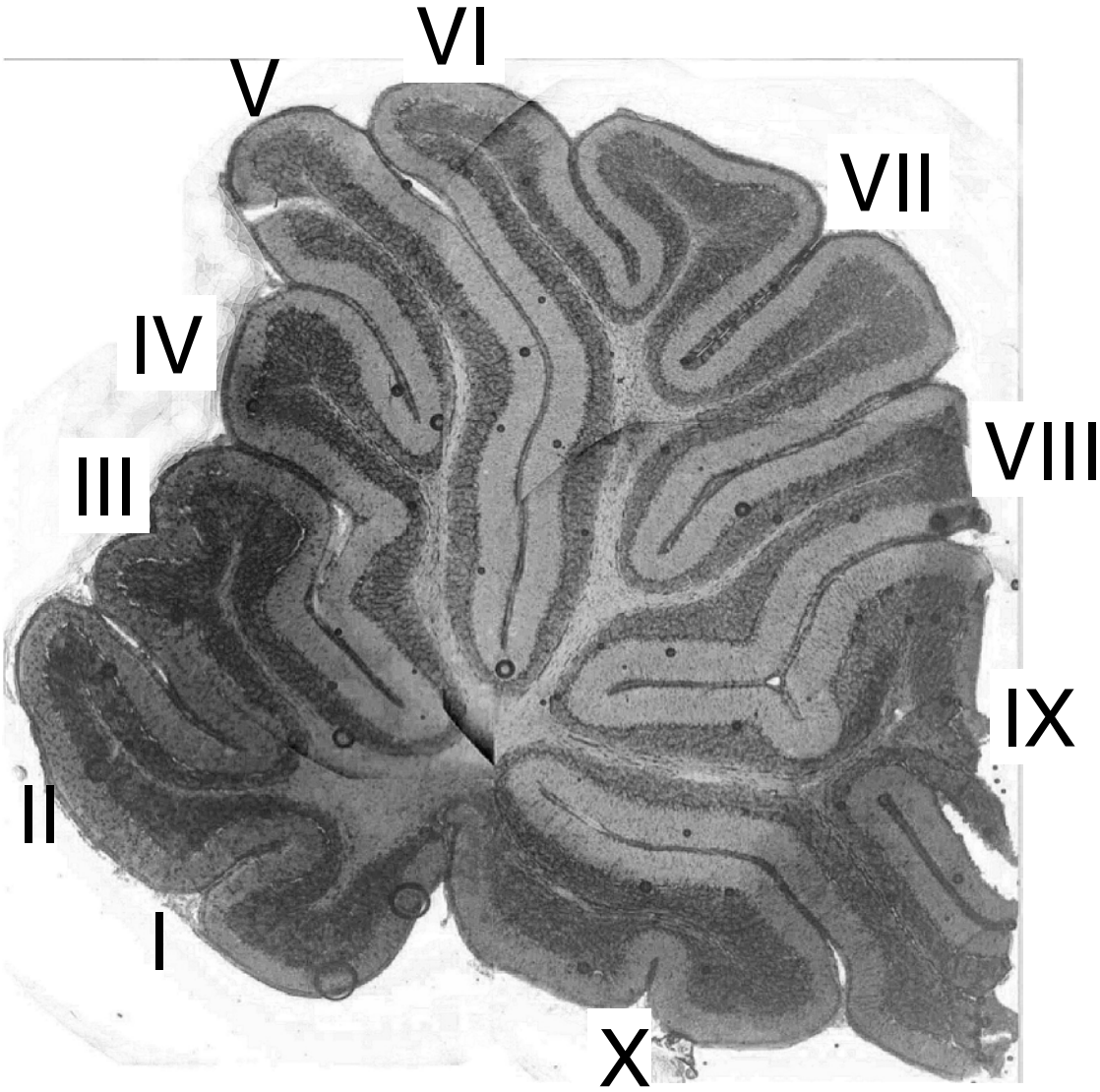

図６　Ｐ１６小脳皮質と小葉Ｉ〜Ｘ

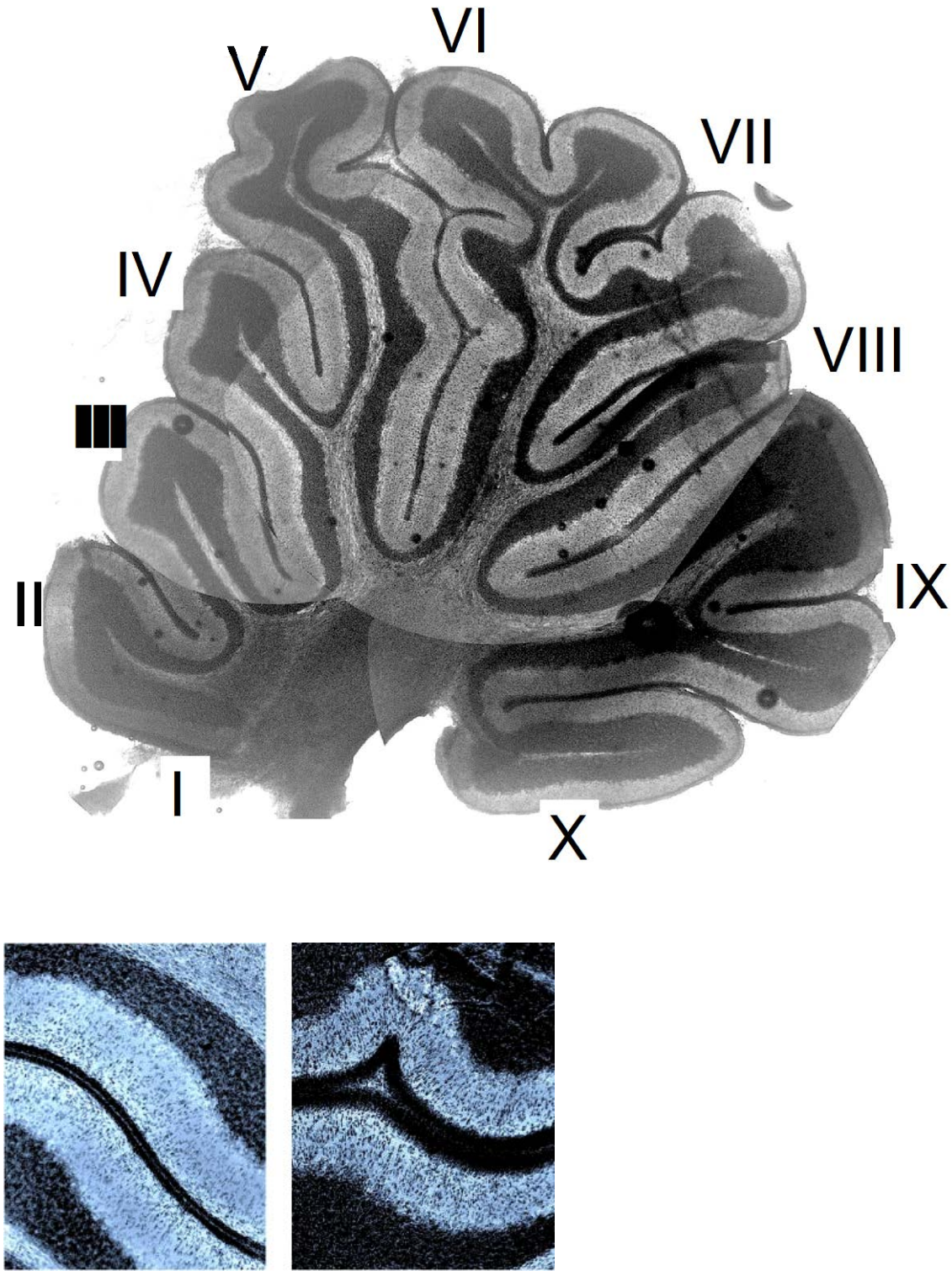

図 7　P16 VPA 投与動物の小脳小葉(A)と拡大図(B:対照動物、C:VPA 投与動物)

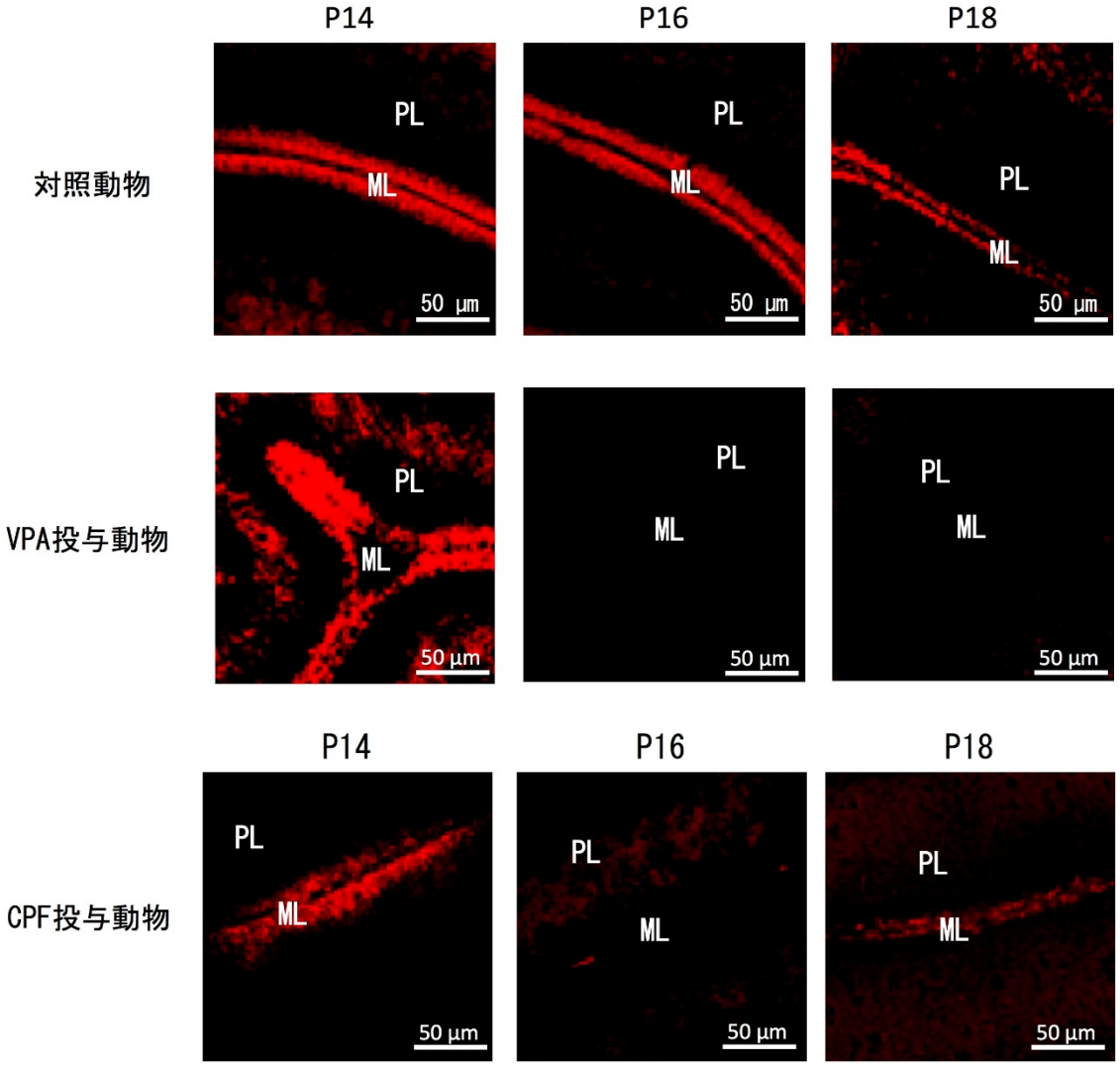

図 8　ブロモデオキシウリジン(BrdU)取り込みによる分裂期細胞の分布。対照動物では P18 まで BrdU 取り込みを示す細胞が分子層上部に分布しているが、VPA 投与動物、CPF 投与動物では P14 以降 BrdU 取り込み能を示す細胞が激減した。

厚生労働科学研究費補助金（化学物質リスク研究事業）
分担研究報告書

幼若期の神経回路機能に対する化学物質の影響評価

研究分担者　産業医科大学　産業生態科学研究所　教授
上野　晋
研究協力者　産業医科大学　産業保健学部　講師
笛田　由紀子
研究協力者　豊橋技術科学大学　環境・生命工学系　講師
吉田祥子

要旨

平成 26 度までのトリブチルスズ（TBT）の胎生期投与ラットを用いた検討で、生後早期の海馬神経回路機能に対して TBT の胎生期曝露は回路機能を抑制することが見出され、海馬神経回路機能の発達遅延を生じる可能性を示唆する結果を得ていた。平成 27 年度は $GABA_A$受容体拮抗薬ビククリンに対する反応性について解析したところ、開眼後となる生後 16 日齢で抑制系に TBT 胎生期曝露による影響が認められた。このことから、VPA と同様に TBT 胎生期投与でも GABA 作動性神経系の生後発達に影響を及ぼしている可能性が示唆された。このように作用機序が異なるとされる VPA および TBT という２種類の化学物質から胎生期曝露の影響を検出できたことから、授乳期内の特定の時期にある仔ラットから作製される海馬スライス標本、ならびにこれを用いた神経回路機能の解析が発達神経毒性評価法として有用である可能性が示された。

また生後 1 週目あたりに出現する不随意運動に着目し、日齢 5〜7 日における不随意運動の出現を調べたところ、対照群ではこの期間で不随意運動量が次第に減少していったが、TBT 胎生期投与群では減少を認めなかった。海馬スライスを用いた指標との関連は不明であるものの、不随意運動も何らかの神経回路発達を反映しているものと考えると、ここにも TBT 胎生期投与が影響している可能性が示唆される。この生後１週齢における不随意運動評価と、２週齢に実施する海馬スライス標本を用いた神経回路機能の評価の関連性が明らかにできれば、発達神経毒性評価も２週齢までは同一の曝露モデルラットを用いることが可能になり、評価に使用する動物数の削減にも貢献することが考えられる。

第 3 の化学物質として有機リン系農薬クロルピリホス（CP）を選択し、同様に胎生期曝露ラットを用いた生後早期の海馬神経回路機能を評価したところ、VPA 胎生期曝露の場合に認められた興奮性神経回路の発達が亢進する傾向が認められた。今後は CP の投与量を増加して再評価する必要があると考えられる。

A. 研究目的

本研究では、胎生期・神経発達期の化学物質曝露に起因する生後の遅発性神経毒性を評価する in vitro 試験法の開発を目指すこととし、発生過程の神経組織を用いて様々な化学物質の発達神経毒性評価へ応用できるか否かを検証していくことを 3 年間の目的とした。当分担研究班では、すでに発達神経毒性が報告されている化学物質を用い、胎生期に曝露された仔ラットの脳スライス標本を採取して、授乳期の神経発達を電気生理学的に解析するという ex vivo の手法を用いて検証した。

B. 研究方法

1. トリブチルスズ（TBT）、酢酸スズ（TA）ならびにクロルピリホス（CP）の胎生期曝露（研究協力者　笛田由紀子、吉田祥子）

妊娠 15 日目（プラグ確認を第 0 日とする）の雌性 Wistar 系ラットに対して、イソフルラン麻酔下に TBT あるいは CP を経口投与した。投与量について、TBT は 20 mg/kg（以下 TBT20 群）、TA は TBT 投与におけるスズの投与量を等しくするために 15 mg/kg（以下 TA15 群）、CP は 10 mg/kg（以下 CP10 群）の割合で投与し、対照として溶媒である 50% ポリエチレングリコール（TBT20 群の対照）、あるいは 0.1%ジメチルスルホキシド（CP10 群の対照）を投与したラットを用いた。

2. 電気生理学的評価のための脳スライス標本の作製（研究協力者　笛田由紀子）

PND（postnatal day の略、ラットが生まれた日を PND 0 としている）13 - 18 の雄性仔ラットをエーテルで深麻酔したのち断頭し、速やかに海馬を取り出した。ティッシュチョッパー（McIlwain tissue chopper）を用いて、すべての日齢について厚さ 600 μm の海馬スライス標本を両側の背側海馬（海馬長軸の中央あたり）から作製した。

スライス時に用いた人工脳脊髄液の組成（mM）は、NaCl, 124; KCl, 2; KH_2PO_4, 1.25; $MgSO_4$, 2; $NaHCO_3$, 26; glucose, 10、実験に用いた人工脳脊髄液は NaCl, 124; KCl, 2; KH_2PO_4, 1.25; $CaCl_2$, 2; $MgSO_4$, 2; $NaHCO_3$, 26; glucose, 10 という組成とした。脳の取り出しからスライス作製までのすべての過程は、混合ガス（O_2/CO_2:95%/5%）で飽和し 3.5 - 4℃に冷やした人工脳脊髄液中ですばやく行った。スライスは Haas 型チャンバー内（32.0±0.1℃）で記録開始まで約 2 時間静置した後に実験に用いた。

3. 刺激応答性の電気生理学的評価法（研究協力者　笛田由紀子）

刺激電極にステンレスの双極電極（直径 50 μm）を用い、CA3 領野から CA1 錐体細胞への入力線維が密集するシナプス層に置いた。記録電極にはガラス微小電極を用い（抵抗 1 - 2 MΩ）、CA1 領野の錐体細胞層からは集合スパイク電位（PS）を、シナプス層から集合シナプス後電位（fEPSP）を記録して『興奮系』神経回路の機能を評価した。

4. 興奮系発達における $GABA_A$ 受容体拮抗薬（ビククリン、BMI）の関与（研究協力者　笛田由紀子）

GABA 抑制系は神経発達において重要な役割を果たすことから、胎生期における化学物質投与によって GABA 抑制系の機能が変化すれば神経発達にも何らかの影響を呈することは容易に予測される。そこで GABA 抑制系の変化を調べるために、PS 振幅の刺激応答性で明らかな変化が認められた日齢での海馬スライスを用いることとし、TBT 胎生期曝露では PND14 と PND16 を対象とした。単回刺激による PS と fEPSP の大きさを $GABA_A$ 受容体拮抗薬（ビククリン、BMI）存在下、および非存在下で比較し、その変化率を検討した。

5. 生後 1 週目に出現する不随意運動を指標とする試験法と解析法（研究協力者　笛田由紀子、吉田祥子）

後述するが、本研究を実施していく中で、生後 1 週目の TBT20 群仔ラットにおいて、持続性は短いものの痙攣用の不随意運動がしばしば観察された。この不随意運動は対照群の仔ラットでも観察されたことから、本来この時期の仔ラットに出現する運動であることが考えられる。そこで胎生期曝露によってこの不随意運動の出現が変化するのではないかと考えて、本研究ではその頻度を定量することにした。具体的には母ラットから離した仔ラットを、約 32℃に保温された箱に入れて体温の低下を防ぎながら 3 分間行動を観察するとともにビデオに記録した。この運動の定量的解析については、計測の個人差

が出ることを考慮し validation を検討するために２名の計測者を決め、ビデオ再生下で１秒ごとに不随意運動の有無を独立して計測し、３分間の観察時間中に生じた不随意運動の合計量を秒数で表記した。すべてのビデオについて計測した後に、２名の計測者による結果の差を検討した。今回の不随意運動評価に用いた対照群および TBT20 群のラットの匹数については表１に示してある。

（倫理面への配慮）

本研究の遂行にあたっては、産業医科大学および豊橋技術科学大学に定められた、関係する遵守すべき指針等を把握して、十分な管理体制のもと、倫理面に万全の配慮をしながらそれぞれの研究が進められた。

C. 研究結果

1. 海馬の興奮系および抑制系神経回路の生後発達に対する $GABA_A$受容体拮抗薬の作用、およびこれに対する TBT、TA および CP 胎生期曝露の影響

単回刺激による興奮系の刺激応答性について、平成 26 年度に引き続き実験数を増やした結果から、対照群では PND15 から PND16 にかけて著明に亢進することが確認できた（図 1、上段）。これに対して TBT20 群ではこの亢進は明確でなく、平成 26 年度に報告したように PND16 においては対照群と比較して減弱した刺激応答性を示した（図 1、中段）。TBT、すなわち有機スズの対照として用いた TA15 群においては、TBT 対照群と類似した刺激応答性のパターンを示した（図 1、下段）。

TBT 対照群の平均開眼時期が日齢 16.7 であり、刺激応答性の変化はこの開眼時期を境に観察されたことから、この前後すなわち PND14 と PND16 について、単回刺激（600 μA）で誘発される PS 振幅に対する $GABA_A$ 受容体拮抗薬ビククリン（BMI、1μM）の効果について検討した（図 2）。TBT 対照群では BMI 存在下で開眼前期において PS 振幅は著増した（平均増加率 52±9.6%）ものの開眼後期ではその増加はわずかなものとなり（平均増加率 9.8±3.0%）、GABA 作動性抑制系の関与が発達に伴い異なることが示唆された。一方、TBT20 群については、PND14 では BMI 存在下での PS 振幅の増加は、対照群の同時期で認められたものと同等（平均増加率 42±5.2%）であった。しかし PND16 になっても増加は認められていた（平均増加率 37±8.3%）。

さらに個々のスライス標本から得られた BMI に対する反応の比（BMI 存在下での PS 振幅／BMI 非存在下で PS 振幅）をその分布ならびに近似曲線により検討した。PND14 では対照群と TBT20 群とでは近似曲線で示されるようにその分布はほぼ等しくなったが（図３）、PND16 では対照群と比べ TBT20 群の分布近似曲線が右方移動していることが見出された（図４）。言い換えると、対照群で見られるように本来は発達（PND14 から PND16）に伴い分布近似曲線が左方移動するところが、TBT 胎生期曝露によって左方への移動が軽度ではあるが抑制されているとも言える。以上のことから、開眼期に認められる GABA 作動性抑制系の関与に対しても TBT の胎生期曝露は影響を与えていることが判明した。

CP 胎生期投与の刺激応答性の検討については実験数が十分とはいえないまでも、VPA 対照群や TBT 対照群の場合と同様に、PND15 から PND16 にかけて刺激応答性の亢進を示した（図５）。

2. 不随意運動の出現、ならびにこれに対する TBT、TA 胎生期曝露の影響

不随意運動量を PND５－７の３日間で解析した結果、対照群では運動量（総秒数）が日齢を経るとともに有意に減少していることが判明した（$p<0.05$）。ところが、TBT20 群と TA15 群については、３日間の不随意運動量には変化が認められなかった。また PND５における不随意運動量については３群間に有意差はなかったが、PND７においては対照群と TBT 群との間に有意な差が認められた。一方、授乳期の後半になるとこの不随意運動は３群ともに認められなくなった。このことから、今回着目したこの不随意運動は授乳期早期に出現し発達とともに減少するものであること、さらに TBT の胎生期投与はこの運動が減少する時期に影響を与えている可能性があることが考えられた。したがってこの不随意運動の発現および発達に伴う変化の背景にも、何らかの神経発達が関与している可能性が考えられる。不随意運動の結

果はTBT対照群とTBT20群についてのみ図６に示している。

D. 考察

本研究では海馬スライス標本を用いた電気生理学的評価手法により、胎生期のVPA、TBT、TAおよびCP投与による発達神経毒性評価を生後早期で実施してきた。その結果として平成25年度は海馬神経回路の興奮性シナプス機能と抑制性シナプス機能がVPA胎生期曝露により亢進していることを見出した。そこで平成26年度は、このメカニズムを解明する目的でGABA作動性抑制系に着目し、授乳期の発達に伴うGABA抑制系の関与が開眼時期に合わせて変化すること、VPA胎生期投与群ではこの発達に伴う変化がすでに開眼時期以前に出現することを見出している。

今回、20 mg/kgのTBTを胎生期に投与することよって、開眼時期であるPND16に興奮系の刺激応答性の発達遅延が出現することが示唆された。さらにGABA抑制系についても、発達に伴ってGABA抑制系に依存した反応性が減弱するという現象がTBT胎生期投与により認められなかったことは発達遅延の可能性を示唆するものである。前述した分布度近似曲線の発達に伴う左方移動が抑制されていることも、発達遅延が生じていることを支持する結果であると言える。

GABA作動性抑制系の生後発達は脳機能に重要な役割を果たしていることが明らかとされている。本研究では$GABA_A$受容体拮抗薬BMIを用いた薬理学的なアプローチにより、VPAの胎生期投与では開眼前期において対照群の開眼期と類似した反応性であることから発達の亢進が示唆され、またTBT胎生期投与では開眼期においても対照群の開眼前期に近い反応性であることから発達の遅延が示唆されており、これら化学物質の発達神経毒性を評価する指標として、生後早期における興奮性・抑制系神経回路特性が有用であることを支持する結果であると考えている。

平成27年度はさらに、その作用ならびに作用機序がVPAやTBTとは異なるCPの胎生期投与の影響を検討する実験を開始したが、現在のところ、VPAやTBTの刺激応答性の発達に伴う変化は認められていない。CPが胎生期に投与された場合、ヒトではVPAの場合のように自閉症が発生することが疫学研究で報告されている。また吉田らの今年度の成果として、(1) 不随意運動量の評価ではVPA胎生期投与群と類似した結果を示すこと、(2) VPA胎生期投与で認められた小脳プルキンエ細胞の細胞死抑制、樹状突起の異常伸長が観察されること、(3) VPA胎生期投与で認められた小脳Ⅴ/Ⅵ層における脳回の過剰形成が観察されること、の3点を速報として得ている。このことから化学物質によって、あるいは投与時期によって、脳内部位の感受性が異なることも考えられたため、今後CPの投与量を増加した胎生期曝露モデルを作成することも視野に入れている。

本年度の結果から、TBT胎生期投与ではVPA胎生期投与とは逆に、発達に伴う刺激応答性の亢進が遅れて出現することが判明し、この『遅れ』を指標とすることで、海馬スライス標本を用いた神経回路機能の解析がTBTの発達神経毒性に対しても早期に評価できる可能性が示唆された。

興味あることに、ヒト多能性幹細胞、胎児期の神経堤細胞、生後初期の神経・グリア細胞を用いた神経新生を指標とするin vitro評価系においても、VPAによる機能亢進、TBTによる抑制が認められた（研究代表者・諫田、研究分担者・宇佐見、研究分担者・佐藤の報告内容を参照）。またCPに関しても条件によりその作用に違いが認められたとの情報もあり、in vivo評価系においても小脳と海馬で影響が異なる可能性は考えられる。

また今年度、本研究分担班では日齢5日から7日における不随意運動の出現に着目してその評価を行ったところ、対照群ではこの3日間で不随意運動量が次第に減少したが、TBT胎生期投与群では減少しなかった。この結果は、吉田らの班においてVPAあるいはCP胎生期投与群に対して実施された運動量の評価結果と類似した傾向を示している。不随意運動を３分間観察するという極めてシンプルな試験方法ではあるが、発達神経毒性評価のin vivo実験系におけるスクリーニング的な指標として応用できる可能性も考えられるだろう。この不随意運動という指標と、海馬スライスを用いた指標との関連はまだ不明であり今後の検討課題であるが、生後１週目の発達期に対しても、TBT胎生期投与が影響を与えていることを今回見出せたこと

は、この評価と２週齢に実施する海馬スライス標本を用いた神経回路機能の評価とを併せた発達神経毒性評価法を確立できることにも繋がる。これが実現すれば２週齢までは同一の曝露モデルラットを用いることが可能になり、評価に使用する動物数の削減にも貢献することが考えられる。

E. 結論

発達神経毒性を早期にスクリーニングできる ex vivo の系の確立を目指しており、平成 27 年度は環境ホルモン様作用を示すものの一つとして知られている TBT を投与した胎生期曝露ラットを用い、授乳期の海馬神経回路の発達を検討した。その結果、TBT 胎生期曝露ラットでは神経回路機能の発達遅延を見出し、神経毒性の早期スクリーニング手法として、授乳期の海馬神経回路発達の評価が有用である可能性が考えられた。

F. 研究発表

1. 論文発表

[1] Ishidao T, Fueta Y, Ueno S, Yoshid a Y, Hori H. A cross-fostering analysi s of bromine ion concentration in rats that that inhaled 1-bromopropane va por. *J. Occup. Health*, in press.

[2] Fueta Y, Kanemitsu M, Egawa S, Is hidao T, Ueno S, Hori H. Prenatal ex posure to 1-bromopropane suppresses kainate-induced wet dog shakes in im mature rats. *J UOEH.* 37:255-261 (20 15).

[3] Li X, Toyohira Y, Horisita T, Satoh N, Takahashi K, Zhang H, Iinuma M, Yoshinaga Y, Ueno S, Tsutsui M, Sata T, Yanagihara N. Ikarisoside A inhibits acetylcholine-induced catecholamine secretion and synthesis by suppressing nicotinic acetylcholine receptor-ion channels in cultured bovine adrenal medullary cells. *Naunyn Schmiedebergs Arch Pharmacol.* 388:1259-1269 (2015).

[4] Okura D, Horishita T, Ueno S, Yanagihara N, Sudo Y, Uezono Y, Minami T, Kawasaki T, Sata T. Lidocaine preferentially inhibits the function of purinergic P2X7 receptors expressed in *Xenopus* Oocytes. *Anesth Analg.* 120:597-605 (2015).

[5] Uchida T, Furuno Y, Tanimoto A, Toyohira Y, Arakaki K, Kina-Tanada M, Kubota H, Sakanashi M, Matsuzaki T, Noguchi K, Nakasone J., Igarashi T, Ueno S, Matsushita M, Ishiuchi S, Masuzaki H, Ohya Y, Yanagihara N., Shimokawa H, Otsuji Y, Tamura M, Tsutsui M. Development of an experimentally useful model of acute myocardial infarction: 2/3 nephrectomized triple nitric oxide synthases-deficient mouse. *J Mol Cell Cardiol.* 77C:29-41 (2014).

[6] Horishita T, Yanagihara N, Ueno S, Sudo Y, Uezono Y, Okura D, Minami T, Kawasaki T, Sata T. Neurosteroids allopregnanolone sulfate and pregnanolone sulfate have diverse effect on the α subunit of the neuronal voltage-gated sodium channels Nav1.2, Nav1.6, Nav1.7, and Nav1.8 expressed in *Xenopus* oocytes. *Anesthesiology.* 121:620-31 (2014).

[7] Okura D., Horishita T., Ueno S., Yanagihara N., Sudo Y., Uezono Y., Sata T. The endocannabinoid anandamide inhibits voltage-gated sodium channels Nav1.2, Nav1.6, Nav1.7 and Nav1.8 in *Xenopus* oocytes. *Anesth. Analg.* 118:554-62 (2014).

[8] Yanagihara N, Zhang H, Toyohira Y, Takahashi K, Ueno S, Tsutsui M, Takahashi K. New insights into the pharmacological potential of plant flavonoids in the catecholamine system. *J Pharmacol Sci.* 124:123-8 (2014)

[9] Inagaki H, Toyohira Y, Takahashi K, Ueno S, Obara G, Kawagoe T, Tsutsui M, Hachisuga T, Yanagihara N. Effects of selective estrogen receptor modulators on plasma membrane estrogen receptors and catecholamine synthesis and secretion in cultured bovine adrenal medullary cells. *J Pharmacol Sci.* 124:66-75 (2014).

[10] 上野　晋 化学物質（金属・有機溶剤）の毒性学と産業医としての対応　*産業医科大学雑誌*　第35巻特集号:91-6 (2013).

[11] Park EK, Wilson D, Choi HJ, Wilson CT, Ueno S. Hazardous metal pollution in the republic of Fiji and the need to elicit human exposure. *Environ Health Toxicol.* doi: 10.5620/eht.2013.28.e2013017 (2013).

[12] Obara G., Toyohira Y., Inagaki H., Takahashi K., Horishita T., Kawasaki

T., Ueno S., Tsutsui M., Sata T., Yanagihara N. Pentazocine inhibits norepinephrine transporter function by reducing its surface expression in bovine adrenal medullary cells. *J Pharmacol Sci*. 121:138-47 (2013).

2. 学会発表

[1] 笛田由紀子、上野　晋. 自閉症モデルラットを用いた早期の発達神経毒性評価－GABA 抑制系の関与. 第 88 回日本産業衛生学会、2015 年 5 月、大阪

[2] Tomida T, Hozumi N, Fueta Y, Ueno S, Sekino Y, Yoshida S. The effects of HDAC inhibitors on developing cerebellar astrocytes. 第 38 回日本神経科学大会、2015 年 7 月、神戸

[3] Waranabe K, Abe T, Fueta Y, Ueno S, Sekino Y, Hozumi N, Yoshida S. Alteration of neurotransmitter release in cerebellar cortex of valproate-administered rat using the enzyme-linked photo assay system.　第 38 回日本神経科学大会、2015 年 7 月、神戸

[4] Nakajima S, Katsumata D, Abe T, Hozumi N, Fueta Y, Ueno S, Sekino Y, Yoshida S. Alteration of neuronal development and behavioral anomaly in autistic-like anomalous developing cerebellum.　第 38 回日本神経科学大会、2015 年 7 月、神戸

[5] Fueta Y, Sekino Y, Yoshida S, Ueno S. Prenatal administration of valproic acid or tributyltin alters developmental transient of hippocampal excitability in juvenile rats.　第 58 回日本神経化学会大会、2015 年 9 月、大宮

[6] Yoshida S, Fueta Y, Ueno S, Sekino Y. Prenatal administration of valproic acid or SAHA alters the development of Purkinje cell dendrites and network formation in rat cerebellum.　第 58 回日本神経化学会大会、2015 年 9 月、大宮

[7] Fueta Y, Sekino Y, Yoshida S, Ueno S. Prenatal single administration of tributyltin alters developmental transient of spontaneous behaviors and basic excitability in the hippocampal slices of immature rats. 55th Annual Meeting of Society for Toxicology. 2015 年 3 月、USA（発表予定）

[8] Yoshida Y, Hozumi N, Fueta Y, Ueno S, Sekino Y. Prenatal administration of valproic acid alters both the Purkinje cell dendrites and the granule cell proliferation in rat developing cerebellum. 55th Annual Meeting of Society for Toxicology.　2015 年 3 月、USA（発表予定）

[9] 笛田由紀子、関野祐子、吉田祥子、上野晋. 胎生期トリブチルスズあるいは酢酸スズ単回投与による授乳期ラットの行動と興奮・抑制系の変化. 第 43 回日本毒性学会学術年会、2016 年 6 月、名古屋(発表予定)

H. 知的財産の出願・登録状況

（該当なし）

	control			TBT		
	PND5	PND6	PND7	PND5	PND6	PND7
腹数	4	6	7	4	5	5
ラット数	40	60	70	37	46	46

表 1. 不随意運動解析に用いた対照群と TBT20 群の腹数および仔ラット数

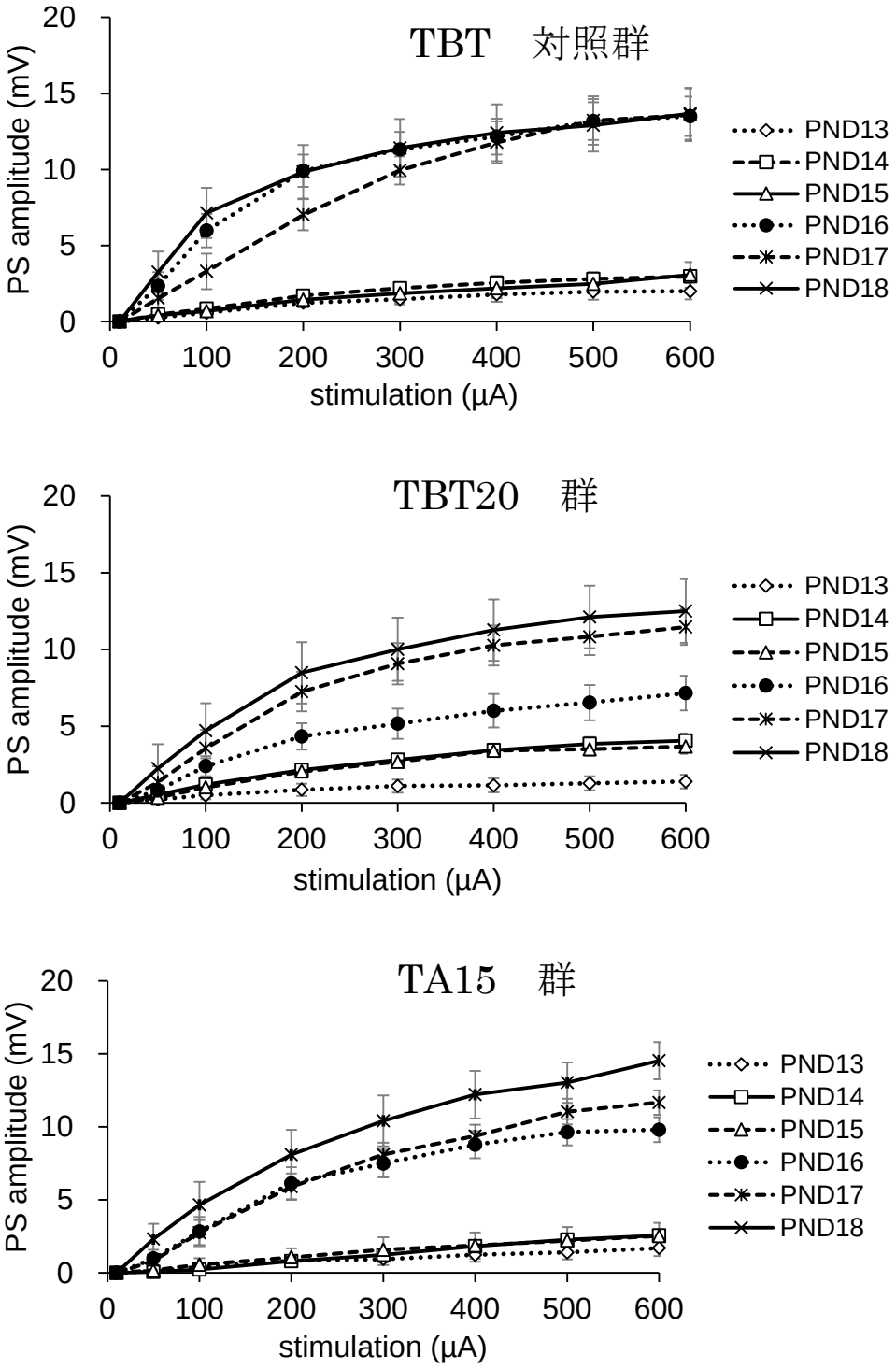

図１．トリブチルスズ（TBT）と無機スズ（TA）を胎生期に曝露された仔ラットを用いて、生後日齢毎に得られた海馬 CA1 領域の集合スパイク電位（PS）の振幅を指標とする刺激応答性。横軸は刺激の大きさ（μA）、縦軸は PS の振幅（mV）である。

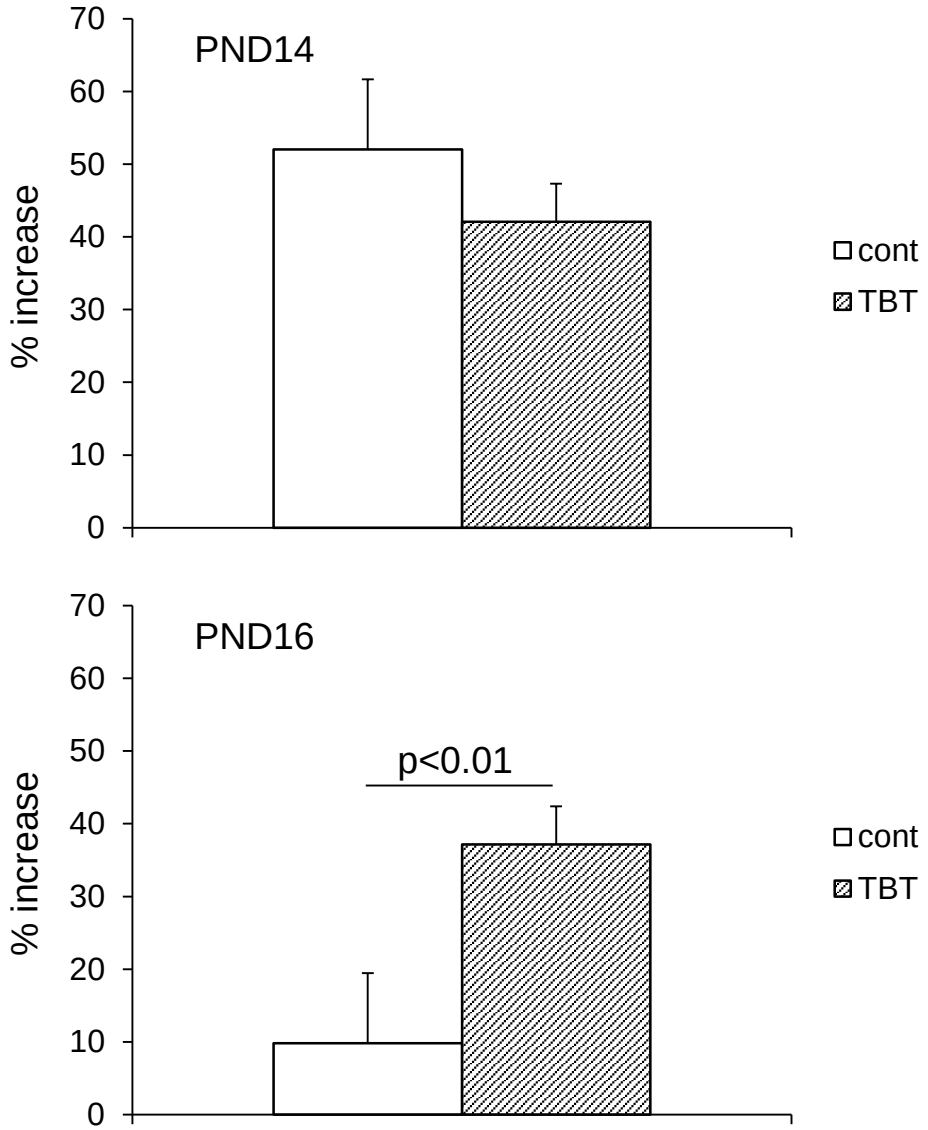

図２．生後 14 日齢および 16 日齢における集合スパイク電位（PS）振幅（刺激電流値 600 μA）に対する $GABA_A$受容体拮抗薬ビククリン（BMI）の増強作用とこれに対する TBT 胎生期曝露の影響。変化率（%increase）は次式で求められている。

%increase＝(BMI 存在下の応答/非存在下の応答 - 1)×100

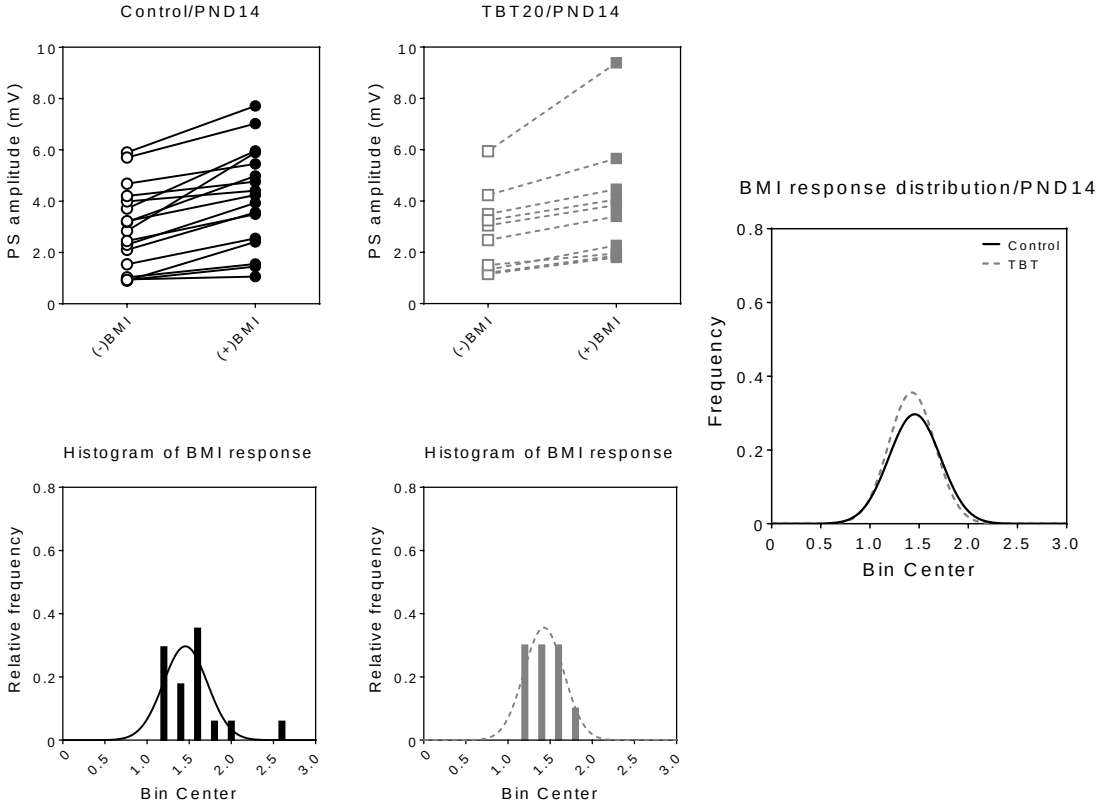

図３．生後 14 日齢における対照群と TBT20 群から得られた $GABA_A$受容体拮抗薬ビククリン（BMI）存在下、非存在下での集合スパイク電位（PS）振幅（刺激電流値 600 μA）、および BMI による増強率の分布近似曲線。

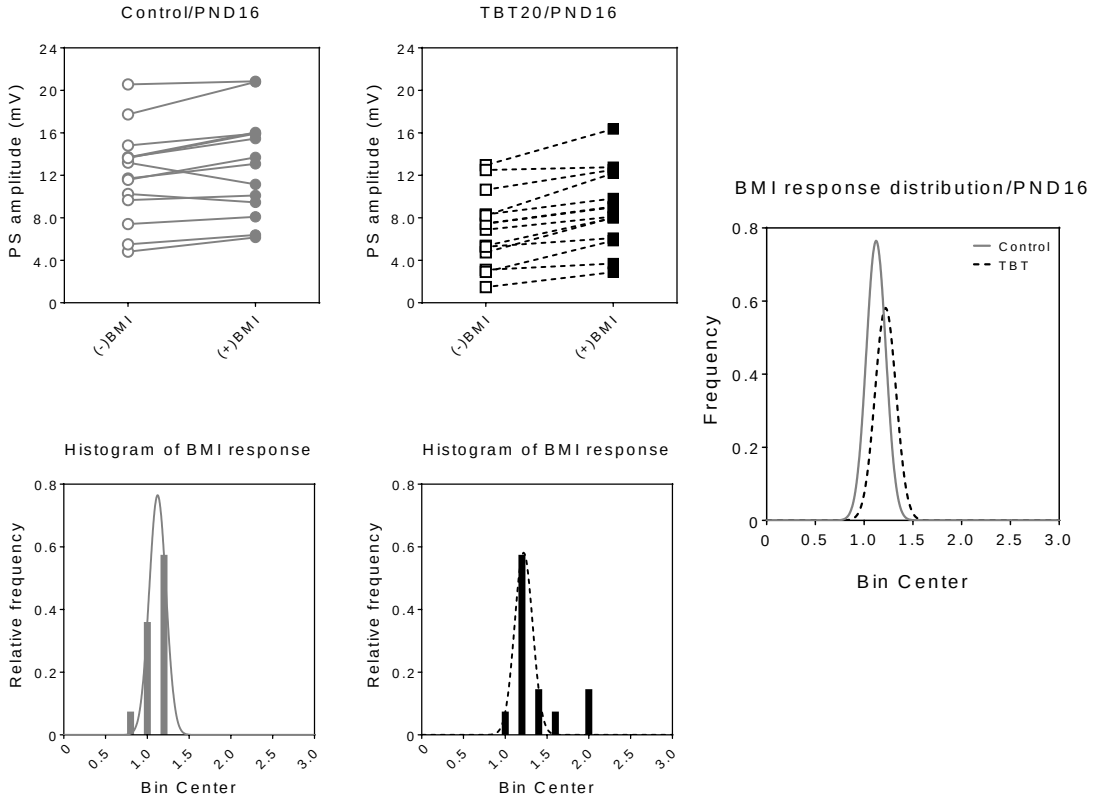

図４．生後 16 日齢における対照群と TBT20 群から得られた $GABA_A$受容体拮抗薬ビククリン（BMI）存在下、非存在下での集合スパイク電位（PS）振幅（刺激電流値 600μA）、および BMI による増強率の分布近似曲線。

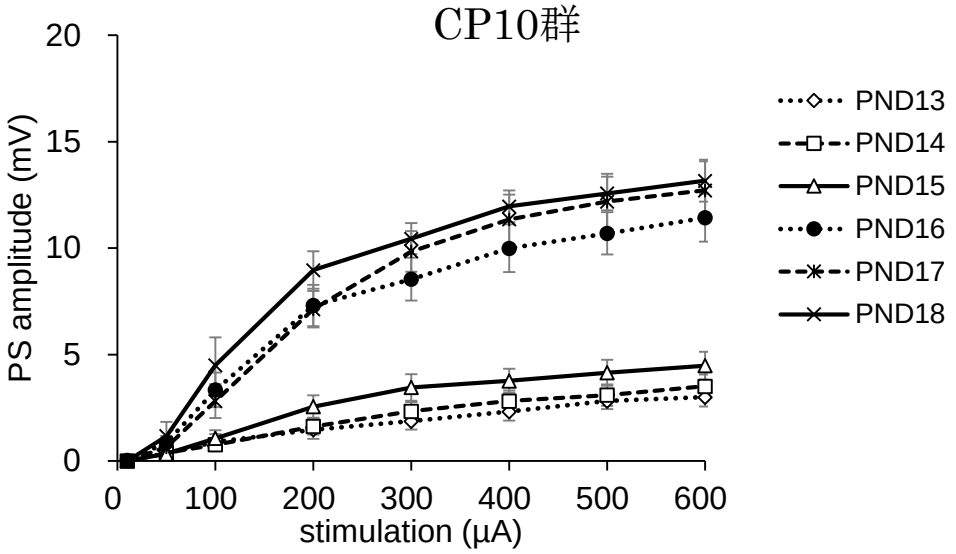

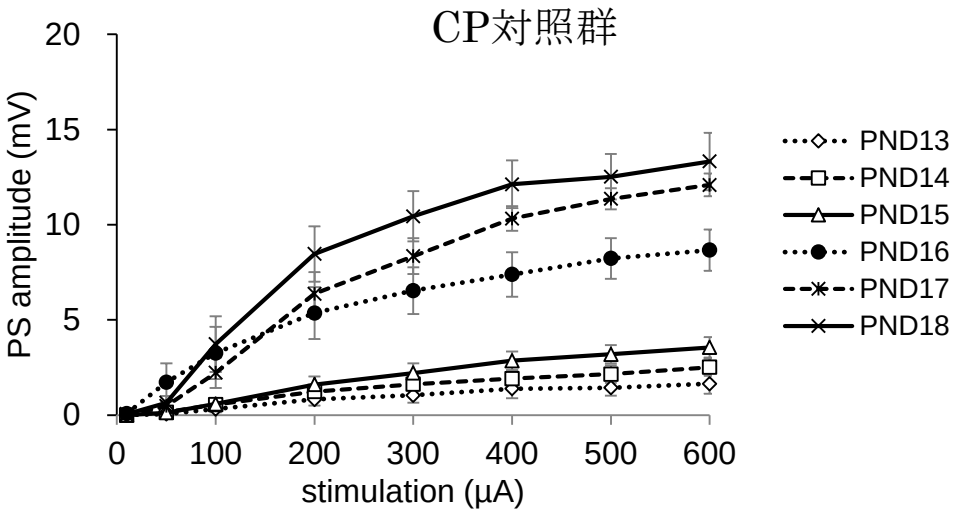

図５．クロルピリホス（CP）胎生期に曝露された仔ラットを用いて、生後日齢毎に得られた海馬 CA1 領域の集合スパイク電位（PS）の振幅を指標とする刺激応答性。横軸は刺激の大きさ（μA）、縦軸は PS の振幅（mV）である。

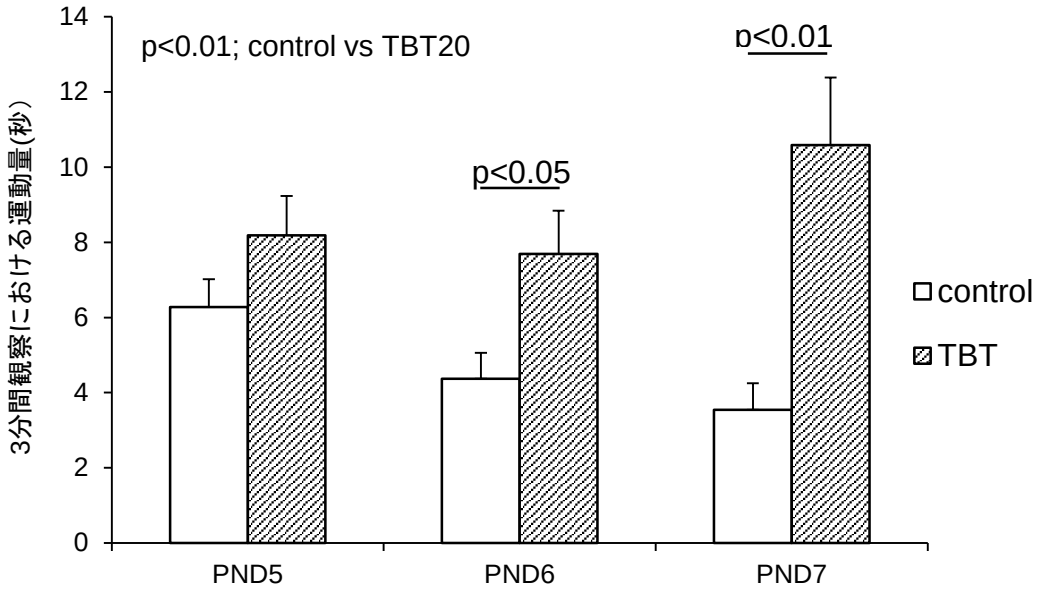

図６．生後５日齢～７日齢の間で観察される不随意運動、およびこれに対する TBT 胎生期曝露の影響。不随意運動は３分間における運動量を秒数で示した（mean±SEM）。

研究成果の刊行に関する一覧表

雑誌

発表者氏名	論文タイトル名	発表誌名	巻号	ページ	出版年
Ishida K., Kotake Y., Miyara M., Aoki K., Sanoh S., Kanda Y., Ohta S.	Involvement of GluR2 decrease in lead-induced neuronal cell death.	J. Toxicol. Sci.	38	513-521	2013
Yamada S., Kotake Y., Sekino Y., Kanda Y.	AMP-activated protein kinase-mediated glucose transport as a novel target of tributyltin in human embryonic carcinoma cells	Metallomics	5	484-491	2013
関野祐子、佐藤薫、諫田泰成、石田誠一	ヒトiPS分化細胞を利用した医薬品のヒト特異的有害反応評価系の開発・標準化	国立医薬品食品衛生研究所報告	131	25-34	2013
諫田泰成	ヒトiPS細胞から心筋細胞への分化誘導法	日本薬理学雑誌	141	32-36	2013
Yamada S., Kotake Y., Demizu Y., Kurihara M.,Sekino Y., Kanda Y.	Isocitrate dehydrogenase 3 as a novel target of tributyltin in human embryonic carcinoma cells.	Sci. Rep.	4	5952	2014
Nagakubo T., Demizu Y., Kanda Y., Misawa T., Shoda T., Okuhira K., Sekino Y., Naito M., Kurihara M.	Development of cell-penetrating R7 fragment-conjugated helical peptides as inhibitors of estrogen receptor-mediated transcription.	Bioconjugate Chem.	25	1921-1924	2014
Hirata N., Yamada S., Shoda T., Kurihara M., Sekino Y., Kanda Y.	Sphingosine-1-phosphate promotes expansion of cancer stem cells via S1PR3 by a ligand-independent Notch activation	Nature Commun.	5	4806	2014
Hayakawa T., Kunihiro T., Ando T., Kobayashi S., Matsui E., Yada H., Kanda Y., Kurokawa J., Furukawa T.	Image-based evaluation of contraction-relaxation kinetics of human-induced pluripotent stem cell-derived cardiomyocytes: correlation and complementarity with extracellular electrophysiology.	J. Mol. Cell. Cardiol.	77	178-191	2014
Hiyoshi H., Goto N., Tsuchiya M., Iida K., Nakajima Y., Hirata N., Kanda Y., Nagasawa K., Yanagisawa J.	YL-109 is a novel antitumor agent suppressing triple-negative breast cancer progression by inducing ubiquitin ligase CHIP.	Sci. Rep.	4	7095	2014
Tsuchiya M, Nakajima Y, Hirata N, Morishita T, Kishimoto H, Kanda Y, Kimura K.	Ubiquitin ligase CHIP suppresses cancer stem cell properties in a population of breast cancer cells.	Biochem Biophys Res Commun.	452	928-932	2014
Nakamura Y., Matsuo J., Miyamoto N., Ojima A., Ando K., Kanda Y., Sawada K., Sugiyama A., Sekino Y.	Assessment of testing methods for drug-induced repolarization delay and arrhythmias in an iPS cell-derived cardiomyocyte sheet: multi-site validation study.	J Pharmacol Sci.	124	494-501	2014
諫田泰成	ヒトiPS細胞を用いた成熟心筋細胞の開発	心電図	34	306-309	2014

澤田光平、松尾純子、長田智治、吉田善紀、白尾智明、佐藤薫、諫田泰成、関野祐子	霧島会議Stem Cell Safety Pharmacology Working Groupまとめ－ヒトES/iPS細胞由来心筋細胞を用いた催不整脈作用検出とその課題－	心電図	34	302-305	2014
諫田泰成	癌幹細胞の受容体を標的とした創薬の可能性	日本薬理学雑誌	144	17-21	2014
Yosuke D, Takashi Mi, Takaya N, Yasunari K, Keiichiro O, Yuko S, Mikihiko N, Masaaki K.	Structural development of stabilized helical peptides as inhibitors of estrogen receptor (ER)-mediated transcription.	Bioorg.Med.Chem.	23	4132-8	2015
Asakura K, Hayashi S, Ojima A, Taniguchi T, Miyamoto N, Nakamori C, Nagasawa C, Kitamura T, Osada T, Honnda Y, Kasai C, Ando H, Kanda Y, Sekino Y, Sawada K.	Improvement of acquisition and analysis methods in multi-electrode array experiments with iPS cell-derived cardiomyocyte.	Journal of Pharmacological and Toxicological Methods			2015
Yamada S., Kotake Y., Nakano M., Sekino Y. Kanda Y.	Tributyltin induces mitochondrial fission through NAD-IDH dependent mitofusin degradation in human embryonic carcinoma cells.	Metallomics	7	1240-6	2015
Asanagi M., Yamada S., Hirata N, Itagaki H., Kotake Y., Sekino Y. Kanda Y.	Tributyltin induces G2/M cell cycle arrest via NAD+-dependent isocitrate dehydrogenase in human embryonic carcinoma cells.	JTS	41	207-215	2016
Hirata N., Yamada S., Asanagi M., Sekino Y., Kanda Y.	Nicotine induces mitochondrial fission through mitofusin degradation in human multipotent embryonic carcinoma cells.	BBRC	470	300-5	2016
Kim S.-R., Kubo T., Kuroda Y., Hojyo M., Matsuo T., Miyajima A., Usami M., Sekino Y., Matsushita T., Ishida S.	Comparative metabolome analysis of cultured fetal and adult hepatocytes in humans.	J Toxicol Sci.	39	717-723	2014
Usami M., Mitsunaga K., Irie T., Miyajima A., Doi O.	Simple in vitro migration assay for neural crest cells and the opposite effects of all-trans-retinoic acid on cephalic- and trunk-derived cells.	Congenit Anom	54	184-188	2014
Usami M., Mitsunaga K., Irie T. Nakajima M.	Various definitions of reproductive indices: a proposal for combined use of brief definitions.	Congenital Anomalies	54	67-68	2014

Usami M., Mitsunaga K., Irie T., Miyajima A. Doi O.	Proteomic analysis of ethanol-induced embryotoxicity in cultured post-implantation rat embryos.	The Journal of Toxicological Sciences	39	285-292	2014
Usami M., Mitsunaga K., Miyajima A., Takamatu M., Kazama S., Irie T., Doi O., Takizawa T.	Effects of 13 developmentally toxic chemicals on the migration of rat cephalic neural crest cels in vitro.	Congenital Anomalies			2015
Irie T., Kikura-Hanajiri R., Usami M., Uchiyama N., Goda Y., Sekino Y	MAM-2201, a synthetic cannabinoid drug of abuse, suppresses the synaptic input to cerebellar Purkinje cells via activation of presynaptic CB1 receptors.	Neuropharmacology	95	479–91	2015
Oguchi-Katayama A., Monma A., Sekino Y., Moriguchi T., Sato K	Comparative gene expression analysis of the amygdalae of juvenile rats exposed to valproic acid at prenatal and postnatal stages.	J Toxicol Sci	38 (3)	381-402	2013
Takahashi K., Ishii-Nozawa R., Takeuchi K., Nakazawa K., Sekino Y., Sato K.	Niflumic acid activates additional currents of the human glial L-glutamate transporter EAAT1 in a substrate-dependent manner.	Biol Pharm Bull	36 (12)	1996-2004	2013
Fujimori, K., Takaki, J., Miura, M., Shigemoto-Mogami, Y., Sekino, Y., Suzuki, T., Sato, K.	Paroxetine prevented the down-regulation of astrocytic L-Glu transporters in neuroinflammation.	J Pharamcol Sci (in press)			
Shigemoto-Mogami, Y., Hoshikawa, K., Goldman, J.E.,Sekino, Y., Sato, K.	Microglia enhances neurogenesis and oligodendrogenesis in the early postnatal subventricular zone.	J Neurosci.	34(5)	2231- 2243	2014
Shigemoto-Mogami, Y., Fujimori, K., Ikarashi, Y., Hirose, A., Sekino, Y., Sato, K.	Residual metals in carbon nanotubes suppress the proliferation of neural stem cells.	Fundam Toxcol Sci.	1(3)	87-94	2014
佐藤　薫	ミクログリアの発生と分化	Clinical Neuroscience	32 (12)	1338-1341	2015
Sato, K.	Microglia effects on neuronal development.	GLIA	63 (8)	1394-495	2015
吉田祥子・穂積直裕	神経伝達物質を視るデバイスが拓く神経科学の展開 ～ 求められる技術を開発する技術 ～	信学技報	112-345	39-40	2012
吉田祥子・穂積直裕	発達期小脳アストロサイトの機能と秩序形成	JNNS.	20	14-18	2013

K. Watanabe, N. Takahashi, N. Hozumi, S. Yoshida,	Improvements in Enzyme-Linked Photo assay Systems for Spatiotemporal Observation of Neurotransmitter Release	Sensors and Materials	27 (10)	1035–1044	2015
H. Mabuchi, HY Ong, K. Watanabe, S. Yoshida, N. Hozumi,	Visualization of Spatially Distributed Bioactive Molecules Using Enzyme-Linked Photo Assay	IEEJ Transactions (in press)			
上野　晋	化学物質（金属・有機溶剤）の毒性学と産業医としての対応	産業医科大学雑誌	第35巻 特集号	91-6	2013
Park EK, Wilson D, Choi HJ, Wilson CT, Ueno S.	Hazardous metal pollution in the republic of Fiji and the need to elicit human exposure.	Environ Health Toxicol.			2013
Obara G., Toyohira Y., Inagaki H., Takahashi K., Horishita T., Kawasaki T., Ueno S., Tsutsui M., Sata T., Yanagihara N.	Pentazocine inhibits norepinephrine transporter function by reducing its surface expression in bovine adrenal medullary cells.	*J Pharmacol Sci.*	121	138-47	2013
Uchida T., Furuno Y., Tanimoto A., Toyohira Y., Arakaki K., Kina-Tanada M., Kubota H., Sakanashi M., Matsuzaki T., Noguchi K. Nakasone J., Igarashi T., Ueno S., Matsushita M., Ishiuchi S., Masuzaki H., Ohya Y., Yanagihara N., Shimokawa H., Otsuji Y., Tamura M., Tsutsui M.	Development of an experimentally useful model of acute myocardial infarction: 2/3 nephrectomized triple nitric oxide synthases-deficient mouse.	J Mol Cell Cardiol.	77	29-41	2014
Horishita T., Yanagihara N., Ueno S., Sudo Y., Uezono Y., Okura D., Minami T., Kawasaki T., Sata T.	Neurosteroids allopregnanolone sulfate and pregnanolone sulfate have diverse effect on the a subunit of the neuronal voltage-gated sodium channels Nav1.2, Nav1.6, Nav1.7, and Nav1.8 expressed in *Xenopus* oocytes.	Anesthesiology.	121	620-631	2014
Okura D., Horishita T., Ueno S., Yanagihara N., Sudo Y., Uezono Y., Sata T.	The endocannabinoid anandamide inhibits voltage-gated sodium channels Nav1.2, Nav1.6, Nav1.7 and Nav1.8 in Xenopus oocytes.	Anesth. Analg.	118	554-62	2014
Yanagihara N, Zhang H, Toyohira Y, Takahashi K, Ueno S, Tsutsui M, Takahashi K.	New insights into the pharmacological potential of plant flavonoids in the catecholamine system.	J Pharmacol Sci.	124	123-8	2014

Inagaki H, Toyohira Y, Takahashi K, Ueno S, Obara G, Kawagoe T, Tsutsui M, Hachisuga T, Yanagihara N.	Effects of selective estrogen receptor modulators on plasma membrane estrogen receptors and catecholamine synthesis and secretion in cultured bovine adrenal medullary cells.	J Pharmacol Sci.	124	66-75	2014
Okura D., Horishita T., Ueno S., Yanagihara N., Sudo Y., Uezono Y., Minami T., Kawasaki T., Sata T.	Lidocaine preferentially inhibits the function of purinergic P2X7 receptors expressed in *Xenopus* Oocytes.	Anesth Analg.	120	597-605	2015
Ishidao T, Fueta Y, Ueno S, Yoshida Y, Hori H.	A cross-fostering analysis of bromine ion concentration in rats that that inhaled 1-bromopropane vapor.	*J. Occup. Health*, in press.			
Fueta Y, Kanemitsu M, Egawa S, Ishidao T, Ueno S, Hori H.	Prenatal exposure to 1-bromopropane suppresses kainate-induced wet dog shakes in immature rats.	*J UOEH.*	37	255-261	2015
Li X, Toyohira Y, Horisita T, Satoh N, Takahashi K, Zhang H, Iinuma M, Yoshinaga Y, Ueno S, Tsutsui M, Sata T, Yanagihara N.	Ikarisoside A inhibits acetylcholine-induced catecholamine secretion and synthesis by suppressing nicotinic acetylcholine receptor-ion channels in cultured bovine adrenal medullary cells.	*Naunyn Schmiedebergs Arch Pharmacol.*	388	1259-1269	2015

書籍

著者氏名	論文タイトル名	書籍全体の編集者名	書　籍　名	出版社名	出版地	出版年	ページ
Kanda Y.	Assessment of cigarette smoking toxicity using cancer stem cells.	Nazmi Sari	Smoking Restrictions, Risk Perceptions and Its Health and Environmental Impacts	Nova Science Publishers	United States of America	2014	185-196
Kanda Y.	1. Cancer Stem Cells - Fact or Fiction?	Dittmar T, Zänker KS	Role of Cancer Stem Cells in Cancer Biology and Therapy	CRC Press	United States of America	2013	1-22
諫田泰成	ヒトiPS細胞を用いた心毒性試験の現状と課題	安全性評価研究会編集委員会	谷本学校毒性質問箱第16号	株式会社サイエンティスト社	東京	2014	91-94
諫田泰成	再生心筋細胞を用いた安全性薬理評価系の開発	エイブル株式会社和田昌憲	再生医療における臨床研究と製品開発	技術情報協会	東京	2013	572-576

IV.　研究成果の刊行物・別刷

Metallomics

PAPER

View Article Online
View Journal

Cite this: DOI: 10.1039/c5mt00033e

Tributyltin induces mitochondrial fission through NAD-IDH dependent mitofusin degradation in human embryonic carcinoma cells

Shigeru Yamada,[a] Yaichiro Kotake,[b] Mizuho Nakano,[a] Yuko Sekino[a] and Yasunari Kanda*[a]

Received 4th February 2015,
Accepted 14th April 2015

DOI: 10.1039/c5mt00033e

www.rsc.org/metallomics

Organotin compounds, such as tributyltin (TBT), are well-known endocrine disruptors. TBT acts at the nanomolar level through genomic pathways *via* the peroxisome proliferator activated receptor (PPAR)/retinoid X receptor (RXR). We recently reported that TBT inhibits cell growth and the ATP content in the human embryonic carcinoma cell line NT2/D1 *via* a non-genomic pathway involving NAD^+-dependent isocitrate dehydrogenase (NAD-IDH), which metabolizes isocitrate to α-ketoglutarate. However, the molecular mechanisms by which NAD-IDH mediates TBT toxicity remain unclear. In the present study, we evaluated the effects of TBT on mitochondrial NAD-IDH and energy production. Staining with MitoTracker revealed that nanomolar TBT levels induced mitochondrial fragmentation. TBT also degraded the mitochondrial fusion proteins, mitofusins 1 and 2. Interestingly, apigenin, an inhibitor of NAD-IDH, mimicked the effects of TBT. Incubation with an α-ketoglutarate analogue partially recovered TBT-induced mitochondrial dysfunction, supporting the involvement of NAD-IDH. Our data suggest that nanomolar TBT levels impair mitochondrial quality control *via* NAD-IDH in NT2/D1 cells. Thus, mitochondrial function in embryonic cells could be used to assess cytotoxicity associated with metal exposure.

Introduction

Growing evidence suggests that environmental organometals contribute to the observed increase in neurodevelopmental disorders, such as learning disabilities, autism spectrum disorder, behavioral abnormalities and teratogenicity.[1–3] Since the developing brain is more vulnerable to injury than the adult brain, exposure to these organometals during early fetal development can cause permanent or delayed neural disorders at much lower doses than in adults.[4–7] Therefore, it is necessary to elucidate the cytotoxic effects of organometals at low levels during development.

Organotin compounds, such as TBT, are well known to cause various types of cytotoxicity *via* genomic and non-genomic pathways. In the genomic pathway, nanomolar concentrations of TBT activate the retinoid X receptor (RXR) and/or peroxisome proliferator-activated receptor γ (PPARγ) and result in neurodevelopmental defects in mammals.[8,9] Conversely, many reports have shown that TBT at micromolar levels causes mitochondorial toxicity in the non-genomic pathway. For example, micromolar TBT and dibutyltin (DBT) levels have been shown to prevent mitochondrial respiration by inhibiting the electron transfer from complexes I and III, and Mg-ATPase activity.[10–12] The non-genomic effect of TBT mediates cell death in rat neurons. TBT induces neuronal death *via* AMPK activation and the phosphorylation of the mammalian target of rapamycin (mTOR) in rat cortical neurons.[13,14] TBT also induces neuronal degeneration *via* mitochondria-mediated ROS generation in rat neurons.[15]

We studied nanomolar TBT toxicity using neuronal precursor NT2/D1 cells as a model of the neurodevelopmental stage[16] and found that nanomolar TBT levels inhibit intracellular energy metabolism, including ATP production, *via* mitochondrial NAD^+-dependent isocitrate dehydrogenase (NAD-IDH), which catalyzes the irreversible conversion of isocitrate to α-ketoglutarate in the tricarboxylic acid (TCA) cycle.[17,18] Based on these observations, we hypothesized that nanomolar TBT levels affect mitochondrial functions, thereby altering the energy metabolism of neuronal precursor cells.[19]

Mitochondria continuously change their morphology through fission and fusion. These mitochondrial dynamics are an important quality control mechanism that maintains mitochondrial function, such as ATP production.[20] Mitochondrial fission and fusion are regulated by several GTPases. In mitochondrial fusion, mitofusins 1 and 2 (Mfn1, 2) and optic atrophy 1 (Opa1) induce the fusion of the outer and inner mitochondrial membranes,

[a] Division of Pharmacology, National Institute of Health Sciences, 1-18-1, Kamiyoga, Setagaya-ku 158-8501, Japan. E-mail: kanda@nihs.go.jp; Fax: +81-3-3700-9704; Tel: +81-3-3700-9704

[b] Department of Xenobiotic Metabolism and Molecular Toxicology, Graduate School of Biomedical and Health Sciences, Hiroshima University, Japan

respectively.[21,22] The deletion of Mfn1 and Mfn2 in mice is embryonically lethal, and cells from these embryos contain fragmented and dysfunctional mitochondria.[23] In contrast, dynamin-related protein 1 (Drp1) is a cytoplasmic protein that assembles into rings surrounding the outer mitochondrial membrane, where it interacts with fission protein 1 (Fis1) to promote fission.[24,25]

In the present study, we have investigated the effect of TBT on mitochondrial quality control in NT2/D1 cells. We found that exposure to 100 nM TBT induced proteasomal degradation of Mfn and mitochondrial fragmentation through an NAD-IDH-dependent mechanism. Thus, impaired mitochondrial quality control is a novel mechanism of nanomolar level TBT-induced toxicity in human embryonic carcinoma cells.

Methods

Cell culture

NT2/D1 cells were obtained from the American Type Culture Collection (Manassas, VA, USA). The cells were cultured in Dulbecco's modified Eagle's medium (DMEM; Sigma-Aldrich, St Louis, MO, USA) supplemented with 10% fetal bovine serum (FBS; Biological Industries, Ashrat, Israel) and 0.05 mg ml^{-1} of the penicillin–streptomycin mixture (Life Technologies, Carlsbad, CA, USA) at 37 °C in 5% CO_2.

Assessment of mitochondrial fusion

After treatment with TBT (100 nM, 24 h), the cells were fixed with 4% paraformaldehyde and stained with 50 nM MitoTracker Red CMXRos (Cell Signaling Technology, Danvers, MA, USA) and 0.1 μg ml^{-1} 4′,6-diamidino-2-phenylindole (DAPI; Dojin, Kumamoto, Japan). Changes in the mitochondrial morphology were observed using confocal laser microscopy (Nicon A1). Images (n = 3–7) of random fields were obtained, and the number of cells displaying mitochondrial fusion (<10% punctiform) was counted in each image, as previously reported.[26]

Real-time PCR

Total RNA was isolated from NT2/D1 cells using the TRIzol reagent (Life Technologies), and quantitative real-time reverse transcription (RT)-PCR using a QuantiTect SYBR Green RT-PCR Kit (QIAGEN, Valencia, CA, USA) was performed using an ABI PRISM 7900HT sequence detection system (Applied Biosystems, Foster City, CA, USA), as previously reported.[27] The relative change in the amount of transcript was normalized to the mRNA levels of glyceraldehyde-3-phosphate dehydrogenase (GAPDH). The following primer sequences were used for real-time PCR analysis: human Drp1: forward, 5-TGGGCGCCGACATCA-3, reverse, 5-GCTCTGCGTTCCCACTACGA-3; human Fis1: forward, 5-TACGTCCGCGGGTTGCT-3, reverse, 5-CCAGTTCCTTGGCCTGGTT-3; human Mfn1: forward, 5-GGCATCTGTGGCCGAGTT-3, reverse, 5-ATTATGCTAAGTCTCCGCTCCAA-3; human Mfn2: forward, 5-GCTCGGAGGCACATGAAAGT-3, reverse, 5-ATCACGGTGCTCTTCCCATT-3; human GAPDH: forward, 5-GTCTCCTCTGACTTCAACAGCG-3, reverse, 5-ACCACCCTGTTGCTGTAGCCAA-3.

Western blot analysis

Western blot analysis was performed as previously reported.[28] Briefly, the cells were lysed with cell lysis buffer (Cell Signaling Technology). The proteins were then separated by sodium dodecyl sulfate-polyacrylamide gel electrophoresis (SDS-PAGE) and electrophoretically transferred to Immobilon-P (Millipore, Billerica, MA, USA). The membranes were probed using the following antibodies: an anti-Mfn1 polyclonal antibody (1 : 1000; Cell Signaling Technology), an anti-Mfn2 monoclonal antibody (1 : 1000; Cell Signaling Technology), an anti-cytochrome c oxidase subunit IV (COX IV) monoclonal antibody (1 : 1000; Cell Signaling Technology), and an anti-β-actin monoclonal antibody (1 : 5000; Sigma-Aldrich). The membranes were then incubated with secondary antibodies against rabbit or mouse IgG conjugated to horseradish peroxidase (Cell Signaling Technology). The bands were visualized using the ECL western blotting analysis system (GE Healthcare, Buckinghamshire, UK), and images were acquired using a LAS-3000 imager (FUJIFILM UK Ltd., Systems, Bedford, UK).

Chemicals and reagents

Tributyltin chloride was obtained from Tokyo Chemical Industry (Tokyo, Japan). Tin acetate (TA), rosiglitazone (RGZ), CD3254,

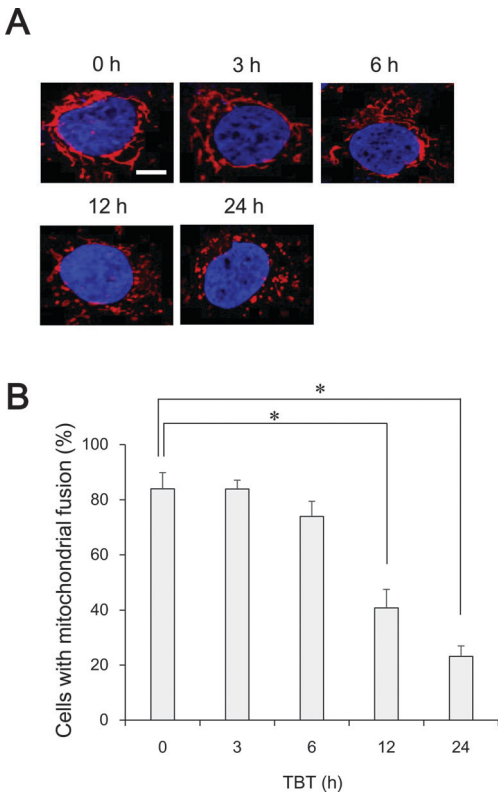

Fig. 1 Effect of TBT on the mitochondrial morphology in NT2/D1 cells. Cells were exposed to 100 nM TBT for 3, 6, 12, or 24 h. (A) The cells were stained with MitoTracker Red CMXRos and DAPI. Mitochondrial morphology was observed by confocal laser microscopy. Bar = 10 μm. (B) The number of cells undergoing mitochondrial fusion (<10% punctiform) was counted in each image. Data represent mean ± s.d. (n = 5). *P < 0.05.

apigenin, cycloheximide (CHX), carbonylcyanide m-chlorophenylhydrazone (CCCP), and MG132 were obtained from Sigma-Aldrich.

Statistical analysis

All data were presented as means ± S.D. ANOVA followed by a *post hoc* Tukey' test was used to analyze data in Fig. 1B, 2B, 3C, 4C, 5B, and 5C. Student's *t*-test was used to analyze data in Fig. 3A and 4B. *P*-values less than 0.05 were considered to be statistically significant.

Results and discussion

Effects of TBT on mitochondrial morphology

We have previously examined the effect of TBT (30–300 nM) on cell growth in NT2/D1 cells and found that TBT levels at the concentrations of 100 nM or more induced growth arrest in the cells.[17] Here we investigated whether 100 nM TBT affects mitochondrial dynamics in the cells. After exposure to 100 nM TBT for 12 h, we observed the increase in the number of cells with fragmented mitochondria, as compared to untreated control cells (Fig. 1A, B). After 24 h, the proportion of cells with mitochondrial fusion was nearly 80%. As a positive control, we used CCCP, which induces mitochondrial uncoupling and mitochondrial fission in other cells.[29] As expected, fragmented mitochondria were also observed following CCCP treatment for 24 h (Fig. 2A and B). In contrast, exposure to tin acetate (TA), which is less toxic, did not affect the mitochondrial morphology. To investigate whether TBT-induced mitochondrial fission was caused by changes in transcription, we treated the cells with the protein synthesis inhibitor cycloheximide. Treatment with cycloheximide did not alter the effects of TBT on the mitochondrial morphology (Fig. 2A and B). Moreover, rosiglitazone, an agonist of the TBT genomic target PPARγ, did not induce mitochondrial fragmentation. These results suggest that TBT induces mitochondrial fission through a non-genomic pathway in NT2/D1 cells.

TBT exposure induces proteasomal degradation of Mfn1 and 2

To examine the molecular mechanism by which TBT induces mitochondrial fragmentation, we assessed the effect of TBT on

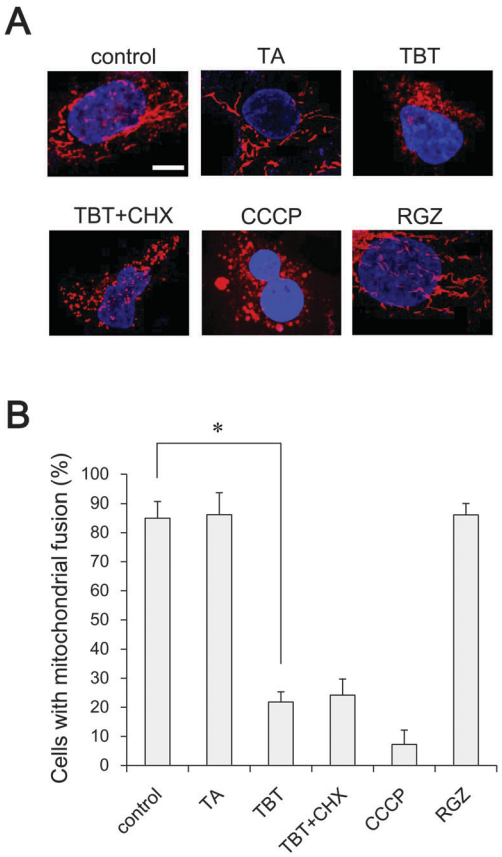

Fig. 2 Non-genomic effect of TBT-induced mitochondrial fission. Cells were exposed to 100 nM TA, 100 nM TBT, 100 nM TBT + 10 μg ml^{-1} cycloheximide (CHX), 1 μM CCCP or 100 nM rosiglitazone (RGZ) for 24 h. (A) The cells were stained with MitoTracker Red CMXRos and DAPI. Mitochondrial morphology was observed by confocal laser microscopy. Bar = 10 μm. (B) The number of cells undergoing mitochondrial fusion (<10% punctiform) was counted in each image. Data represent mean ± s.d. (n = 5). *P < 0.05.

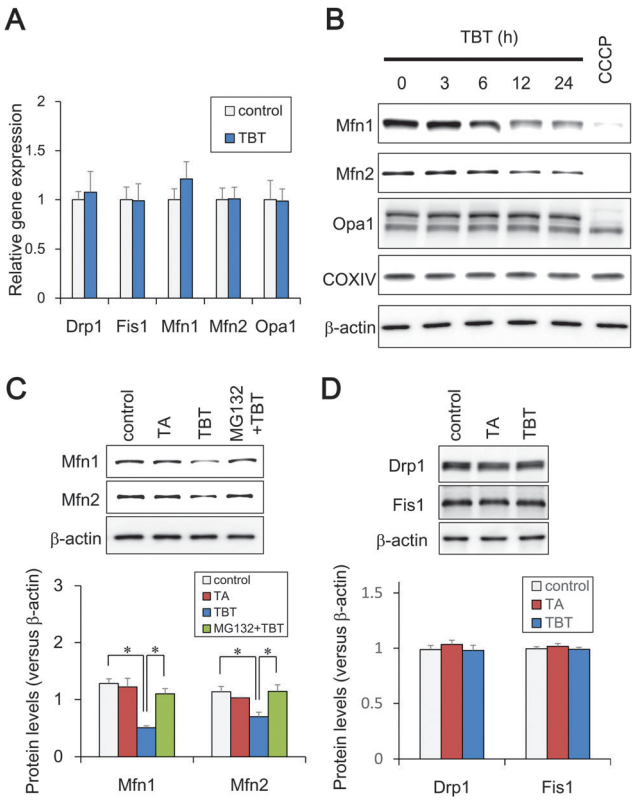

Fig. 3 Effect of TBT on mitochondrial protein levels in NT2/D1 cells. (A) After 24 h TBT exposure, the expression of mitochondrial genes was analyzed by real time PCR. The gene expression was not significantly altered by TBT exposure. (B) After TBT exposure for 3, 6, 12, or 24 h, mitochondrial proteins were analyzed by western blot using anti-Mfn1, Mfn2, Opa1, COXIV, or β-actin antibodies. (C) Cells were exposed to 100 nM TA, 100 nM TBT, or 100 nM TBT + 3 μM MG132 for 6 h. Mitochondrial proteins were analyzed by western blot using anti-Mfn1 or Mfn2 antibodies. (D) After 6 h TBT exposure, other mitochondrial proteins were analyzed by western blot using anti-Drp1, Fis1, or β-actin antibodies. Data represent mean ± s.d. (n = 3). *P < 0.05.

mitochondrial fission (Fis1, Drp1) and fusion genes (Mfn1, Mfn2, OPA1). Real-time PCR analysis showed that each gene expression was not significantly altered by TBT exposure (Fig. 3A). Fusion allows damaged mitochondria to incorporate into intact mitochondria, thereby maintaining mitochondrial function.[30] Dysfunctional mitochondria may lose their fusion capacity by the degradation of fusion proteins, resulting in the accumulation of fragmented mitochondria. Thus, we assessed the protein expression of Mfn1, Mfn2, and OPA1 in the presence or absence of TBT. Western blot analysis revealed that Mfn1 and Mfn2 protein levels were significantly reduced after 6 h, whereas OPA1 protein expression was not changed after 24 h (Fig. 3B and C). The other mitochondrial inner membrane protein, cytochrome *c* oxidase subunit IV (COX IV), was also not changed after 24 h (Fig. 3B). Moreover, MG132, a proteasome inhibitor, recovered the TBT-induced reduction in Mfn1 and Mfn2 (Fig. 3C). In contrast, the fusion proteins Fis1 and Drp1 were not affected by TBT (Fig. 3D). These data suggest that TBT-induced mitochondrial fragmentation is caused by the proteasomal degradation of Mfn1 and Mfn2.

Consistent with our data, chemical stressors have been reported to cause mitochondrial fission through the proteasomal degradation of Mfn. For example, doxorubicin induces ubiquitin-mediated proteasomal degradation of Mfn2, which facilitates mitochondrial fragmentation and apoptosis in sarcoma U2OS cells.[31] Another study has shown that CGP37157, an inhibitor of mitochondrial calcium efflux, mediates mitochondrial fission through Mfn1 degradation *via* ubiquitin ligase in prostate cancer LNCaP cells.[32] Since it remains unknown if ubiquitin ligases are involved or not in these TBT actions, further studies should be addressed to clarify the TBT-induced mechanism of proteasomal degradation of Mfn1 and Mfn2.

TBT induces mitochondrial defects *via* NAD-IDH

To investigate whether Mfn degradation and mitochondrial dysfunction are mediated through the non-genomic TBT target NAD-IDH, we examined the effects of apigenin, an NAD-IDH inhibitor,[33] on mitochondrial function. Apigenin (10 μM) decreased the number of cells undergoing mitochondrial fusion and induced mitochondrial fragmentation after 24 h (Fig. 4A and B). Furthermore, apigenin significantly reduced Mfn1 and Mfn2 protein expression, which was recovered by MG132 treatment (Fig. 4C). Apigenin has been reported to inhibit not only NAD-IDH but also hnRNPA2 and NF-κB.[33]

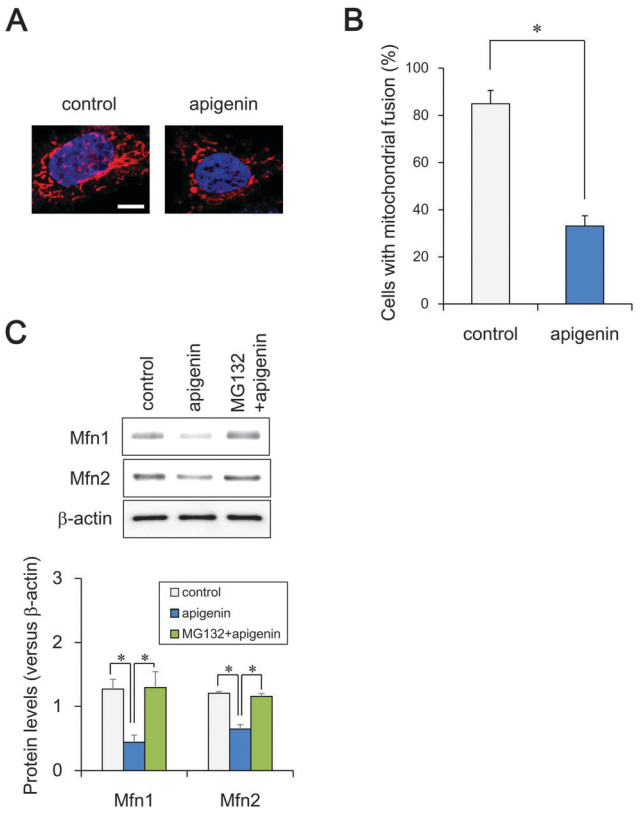

Fig. 4 Effect of apigenin on mitochondrial function in NT2/D1 cells. Cells were exposed to 10 μM apigenin. (A) Cells were stained with MitoTracker Red CMXRos and DAPI. Mitochondrial morphology was observed by confocal laser microscopy. Bar = 10 μm. (B) The number of cells undergoing mitochondrial fusion (<10% punctiform) was counted in each image. Data represent mean ± s.d. (n = 5). (C) Mitochondrial proteins in the cell lysate were analyzed by western blotting using anti-Mfn1 or Mfn2 antibodies. Data represent mean ± s.d. (n = 3). *P < 0.05.

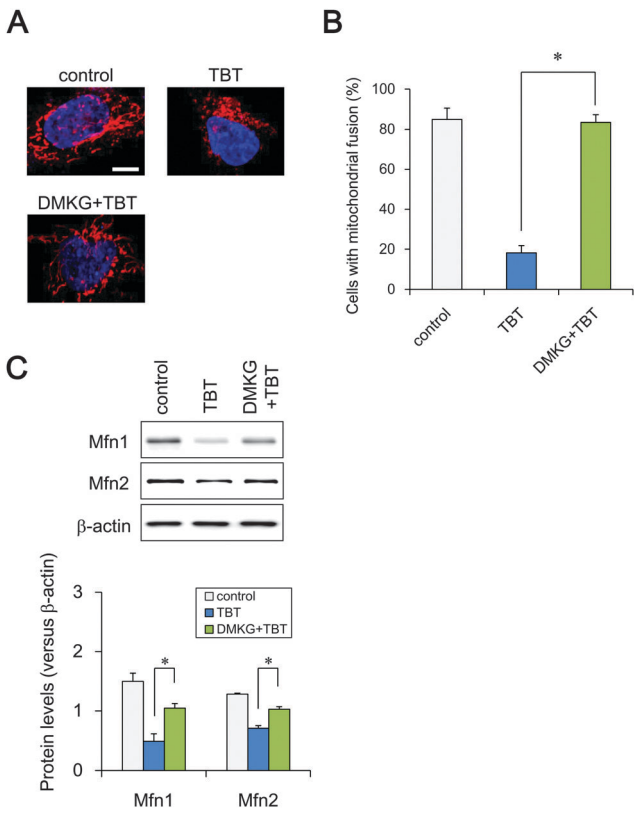

Fig. 5 Effect of DMKG on TBT-induced mitochondrial dysfunctions in NT2/D1 cells. Cells were exposed to 100 nM TBT and 7 mM DMKG. (A) Cells were stained with MitoTracker Red CMXRos and DAPI. Mitochondrial morphology was observed by confocal laser microscopy. Bar = 10 μm. (B) The number of cells undergoing mitochondrial fusion (<10% punctiform) was counted in each image. Data represent mean ± s.d. (n = 5). (C) Mitochondrial proteins were analyzed by western blotting using anti-Mfn1 or Mfn2 antibodies. Data represent mean ± s.d. (n = 3). *P < 0.05.

We cannot rule out the possibility that apigenin-induced mitochondrial dysfunction was induced by other targets. It is necessary to confirm our data by shRNA against NAD-IDH. To further confirm the involvement of NAD-IDH, we used dimethyl α-ketoglutarate (DMKG), a cell-permeable analog of α-ketoglutarate.[34] Incubation with DMKG prevented TBT-induced mitochondrial fragmentation in NT2/D1 cells (Fig. 5A) and recovered the number of cells undergoing mitochondrial fusion to the basal level (Fig. 5B). Furthermore, DMKG significantly recovered the TBT-induced the proteasomal degradation of Mfn1 and Mfn2 (Fig. 5C). Taken together, these data suggest that NAD-IDH mediates TBT-induced mitochondrial dysfunction *via* Mfn degradation in NT2/D1 cells. In addition to NAD-IDH, citrate synthase and α-ketoglutarate dehydrogenase also work as rate-limiting enzymes in the TCA cycle. Aluminium has been shown to induce oxidative stress *via* the negative regulation of citrate synthase and α-ketoglutarate dehydrogenase.[35,36] We could not rule out the possibility that TBT affects these enzymes. Several reports indicate that knockdown of Mfn1 and Mfn2 in the cells induces mitochondrial fragmentation and shows severe cellular defects, including decreased ATP content and poor cell growth.[30,37] Especially, Mfn2 has been reported to be necessary for striatal axonal projections of midbrain dopamine neurons by studies using dopamine neuron-specific Mfn2 knockout mice.[38] Taken together, Mfn1 and Mfn2 might be involved in several TBT actions *via* NAD-IDH, such as the reduction of ATP content, growth inhibition and enhancement of neuronal differentiation.

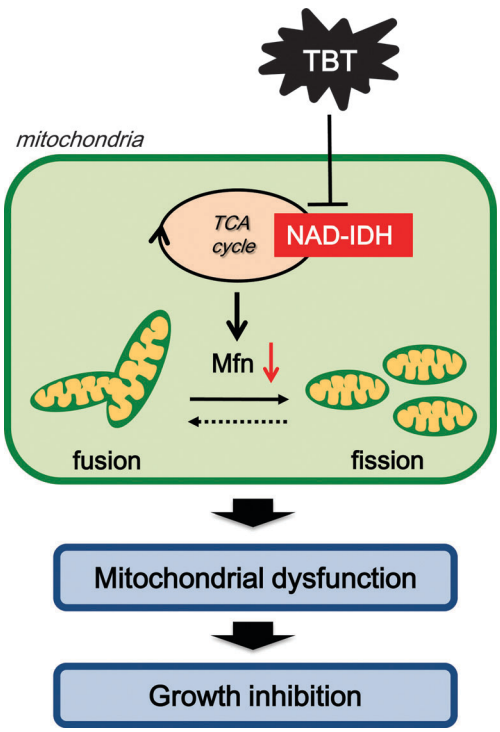

Fig. 6 Proposed model of TBT toxicity through non-genomic pathways in human embryonic carcinoma cells. Nanomolar TBT levels induce Mfn degradation and mitochondrial fission through NAD-IDH inhibition. These negative effects of TBT on mitochondrial quality control could mediate cell growth inhibition.

Conclusions

Based on our data, we have proposed a model of nanomolar TBT-induced mitochondrial dysfunction in neuronal precursor cells (Fig. 6). We demonstrated that TBT mediates the inhibition of NAD-IDH and the loss of mitochondrial quality control, representing a novel non-genomic pathway of TBT-induced toxicity. These negative effects of TBT on mitochondria could inhibit ATP production and cell growth. Since TBT at micromolar levels is known to cause neuronal degeneration *via* multiple mitochondrial defects, similar mitochondrial dysfunction might be also observed in immature neuronal precursor cells. We have previously revealed TBT-induced NAD-IDH inhibition in the rat brain. It would be interesting to study whether TBT-induced mitochondrial dysfunction *via* NAD-IDH might be also observed *in vivo*. We are now conducting experiments to determine how TBT degrades Mfn proteins both *in vitro* and *in vivo*. It remains to be determined if micromolar concentrations of TBT induce other mitochondrial dysfunctions in NT2/D1 cells and if the mechanisms pointed out here are selective for immature cells.

List of abbreviations

CCCP	Carbonylcyanide *m*-chlorophenylhydrazone
CHX	Cycloheximide
COX IV	Cytochrome *c* oxidase subunit IV
DAPI	4′,6-Diamidino-2-phenylindole
DMEM	Dulbecco's modified Eagle's medium
DMKG	Dimethyl α-ketoglutarate
Drp1	Dynamin-related protein 1
FBS	Fetal bovine serum
Fis1	Fission protein 1
GAPDH	Glyceraldehyde-3-phosphate dehydrogenase
Mfn	Mitofusin
NAD-IDH	NAD^+-dependent isocitrate dehydrogenase
Opa1	Optic atrophy 1
PPAR	Peroxisome proliferator activated receptor
RGZ	Rosiglitazone
RXR	Retinoid X receptor
TA	Tin acetate
TBT	Tributyltin
TCA	Tricarboxylic acid

Conflict of interest

The authors declare that there are no conflicts of interest.

Acknowledgements

This work was supported by a Health and Labour Sciences research grant from the Ministry of Health, Labour and Welfare, Japan (#H25-Kagaku-Ippan-002 to Y.Ka.), a grant-in-aid for scientific research from the Ministry of Education, Culture, Sports, Science, and Technology, Japan (#26293056, #26670041 to Y. Kanda), and a grant from the Smoking Research Foundation (Y. Kanda).

References

1 E. Dopp, L. M. Hartmann, A. M. Florea, A. W. Rettenmeier and A. V. Hirner, Environmental distribution, analysis, and toxicity of organometal(loid) compounds, *Crit. Rev. Toxicol.*, 2004, **34**, 301–333.

2 A. T. Gardlund, T. Archer, K. Danielsen, B. Danielsson, A. Frederiksson, N. G. Lindquist, H. Lindstrom and J. Luthman, Effects of prenatal exposure to tributyltin and trihexyltin on behavior in rats, *Neurotoxicol. Teratol.*, 1991, **13**, 99–105.

3 A. Mariani, R. Fanelli, A. Re Depaolini and M. De Paola, Decabrominated diphenyl ether and methylmercury impair fetal nervous system development in mice at documented human exposure levels, *Dev. Neurobiol.*, 2015, **75**, 23–38.

4 G. Winneke, Developmental aspects of environmental neurotoxicology: lessons from lead and polychlorinated biphenyls, *J. Neurol. Sci.*, 2011, **308**, 9–15.

5 L. G. Costa, M. Aschne, A. Vitalone, T. Syversen and O. P. Soldin, Developmental neuropathology of environmental agents, *Annu. Rev. Pharmacol. Toxicol.*, 2004, **44**, 87–110.

6 J. Dobbing, Vulnerable periods in developing brain, in *Appl. Neurochem*, ed. A. N. Davison and J. Dobbing, Davis, Philadelphia, 1968, pp. 287–316.

7 P. M. Rodier, Developing brain as a target of toxicity, *Environ. Health Perspect.*, 1995, **103**(suppl 6), 73–76.

8 T. Kanayama, N. Kobayashi, S. Mamiya, T. Nakanishi and J. Nishikawa, Organotin compounds promote adipocyte differentiation as agonists of the peroxisome proliferator-activated receptor gamma/retinoid X receptor pathway, *Mol. Pharmacol.*, 2005, **67**, 766–774.

9 M. Kajta and A. K. Wójtowicz, Impact of endocrine-disrupting chemicals on neural development and the onset of neurological disorders, *Pharmacol. Rep.*, 2013, **65**, 1632–1639.

10 H. S. Elsabbagh, S. Z. Moussa and O. S. El-tawil, Neurotoxicologic sequelae of tributyltin intoxication in rats, *Pharmacol. Res.*, 2002, **45**, 201–206.

11 S. Nesci, V. Ventrella, F. Trombetti, M. Pirini and A. Pagliarani, Tributyltin (TBT) and mitochondrial respiration in mussel digestive gland, *Toxicol. in Vitro*, 2011, **25**, 951–959.

12 S. Nesci, V. Ventrella, F. Trombetti, M. Pirini, A. R. Borgatti and A. Pagliarani, Tributyltin (TBT) and dibutyltin (DBT) differently inhibit the mitochondrial Mg-ATPase activity in mussel digestive gland, *Toxicol. in Vitro*, 2011, **25**, 117–124.

13 Y. Nakatsu, Y. Kotake, N. Takai and S. Ohta, Involvement of autophagy *via* mammalian target of rapamycin (mTOR) inhibition in tributyltin-induced neuronal cell death, *J. Toxicol. Sci.*, 2010, **35**, 245–251.

14 Y. Kotake, Molecular mechanisms of environmental organotin toxicity in mammals, *Biol. Pharm. Bull.*, 2012, **35**, 1876–1880.

15 S. Mitra, R. Gera, W. A. Siddiqui and S. Khandelwal, Tributyltin induces oxidative damage, inflammation and apoptosis *via* disturbance in blood–brain barrier and metal homeostasis in cerebral cortex of rat brain: an *in vivo* and *in vitro* study, *Toxicology*, 2013, **310**, 39–52.

16 M. Bani-Yaghoub, J. M. Felker and C. C. Naus, Human NT2/D1 cells differentiate into functional astrocytes, *NeuroReport*, 1999, **10**, 3843–3846.

17 S. Yamada, Y. Kotake, Y. Sekino and Y. Kanda, AMP-activated protein kinase-mediated glucose transport as a novel target of tributyltin in human embryonic carcinoma cells, *Metallomics*, 2013, **5**, 484–491.

18 S. Yamada, Y. Kotake, Y. Demizu, M. Kurihara, Y. Sekino and Y. Kanda, NAD-dependent isocitrate dehydrogenase as a novel target of tributyltin in human embryonic carcinoma cells, *Sci. Rep.*, 2014, **4**, 5952.

19 C. M. Nasrallah and T. L. Horvath, Mitochondrial dynamics in the central regulation of metabolism, *Nat. Rev. Endocrinol.*, 2014, **10**, 650–658.

20 R. J. Youle and A. M. van der Bliek, Mitochondrial fission, fusion, and stress, *Science*, 2012, **337**, 1062–1065.

21 T. Koshiba, S. A. Detmer, J. T. Kaiser, H. Chen, J. M. McCaffery and D. C. Chan, Structural basis of mitochondrial tethering by mitofusin complexes, *Science*, 2004, **305**, 858–862.

22 S. Cipolat, O. M. De Brito, B. Dal Zilio and L. Scorrano, OPA1 requires mitofusin 1 to promote mitochondrial fusion, *Proc. Natl. Acad. Sci. U. S. A.*, 2004, **101**, 15927–15932.

23 H. Chen, S. A. Detmer, A. J. Ewald, E. Erik, S. E. F. Griffin and D. C. Chan, Mitofusins mfn1 and mfn2 coordinately regulate mitochondrial fusion and are essential for embryonic development, *J. Cell Biol.*, 2003, **160**, 189–200.

24 E. Smirnova, L. Griparic, D.-L. Shurland and A. M. van der Bliek, Dynamin-related protein Drp1 is required for mitochondrial division in mammalian cells, *Mol. Biol. Cell*, 2001, **12**, 2245–2256.

25 Y. Yoon, E. W. Krueger, B. J. Oswald and M. A. McNiven, The mitochondrial protein hFis1 regulates mitochondrial fission in mammalian cells through an interaction with the dynamin-like protein DLP1, *Mol. Biol. Cell*, 2003, **23**, 5409–5420.

26 X. Fan, R. Hussien and G. A. Brooks, H_2O_2-induced mitochondrial fragmentation in C2C12 myocytes, *Free Radical Biol. Med.*, 2010, **49**, 1646–1654.

27 N. Hiarta, S. Yamada, T. Shoda, M. Kurihara, Y. Sekino and Y. Kanda, Sphingosine-1-phosphate promotes expansion of cancer stem cells *via* S1PR3 by a ligand-independent Notch activation, *Nat. Commun.*, 2014, **5**, 4806.

28 Y. Kanda, T. Hinara, S. W. Kang and Y. Watanabe, Reactive oxygen species mediate adipocyte differentiation in mesenchymal stem cells, *Life Sci.*, 2011, **89**, 250–258.

29 A. Tanaka, M. M. Cleland, S. Xu, D. P. Narendra, D. F. Suen, M. Karbowski and R. J. Youle, Proteasome and p97 mediate mitophagy and degradation of mitofusins induced by Parkin, *J. Cell Biol.*, 2010, **191**, 1367–1380.

30 H. Chen, A. Chomyn and D. C. Chan, Disruption of fusion results in mitochondrial heterogeneity and dysfunction, *J. Biol. Chem.*, 2005, **280**, 26185–26192.

31 G. P. Leboucher, Y. C. Tsai, M. Yang, K. C. Shaw, M. Zhou, T. D. Veenstra, M. H. Glickman and A. M. Weissman, Stress-induced phosphorylation and proteasomal degradation of mitofusin 2 facilitates mitochondrial fragmentation and apoptosis, *Mol. Cell*, 2012, **47**, 547–557.

32 V. Choudhary, I. Kaddour-Djebbar, R. Alaisami, M. V. Kumar and W. B. Bollag, Mitofusin 1 degradation is induced by a disruptor of mitochondrial calcium homeostasis, CGP37157: a role in apoptosis in prostate cancer cells, *Int. J. Oncol.*, 2014, **44**, 1767–1773.

33 D. Arango, K. Morohashi, A. Yilmaz, K. Kuramochi, A. Parihar, B. Brahimaj, E. Grotewold and A. I. Doseff, Molecular basis for the action of a dietary flavonoid revealed by the comprehensive identification of apigenin human targets, *Proc. Natl. Acad. Sci. U. S. A.*, 2013, **110**, E2153–E2162.

34 M. Willenborg, U. Panten and I. Rustenbeck, Triggering and amplification of insulin secretion by dimethyl alpha-ketoglutarate, a membrane permeable alpha-ketoglutarate analogue, *Eur. J. Pharmacol.*, 2009, **607**, 41–46.

35 D. R. Sharma, A. Sunkaria, W. Y. Wani, R. K. Sharma, R. J. Kandimalla, A. Bal and K. D. Gill, Aluminium induced oxidative stress results in decreased mitochondrial biogenesis *via* modulation of PGC-1α expression, *Toxicol. Appl. Pharmacol.*, 2013, **273**, 365–380.

36 R. J. Mailloux, J. Lemire and V. D. Appanna, Hepatic response to aluminum toxicity: dyslipidemia and liver diseases, *Exp. Cell Res.*, 2011, **317**, 2231–2238.

37 W. Yue, Z. Chen, H. Liu, C. Yan, M. Chen, D. Feng, C. Yan, H. Wu, L. Du, Y. Wang, J. Liu, X. Huang, L. Xia, L. Liu, X. Wang, H. Jin, J. Wang, Z. Song, X. Hao and Q. Chen, A small natural molecule promotes mitochondrial fusion through inhibition of the deubiquitinase USP30, *Cell Res.*, 2014, **24**, 482–496.

38 S. Lee, F. H. Sterky, A. Mourier, M. Terzioglu, S. Cullheim, L. Olson and N. G. Larsson, Mitofusin 2 is necessary for striatal axonal projections of midbrain dopamine neurons, *Hum. Mol. Genet.*, 2012, **21**, 4827–4835.

The Journal of Toxicological Sciences (J. Toxicol. Sci.)
Vol.41, No.2, 207-215, 2016

Original Article

Tributyltin induces G2/M cell cycle arrest via NAD+-dependent isocitrate dehydrogenase in human embryonic carcinoma cells

Miki Asanagi[1,2,*], Shigeru Yamada[1,*], Naoya Hirata[1], Hiroshi Itagaki[2], Yaichiro Kotake[3], Yuko Sekino[1] and Yasunari Kanda[1]

[1]*Division of Pharmacology, National Institute of Health Sciences, 1-18-1 Kamiyoga, Setagaya-ku, Tokyo 158-8501, Japan*
[2]*Faculty of Engineering, Department of Materials Science and Engineering, Yokohama National University, 79-5 Tokiwadai, Hodogaya-ku, Yokohama, Kanagawa 240-8501, Japan*
[3]*Department of Xenobiotic Metabolism and Molecular Toxicology, Graduate School of Biomedical and Health Sciences, Hiroshima University, 1-2-3 Kasumi, Minami-ku, Hiroshima 734-8553, Japan*

(Received November 16, 2015; Accepted December 28, 2015)

ABSTRACT — Organotin compounds, such as tributyltin (TBT), are well-known endocrine-disrupting chemicals (EDCs). We have recently reported that TBT induces growth arrest in the human embryonic carcinoma cell line NT2/D1 at nanomolar levels by inhibiting NAD+-dependent isocitrate dehydrogenase (NAD-IDH), which catalyzes the irreversible conversion of isocitrate to α-ketoglutarate. However, the molecular mechanisms by which NAD-IDH mediates TBT toxicity remain unclear. In the present study, we examined whether TBT at nanomolar levels affects cell cycle progression in NT2/D1 cells. Propidium iodide staining revealed that TBT reduced the ratio of cells in the G1 phase and increased the ratio of cells in the G2/M phase. TBT also reduced cell division cycle 25C (cdc25C) and cyclin B1, which are key regulators of G2/M progression. Furthermore, apigenin, an inhibitor of NAD-IDH, mimicked the effects of TBT. The G2/M arrest induced by TBT was abolished by NAD-IDHα knockdown. Treatment with a cell-permeable α-ketoglutarate analogue recovered the effect of TBT, suggesting the involvement of NAD-IDH. Taken together, our data suggest that TBT at nanomolar levels induced G2/M cell cycle arrest via NAD-IDH in NT2/D1 cells. Thus, cell cycle analysis in embryonic cells could be used to assess cytotoxicity associated with nanomolar level exposure of EDCs.

Key words: Embryonic carcinoma cells, Tributyltin, Cell cycle, Isocitrate dehydrogenase

INTRODUCTION

Organotin compounds, such as tributyltin (TBT) are typical environmental contaminants and are categorized as endocrine-disrupting chemicals (EDCs), which cause neurodevelopmental defects including behavioral abnormality and teratogenicity (Dopp *et al.*, 2004; Gårdlund *et al.*, 1991). Although the use of TBT has already been restricted, butyltin compounds, including TBT, can still be found in human blood at concentrations between 50 and 400 nM. There is still concern about TBT toxicity for human health (Whalen *et al.*, 1999).

Several studies have revealed that TBT activates retinoid X receptor (RXR) and/or peroxisome proliferator-activated receptor γ (PPARγ) (Kanayama *et al.*, 2005). TBT at nanomolar levels has the ability to bind with higher affinity than the intrinsic ligands and these genomic transcriptional activations have been reported to mediate neurodevelopmental defects in *Xenopus* (Yu *et al.*, 2011). In contrast, TBT elicits non-genomic pathway in mature rat neurons and brain tissues at nearly micromolar levels. For instance, TBT induces neuronal death by inhibiting mammalian target of rapamycin (mTOR) in rat cortical neurons (Nakatsu *et al.*, 2010). TBT also induces neuronal degeneration via the generation of reactive oxygen species along with marked reduction of GSH/GSSG levels in the rat brain (Mitra *et al.*, 2013).

Cell stress is known to trigger a checkpoint that arrests cells in the G1 or G2 phase (Gabrielli *et al.*, 2012). The cell cycle is tightly regulated by spatial and temporal

Correspondence: Yasunari Kanda (E-mail: kanda@nihs.go.jp)
*These authors equally contributed to this work.

expression of cell cycle proteins and divided into p53-dependent and p53-independent regulations (Shackelford *et al.*, 1999). In the p53-independent regulations, cdc25C phosphatase, a mitotic inducer, plays a central role in G2/M phase regulation. Cdc25C activates cyclin B1/cyclin-dependent kinase (Cdk) 1 complex, which triggers mitosis (Donzelli and Draetta, 2003) and cyclin B1 accumulates during the S and G2 phases, followed by nuclear translocation and association with Cdk1. Protein levels of these cell cycle regulators are strictly regulated during cell cycle progression. Ultraviolet irradiation or toxic drugs are known to cause G2 arrest by the inactivation of cyclin B1/Cdk1 via p53 induction followed by the upregulation of p21, a Cdk inhibitor and/or cdc25C downregulation by degradation (Chaudhary *et al.*, 2013; Kawabe, 2004; Nam *et al.*, 2010; Ouyang *et al.*, 2009).

We have previously reported that nanomolar levels of TBT induce growth arrest of neuronal precursor NT2/D1 cells as a model of neurodevelopmental stage (Yamada *et al.*, 2013). We found that TBT causes growth arrest via mitochondrial NAD^+-dependent isocitrate dehydrogenase (NAD-IDH), which catalyzes the irreversible conversion of isocitrate to α-ketoglutarate in the tricarboxylic acid (TCA) cycle (Yamada *et al.*, 2014). Based on these observations, we hypothesized that nanomolar levels of TBT could also affect cell cycle progression via NAD-IDH in NT2/D1 cells.

In the present study, we investigated the effect of TBT on cell cycle progression in NT2/D1 cells. We found that exposure to 100 nM TBT reduced the protein levels of cell cycle regulators and induced G2/M cell cycle arrest through an NAD-IDH-dependent mechanism. Thus, cell cycle regulation via NAD-IDH is a novel target of TBT-induced toxicity in human embryonic carcinoma cells.

MATERIALS AND METHODS

Cell culture

NT2/D1 cells were obtained from the American Type Culture Collection (Manassas, VA, USA). The cells were cultured in Dulbecco's modified Eagle's medium (DMEM; Sigma-Aldrich, St. Louis, MO, USA) supplemented with 10% fetal bovine serum (FBS; Biological Industries, Ashrat, Israel) and 0.05 mg/mL penicillin-streptomycin mixture (Life Technologies, Carlsbad, CA, USA) at 37°C in 5% CO_2.

Cell cycle analysis

The cells were trypsinized and harvested in phosphate buffered saline. Then the cells were resuspended in 70% ethanol for 30 min at -20°C. The fixed cells were collected by centrifugation and resuspended in propidium iodide (PI)/RNase Staining Buffer (BD Biosciences, San Jose, CA, USA) followed by incubation at room temperature for 30 min in the dark. Cell cycle distribution was determined by flow cytometric analysis of the DNA content using the BD FACS Aria II system (BD Biosciences). Data were analyzed by Modfit LT 4.0 (Verity Software House, Topsham, ME, USA).

Real-time PCR

Total RNA was extracted from NT2/D1 cells using TRIzol reagent (Life Technologies), and quantitative real-time reverse transcription (RT)-PCR was performed with QuantiTect SYBR Green RT-PCR Kit (QIAGEN, Valencia, CA, USA) using an ABI PRISM 7900HT sequence detection system (Applied Biosystems, Foster City, CA, USA) as previously reported (Hirata *et al.*, 2014). The relative change in transcript amounts was normalized to the expression levels of glyceraldehyde-3-phosphate dehydrogenase (GAPDH). The following primer sequences were used for real-time PCR analysis: human cdc25C: forward, 5′-AGGCAGCCTTGAGTTGCATAGAGA-3′, reverse, 5′-AGAGTTGGCTGGCTTGTGAGAAGA-3′;humancyclin B1:forward,5′-CGGGAAGTCACTGGAAACAT-3′,reverse, 5′-AAACATGGCAGTGACACCAA-3′; human GAPDH: forward, 5′-GTCTCCTCTGACTTCAACAGCG-3′, reverse, 5′-ACCACCCTGTTGCTGTAGCCAA-3′.

Western blot analysis

Western blot analysis was performed as previously reported (Kanda *et al.*, 2011). Briefly, cells were lysed with Cell Lysis Buffer (Cell Signaling Technology, Danvers, MA, USA). The proteins were then separated by sodium dodecyl sulfate-polyacrylamide gel electrophoresis (SDS-PAGE) and electrophoretically transferred to Immobilon-P membrane (Millipore, Billerica, MA, USA). The membranes were probed with an anti-cdc25C monoclonal antibody (1:1,000; Cell Signaling Technology), an anti-cyclin B1 monoclonal antibody (1:1,000; Cell Signaling Technology), and an anti-GAPDH polyclonal antibody (1:2,500; Abcam, Cambridge, UK) followed by incubation with horseradish peroxidase-conjugated secondary antibodies against rabbit or mouse IgG (Cel Signaling Technology). The bands were visualized using the ECL Western Blotting Analysis System (GE Healthcare, Buckinghamshire, UK), and images were acquired using a LAS-3000 Imager (FUJIFILM UK Ltd., Systems, Bedford, UK).

NAD-IDH activity assay

NAD-IDH activity was determined using the

Isocitrate Dehydrogenase Activity Colorimetric Assay Kit (Biovision, Mountain View, CA, USA), according to the manufacturer's instructions. Briefly, NT2/D1 cells were lysed in an assay buffer provided in the kit. The lysate was centrifuged at 14,000 *g* for 15 min, and the cleared supernatant was used for the assay.

NAD-IDHα knockdown

Knockdown studies were performed using NAD-IDHα shRNA lentiviruses from Sigma-Aldrich (MISSION shRNA) according to the manufacturer's protocol. A scrambled hairpin sequence was used as a negative control. Briefly, the cells were infected with the viruses at a multiplicity of infection of 10 in presence of 8 μg/mL hexadimethrine bromide (Sigma-Aldrich) for 24 hr, and were then subjected to selection with 0.5 μg/mL puromycin for 72 hr for further functional analyses.

Chemicals and reagents

Tributyltin Chloride was obtained from Tokyo Chemical Industry (Tokyo, Japan). Tin acetate (TA), apigenin, and dimethyl α-ketoglutarate (DMKG) were obtained from Sigma-Aldrich.

Statistical analysis

All data were presented as mean ± S.D. Analysis of variance (ANOVA) followed by post hoc Tukey's test was used to analyze the data in Figs. 1C, 1D, 1E, 2A, 2B, 3C, 4E, 5A, 5B, 6A and 6B. Student's t test was used to analyze the data in Figs. 3A, 3B, 4A, 4B and 4C. P-values less than 0.05 were considered to be statistically significant.

RESULTS

Effect of TBT on cell cycle progression

We have previously found that 100 nM TBT induced growth arrest in NT2/D1 cells (Yamada *et al.*, 2013). Here we investigated whether TBT affects cell cycle progression. Exposure to 100 nM TBT for 48 hr decreased the proportion of cells in the G1 phase (51.9% decrease) and increased of the proportion of cells in the G2/M phase (79.6% increase), compared with untreated control cells (Figs. 1A-E). In contrast, TBT did not affect the proportion of cells in the S phase. Moreover, exposure to tin acetate (TA), which is less toxic, did not affect cell cycle progression. These data suggest that TBT induces G2/M cell cycle arrest in the cells.

TBT exposure reduces G2/M cell cycle regulators, cdc25C and cyclin B1

To examine the molecular mechanism by which TBT induces G2/M cell cycle arrest, we assessed the protein levels of p53, a major cell cycle regulator. We found that p53 protein level was reduced after 24 hr of TBT treatment, whereas cisplatin, which is known to cause p53-dependent G2/M cell cycle arrest (Pani *et al.*, 2007), increased p53 levels (Supplementary Fig. 1). Since we could not observe p53-dependency in TBT-induced G2/M cell cycle arrest, we assessed cdc25C and its downstream factor, cyclin B1, which are also involved in G2/M progression of cell cycle. Western blot analysis revealed that cdc25C and cyclin B1 protein levels were reduced after 24 hr of TBT treatment (Fig. 2A). In contrast, exposure to TA did not affect cdc25C and cyclin B1 protein levels. Equal GAPDH protein expression levels were confirmed as a loading control. Next, we assessed the gene expression of cdc25C and cyclin B1. However, real-time PCR analysis showed that gene expression was not significantly altered by TBT exposure for both 24 and 48 hr (Fig. 2B). These data suggest that TBT-induced G2/M cell cycle arrest is caused by reduction of cdc25C and cyclin B1 proteins.

TBT induces G2/M cell cycle arrest via NAD-IDH

To investigate the molecular mechanisms by which cdc25C is degraded and G2/M cell cycle arrest is induced, we examined the effect of the PPARγ agonist rosiglitazone (RGZ), which is the genomic target of TBT. We found that RGZ did not induce G1 phase reduction and G2/M phase increase (Figs. 3A and B). RGZ at 100 nM induced PPARγ gene expression at similar level to 100 nM TBT in NT2/D1 cells (Fig. 3C), confirming the agonistic effect of RGZ on PPARγ expression described in previous report (Benkirane *et al.*, 2006). These data suggest that TBT induces G2/M cell cycle arrest in NT2/D1 cells through a non-genomic pathway. We next examined the involvement of the non-genomic target NAD-IDH. We used an NAD-IDH inhibitor apigenin (Arango *et al.*, 2013) at 10 μM, which reduced NAD-IDH activity to a level (22.4%) (Fig. 4A). As previously reported, 100 nM TBT had a similar inhibitory effect (24.4%; Yamada *et al.*, 2014). Treatment with apigenin (10 μM, 48 hr) decreased G1 phase ratio (58.6% decrease) and increased G2/M phase ratio (98.1% increase) (Figs. 4B and C). Similar to TBT, apigenin reduced protein expression of cdc25C and cyclin B1 without affecting gene expression (Figs. 4D and E). To further confirm the effect of apigenin, we performed knockdown (KD) experiments of NAD-IDHα, the catalytic subunit of NAD-IDH, using lentivirus-delivered shRNAs. Real-time PCR analysis showed that KD efficiency was approximately 40% (Yamada *et al.*, 2014). We could not obtain more highly KD cells because of cell

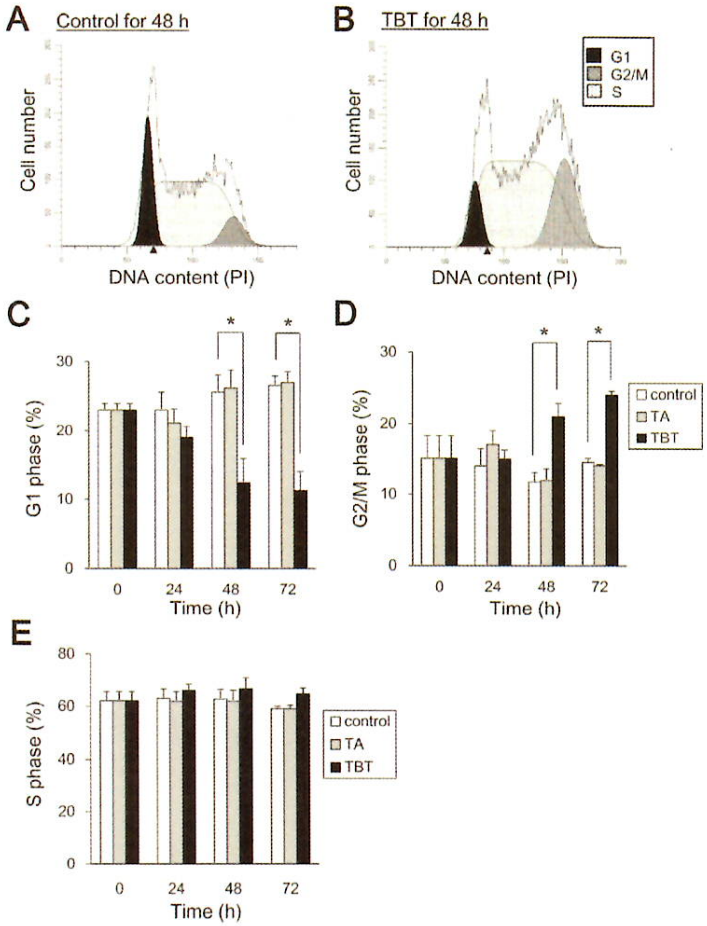

Fig. 1. Effect of TBT on cell cycle progression in NT2/D1 cells. Cells were exposed to 100 nM TA or TBT for 24, 48 or 72 hr. Cells were stained with propidium iodide (PI). Cell cycle distribution was determined by flow cytometric analysis of the DNA content on BD FACS Aria II. Representative cell cycle data in control (A) and TBT (B)-treated cells. The area ratio of G1 (C), G2/M (D) and S (E) phases was determined by Modfit LT 4.0. Data represent mean ± S.D. (n = 3). *P < 0.05.

death. Due to partial KD of the NAD-IDHα gene, NAD-IDH activity decreased by 22%, which is comparable to its decreased levels by TBT. In our previous studies, we observed that NAD-IDHα KD recovered the inhibitory effect of TBT on ATP content (Yamada *et al.*, 2014). This might be because the TBT target NAD-IDHα was already inhibited by shRNA and further inhibition by TBT was not observed in the knockdown cells. Similar to these data, NAD-IDHα KD abolished the TBT-induced G1 phase reduction and G2/M phase increase (Figs. 5A and B), suggesting the involvement of NAD-IDH on TBT effects. NAD-IDHα KD tended to decrease the proportion of cells in the G1 phase (24.1% ± 0.55 to 23.2% ± 0.34) and increase the proportion of cells in the G2/M phase (17.5% ± 1.6 to 20.3% ± 0.62), compared with control (Figs. 5A and B). Moreover, NAD-IDHα KD also abolished the TBT-induced reduction of cdc25C and cyclin B1 proteins (Fig. 5C). NAD-IDHα KD reduced the basal levels of cdc25C and cyclin B1 proteins, compared with control (Fig. 5C). These data suggest that NAD-IDH mediates TBT-induced G2/M cell cycle arrest in NT2/D1 cells. To further confirm the involvement of NAD-IDH, we treated the cells with dimethyl α-ketoglutarate (DMKG), a cell-permeable analog of α-ketoglutarate (Willenborg *et al.*, 2009). Incubation with DMKG prevented TBT-induced G2/M cell cycle arrest in NT2/D1 cells and

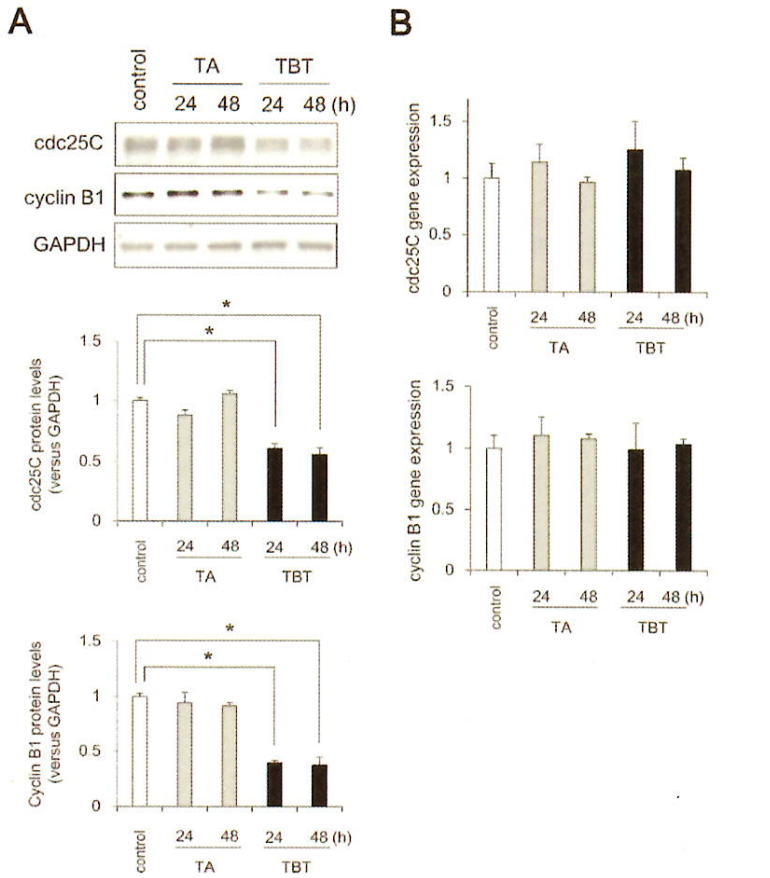

Fig. 2. Effect of TBT on expression levels of G2/M cell cycle regulators in NT2/D1 cells. After TBT exposure for 24 and 48 hr, protein expression was analyzed by western blot using anti-cdc25C, cyclin B1, or GAPDH antibodies (A). After TBT exposure for 24 or 48 hr, the expression of G2/M cell cycle regulators was analyzed by real time PCR (B). The gene expression was not significantly altered by TBT exposure. Data represent mean ± S.D. (n = 3).

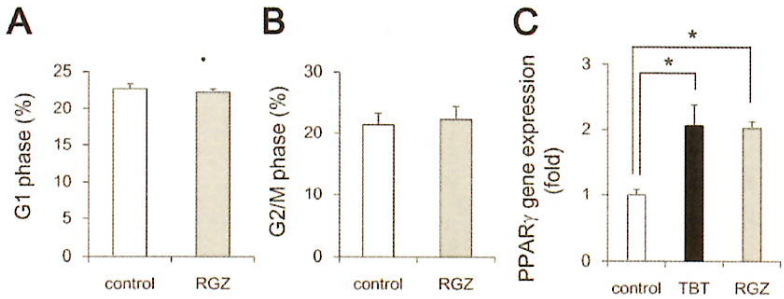

Fig. 3. Effect of RGZ on cell cycle progression in NT2/D1 cells. After RGZ exposure for 48 hr, cells were stained with propidium iodide (PI). The cell cycle distribution was determined by flow cytometric analysis of the DNA content using BD FACS Aria II. The ratio of G1 (A) and G2/M (B) phases was determined by Modfit LT 4.0. After exposure to TBT or RGZ, the expression of PPARγ was analyzed by real time PCR (C). The gene expression was comparably increased upon TBT or RGZ exposure. Data represent mean ± S.D. (n = 3). *P < 0.05.

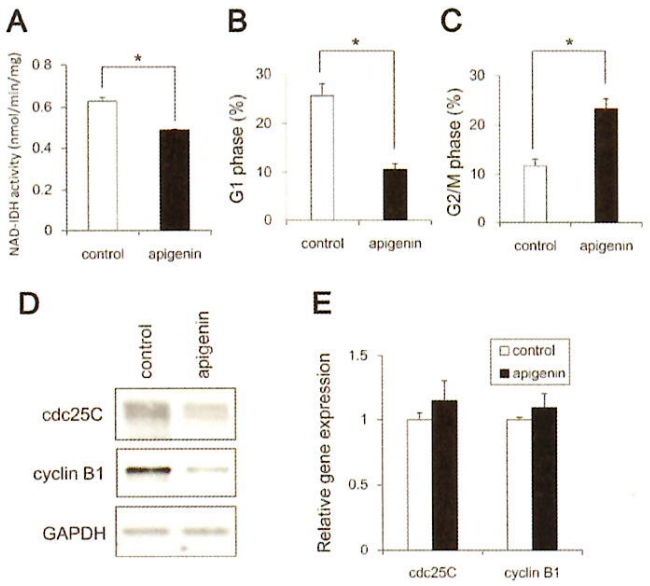

Fig. 4. Effect of apigenin on cell cycle progression in NT2/D1 cells. Cells were exposed to 10 μM apigenin for 24 hr and then determined NAD-IDH activity (A). Moreover, after exposure to apigenin for 48 hr, the cell cycle distribution was determined by flow cytometric analysis of the DNA content using BD FACS Aria II. The ratio of G1 (B) and G2/M (C) phases was determined by Modfit LT 4.0. The protein expressions in the cell lysate were analyzed by western blot using anti-cdc25C, cyclin B1, or GAPDH antibodies (D). The expression of G2/M cell cycle regulators was analyzed by real time PCR (E). The gene expression was not significantly altered upon apigenin exposure. Data represent mean ± S.D. (n = 3). *P < 0.05.

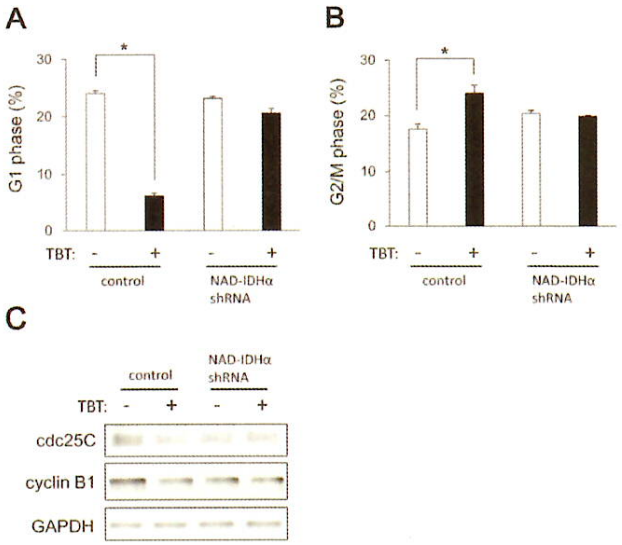

Fig. 5. Effect of NAD-IDH knockdown on cell cycle progression in NT2/D1 cells. Cells were infected with lentiviruses to express a shRNA against NAD-IDHα or a scrambled sequence shRNA (control). The infected cells were subjected to selection with 0.5 μg/mL puromycin for 72 hr and were then exposed to TBT at 100 nM for 48 hr. After staining with PI, cell cycle distribution was determined by flow cytometric analysis of the DNA content using BD FACS Aria II. The ratio of G1 (A) and G2/M (B) phases was analyzed by Modfit LT 4.0. The protein expressions in cell lysates were analyzed by western blot using anti-cdc25C, cyclin B1, or GAPDH antibodies (C). Data represent mean ± S.D. (n = 3). *P < 0.05.

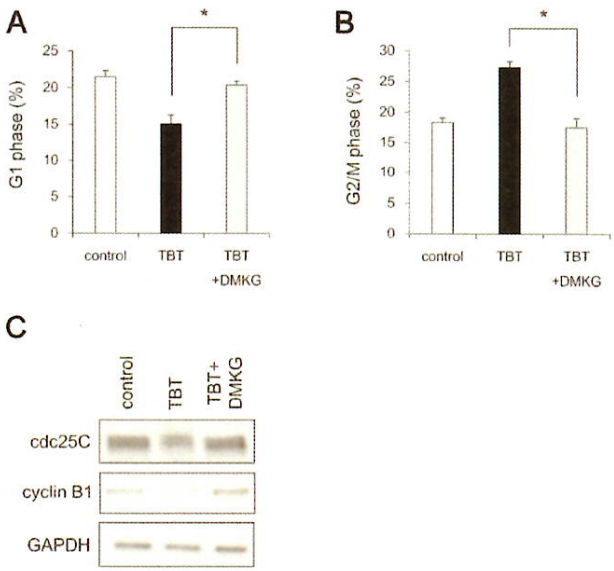

Fig. 6. Effect of dimethyl α-ketoglutarate (DMKG) on TBT-induced G2/M cell cycle arrest in NT2/D1 cells. Cells were exposed to 100 nM TBT and 7 mM DMKG for 48 hr. Cells were then stained with propidium iodide (PI) and cell cycle distribution was determined by flow cytometric analysis of the DNA content using BD FACS Aria II. The ratio of G1 (A) and G2/M (B) phases was analyzed by Modfit LT 4.0. Next, the protein expressions in cell lysates were analyzed by western blot using anti-cdc25C, cyclin B1, or GAPDH antibodies (C). Data represent mean ± S.D. (n = 3). *P < 0.05.

recovered the ratio of G1 and G2/M phases to the basal level (Figs. 6A and B). DMKG treatment also recovered TBT-induced protein reduction of cdc25C and cyclin B1 (Fig. 6C). Taken together, these data suggest that NAD-IDH mediates TBT-induced G2/M cell cycle arrest via cdc25C reduction in NT2/D1 cells.

DISCUSSION

Our data suggest that nanomolar TBT levels induce G2/M cell cycle arrest through the protein reduction of cdc25C and thereafter cyclin B1 (Figs. 1 and 2). Since the protein expression of p53 is decreased after TBT exposure, TBT-induced G2/M cell cycle arrest seems to be p53 independent. Consistent with our data, recent study has reported that nearly micromolar TBT levels induce G2/M cell cycle arrest in human amniotic cells via protein phosphatase (PP) 2A inhibition-mediated extracellular-signal-regulated kinase (ERK) inactivation (Zhang *et al.*, 2014). Since we did not observe the reduction of phospho-ERK in NT2/D1 cells after nanomolar levels of TBT exposure (data not shown), the mechanism of inducing G2 arrest may differ depending on the TBT levels and cell type. Moreover, several chemical stressors have been reported to cause G2/M cell cycle arrest through the protein reduction of cell cycle regulators (Chaudhary *et al.*, 2013; Nam *et al.*, 2010; Ouyang *et al.*, 2009). For instance, 4-Hydroxynonenal, an inducer of oxidative stress, causes DNA damage and induces G2/M cell cycle arrest in hepatocellular carcinoma HepG2 and Hep3B cells, following reduction of cdc25C and thereafter cyclin B1 proteins in a p53-independent manner (Chaudhary *et al.*, 2013). Reduction of cdc25C protein may be mediated by the ubiquitin-proteasome system in NT2/D1 cells. Cdc25C has been reported to be degraded via ubiquitination by BRCA1 during G2/M cell cycle arrest in breast cancer cell lines (Shabbeer *et al.*, 2013). During G2/M cell cycle arrest, another cell cycle regulators, such as Plk1, cdc25A and CDK1, are also known to be degraded by ubiquitin ligases, such as multi-subunit E3 ubiquitin ligases, Skp1-Cullin1-F-box Complex (SCF) or Anaphase Promoting Complex (APC) (Bassermann and Pagano, 2010). Further studies should determine whether ubiquitin ligases are involved in TBT-induced cdc25C reduction and subsequent G2/M cell cycle arrest in embryonic cells.

Our data using apigenin showed that TBT-induced G2/M cell cycle arrest is caused by NAD-IDH inhibition

(Fig. 4) and the data were verified by NAD-IDH knockdown and DMKG experiments (Figs. 5, 6). We used apigenin as a NAD-IDH inhibitor. We also confirmed the data by knockdown experiments. Since Apigenin has been reported to inhibit not only NAD-IDH but also hnRNPA2 and NF-κB (Arango *et al.*, 2013), we can not rule out the possibility that apigenin-induced G2/M cell cycle arrest was induced by other targets. Our previous report indicates that TBT induces mitochondrial dysfunction, such as impaired mitochondrial morphological dynamics and reduced ATP production via NAD-IDH in embryonic carcinoma cells (Yamada *et al.*, 2015). Considering that NAD-IDH is a mitochondrial enzyme, TBT-induced G2/M cell cycle arrest is caused by mitochondrial dysfunction through NAD-IDH inhibition. NAD-IDH catalyzes the reduction of NAD to NADH, which is oxidized by the electron transport chain and is required to generate proton electrochemical gradients across the inner mitochondrial membrane (Saraste, 1999). Thus, inhibition of NAD-IDH by TBT may reduce the NADH supply, thereby dissipating the proton electrochemical gradient. Intracellular Ca^{2+} may be also involved in mitochondrial dysfunction. Previous reports have shown that several anticancer drugs induce G2/M cell cycle arrest and apoptosis by depolarizing mitochondrial membrane potential and increasing intracellular Ca^{2+} (Fang *et al.*, 2014; Guo *et al.*, 2014). With respect to intracellular Ca^{2+}, there has been also reported that TBT induces mobilization of Ca^{2+} from intracellular stores and results in phosphorylation of MAPKs because its suppression by chelation of intracellular Ca^{2+} in human T lymphoblastoid cells (Yu *et al.*, 2000). Thus, Ca^{2+} release from depolarized mitochondria may induce G2/M cell cycle arrest after TBT exposure. Further studies should determine how the downstream signaling of NAD-IDH induces reduction of the cdc25C protein and subsequent G2/M cell cycle arrest after TBT exposure in embryonic cells.

In our previous studies, we have observed that TBT degrades mitofusin proteins and induces mitochondrial fission via the NAD-IDH inhibition. Moreover, we have also shown that TBT results in growth arrest by targeting the glycolytic systems (Yamada *et al.*, 2014). Both mitochondrial fission and glycolysis have been reported to be linked to cell cycle alterations (Yamamori *et al.*, 2015; Zhai *et al.*, 2013). Thus, we are currently investigating whether TBT-induced mitochondrial fission or glycolytic inhibition are linked to G2/M cell cycle arrest or not.

In summary, we demonstrate that TBT mediates G2/M cell cycle arrest through inhibition of NAD-IDH, representing a novel non-genomic pathway of TBT-induced toxicity (Fig. 7). These negative effects of TBT on the cell cycle could result in direct inhibition of cell growth. Thus, TBT-induced G2/M cell cycle arrest via NAD-IDH in embryonic cells may represent a novel mechanism of cytotoxicity associated with nanomolar level exposure of EDCs.

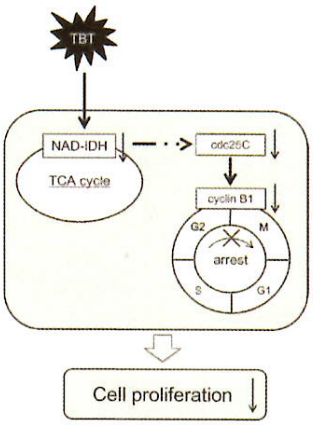

Fig. 7. Proposed model of TBT toxicity through non-genomic pathways in human embryonic carcinoma cells. Nanomolar TBT levels inhibit NAD-IDH activity. TBT induces G2/M cell cycle arrest via the protein reduction of cdc25C and its downstream target, cyclin B1. This TBT-induced G2/M cell cycle arrest may mediate cell growth inhibition.

ACKNOWLEDGMENTS

This work was supported by a Health and Labour Sciences Research Grant from the Ministry of Health, Labour and Welfare, Japan (#H25-Kagaku-Ippan-002 to Y. Kanda), a Grant-in-Aid for Scientific Research from the Ministry of Education, Culture, Sports, Science, and Technology, Japan (#26293056, #26670041 to Y. Kanda), the Research on Regulatory Harmonization and Evaluation of Pharmaceuticals, Medical Devices, Regenerative and Cellular Therapy Products, Gene Therapy Products, and Cosmetics from Japan Agency for Medical Research and development, AMED (To Y. Sekino), and a grant from the Smoking Research Foundation (Y. Kanda).

Conflict of interest---- The authors declare that there is no conflict of interest.

REFERENCES

Arango, D., Morohashi, K., Yilmaz, A., Kuramochi, K., Parihar, A., Brahimaj, B., Grotewold, E. and Doseff, A.I. (2013): Molecular basis for the action of a dietary flavonoid revealed by the com-

prehensive identification of apigenin human targets. Proc. Natl. Acad. Sci. USA, **110**, E2153-E2162.

Bassermann, F. and Pagano, M. (2010): Dissecting the role of ubiquitylation in the DNA damage response checkpoint in G2. Cell Death Differ., **17**, 78-85.

Benkirane, K., Amiri, F., Diep, Q.N., El Mabrouk, M. and Schiffrin, E.L. (2006): PPAR-gamma inhibits ANG II-induced cell growth via SHIP2 and 4E-BP1. Am. J. Physiol. Heart Circ. Physiol., **290**, H390-H397.

Chaudhary, P., Sharma, R., Sahu, M., Vishwanatha, J.K., Awasthi, S. and Awasthi, Y.C. (2013): 4-Hydroxynonenal induces G2/M phase cell cycle arrest by activation of the ataxia telangiectasia mutated and Rad3-related protein (ATR)/checkpoint kinase 1 (Chk1) signaling pathway. J. Biol. Chem., **288**, 20532-20546.

Donzelli, M. and Draetta, G.F. (2003): Regulating mammalian checkpoints through Cdc25 inactivation. EMBO Rep., **4**, 671-677.

Dopp, E., Hartmann, L.M., Florea, A.M., Rettenmeier, A.W. and Hirner, A.V. (2004): Environmental distribution, analysis, and toxicity of organometal(loid) compounds. Crit. Rev. Toxicol., **34**, 301-333.

Fang, C., Zhang, J., Qi, D., Fan, X., Luo, J., Liu, L. and Tan, Q. (2014): Evodiamine induces G2/M arrest and apoptosis via mitochondrial and endoplasmic reticulum pathways in H446 and H1688 human small-cell lung cancer cells. PLoS One, **9**, e115204.

Gabrielli, B., Brooks, K. and Pavey, S. (2012): Defective cell cycle checkpoints as targets for anti-cancer therapies. Front. Pharmacol., **3**, 9.

Gårdlund, A.T., Archer, T., Danielsen, K., Danielsson, B., Frederiksson, A., Lindquist, N.G., Lindström, H. and Luthman, J. (1991): Effects of prenatal exposure to tributyltin and trihexyltin on behaviour in rats. Neurotoxicol. Teratol., **13**, 99-105.

Guo, J., Zhao, W., Hao, W., Ren, G., Lu, J. and Chen, X. (2014): Cucurbitacin B induces DNA damage, G2/M phase arrest, and apoptosis mediated by reactive oxygen species (ROS) in leukemia K562 cells. Anticancer Agents Med. Chem., **14**, 1146-1153.

Hirata, N., Yamada, S., Shoda, T., Kurihara, M., Sekino, Y. and Kanda, Y. (2014): Sphingosine-1-phosphate promotes expansion of cancer stem cells via S1PR3 by a ligand-independent Notch activation. Nat. Commun., **5**, 4806.

Kanayama, T., Kobayashi, N., Mamiya, S., Nakanishi, T. and Nishikawa, J. (2005): Organotin compounds promote adipocyte differentiation as agonists of the peroxisome proliferator-activated receptor gamma/retinoid X receptor pathway. Mol. Pharmacol., **67**, 766-774.

Kanda, Y., Hinata, T., Kang, S.W. and Watanabe, Y. (2011): Reactive oxygen species mediate adipocyte differentiation in mesenchymal stem cells. Life Sci., **89**, 250-258.

Kawabe, T. (2004): G2 checkpoint abrogators as anticancer drugs. Mol. Cancer Ther., **3**, 513-519.

Mitra, S., Gera, R., Siddiqui, W.A. and Khandelwal, S. (2013): Tributyltin induces oxidative damage, inflammation and apoptosis via disturbance in blood–brain barrier and metal homeostasis in cerebral cortex of rat brain: an *in vivo* and *in vitro* study. Toxicology, **310**, 39-52.

Nakatsu, Y., Kotake, Y., Takai, N. and Ohta, S. (2010): Involvement of autophagy via mammalian target of rapamycin (mTOR) inhibition in tributyltin-induced neuronal cell death. J. Toxicol. Sci., **35**, 245-251.

Nam, C., Doi, K. and Nakayama, H. (2010): Etoposide induces G2/M arrest and apoptosis in neural progenitor cells via DNA damage and an ATM/p53-related pathway. Histol. Histopathol., **25**, 485-493.

Ouyang, G., Yao, L., Ruan, K., Song, G., Mao, Y. and Bao, S. (2009): Genistein induces G2/M cell cycle arrest and apoptosis of human ovarian cancer cells via activation of DNA damage checkpoint pathways. Cell Biol. Int., **33**, 1237-1244.

Pani, E., Stojic, L., El-Shemerly, M., Jiricny, J. and Ferrari, S. (2007): Mismatch repair status and the response of human cells to cisplatin. Cell Cycle, **6**, 1796-1802.

Saraste, M. (1999): Oxidative phosphorylation at the fin de siècle. Science, **283**, 1488-1493.

Shabbeer, S., Omer, D., Berneman, D., Weitzman, O., Alpaugh, A., Pietraszkiewicz, A., Metsuyanim, S., Shainskaya, A., Papa, M.Z. and Yarden, R.I. (2013): BRCA1 targets G2/M cell cycle proteins for ubiquitination and proteasomal degradation. Oncogene, **32**, 5005-5016.

Shackelford, R.E., Kaufmann, W.K. and Paules, R.S. (1999): Cell cycle control, checkpoint mechanisms, and genotoxic stress. Environ. Health Perspect., **107**, 5-24.

Whalen, M.M., Loganathan, B.G. and Kannan, K. (1999): Immunotoxicity of environmentally relevant concentrations of butyltins on human natural killer cells *in vitro*. Environ. Res., **81**, 108-116.

Willenborg, M., Panten, U. and Rustenbeck, I. (2009): Triggering and amplification of insulin secretion by dimethyl alpha-ketoglutarate, a membrane permeable alpha-ketoglutarate analogue. Eur. J. Pharmacol., **607**, 41-46.

Yamada, S., Kotake, Y., Sekino, Y. and Kanda, Y. (2013): AMP-activated protein kinase-mediated glucose transport as a novel target of tributyltin in human embryonic carcinoma cells. Metallomics, **5**, 484-491.

Yamada, S., Kotake, Y., Demizu, Y., Kurihara, M., Sekino, Y. and Kanda, Y. (2014): NAD-dependent isocitrate dehydrogenase as a novel target of tributyltin in human embryonic carcinoma cells. Sci. Rep., **4**, 5952.

Yamada, S., Kotake, Y., Nakano, M., Sekino, Y. and Kanda, Y. (2015): Tributyltin induces mitochondrial fission through NAD-IDH dependent mitofusin degradation in human embryonic carcinoma cells. Metallomics, **7**, 1240-1246.

Yamamori, T., Ike, S., Bo, T., Sasagawa, T., Sakai, Y., Suzuki, M., Yamamoto, K., Nagane, M., Yasui, H. and Inanami, O. (2015): Inhibition of the mitochondrial fission protein dynamin-related protein 1 (Drp1) impairs mitochondrial fission and mitoticcatastrophe after X-irradiation. Mol. Biol. Cell, **26**, 4607-4617.

Yu, L., Zhang, X., Yuan, J., Cao, Q., Liu, J., Zhu, P. and Shi, H. (2011): Teratogenic effects of triphenyltin on embryos of amphibian (*Xenopus tropicalis*): a phenotypic comparison with the retinoid X and retinoic acid receptor ligands. J. Hazard Mater., **192**, 1860-1868.

Yu, Z.P., Matsuoka, M., Wispriyono, B., Iryo, Y. and Igisu, H. (2000): Activation of mitogen-activated protein kinases by tributyltin in CCRF-CEM cells: role of intracellular Ca(2+). Toxicol. Appl. Pharmacol., **168**, 200-207.

Zhai, X., Yang, Y., Wan, J., Zhu, R. and Wu, Y. (2013): Inhibition of LDH-A by oxamate induces G2/M arrest, apoptosis and increases radiosensitivity in nasopharyngeal carcinoma cells. Oncol. Rep., **30**, 2983-2991.

Zhang, Y., Go, Z. and Xu, L. (2014): Tributyltin induces a G2/M cell cycle arrest in human amniotic cells via PP2A inhibition-mediated inactivation of the ERK1/2 cascades. Environ. Toxicol. Pharmacol., **37**, 812-818.

Biochemical and Biophysical Research Communications 470 (2016) 300–305

Contents lists available at ScienceDirect

Biochemical and Biophysical Research Communications

journal homepage: www.elsevier.com/locate/ybbrc

Nicotine induces mitochondrial fission through mitofusin degradation in human multipotent embryonic carcinoma cells

Naoya Hirata [a, 1], Shigeru Yamada [a, 1], Miki Asanagi [a, b], Yuko Sekino [a], Yasunari Kanda [a, *]

[a] Division of Pharmacology, National Institute of Health Sciences, Japan
[b] Faculty of Engineering, Department of Materials Science and Engineering, Yokohama National University, Japan

ARTICLE INFO

Article history:
Received 5 January 2016
Accepted 10 January 2016
Available online 13 January 2016

Keywords:
Embryonic cells
Cigarette smoking
Nicotine
Mitochondrial fission
Mitofusin

ABSTRACT

Nicotine is considered to contribute to the health risks associated with cigarette smoking. Nicotine exerts its cellular functions by acting on nicotinic acetylcholine receptors (nAChRs), and adversely affects normal embryonic development. However, nicotine toxicity has not been elucidated in human embryonic stage. In the present study, we examined the cytotoxic effects of nicotine in human multipotent embryonal carcinoma cell line NT2/D1. We found that exposure to 10 μM nicotine decreased intracellular ATP levels and inhibited proliferation of NT2/D1 cells. Because nicotine suppressed energy production, which is a critical mitochondrial function, we further assessed the effects of nicotine on mitochondrial dynamics. Staining with MitoTracker revealed that 10 μM nicotine induced mitochondrial fragmentation. The levels of the mitochondrial fusion proteins, mitofusins 1 and 2, were also reduced in cells exposed to nicotine. These nicotine effects were blocked by treatment with mecamylamine, a nonselective nAChR antagonist. These data suggest that nicotine degrades mitofusin in NT2/D1 cells and thus induces mitochondrial dysfunction and cell growth inhibition in a nAChR-dependent manner. Thus, mitochondrial function in embryonic cells could be used to assess the developmental toxicity of chemicals.

1. Introduction

Growing evidence suggest that maternal smoking during pregnancy is related to adverse neurodevelopmental outcomes in the offspring, including lower intelligence quotients and deficits in learning and memory [1,2]. Nicotine is a naturally occurring alkaloid that is present in tobacco leaves and is considered to contribute to the negative effects of cigarette smoking on health [2,3]. Nicotine exerts its cellular functions by activating nicotinic acetylcholine receptors (nAChRs), which are heterodimers composed of combinations of different types of α subunit (α1–α10) and β subunit (β1–β4) [4]. α8-nAChR has not been identified in human. Recent studies have shown that nAChRs are present in a variety of cells, such as cancer cells, vascular smooth muscle, and neural cells [3–6]. Activation of nAChRs by nicotine promotes the release of various neurotransmitters (including dopamine, norepinephrine, acetylcholine, glutamate) [7]. Altered regulation of neurotransmitter levels can adversely affect key events in normal brain development, such as the formation of neural circuits and neurotransmitter systems [7,8]. Therefore, it is necessary to elucidate the cytotoxic effects of nicotine on embryonic development.

Nicotine toxicity has been reported to affect mitochondrial function both *in vitro* and *in vivo*. For example, nicotine exposure alters mitochondrial membrane potential (MMP), increases an oxidative stress, and induces apoptosis in colon adenocarcinoma HCT-116 cell [9]. Another study has shown that nicotine exposure reduced the activity of an enzyme in the pancreatic mitochondrial respiratory chain, and impaired glucose-stimulated insulin secretion in neonatal rats [10]. However, the precise mechanisms underlying the effects of nicotine on mitochondrial function remain largely unknown.

Growing evidence suggest that mitochondria undergo continuous morphological dynamics involving fusion and fission cycles. These dynamics play a key role in maintenance of normal mitochondrial functions, such as ATP production [11]. Mitochondrial fusion and fission are regulated by several GTPases. Mitofusin 1 and 2 (Mfn1, 2) and optic atrophy 1 (Opa1) induce fusion of the outer and inner mitochondrial membranes, respectively [12,13]. In contrast, dynamin-related protein 1 (Drp1) is a cytoplasmic protein that assembles into rings surrounding the outer mitochondrial

* Corresponding author. 1-18-1, Kamiyoga, Setagaya-ku, 158-8501, Japan.
E-mail address: kanda@nihs.go.jp (Y. Kanda).
[1] Equally contributed.

http://dx.doi.org/10.1016/j.bbrc.2016.01.063
0006-291X/

membrane, where it interacts with fission protein 1 (Fis1) to promote fission [14,15]. For example, pigment epithelium-derived factor is reported to improve mitochondrial function by stabilizing mitochondrial fusion in retinal pigment epithelial cells [16]. In contrast, the anti-tumor agent, doxorubicin, facilitates mitochondrial fragmentation and apoptosis by promoting Mfn2 degradation in sarcoma U2OS cells [17].

In the present study, we hypothesized a possible link between nicotine toxicity and mitochondrial function in human mulitpotent NT2/D1 cells, which have neural differentiation capability. Our results showed that exposure to 10 μM nicotine decreased intracellular ATP levels and inhibited cell growth. Moreover, nicotine exposure induced Mfn degradation and mitochondrial fragmentation via nicotinic acetylcholine receptors (nAChRs). Thus, nicotine induces toxicity through impairment of mitochondrial quality control in human NT2/D1 cells.

2. Materials and methods

2.1. Cell culture

The human multipotent embryonal carcinoma NT2/D1 cells were obtained from the American Type Culture Collection (Manassas, VA, USA). SH-SY5Y cells were obtained from European Collection of Animal Cell Culture (Salisbury, Wiltshire, UK). The cells were cultured in Dulbecco's modified Eagle's medium (DMEM; Sigma–Aldrich, St. Louis, MO, USA) supplemented with 10% fetal bovine serum (FBS; Biological Industries, Ashrat, Israel) and 0.05 mg/ml penicillin-streptomycin mixture (Life Technologies, Carlsbad, CA, USA) at 37 °C in the presence of 5% CO_2.

2.2. Cell proliferation assay

Cell viability was measured using the CellTiter 96 AQueous One Solution Cell Proliferation Assay (Promega, Madison, WI, USA), as previously described [18]. Briefly, NT2/D1 cells were seeded into 96-well plate and exposed to different concentrations of nicotine. After exposure to nicotine, One Solution Reagent was added to each well, and the plate was incubated at 37 °C for another 2 h. Absorbance was measured at 490 nm by iMark microplate reader (Bio-Rad, Hercules, CA, USA).

2.3. Measurement of intracellular ATP levels

The intracellular ATP content was measured using the ATP Determination Kit (Life Technologies), as previously described [19]. Briefly, the cells were washed and lysed with phosphate-buffered saline containing 0.1% Triton X-100. The resulting cell lysates were added to a reaction mixture containing 0.5 mM D-luciferin, 1 mM dithiothreitol, and 1.25 μg/ml luciferase and incubated for 30 min at room temperature. Luminescence was measured using a Wallac1420ARVO fluoroscan (Perkin–Elmer, Waltham, MA, USA). The luminescence intensities were normalized to the total protein content.

2.4. Assessment of mitochondrial fusion

After treatment with nicotine (10 μM, 24 h), cells were fixed with 4% paraformaldehyde and stained with 50 nM MitoTracker Red CMXRos (Cell Signaling Technology, Danvers, MA, USA) and 0.1 μg/ml 4′,6-diamidino-2-phenylindole (DAPI; Dojin, Kumamoto, Japan). Changes in mitochondrial morphology were observed using a confocal laser microscope (Nikon A1). Images (n = 3–7) of random fields were taken, and the number of cells displaying mitochondrial fusion (<10% punctiform) was counted in each image, as previously described [20]. The number of cells showing mitochondrial fission was calculated by subtracting the number of cells with mitochondrial fusion from the total cell number.

2.5. Real-time PCR

Total RNA was isolated from NT2/D1 cells using TRIzol reagent (Life Technologies), and quantitative real-time reverse transcription (RT)-PCR with QuantiTect SYBR Green RT-PCR Kit (QIAGEN, Valencia, CA, USA) was performed using an ABI PRISM 7900HT sequence detection system (Applied Biosystems, Foster City, CA, USA) as previously described [21]. The relative change in the amount of transcript was normalized to the mRNA levels of glyceraldehyde-3-phosphate dehydrogenase (GAPDH). The following primer sequences were used for real-time PCR analysis: *nAChRα1*, forward, 5′-CTGGACCTACGACGGCTCT-3′ and reverse, 5′-CGCTGCATGACGAAGTGGT-3′; *nAChRα2*, forward, 5′-ACACTTCAGACGTGGTGATTG-3′ and reverse, 5′-CCACTCCTGTTTTAGCCAGAC-3′; *nAChRα3*, forward, 5′-ACCTGTGGCTCAAGCAAATCT-3′ and reverse, 5′-GCAGGGACACGCATGAACT-3′; *nAChRα4*, forward, 5′-GGAGGGCGTCCAGTACATTG-3′ and reverse, 5′-GAAGATGCGGTCGATGACCA-3′; *nAChRα5*, forward, 5′-AGATGGAACCCTGATGACTATGGT-3′ and reverse, 5′-AAACGTCCATCTGCATTATCAAAC-3′; *nAChRα6*, forward, 5′-GGCAGGGATTCCTTCATGGG-3′ and reverse, 5′-GCCTCTCCTCAGTTGCACAG-3′; *nAChRα7*, forward, 5′-CATGGCCTTCTCGGTCTTCA-3′ and reverse, 5′-CACGGCCTCCACGAAGTT-3′; *nAChRα10*, forward, 5′-CAGATGCCTACCTACGATGGG-3′ and reverse, 5′-GGGAAGGCTGCTACATCCA-3′; *nAChRβ1*, forward, 5′-TGAGACCTCACTATCAGTACCCA-3′ and reverse, 5′-AGAACCACGACACTAAGGATGA-3′; *nAChRβ2*, forward, 5′-GGTGACAGTACAGCTTATGGTG-3′ and reverse, 5′-AGGCGATAATCTTCCCACTCC-3′; *nAChRβ3*, forward, 5′-TGCTGGTTCTCATCGTCCTTG-3′ and reverse, 5′-GCATCTTCATTTTCGGCGATTGA-3′; *nAChRβ4*, forward, 5′-CAGCTTATCAGCGTGAATGAGC-3′ and reverse, 5′-GTCAGGCGGTAATCAGTCCAT-3′; *Drp1*, forward, 5′-TGGGCGCCGACATCA-3′ and reverse, 5′-GCTCTGCGTTCCCACTACGA-3′; *Fis1*, forward, 5′-TACGTCCGCGGGTTGCT-3′ and reverse, 5′-CCAGTTCCTTGGCCTGGTT-3′; *Mfn1*, forward, 5′-GGCATCTGTGGCCGAGTT-3′ and reverse, 5′-ATTATGCTAAGTCTCCGCTCCAA-3′; *Mfn2*, forward, 5′-GCTCGGAGGCACATGAAAGT-3′ and reverse, 5′-ATCACGGTGCTCTTCCCATT-3′; *Opa1*, forward, 5′-GTGCTGCCCGCCTAGAAA-3′ and reverse, 5′-TGACAGGCACCCGTACTCAGT-3′; *GAPDH*, forward, 5′-GTCTCCTCTGACTTCAACAGCG-3′ and reverse, 5′-ACCACCCTGTTGCTGTAGCCAA-3′.

2.6. Western blot analysis

Western blot analysis was performed as previously reported [22]. Briefly, the cells were lysed with Cell Lysis Buffer (Cell Signaling Technology). The proteins were then separated by sodium dodecyl sulfate-polyacrylamide gel electrophoresis (SDS-PAGE) and electrophoretically transferred to Immobilon-P (Millipore, Billerica, MA, USA). The membranes were probed with anti-Drp1 monoclonal antibodies (1:1000; Cell Signaling Technology), anti-Fis1 polyclonal antibodies (1:200; Santa Cruz Biotechnology, Santa Cruz, CA, USA), anti-Mfn1 polyclonal antibodies (1:1000; Cell Signaling Technology), anti-Mfn2 monoclonal antibodies (1:1000; Cell Signaling Technology), anti-Opa1 monoclonal antibodies (1:1000; BD Biosciences), and anti-β-actin monoclonal antibodies (1:5000; Sigma–Aldrich). The membranes were then incubated with secondary antibodies against rabbit or mouse IgG conjugated to horseradish peroxidase (Cell Signaling Technology). The bands were visualized using the ECL Western Blotting Analysis System (GE

Healthcare, Buckinghamshire, UK), and images were acquired using a LAS-3000 Imager (FUJIFILM UK Ltd., Systems, Bedford, UK).

2.7. Chemicals and reagents

Nicotine was obtained from Wako Pure Chemicals (Osaka, Japan). Mecamylamine hydrochloride (MCA) and m-chlorophenylhydrazone (CCCP) were obtained from Sigma–Aldrich.

2.8. Statistical analysis

All data were presented as means ± S.D. ANOVA followed by post hoc Fisher test was used to analyze data in Fig. 1A and B and Figs. 2–4C. Student's *t*-test was used to analyze data in Fig. 4A. *P*-values less than 0.05 were considered to be statistically significant.

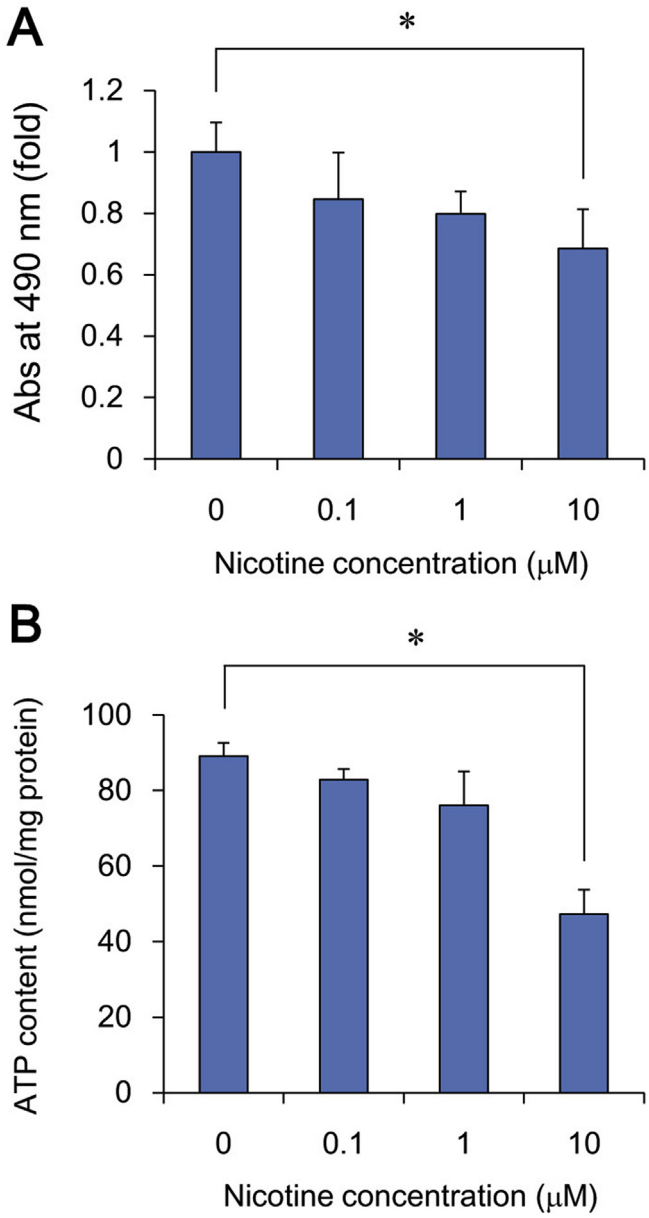

Fig. 1. Nicotine inhibits cell proliferation via intracellular ATP decrease in NT2/D1 cells. A. Cells were exposed to different concentrations of nicotine for 72 h. Cell viability was examined using the CellTiter 96 AQueous One Solution Cell Proliferation Assay. B. After treatment with different concentrations of nicotine for 24 h, intracellular ATP content was determined in cell lysates. Data represent the mean ± SD (n = 3). *P < 0.05.

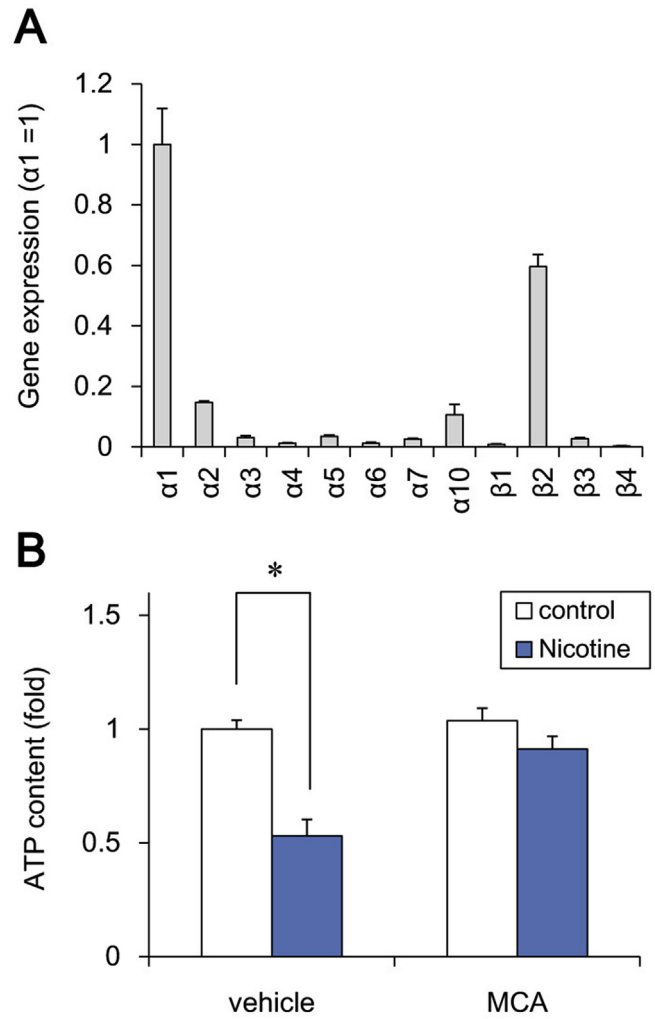

Fig. 2. Nicotine reduces intracellular ATP levels via nAChRs in NT2/D1 cells. A. Expression of AChR subtypes was analyzed by real-time PCR in NT2/D1 cells. The relative changes were determined by normalizing with GAPDH. B. After treatment with 10 μM nicotine and/or 30 μM MCA for 24 h, intracellular ATP content was determined in cell lysates. Data represent the mean ± SD (n = 3). *P < 0.05.

3. Results

3.1. Cytotoxic effects of nicotine in NT2/D1 cells

To examine the effects of nicotine on human multipotent embryonic cells, we exposed the cells to different concentrations of nicotine for 72 h and measured cell viability by MTT assay using human multipotent embryonic carcinoma NT2/D1 cells, which have an ability to differentiate into neuronal cells. We found that treatment with 10 μM nicotine significantly inhibited cell proliferation (Fig. 1A). Similarly, exposure to 10 μM nicotine significantly reduced the ATP content of the cells (Fig. 1B). To further investigate whether the nicotine effects are selective for undifferentiated cells, we used human SH-SY5Y neuroblastoma cells. We found that exposure to 10 μM nicotine had little effect on proliferation and ATP content of SH-SY5Y cells (Fig. S1).

We next examined the nAChR mRNA levels by real-time PCR and confirmed that nAChR subtypes except α9-nAChR were expressed in NT2/D1 cells (Fig. 2A). To examine whether the inhibition of ATP

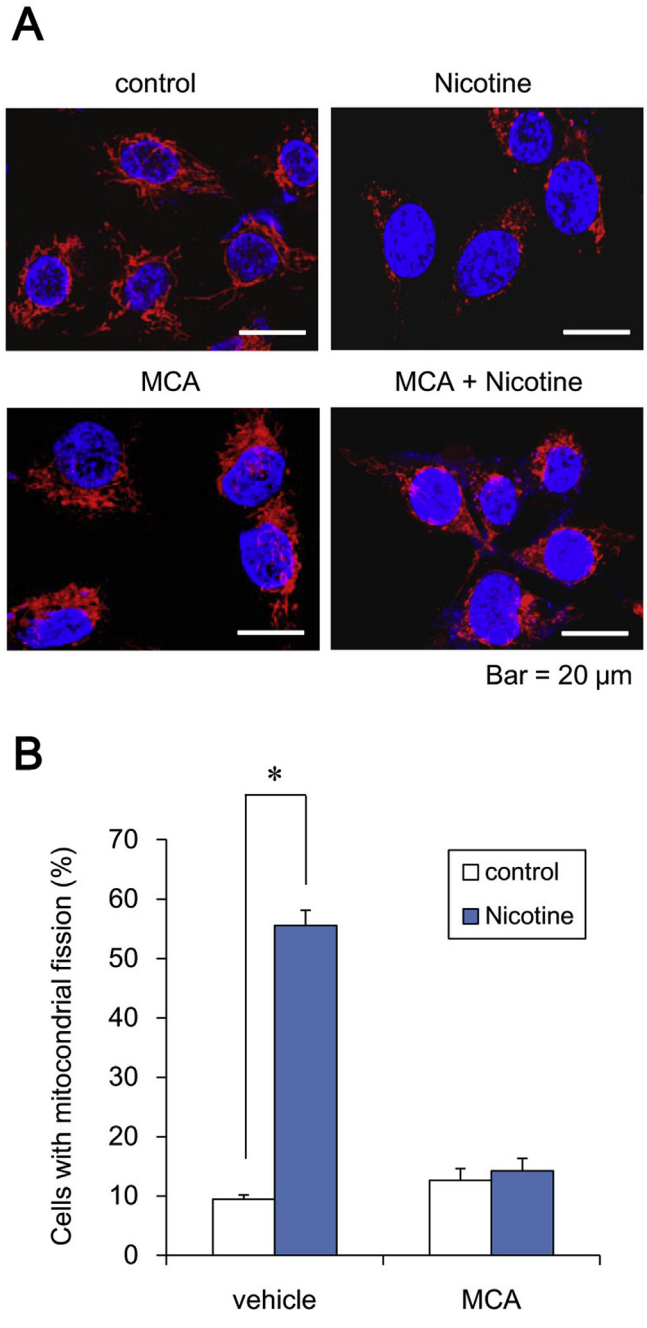

Fig. 3. Nicotine induces mitochondrial fission via nAChRs in NT2/D1 cells. A. Cells were exposed to 10 μM nicotine, in the presence or absence of 30 μM MCA, for 24 h. The cells were stained with MitoTracker Red CMXRos and DAPI and mitochondrial morphology was observed by confocal laser microscopy. Bar = 20 μm. B. The number of cells showing mitochondrial fusion (<10% punctiform) was counted in three independent captured images. The number of cells showing mitochondrial fission was calculated by subtracting the number of cells with mitochondrial fusion from the total cell number. *$P < 0.05$.

production is mediated via the nAChRs, we tested the effect of nAChR antagonist on the ATP content. As shown in Fig. 2B, a non-selective nAChR antagonist mecamylamine (MCA) abolished the nicotine-induced reduction of ATP content. MCA alone did not affect the ATP level. These data suggest that nicotine decreases the ATP content via its nAChR and inhibits cell proliferation in NT2/D1 cells.

3.2. Effects of nicotine on mitochondrial morphology in NT2/D1 cells

Mitochondrial function, including ATP production, are maintained by mitochondrial fusion and fission [11]. Since nicotine reduced intracellular ATP levels, we next focused on the mitochondrial dynamics in NT2/D1 cells. Nicotine exposure (10 μM, 24 h) significantly increased the number of fragmented mitochondria with punctate morphology, as compared to the level observed in untreated control cells (Fig. 3). Moreover, MCA abolished this nicotine-induced mitochondrial fragmentation (Fig. 3). MCA alone did not affect mitochondrial dynamics. In contrast to NT2/D1 cells, nicotine did not significantly affect the mitochondrial dynamics in SH-SY5Y neuroblastoma cells (Fig. S1). These results suggest that nicotine induces mitochondrial fission via nAChRs in NT2/D1 cells.

3.3. Nicotine reduces Mfn1 and Mfn2 protein levels in NT2/D1 cells

To examine the molecular mechanism by which nicotine induces mitochondrial fragmentation, we assessed its effects on mitochondrial fission (Fis1, Drp1) and fusion genes (Mfn1, Mfn2, Opa1). Real-time PCR analysis showed that each gene expression was not significantly altered by nicotine exposure (Fig. 4A). Interestingly, western blot analysis revealed that nicotine did significantly decrease the levels of Mfn1 and Mfn2 proteins (Fig. 4B and C). In contrast, the levels of other proteins, including Fis1, Drp1, and Opa1, were not affected by nicotine. These data suggest that nicotine-induced mitochondrial fragmentation is caused by the degradation of Mfn1 and Mfn2 proteins.

4. Discussion

In the present study, we demonstrated that exposure to micromolar levels of nicotine impairs mitochondrial quality control in human multipotent embryonic carcinoma cells. Exposure to nicotine induces nAChR-dependent degradation of Mfn1 and Mfn2, thereby promoting mitochondrial fragmentation. These negative nAChR-mediated effects of nicotine on mitochondrial quality control could inhibit ATP production and cell viability.

Undifferentiated embryonic cells may tend to be sensitive to the growth inhibitory effects of nicotine, whereas proliferative and protective effects of nicotine have been described in more developed somatic cells [23–27]. Our studies showed that treatment with 10 μM nicotine reduces cell growth in human embryonic cells (Fig. 1), whereas the growth of human neuroblastoma SH-SY5Y cells is not affected (Fig. S1). Previous study has also shown that exposure to more than 1.8 μM nicotine inhibits cell adhesion and induces apoptosis in human embryonic stem cells [28]. The concentrations of nicotine tested in our study were relevant to the circulating levels of nicotine in cigarette smokers, which have been reported to range from 10 nM to 10 μM [29]; these have the potential to inhibit the growth of embryonic cells. In contrast to these growth inhibitory effects, nicotine is known to stimulate the proliferation of hematopoietic and neuronal progenitors [23–25]. In addition, nicotine is reported to protect rat basal forebrain neurons or rat hippocampal neurons from the cytotoxicity of β-amyloid protein [26,27]. Taken together, nicotine effects in undifferentiated embryonic cells contains different mechanisms from developed somatic cells. Therefore, further studies are required to elucidate the mechanism of cell stage-specific effects using embryonic and differentiated cells.

Our data suggest that nicotine induces mitochondrial fission through the degradation of Mfn1 and Mfn2 (Figs. 3 and 4). Consistent with this finding, chemical stressors have been reported

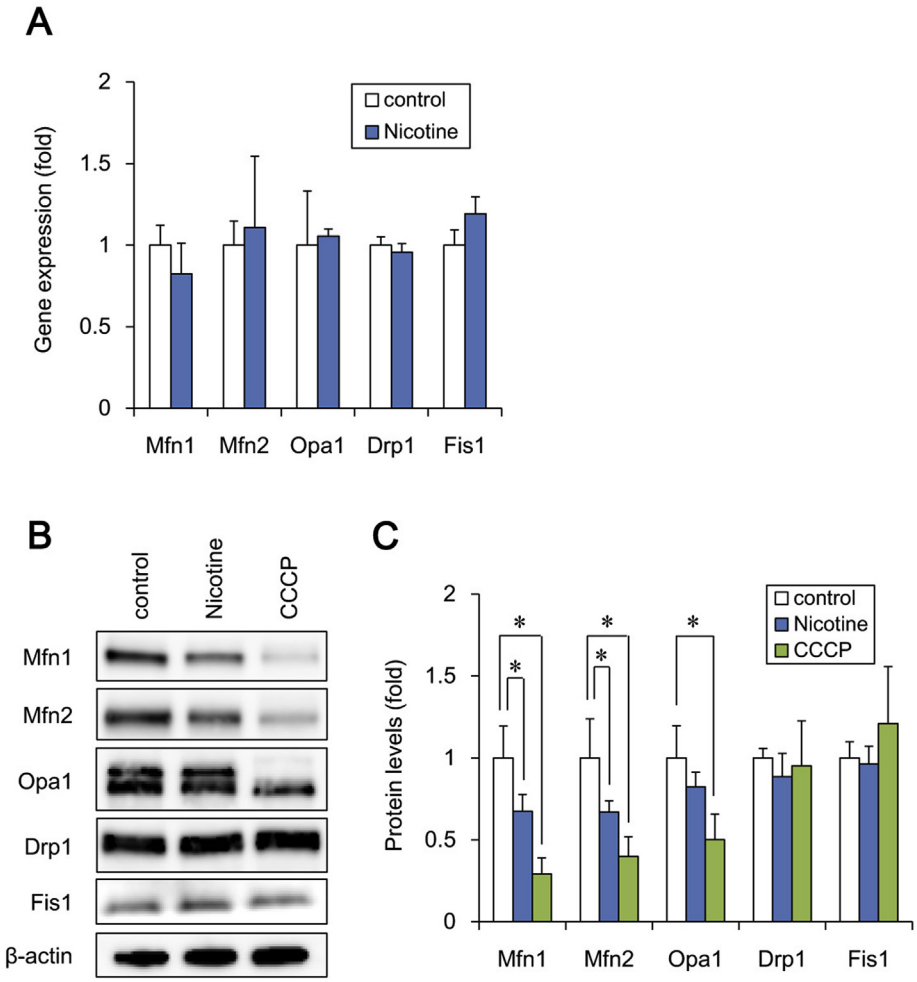

Fig. 4. Nicotine reduces Mfn1 and Mfn2 protein levels in NT2/D1 cells. A. After exposure to 10 μM nicotine for 24 h, the expression of the indicated mitochondrial genes was analyzed by real-time PCR. The relative changes were determined by normalizing with GAPDH. B. After exposure to 10 μM nicotine or 10 μM CCCP for 24 h, the expression of mitochondrial proteins was analyzed by western blot using anti-Drp1, anti-Fis1, anti-Mfn1, anti-Mfn2, anti-Opa1, or anti-β-actin antibodies. C. The band densities were analyzed by ImageJ software. Relative changes in expression were determined by normalization to β-actin. Data represent the mean ± SD (n = 3). *P < 0.05.

to cause mitochondrial fission via Mfn degradation. For example, organotin compounds such as tributyltin induce proteasomal degradation of Mfn1 and Mfn2, which facilitates mitochondrial fragmentation and growth arrest in NT2/D1 cells [30,31]. Since nicotine showed similar effects in NT2/D1 cells, nicotine exposure may also degrade Mfn1 and Mfn2 via proteasome. Moreover, an inhibitor of mitochondrial calcium efflux, CGP37157, is reported to degrade Mfn1 via E3 ubiquitin ligase and induce mitochondrial fission in prostate cancer LNCaP cells [32]. Further studies will be necessary to determine whether ubiquitin ligases are involved in nicotine-induced Mfn1 and Mfn2 degradation in embryonic cells.

Our data suggest that nicotine toxicity is mediated by dysfunctional mitochondrial quality control, which occurs via a nAChR-dependent mechanism (Figs. 2 and 3). Nicotine has been reported to evoke extracellular calcium influx through plasma membrane nAChRs [4]. Moreover, a transient increase in intracellular calcium levels is known to cause mitochondrial calcium overload, which is followed by the depolarization of the mitochondrial membrane, resulting in a loss of MMP [33,34]. In other cell lines, MMP reduction is reported to induce the mitochondrial translocation of the E3 ubiquitin ligase, Parkin, which targets the Mfn protein for proteasomal degradation [35]. Therefore, nicotine may increase intracellular calcium entry via nAChRs, thus reducing the MMP and inducing mitochondrial translocation of E3 ubiquitin ligases; this increases the proteasomal degradation of Mfn1 and Mfn2. Several reports indicate that knockdown of Mfn1 and Mfn2 in the cells induces mitochondrial fragmentation and shows severe cellular defects, including decreased ATP content and poor cell growth [36,37]. Especially, Mfn2 has been reported to be necessary for striatal axonal projections of midbrain dopamine neurons by the studies using dopamine neuron-specific Mfn2 knockout mice [38]. Taken together, Mfn1 and Mfn2 might be involved in several nAChR-mediated effects of nicotine, such as the reduction of ATP content, growth inhibition, and modulation of synaptic transmission. In future studies, it will be necessary to investigate the precise mechanism involved in nicotine-induced Mfn degradation, which results in mitochondrial fission and impaired function.

Conflict of interest

The authors declare that there are no conflicts of interest.

Acknowledgments

This work was supported by a Health and Labour Sciences Research Grant from the Ministry of Health, Labour and Welfare,

Japan (#H25-Kagaku-Ippan-002 to Y. Kanda), a Grant-in-Aid for Scientific Research from the Ministry of Education, Culture, Sports, Science, and Technology, Japan (#26293056, #26670041 to Y. Kanda), the Research on Regulatory Harmonization and Evaluation of Pharmaceuticals, Medical Devices, Regenerative and Cellular Therapy Products, Gene Therapy Products, and Cosmetics from Japan Agency for Medical Research and development, AMED (to Y. Sekino), and a grant from the Smoking Research Foundation (Y. Kanda).

Transparency document

Transparency document related to this article can be found online at http://dx.doi.org/10.1016/j.bbrc.2016.01.063.

Appendix A. Supplementary data

Supplementary data related to this article can be found at http://dx.doi.org/10.1016/j.bbrc.2016.01.063.

References

[1] V.S. Knopik, Maternal smoking during pregnancy and child outcomes: real or spurious effect? Dev. Neuropsychol. 34 (2009) 1–36.
[2] C.M. Tiesler, J. Heinrich, Prenatal nicotine exposure and child behavioural problems, Eur. Child. Adolesc. Psychiatry 23 (2014) 913–929.
[3] B.M. Conti-Fine, D. Navaneetham, S. Lei, A.D. Maus, Neuronal nicotinic receptors in non-neuronal cells: new mediators of tobacco toxicity? Eur. J. Pharmacol. 393 (2000) 279–284.
[4] E.X. Albuquerque, E.F. Pereira, M. Alkondon, S.W. Rogers, Mammalian nicotinic acetylcholine receptors: from structure to function, Physiol. Rev. 89 (2009) 73–120.
[5] Y. Kanda, Y. Watanabe, Nicotine-induced vascular endothelial growth factor release via the EGFR-ERK pathway in rat vascular smooth muscle cells, Life Sci. 80 (2007) 1409–1414.
[6] N. Hirata, Y. Sekino, Y. Kanda, Nicotine increases cancer stem cell population in MCF-7 cells, Biochem. Biophys. Res. Commun. 403 (2010) 138–143.
[7] N.L. Benowitz, Pharmacology of nicotine: addiction, smoking-induced disease, and therapeutics, Annu. Rev. Pharmacol. Toxicol. 49 (2009) 57–71.
[8] J.B. Dwyer, S.C. McQuown, F.M. Leslie, The dynamic effects of nicotine on the developing brain, Pharmacol. Ther. 122 (2009) 125–139.
[9] C.L. Crowley-Weber, K. Dvorakova, C. Crowley, H. Bernstein, C. Bernstein, H. Garewal, C.M. Payne, Nicotine increases oxidative stress, activates NF-kappaB and GRP78, induces apoptosis and sensitizes cells to genotoxic/xenobiotic stresses by a multiple stress inducer, deoxycholate: relevance to colon carcinogenesis, Chem. Biol. Interact. 145 (2003) 53–66.
[10] J.E. Bruin, M.A. Petre, S. Raha, K.M. Morrison, H.C. Gerstein, A.C. Holloway, Fetal and neonatal nicotine exposure in wistar rats causes progressive pancreatic mitochondrial damage and beta cell dysfunction, PLoS One 3 (2008) e3371.
[11] R.J. Youle, A.M. van der Bliek, Mitochondrial fission, fusion, and stress, Science 337 (2012) 1062–1065.
[12] T. Koshiba, S.A. Detmer, J.T. Kaiser, H. Chen, J.M. McCaffery, D.C. Chan, Structural basis of mitochondrial tethering by mitofusin complexes, Science 305 (2004) 858–862.
[13] S. Cipolat, O.M. De Brito, B. Dal Zilio, L. Scorrano, OPA1 requires mitofusin 1 to promote mitochondrial fusion, Proc. Natl. Acad. Sci. U. S. A. 101 (2004) 15927–15932.
[14] E. Smirnova, L. Griparic, D.-L. Shurland, A.M. van der Bliek, Dynamin-related protein Drp1 is required for mitochondrial division in mammalian cells, Mol. Biol. Cell 12 (2001) 2245–2256.
[15] Y. Yoon, E.W. Krueger, B.J. Oswald, M.A. McNiven, The mitochondrial protein hFis1 regulates mitochondrial fission in mammalian cells through an interaction with the dynamin-like protein DLP1, Mol. Biol. Cell 23 (2003) 5409–5420.
[16] Y. He, K.W. Leung, Y. Ren, J. Pei, J. Ge, J. Tombran-Tink, PEDF improves mitochondrial function in RPE cells during oxidative stress, Investig. Ophthalmol. Vis. Sci. 55 (2014) 6742–6755.
[17] G.P. Leboucher, Y.C. Tsai, M. Yang, K.C. Shaw, M. Zhou, T.D. Veenstra, M.H. Glickman, A.M. Weissman, Stress-induced phosphorylation and proteasomal degradation of mitofusin 2 facilitates mitochondrial fragmentation and apoptosis, Mol. Cell 47 (2012) 547–557.
[18] S. Yamada, Y. Kotake, Y. Sekino, Y. Kanda, AMP-activated protein kinase-mediated glucose transport as a novel target of tributyltin in human embryonic carcinoma cells, Metallomics 5 (2013) 484–491.
[19] S. Yamada, Y. Kotake, Y. Demizu, M. Kurihara, Y. Sekino, Y. Kanda, NAD-dependent isocitrate dehydrogenase as a novel target of tributyltin in human embryonic carcinoma cells, Sci. Rep. 4 (2014) 5952.
[20] X. Fan, R. Hussien, G.A. Brooks, H_2O_2-induced mitochondrial fragmentation in C2C12 myocytes, Free Radic. Biol. Med. 49 (2010) 1646–1654.
[21] N. Hirata, S. Yamada, T. Shoda, M. Kurihara, Y. Sekino, Y. Kanda, Sphingosine-1-phosphate promotes expansion of cancer stem cells via S1PR3 by a ligand-independent Notch activation, Nat. Commun. 5 (2014) 4806.
[22] Y. Kanda, T. Hinara, S.W. Kang, Y. Watanabe, Reactive oxygen species mediate adipocyte differentiation in mesenchymal stem cells, Life Sci. 89 (2011) 250–258.
[23] M.V. Skok, R. Grailhe, F. Agenes, J.P. Changeux, The role of nicotinic receptors in B-lymphocyte development and activation, Life Sci. 80 (2007) 2334–2336.
[24] L.M. Koval, A.S. Zverkova, R. Grailhe, Y.N. Utkin, V.I. Tsetlin, S.V. Komisarenko, M.V. Skok, Nicotinic acetylcholine receptors alpha4beta2 and alpha7 regulate myelo- and erythropoiesis within the bone marrow, Int. J. Biochem. Cell Biol. 40 (2008) 980–990.
[25] N. He, Z. Wang, Y. Wang, H. Shen, M. Yin, ZY-1, a novel nicotinic analog, promotes proliferation and migration of adult hippocampal neural stem/progenitor cells, Cell Mol. Neurobiol. 33 (2013) 1149–1157.
[26] C.N. Guo, L. Sun, G.L. Liu, S.J. Zhao, W.W. Liu, Y.B. Zhao, Protective effect of nicotine on the cultured rat basal forebrain neurons damaged by β-Amyloid (Aβ)25-35 protein cytotoxicity, Eur. Rev. Med. Pharmacol. Sci. 19 (2015) 2964–2972.
[27] Q. Liu, B. Zhao, Nicotine attenuates beta-amyloid peptide-induced neurotoxicity, free radical and calcium accumulation in hippocampal neuronal cultures, Br. J. Pharmacol. 141 (2004) 746–754.
[28] T. Zdravkovic, O. Genbacev, N. LaRocque, M. McMaster, S. Fisher, Human embryonic stem cells as a model system for studying the effects of smoke exposure on the embryo, Reprod. Toxicol. 26 (2008) 86–93.
[29] E.R. Gritz, V. Baer-Weiss, N.L. Benowitz, M.E. Van VunakisHjarvik, Plasma nicotine and cotine concentrations in habitual smokeless tobacco users, Clin. Pharmacol. Ther. 30 (1981) 201–209.
[30] S. Yamada, Y. Kotake, M. Nakano, Y. Sekino, Y. Kanda, Tributyltin induces mitochondrial fission through NAD-IDH dependent mitofusin degradation in human embryonic carcinoma cells, Metallomics 7 (2015) 1240–1246.
[31] M. Asanagi, S. Yamada, N. Hirata, H. Itagaki, Y. Kotake, Y. Sekino, Y. Kanda, Tributyltin induces G2/M cell cycle arrest via NAD^+-dependent isocitrate dehydrogenase in human embryonic carcinoma cells, J. Toxicol. Sci. (2016) in press.
[32] V. Choudhary, I. Kaddour-Djebbar, R. Alaisami, M.V. Kumar, W.B. Bollag, Mitofusin 1 degradation is induced by a disruptor of mitochondrial calcium homeostasis, CGP37157: a role in apoptosis in prostate cancer cells, Int. J. Oncol. 44 (2014) 1767–1773.
[33] M.R. Duchen, Mitochondria and calcium: from cell signalling to cell death, J. Physiol. 529 (2000) 57–68.
[34] N. Demaurex, D. Poburko, M. Frieden, Regulation of plasma membrane calcium fluxes by mitochondria, Biochim. Biophys. Acta 1787 (2009) 1383–1394.
[35] A. Tanaka, M.M. Cleland, S. Xu, D.P. Narendra, D.F. Suen, M. Karbowski, R.J. Youle, Proteasome and p97 mediate mitophagy and degradation of mitofusins induced by Parkin, J. Cell Biol. 191 (2010) 1367–1380.
[36] H. Chen, A. Chomyn, D.C. Chan, Disruption of fusion results in mitochondrial heterogeneity and dysfunction, J. Biol. Chem. 280 (2005) 26185–26192.
[37] W. Yue, Z. Chen, H. Liu, C. Yan, M. Chen, D. Feng, C. Yan, H. Wu, L. Du, Y. Wang, J. Liu, X. Huang, L. Xia, L. Liu, X. Wang, H. Jin, J. Wang, Z. Song, X. Hao, Q. Chen, A small natural molecule promotes mitochondrial fusion through inhibition of the deubiquitinase USP30, Cell Res. 24 (2014) 482–496.
[38] S. Lee, F.H. Sterky, A. Mourier, M. Terzioglu, S. Cullheim, L. Olson, N.G. Larsson, Mitofusin 2 is necessary for striatal axonal projections of midbrain dopamine neurons, Hum. Mol. Genet. 21 (2012) 4827–4835.

Title

Effects of 13 developmentally toxic chemicals on the migration of rat cephalic neural crest cells in vitro

First author's surname

Usami

Short title

Chemical effects on neural crest cells

Names of authors

Makoto Usami[1], Katsuyoshi Mitsunaga[2], Atsuko Miyajima[3], Mina Takamatu[4], Shugo Kazama[4], Tomohiko Irie[1], Osamu Doi[5], TatsuyaTakizawa[4]

Affiliation

[1]Division of Pharmacology, National Institute of Health Sciences, Tokyo 158-8501, [2]School of Pharmaceutical Sciences, Toho University, Chiba 274-8510, [3]Division of Medical Devices, National Institute of Health Sciences, Tokyo 158-8501, [4]School of Veterinary Medicine, Azabu University, Kanagawa 252-5201, [5]United Graduate School of Agricultural Science, Gifu University, Gifu 501-1193.

Corresponding author

Makoto Usami, Ph.D.

Division of Pharmacology, National Institute of Health Sciences,

1-18-1, Kamiyoga, Setagaya, Tokyo 158-8501, Japan

Tel: +81-3-3700-1141(ext.342); Fax: +81-3-3707-6950

E-mail: usami@nihs.go.jp

This article has been accepted for publication and undergone full peer review but has not been through the copyediting, typesetting, pagination and proofreading process, which may lead to differences between this version and the Version of Record. Please cite this article as doi: 10.1111/cga.12121

ABSTRACT

The inhibition of neural crest cell (NCC) migration has been considered as a possible pathogenic mechanism underlying chemical developmental toxicity. In this study, we examined the effects of 13 developmentally toxic chemicals on the migration of rat cephalic NCCs (cNCCs) by using a simple in vitro assay. cNCCs were cultured for 48 h as emigrants from rhombencephalic neural tubes explanted from rat embryos at day 10.5 of gestation. The chemicals were added to the culture medium at 24h of culture. Migration of cNCCs was measured as the change in the radius (radius ratio) calculated from the circular spread of cNCCs between 24 and 48 h of culture. Of the chemicals examined, 13-*cis*-retinoic acid, ethanol, ibuprofen, lead acetate, salicylic acid, and selenate inhibited the migration of cNCCs at their embryotoxic concentrations; no effects were observed for acetaminophen, caffeine, indium, phenytoin, selenite, tributyltin, and valproic acid. In a cNCC proliferation assay, ethanol, ibuprofen, salicylic acid, selenate, and tributyltin inhibited cell proliferation, suggesting the contribution of the reduced cell number to the inhibited migration of cNCCs. It was determined that several developmentally toxic chemicals inhibited the migration of cNCCs, the effects of which were manifested as various craniofacial abnormalities.

Key words

Developmental toxicity; Embryo; Migration assay; Neural crest cell; Rat

INTRODUCTION

In vertebrate embryos, neural crest cells (NCCs) migrate to various tissues throughout the body and contribute to tissue organization; malfunction NCCs of can lead to dysmorphologies, tumors and syndromes called neurocristopathies (Hall 2009; Le Douarin & Kalcheim 1999). The inhibition of NCC migration has, therefore, been considered as a possible pathogenic mechanism underlying chemical developmental toxicity. It has been shown, for example, that all-*trans*-retinoic acid, a well-known teratogen, inhibits the migration of cephalic NCCs (cNCCs), causing branchial abnormalities in cultured mouse and rat embryos (Menegola et al. 2004).

The effects of chemicals on the migration of NCCs in mammals, however, have not been fully investigated, probably because no convenient experimental methods are available. The migration of NCCs has been examined by time-lapse video image analysis of fluorescence-labeled cells (Fuller et al. 2002; Kawakami et al. 2011), or by human neural crest stem cells with scratch assay (Zimmer et al. 2012). These methods are complicated and therefore not ideal for testing of chemicals in a common toxicity laboratory.

Recently, we established a simple in vitro assay that enabled examination of the effects of chemicals on the migration of cNCCs and trunk NCCs (tNCCs) (Usami et al. 2014b). In this method, NCCs are cultured as emigrants from isolated neural tubes of day 10.5 rat embryos. The cultured NCCs are exposed to test chemicals and their migration is determined as the radius ratio calculated from circular spread of the NCCs during the exposure period. Using this method we examined the effects of 13 developmentally toxic chemicals on the migration of cNCCs. We also examined the effects of chemicals on the proliferation of cNCCs, because this migration assay depends on the spread of cells and

can therefore be influenced by the cell number.

We selected developmentally toxic chemicals on the basis of our interest in our related study such as proteomics of embryos (Usami et al. 2014a; Usami et al. 2009; Usami et al. 2008) and metabolomics of hepatocytes (Kim et al. 2014) since there was little information about the effects of chemicals on the migration of cNCCs. However, we considered that the chemicals include both ones might affect cNCC migration, e.g., ethanol, and selenate, and ones might not, e.g., indium, and tributyltin, which was speculated from their potential to cause craniofacial abnormality.

MATERIALS AND METHODS

Animals

Wistar rats (Crj: WI, Charles River Japan Inc., Kanagawa, Japan) were used. Pregnant rats were obtained by mating female and male rats overnight, and the plug day was designated as day 0.5 of gestation. All the animal experiments were performed according to the guidelines for animal experiments of the National Institute of Health Sciences.

Chemicals

Acetaminophen (CAS 103-90-2), 13-*cis*-retinoic acid (CAS 4759-48-2), ibuprofen (CAS 31121-93-4), salicylic acid (CAS 54-21-7), selenate (CAS 13410-01-0), and selenite (CAS 10102-18-8) were purchased from Sigma-Aldrich Co. (St. Louis, MO). Caffeine (CAS 58-08-2), ethanol (CAS 64-17-5), indium (CAS 22519-64-8), lead acetate (CAS 6080-56-4), phenytoin (CAS 57-41-0), and tributyltin (CAS 1461-22-9) were purchased from Wako Pure Chemical Industries (Osaka, Japan). Valproic acid (CAS 1069-66-5) was purchased from Merck Co. (Darmstadt, Germany).

Culture of NCCs

Rat NCCs were cultured as emigrated cells from neural tubes of rat embryos at day 10.5 of gestation as previously described (Usami et al. 2014b), according to the culture schedule shown in Fig. 1. Neural tubes were excised from the rhombencephalic (for cNCCs) or trunk (for tNCCs) region of the embryos in Hanks' balanced salt solution with sharpened tungsten needles. The excised neural tubes were cultured in 35-mm culture dishes (BD Primaria; Becton, Dickinson and Company, Franklin Lakes, NJ) containing 2 ml of Dulbecco's Modified Eagle Medium with high glucose (DMEM; GIBCO, Life

Technologies Corp., Carlsbad, CA) and 10% (v/v) fetal bovine serum (GIBCO) at 37°C with 5% CO_2 for 48 h.

Phase-contrast images of cultured NCCs were recorded digitally at a magnification of ×10 with a microscope at 24 and 48 h of culture (BZ-9000; Keyence, Osaka, Japan). In the proliferation assay, the neural tube was removed at 18 h of culture, and the cell nuclei were stained with 4',6- diaminodino-2-phenylindole (DAPI, Invitrogen) and fluorescent images were photographed with the microscope at 48 h of culture. Representative photographs of the cNCCs are shown in Fig. 2.

Addition of chemicals

The chemicals were added at 24 h of culture by replacing the culture medium. For addition to the culture medium, caffeine, ethanol, salicylic acid, selenate, selenite, and valproic acid were directly dissolved in or diluted with the culture medium. Acetaminophen, 13-*cis*-retinoic acid, phenytoin, and tributyltin were dissolved in or diluted with dimethyl sulfoxide and 5 µl each of the solutions was added to 5 ml of the culture medium. Ibuprofen, indium, and lead acetate were dissolved in pure water and 100 µl each of the solutions was added to 4.9 ml of the culture medium.

The concentrations of the following chemicals in the culture medium were their embryotoxic concentrations obtained from the literature: acetaminophen (Weeks et al. 1990), caffeine (Robinson et al. 2010; Shreiner et al. 1986), 13-*cis*-retinoic acid (Lee et al. 1991), ethanol (Usami et al. 2014a), ibuprofen (Guest et al. 1994), indium (Usami et al. 2009), lead acetate (Zhao et al. 1997), phenytoin (Winn 2002), salicylic acid (Greenaway et al. 1985), selenate (Usami et al. 2008), selenite (Usami et al. 2008), tributyltin (Cooke et al. 2008; Adeeko et al. 2003), and valproic acid (Guest et al. 1994)

Migration assay of NCCs

The migration distance of NCCs was calculated as the increased radius of the circular spread of NCCs that emigrated from the neural tubes between 24 and 48 h of culture (Usami et al. 2014b). The outermost NCCs in each of the cultured neural tubes were connected with the polygon tool as if a rubber band were put around the cells, and its inner area was measured as a pixel count. Considering the polygon as a circle, its radius ratio was calculated: radius ratio = (radius at 48 h - radius at 24 h)/radius at 24 h. This ratio was then normalized as a percent of the simultaneous control to express the NCC migration for comparisons among experiments.

Proliferation assay for NCCs

NCC proliferation was evaluated as a ratio of the cell count at 48 h to that at 24 h of culture, and the effects of chemicals were examined. The cells were counted manually at 24 h on the phase-contrast image with the Cell Counter plugin of the ImageJ software (http://rsb.info.nih.gov/ij/, 1997–2009; Rasband, W.S., ImageJ, U. S. National Institutes of Health, Bethesda, MD, USA). The cell count at 48 h was estimated as the count of stained cell nuclei from the fluorescence image with the Hybrid Cell Count function of the BZ-X Analyzer software (Keyence). The average cell counts in an intact control group were 170.6 at 24 h and 272.1 at 48 h (n = 10). Two proliferation indices, the cell count ratio and the cell proliferation ratio, were calculated as follows: cell count ratio = cell count at 48 h/cell count at 24 h, and cell proliferation ratio = (cell count at 48 h - cell count at 24 h)/cell count at 24 h.

Although these indices are basically the same, the latter is more suitable for representing

the proliferation rate and the former is more useful for comparison with the migration index. These indices were normalized to the control to allow for comparisons among experiments.

Statistical analysis

Statistical significance of the difference between the experimental groups was examined by the Student *t* test at a probability level of 5%.

RESULTS

Effects of chemicals on the migration of cNCCs

Of the 13 chemicals we tested, six chemicals, that is, 13-*cis*-retinoic acid, ethanol, ibuprofen, lead acetate, salicylic acid, and selenate, significantly inhibited the migration of cNCCs at their embryotoxic concentrations. 13-*cis*-Retinoic acid reduced the migration of cNCCs by approximately 13% at concentrations of 3 and 10 μM (Fig. 3A). Ethanol, ibuprofen, salicylic acid and selenate reduced the migration of cNCCs by 10.5% at 195 mM, 15.9% at 2 mM, 8.5% at 3 mM and 16.2% at 150 μM, respectively (Figs. 3B - E).

Lead acetate reduced the migration of cNCCs by 11.6% at 3 μM and by 30.0% at 10 μM in an initial experiment (Fig. 3F). Because evaluation of the toxic effects of lead at low exposure levels is important for human health, two lower concentrations were added stepwise so that the no-observed-effect level could be estimated. Lead acetate reduced the migration of cNCCs significantly by 8.7% at 1 μM; however, the decrease (6.4%) was not significant at 0.1 μM (Fig. 3G).

The remaining seven chemicals, that is, acetaminophen, caffeine, indium, phenytoin, selenite, tributyltin, and valproic acid, had no significant effects on the migration of cNCCs even at high concentrations (Figs. 4A-G). Indium did not affect the migration of cNCCs and tNCCs in the experiments (Fig. 4C). These experiments for indium were performed at a single concentration for cNCCs and tNCCs because indium showed no effects on the migration of cNCCs in a pilot study and because indium has been reported to cause malformation in the caudal part of rat embryos (Nakajima et al. 2008).

Effects of chemicals on the proliferation of cNCCs

Effects on the proliferation of cNCCs were examined in the case of six chemicals (i.e., 13-*cis*-retinoic acid, ethanol, ibuprofen, lead acetate, salicylic acid, and selenate) that showed inhibitory effects on the migration of cNCCs. The effects of tributyltin on cNCC proliferation were also examined because of our interest in another research project. To reduce the number of animals to be used, two chemicals with the same vehicle were examined concomitantly when possible. In the control groups, the actual cell count increased by approximately 50% during the 24-h exposure period.

13-*cis*-Retinoic acid did not significantly reduce the proliferation of cNCCs at concentrations of 3 and 10 µM, the same concentrations at which it inhibited the migration of cNCCs, although the cell count ratio and the cell proliferation ratio were lowered by 2.5% and 9.7%, respectively, at 3 µM compared to the control group (Fig. 5A).

Ethanol, ibuprofen, salicylic acid, and selenate significantly reduced the cell count ratio by 16.3%, 14.1%, 12.3%, and 20.6%, and the cell proliferation ratio by 59.0%, 43.0%, 33.1%, and 55.4%, respectively, at the same concentrations (195 mM, 2 mM, 3 mM, and 150 µM, respectively) at which they inhibited the migration of cNCCs (Fig. 5B - D).

Lead acetate increased the cell count ratio by 2.2% and the cell proliferation ratio by 6.6% at 1 µM concentration, the lowest effective concentration for inhibiting the migration of cNCCs, although these differences were not statistically significant (Fig. 5C).

Tributyltin reduced the cell count ratio by 9.2% and the cell proliferation ratio by 27.0% at 100 nM concentration, although no reduction in the migration of cNCCs was observed (Fig. 5E).

There was no significant correlation between proliferation inhibition and migration inhibition when the reduced migration was plotted against the reduced cell count ratio, suggesting a varied contribution of the latter to the former (Fig. 6).

DISCUSSION

Here, we observed inhibition of the migration of rat cNCCs by six developmentally toxic chemicals including those not previously reported to have the inhibitory effects: ibuprofen, salicylic acid, and selenate. It is speculated that inhibition of the migration of cNCCs results in reduction of the number of cNCCs at their destination tissues. The inhibited migration of cNCCs by itself, however, seems insufficient as a pathogenic mechanism underlying teratogenicity because these chemicals do not necessarily cause similar malformations. It is probable that the inhibited migration of cNCCs that is not accompanied by an excessive cell shortage is compensated by accelerated cell proliferation at their destination tissues. Alternatively, these inhibitory effects may occur differently in the body of embryos.

From the results of the proliferation assay, it is considered that the reduced cell number may contribute to the inhibited migration of cNCCs to varying extents depending on the test chemicals. It is suggested that the migration-inhibitory effects of ethanol, ibuprofen, and selenate are due in part to the reduced number of cNCCs. In contrast, in the case of tributyltin, the reduced cell number did not affect the migration of cNCCs. Chemicals that did not inhibit cell proliferation, for example, 13-*cis*-retinoic acid, and lead acetate, appeared to inhibit the migration of cNCCs independent of the cell number.

13-*cis*-Retinoic acid appeared to more potently inhibit the migration of cNCCs than all-*trans*-retinoic acid, because the inhibitory concentration of the former (3 μM) was found to be lower than that of the latter (10 μM) in our previous study (Usami et al. 2014b). This is inconsistent with the teratogenic potential of the retinoic acids in rats, where 13-*cis*-retinoic acid is less teratogenic because of its faster elimination from the body (Collins et al. 1994). Isolated cNCCs themselves may be more susceptible to

13-*cis*-retinoic acid than all-*trans*-retinoic acid, as suggested by the lower affinity of 13-*cis*-retinoic acid for cytoplasmic retinoid binding proteins, which may enable easy access to the cell nucleus (Rühl et al. 2001).

Ethanol is a well-known teratogen causing craniofacial malformations (Schardein & Macina 2006) and its toxic effects on NCCs have often been investigated. It was previously shown that ethanol caused apoptotic cell death (Yan et al. 2010) and inhibited migration (Shi et al. 2014) of NCCs. In the present study, both reduced cell number and inhibited migration of cNCCs were observed as the effects of ethanol, although the effective concentration of ethanol was relatively higher than those reported in previous studies, probably because of species and strain differences in the susceptibility to ethanol (Wentzel & Eriksson 2008).

Inhibitory effects of ibuprofen and salicylic acid, which are non-steroidal anti-inflammatory drugs (NSAIDs), on the migration of NCCs have not been reported to date. Although these NSAIDs are considered non-teratogenic in humans, their embryotoxic effects, including craniofacial malformations, observed in animal experiments (Joschko et al. 1993; Kosar 1993) may be related to their migration-inhibitory effects on cNCCs.

The migration-inhibitory effects of lead acetate in the present study are consistent with previously reported results for human NCCs derived from embryonic stem cells (Zimmer et al. 2012). In both studies, lead acetate at 1 μM (20 μg/dl) or higher concentrations inhibited the migration of NCCs without reduced cell proliferation. It is noted that this inhibitory concentration is comparable to blood lead levels (40.0 ± 16.5 μg/dl, mean ± SD) in a certain proportion of pregnant women (Ugwuja et al. 2012). Although lead caused craniofacial malformations only in cultured rat embryos (Zhao et al. 1997)

and does not cause major malformations in humans, its migration-inhibitory effects on cNCCs, as a neuronal progenitor, may be related to functional deficiencies such as neurological alterations (Flora et al. 2011).

The effects of the two selenium compounds on the migration of cNCCs were different in the present study; i.e., selenate inhibited the migration of cNCCs while selenite did not. This difference may be related to the difference in malformed optic vesicles and the protein expression changes caused by the selenium compounds in cultured rat embryos; selenate caused enlargement of the optic vesicle (Usami et al. 2008), a destination of migrating cNCCs (Le Douarin & Kalcheim 1999), and increased the phosphorylated form (inactive form) of cofilin 1 (Usami et al. 2008), an actin-binding protein essential for the migration of NCCs (Gurniak et al. 2005), while selenite did not cause either (Usami et al. 2008). It is thus speculated that selenate inhibits the migration of cNCCs through inactivation of cofilin 1, which results in malformation of the optic vesicle.

In this context, it is intriguing that ethanol and indium also increased phosphorylated cofiline 1 in cultured rat embryos (Usami et al. 2014a; Usami et al. 2009). However, indium did not have inhibitory effects on the migration of cNCCs or tNCCs in the present study. This may indicate that the increase in phosphorylated cofilin 1 alone is not a sufficient condition for inhibition of the migration of NCCs, or that it could occur in different embryonic cells.

The proliferation-inhibitory effects of tributyltin on cNCCs without reduced migration may be related to its developmental toxicity; treatment of pregnant rats with tributyltin that caused blood concentrations comparable to those in the present study, reduced the body weights of pups without causing external malformations (Adeeko et al. 2003; Cooke et al. 2008).

It is unknown at present why the proliferation-inhibitory effects of tributyltin were not accompanied by the inhibited migration of cNCCs. It is unlikely that tributyltin increased the migration of cNCCs, compensating its proliferation-inhibitory effects. This is because tributyltin did not have any effects on the migration of cNCCs over the concentration tested even when the neural tube was removed at 18 h of culture and the cNCCs could move more freely during the exposure period (data not shown). Rather, the relatively selective toxicity and accumulation of tributyltin in the mitochondria (Doherty & Irwin 2011) might have no effects on the migration of cNCCs. In any case, no correlation between proliferation inhibition and migration inhibition means that the NCC migration assay can not be replaced by usual cytotoxicity assays based on the cell number and is valuable to investigate the effects of chemicals on the function of NCCs.

While valproic acid did not inhibit the migration of cNCCs in the present study, the effects of valproic acid on the migration of NCCs are controversial. Valproic acid inhibited the migration of human NCCs in a scratch assay (Zimmer et al. 2012), but did not inhibit the migration of chick NCCs in cultured neural tubes (Fuller et al. 2002). Currently available data indicate that the effects of valproic acid on the migration of NCCs seem to depend on the assay method and the species used in which it is used.

For other chemicals (acetaminophen, caffeine, and phenytoin) that did not inhibit the migration of cNCCs, no particular information concerning the involvement of NCCs' malfunction in their developmental toxicity was found, except that acetaminophen did not inhibit the migration of human NCCs either (Zimmer et al. 2012).

In conclusion, it was established that several developmentally toxic chemicals inhibit the migration of cNCCs, which appears differently as craniofacial abnormalities. Mechanistic investigation is needed to understand the variability in the outcomes of the

inhibited migration of cNCCs. Our migration assay method will be useful for this purpose because of its simplicity.

CONFLICT OF INTEREST

The authors declare that there are no conflicts of interest.

ACKNOWLEDGEMENTS

This work was supported by a Health and Labor Science Research Grant from the Ministry of Health, Labour and Welfare in Japan.

REFERENCES

Adeeko A, Li D, Forsyth DS, Casey V, Cooke GM, Barthelemy J, Cyr DG, Trasler JM, Robaire B, Hales BF. 2003. Effects of in utero tributyltin chloride exposure in the rat on pregnancy outcome. Toxicol Sci 74: 407–15.

Collins MD, Tzimas G, Hummler H, Bürgin H, Nau H. 1994. Comparative teratology and transplacental pharmacokinetics of all-*trans*-retinoic acid, 13-*cis*-retinoic acid, and retinyl palmitate following daily administrations in rats. Toxicol Appl Pharmacol 127: 132–44.

Cooke GM, Forsyth DS, Bondy GS, Tachon R, Tague B, Coady L. 2008. Organotin speciation and tissue distribution in rat dams, fetuses, and neonates following oral administration of tributyltin chloride. J Toxicol Environ Health A 71: 384–95.

Doherty JD, Irwin WA. 2011. Organotins (tributyltin and triphenyltin). In: Gupta RC, editor. Reproductive and Developmental Toxicology. Sandiego, California: Elsevier. p. 657–672.

Flora SJS, Pachauri V, Saxena G. 2011. Arsenic, cadmium and lead. In: Gupta RC, editor. Reproductive and Developmental Toxicology. Sandiego, California: Elsevier. p. 415–438.

Fuller LC, Cornelius SK, Murphy CW, Wiens DJ. 2002. Neural crest cell motility in valproic acid. Reprod Toxicol 16: 825–839.

Greenaway JC, Mirkes PE, Walker EA, Juchau MR, Shepard TH, Fantel AG. 1985. The effect of oxygen concentration on the teratogenicity of salicylate, niridazole, cyclophosphamide, and phosphoramide mustard in rat embryos in vitro. Teratology 32: 287–295.

Guest I, Buttar HS, Smith S, Varma DR. 1994. Evaluation of the rat embryo culture system as a predictive test for human teratogens. Can J Physiol Pharmacol 72: 57–62.

Gurniak CB, Perlas E, Witke W. 2005. The actin depolymerizing factor n-cofilin is essential for neural tube morphogenesis and neural crest cell migration. Dev Biol 278: 231–241.

Hall BK. 2009. Neurocristopathies. In: The Neural Crest and Neural Crest Cells in Vertebrate Development and Evolution. 2nd ed. New York: Springer. p. 269–293.

Joschko MA, Dreosti IE, Tulsi RS. 1993. The teratogenic effects of salicylic acid on the developing nervous system in rats in vitro. Teratology 48: 104–114.

Kawakami M, Umeda M, Nakagata N, Takeo T, Yamamura K-I. 2011. Novel migrating mouse neural crest cell assay system utilizing P0-Cre/EGFP fluorescent time-lapse imaging. BMC Dev Biol 11: 68.

Kim S-R, Kubo T, Kuroda Y, Hojyo M, Matsuo T, Miyajima A, Usami M, Sekino Y, Matsushita T, Ishida S. 2014. Comparative metabolome analysis of cultured fetal and adult hepatocytes in humans. J Toxicol Sci 39: 717–23.

Kosar K. 1993. Interaction of ibuprofen with early chick embryogenesis. Pharmazie 48: 207–9.

Le Douarin N, Kalcheim C. 1999. The Neural Crest. 2nd ed. New York: Cambridge University Press.

Lee QP, Juchau MR, Kraft JC. 1991. Microinjection of cultured rat embryos: studies with retinol, 13-cis- and all-trans-retinoic acid. Teratology 44: 313–23.

Menegola E, Broccia ML, Di Renzo F, Massa V, Giavini E. 2004. Relationship between hindbrain segmentation, neural crest cell migration and branchial arch abnormalities in rat embryos exposed to fluconazole and retinoic acid *in vitro*. Reprod Toxicol 18: 121–130.

Nakajima M, Mitsunaga K, Nakazawa K, Usami M. 2008. In vivo/in vitro study in rat embryos on indium-caused tail malformations. Reprod Toxicol 25: 426–32.

Robinson JF, van Beelen VA, Verhoef A, Renkens MFJ, Luijten M, van Herwijnen MHM, Westerman A, Pennings JLA, Piersma AH. 2010. Embryotoxicant-specific transcriptomic responses in rat postimplantation whole-embryo culture. Toxicol Sci 118: 675–85.

Rühl R, Plum C, Elmazar MM, Nau H. 2001. Embryonic subcellular distribution of 13-*cis*- and all-*trans*-retinoic acid indicates differential cytosolic/nuclear localization. Toxicol Sci 63: 82–9.

Schardein JL, Macina OT. 2006. Ethanol. In: Human Developmental Toxicants: Aspects of Toxicology and Chemistry. Boca Raton, Florida: Taylor & Francis. p. 301–322.

Shi Y, Li J, Chen C, Gong M, Chen Y, Liu Y, Chen J, Li T, Song W. 2014. 5-mehtyltetrahydrofolate rescues alcohol-induced neural crest cell migration abnormalities. Mol Brain 7: 67.

Shreiner CM, Zimmerman EF, Wee EL, Scott Jr WJ. 1986. Caffein effects on cyclic AMP levels in the mouse embryonic limb and palate in vitro. Teratology 34: 21–27.

Ugwuja EI, Ibiam UA, Ejikeme BN, Obuna JA, Agbafor KN. 2012. Blood Pb Levels in pregnant Nigerian women in Abakaliki, South-Eastern Nigeria. Environ Monit Assess.

Usami M, Mitsunaga K, Irie T, Miyajima A, Doi O. 2014a. Proteomic analysis of ethanol-induced embryotoxicity in cultured post-implantation rat embryos. J Toxicol Sci 39: 285–92.

Usami M, Mitsunaga K, Irie T, Miyajima A, Doi O. 2014b. Simple in vitro migration assay for neural crest cells and the opposite effects of all-trans-retinoic acid on cephalic- and trunk-derived cells. Congenit Anom (Kyoto) 54: 184–188.

Usami M, Mitsunaga K, Nakazawa K, Doi O. 2008. Proteomic analysis of selenium embryotoxicity in cultured postimplantation rat embryos. Birth Defects Res B Dev Reprod Toxicol 83: 80–96.

Usami M, Nakajima M, Mitsunaga K, Miyajima A, Sunouchi M, Doi O. 2009. Proteomic analysis of indium embryotoxicity in cultured postimplantation rat embryos. Reprod Toxicol 28: 477–88.

Weeks BS, Gamache P, Klein NW, Hinson JA, Bruno M, Khairallah E. 1990. Acetaminophen toxicity to cultured rat embryos. Teratog Carcinog Mutagen 10: 361–71.

Wentzel P, Eriksson UJ. 2008. Genetic influence on dysmorphogenesis in embryos from different rat strains exposed to ethanol in vivo and in vitro. Alcohol Clin Exp Res 32: 874–887.

Winn L. 2002. Evidence for Ras-Dependent Signal Transduction in Phenytoin Teratogenicity. Toxicol Appl Pharmacol 184: 144–152.

Yan D, Dong J, Sulik KK, Chen S. 2010. Induction of the Nrf2-driven antioxidant response by tert-butylhydroquinone prevents ethanol-induced apoptosis in cranial neural crest cells. Biochem Pharmacol 80: 144–9.

Zhao SF, Zhang XC, Zhang LF, Zhou SS, Zhang F, Wang QF, Wang YL, Bao YS. 1997. The evaluation of developmental toxicity of chemicals exposed occupationally using whole embryo culture. Int J Dev Biol 41: 275–282.

Zimmer B, Lee G, Balmer N V, Meganathan K, Sachinidis A, Studer L, Leist M. 2012. Evaluation of developmental toxicants and signaling pathways in a functional test based on the migration of human neural crest cells. Environ Health Perspect 120: 1116–22.

Legends to the figures

Fig. 1. Culture schedule of for the migration and proliferation assays of cephalic neural crest cells (cNCCs)

Neural tubes were excised from the rhombencephalic region of day 10.5 rat embryos and cultured for 48 h to allow the emigration of cNCCs. Chemicals were added to the culture medium at 24 h. In the proliferation assay, the neural tubes were removed from the culture dishes at 18h leaving the cNCCs behind, and the cell nuclei were fluorescently stained before the photography at 48 h.

Fig. 2. Photographs of cephalic neural crest cells (cNCCs) cultured in the migration and proliferation assays

(A) cNCCs cultured in the migration assay are shown with blue polygons connecting the outermost cells for the calculation of the cell migration. (B) cNCCs cultured in the proliferation assay are shown with blue dots (24 h) or stained cell nuclei (48 h) for the determination of the cell count.

Fig. 3. Migration of cephalic neural crest cells (cNCCs) cultured in the presence of developmentally toxic chemicals with migration-inhibitory effects

Migration indices were calculated as the radius ratio from the circular spread of cNCCs at 24 and 48 h of culture. The mean ± standard error of the mean (SEM) values of 6–27 neural tubes are shown. Asterisks indicate statistically significant differences from the corresponding control (*, $p < 0.05$; **, $p < 0.01$; ***, $p < 0.001$; ****, $p < 0.0001$).

Fig. 4. Migration of cephalic neural crest cells (cNCCs) cultured in the presence of

developmentally toxic chemicals without migration-inhibitory effects

Migration indices were calculated as the radius ratio from the circular spread of cNCCs at 24 and 48 h of culture. The mean ± standard error of the mean (SEM) values of 8–16 neural tubes are shown. Effects of indium were examined also in trunk neural crest cells as shown in (C).

Fig. 5. Proliferation of cephalic neural crest cells (cNCCs) cultured in the presence of developmentally toxic chemicals

The cNCCs were counted at 24 and 48h of culture, and the proliferation indices were calculated. The mean ± standard error of the mean (SEM) values of 7–10 neural tubes are shown. Asterisks indicate statistically significant differences from the corresponding control (*, $p < 0.05$; **, $p < 0.01$; ***, $p < 0.001$).

Fig. 6. Plot of the reduced migration versus the reduced cell count ratio of neural crest cells cultured in the presence of developmentally toxic chemicals

The reduced migration and reduced cell count ratio were calculated by subtracting the corresponding data in Figs. 1–3 from 100%. The linear regression line and correlation coefficient (r) for all the plotted data are shown.

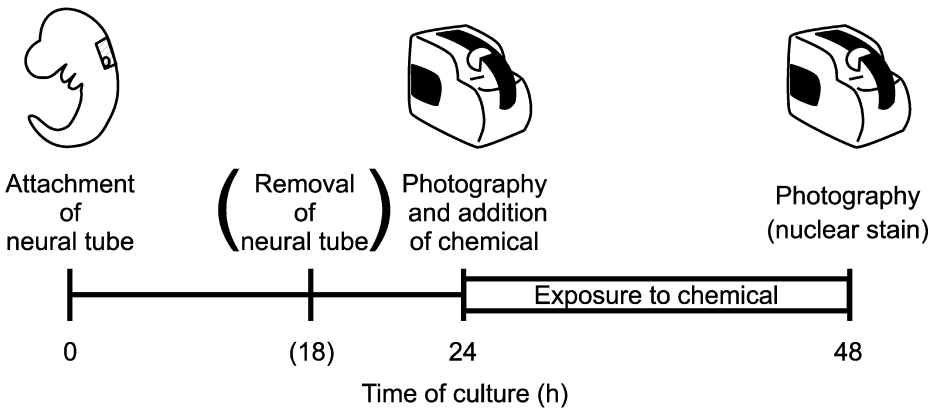

Fig. 1

CGA_12121_F1

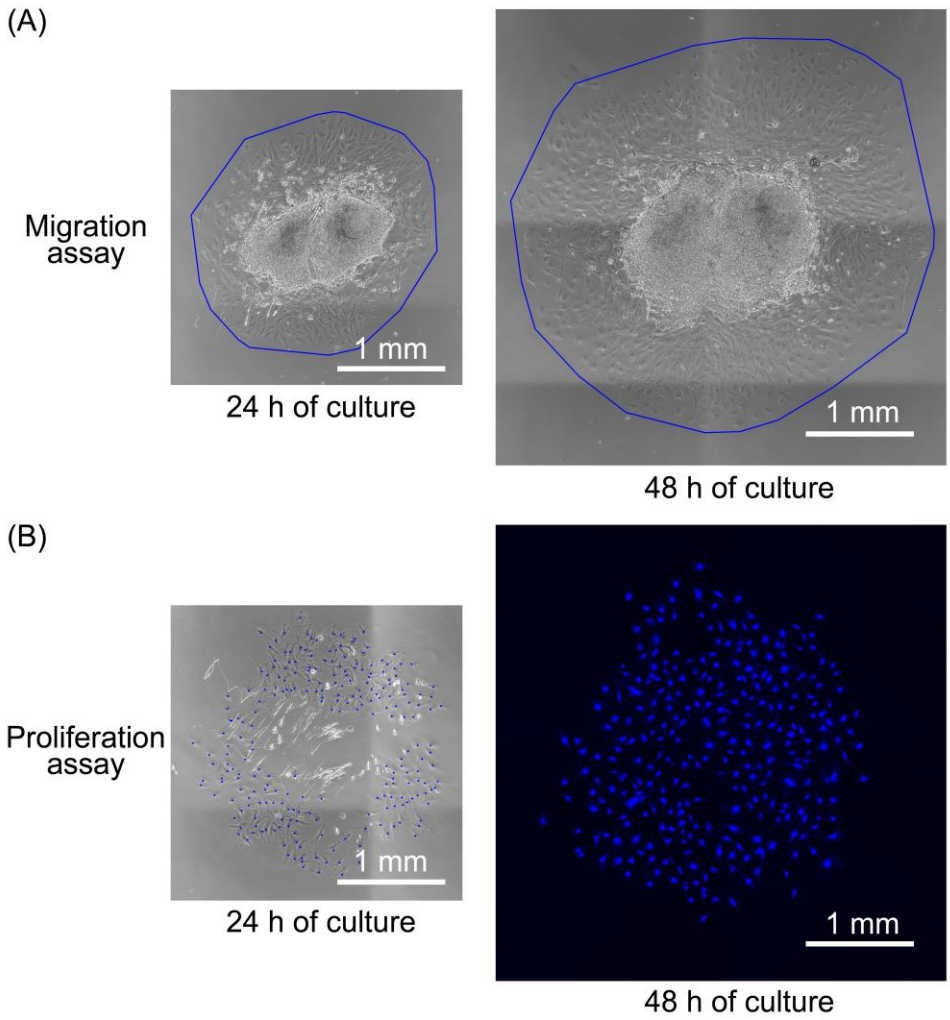

Fig.2

CGA_12121_F2

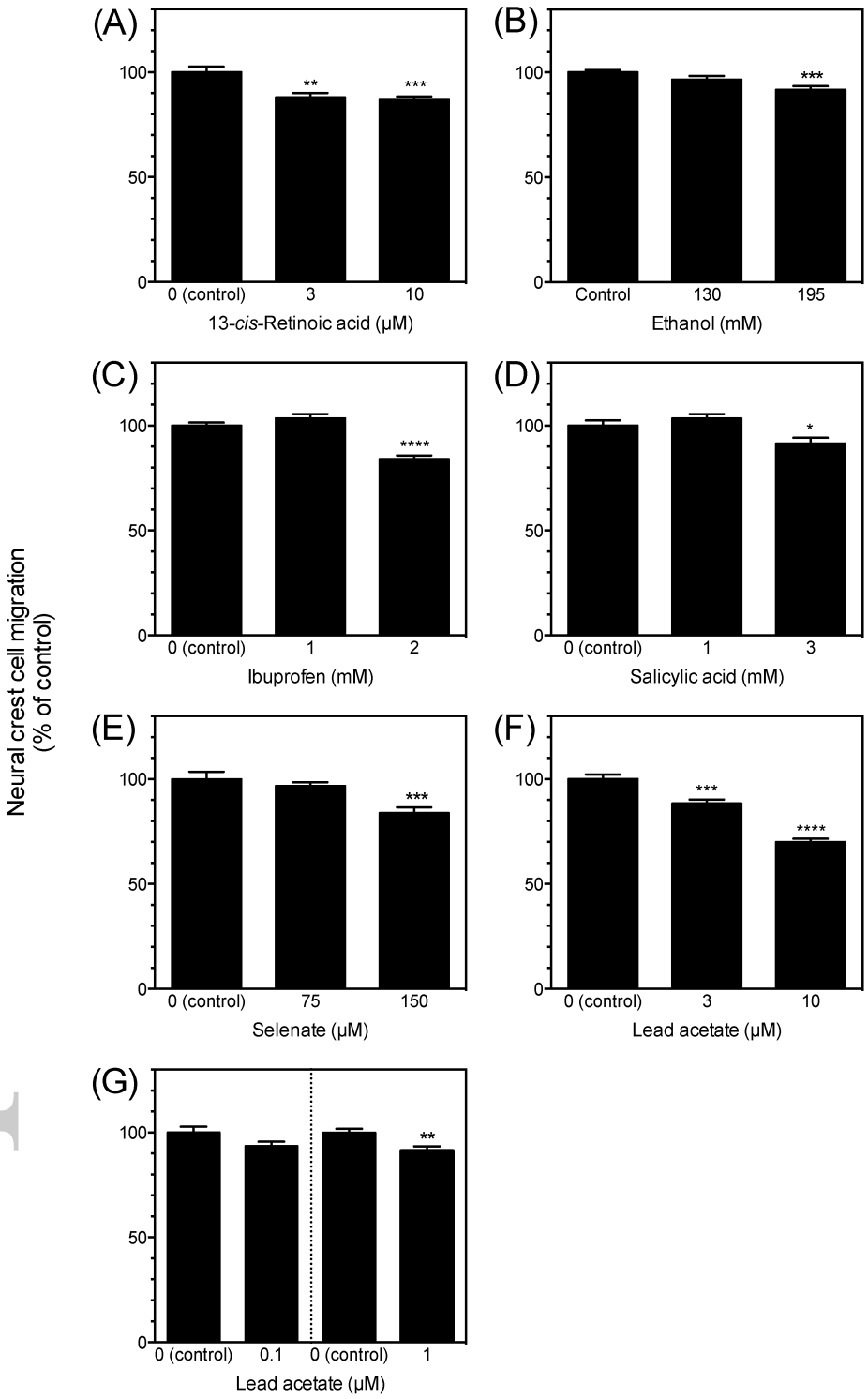

Fig.3

CGA_12121_F3

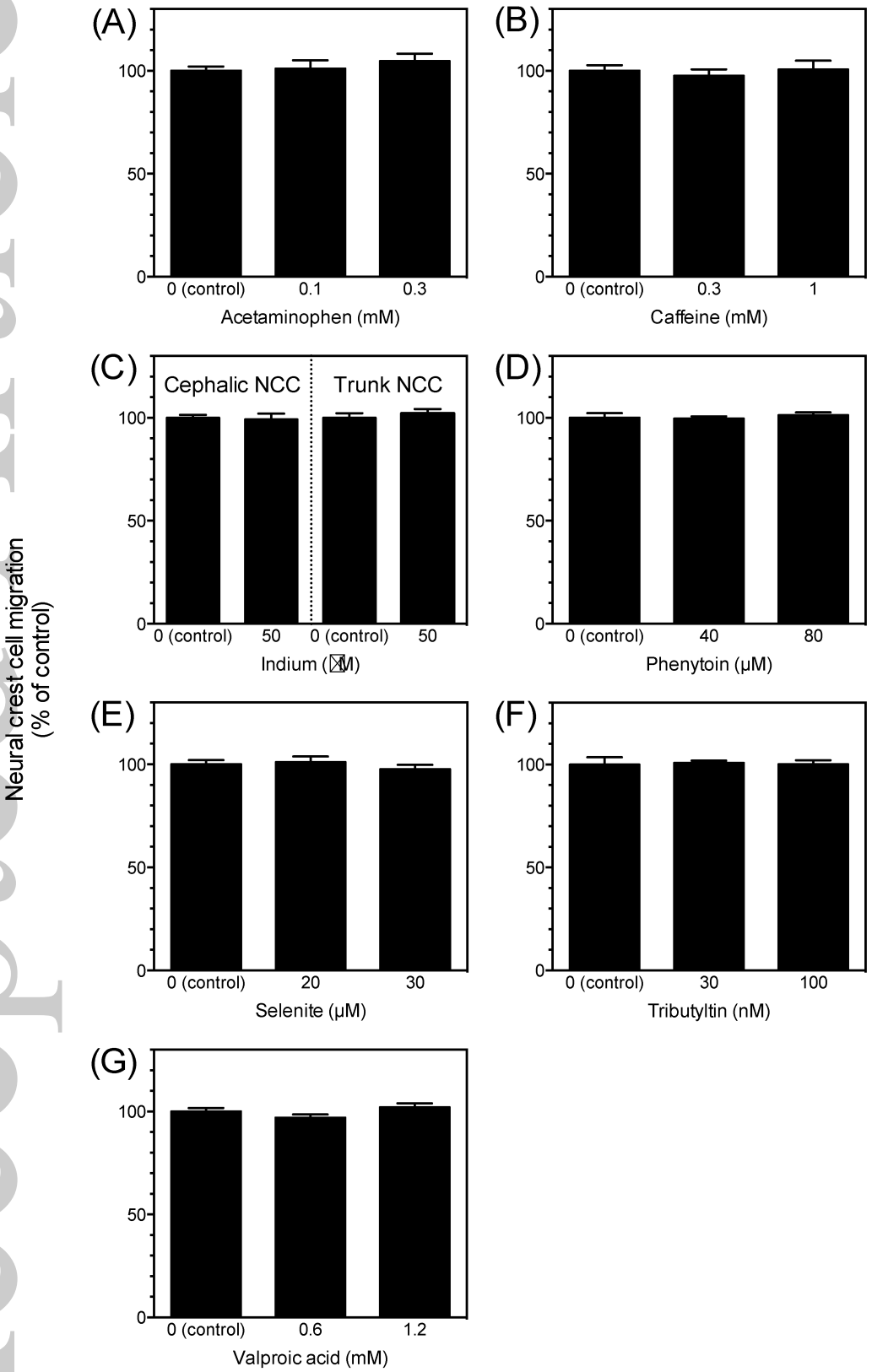

Fig.4

CGA_12121_F4

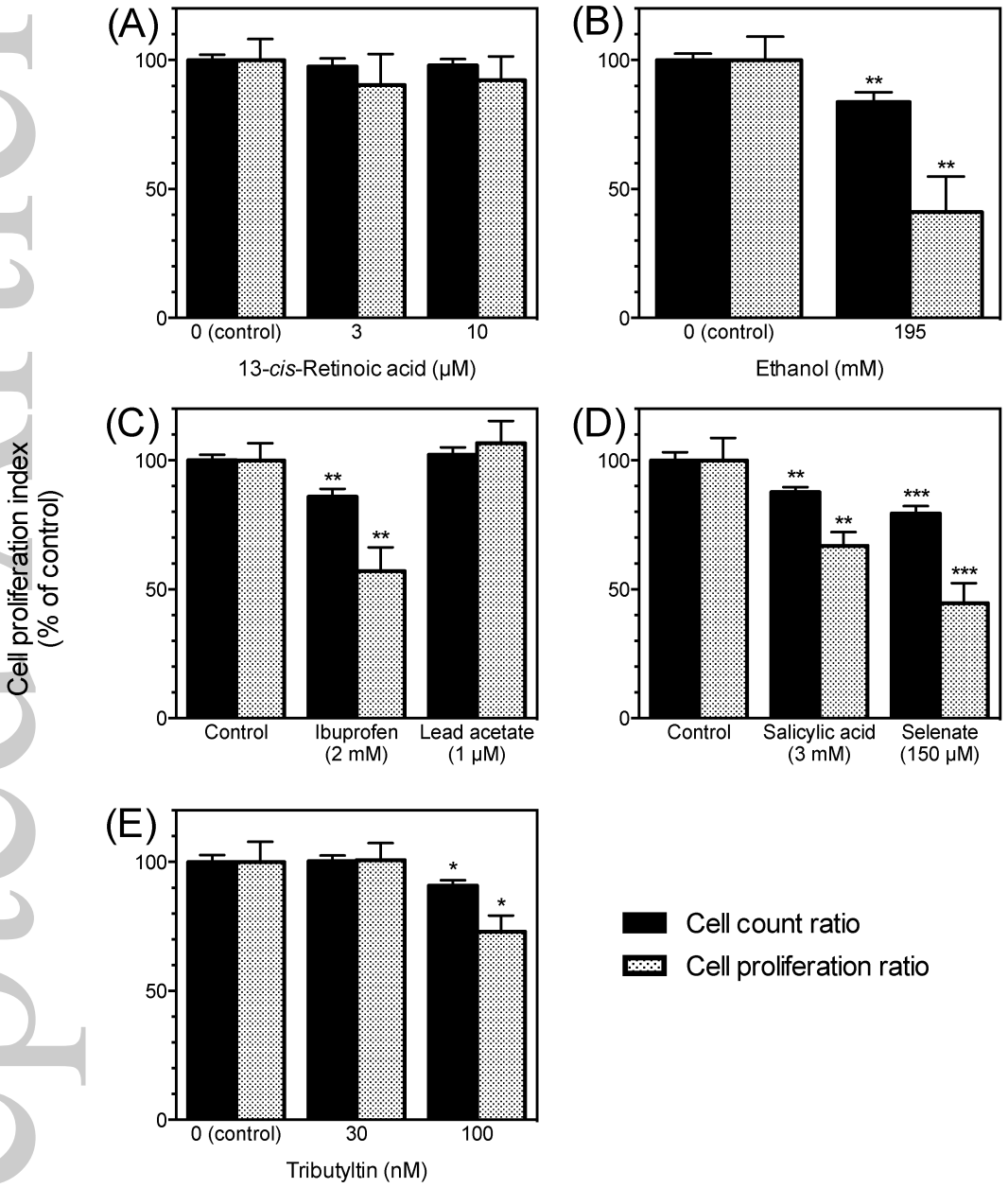

Fig.5

CGA_12121_F5

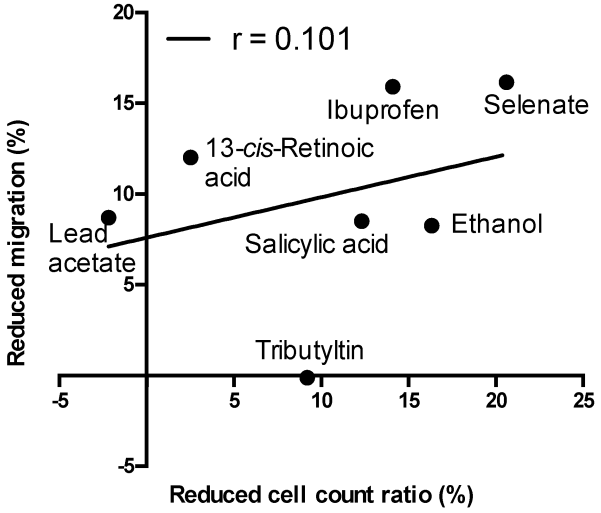

Fig.6

CGA_12121_F6

Neuropharmacology 95 (2015) 479–491

Contents lists available at ScienceDirect

Neuropharmacology

journal homepage: www.elsevier.com/locate/neuropharm

MAM-2201, a synthetic cannabinoid drug of abuse, suppresses the synaptic input to cerebellar Purkinje cells via activation of presynaptic CB1 receptors

Tomohiko Irie [a, *], Ruri Kikura-Hanajiri [b], Makoto Usami [a], Nahoko Uchiyama [b], Yukihiro Goda [c], Yuko Sekino [a, **]

[a] Division of Pharmacology, National Institute of Health Sciences, Tokyo, Japan
[b] Division of Pharmacognosy, Phytochemistry, and Narcotics, National Institute of Health Sciences, Tokyo, Japan
[c] Division of Drugs, National Institute of Health Sciences, Tokyo, Japan

ARTICLE INFO

Article history:
Received 26 June 2014
Received in revised form
18 December 2014
Accepted 20 February 2015
Available online 5 March 2015

Keywords:
Synthetic cannabinoids
MAM-2201
Cannabinoid receptor type 1
Purkinje cell
Cerebellum
Neurotransmitter release

ABSTRACT

Herbal products containing synthetic cannabinoids—initially sold as legal alternatives to marijuana—have become major drugs of abuse. Among the synthetic cannabinoids, [1-(5-fluoropentyl)-1*H*-indol-3-yl](4-methyl-1-naphthalenyl)-methanone (MAM-2201) has been recently detected in herbal products and has psychoactive and intoxicating effects in humans, suggesting that MAM-2201 alters brain function. Nevertheless, the pharmacological actions of MAM-2201 on cannabinoid receptor type 1 (CB1R) and neuronal functions have not been elucidated. We found that MAM-2201 acted as an agonist of human CB1Rs expressed in AtT-20 cells. In whole-cell patch-clamp recordings made from Purkinje cells (PCs) in slice preparations of the mouse cerebellum, we also found that MAM-2201 inhibited glutamate release at parallel fiber-PC synapses via activation of presynaptic CB1Rs. MAM-2201 inhibited neurotransmitter release with an inhibitory concentration 50% of 0.36 μM. MAM-2201 caused greater inhibition of neurotransmitter release than Δ^9-tetrahydrocannabinol within the range of 0.1–30 μM and JWH-018, one of the most popular and potent synthetic cannabinoids detected in the herbal products, within the range of 0.03–3 μM. MAM-2201 caused a concentration-dependent suppression of GABA release onto PCs. Furthermore, MAM-2201 induced suppression of glutamate release at climbing fiber-PC synapses, leading to reduced dendritic Ca^{2+} transients in PCs. These results suggest that MAM-2201 is likely to suppress neurotransmitter release at CB1R-expressing synapses in humans. The reduction of neurotransmitter release from CB1R-containing synapses could contribute to some of the symptoms of synthetic cannabinoid intoxication including impairments in cerebellum-dependent motor coordination and motor learning.

Abbreviations: ACSF, artificial cerebrospinal fluid; AM251, *N*-(piperidin-1-yl)-5-(4-iodophenyl)-1-(2,4-dichlorophenyl)-4-methyl-1*H*-pyrazole-3-carboxamide; CB1R, cannabinoid receptor type 1; CB2R, cannabinoid receptor type 2; CF, climbing fiber; CI, confidence interval; CV, coefficient of variation; DNQX, 6,7-dinitroquinoxaline-2,3-dione; EC50, effective concentration 50%; eCBs, endocannabinoids; EGTA, ethylene glycol tetraacetic acid; EPSC, excitatory postsynaptic current; GFP, green fluorescent protein; hCB1R, human CB1R; HEPES, 4-(2-hydroxyethyl)-1-piperazineethanesulfonic acid; IC50, inhibitory concentration 50%; IEI, inter-event interval; IPSC, inhibitory postsynaptic current; JWH-018, naphthalen-1-yl-(1-pentylindol-3-yl)methanone; LTD, long-term depression; MAM-2201, [1-(5-fluoropentyl)-1*H*-indol-3-yl](4-methyl-1-naphthalenyl)-methanone; mCB1R, mouse CB1R; mIPSC, miniature IPSC; OGB-1, Oregon Green 488 BAPTA-1 hexapotassium salt; P, postnatal day; PC, Purkinje cell; PF, parallel fiber; PPR, paired-pulse ratio; qEPSC, quantal EPSC; THC, tetrahydrocannabinol; TTX, tetrodotoxin; WIN, WIN 55,212-2 mesylate, (*R*)-(+)-[2,3-Dihydro-5-methyl-3-(4-morpholinylmethyl)pyrrolo[1,2,3-de]-1,4-benzoxazin-6-yl]-1-naphthalenylmethanone mesylate.

* Corresponding author. Division of Pharmacology, National Institute of Health Sciences, 1-18-1 Kamiyoga, Setagaya-ku, Tokyo 158-8501, Japan. Tel.: +81 3 3700 9762.
** Corresponding author. Division of Pharmacology, National Institute of Health Sciences, 1-18-1 Kamiyoga, Setagaya-ku, Tokyo 158-8501, Japan. Tel.: +81 3 3700 9692.
E-mail addresses: irie@nihs.go.jp (T. Irie), yukos@nihs.go.jp (Y. Sekino).

http://dx.doi.org/10.1016/j.neuropharm.2015.02.025
0028-3908/

1. Introduction

Marijuana (*Cannabis sativa*) has been widely abused for recreational purposes and contains the psychoactive compound Δ^9-tetrahydrocannabinol (Δ^9-THC) (Taura et al., 2007). Δ^9-THC binds to cannabinoid receptors type 1 and 2 (CB1R and CB2R), which are G protein-coupled receptors. CB1Rs are abundantly expressed in the mammalian brain, whereas CB2Rs are expressed mainly in the immune system (Showalter et al., 1996; Mackie, 2008; Kano et al., 2009). The psychoactive effects of Δ^9-THC are mediated by CB1Rs (Huestis et al., 2001; Monory et al., 2007). Starting in the late 2000s, herbal products containing synthetic cannabinoids, which are chemical compounds produced for the purpose of mimicking the effects of Δ^9-THC, became a major class of drugs of abuse, and are sold as alternatives to marijuana around the world (Auwarter et al., 2009; Vardakou et al., 2010; Seely et al., 2012; Kikura-Hanajiri et al., 2013). Among the synthetic cannabinoids, [1-(5-fluoropentyl)-1*H*-indol-3-yl](4-methyl-1-naphthalenyl)-methanone (MAM-2201, Fig. 1*A*) was recently identified in these herbal products (Moosmann et al., 2012; Derungs et al., 2013; Kikura-Hanajiri et al., 2013; Saito et al., 2013; Uchiyama et al., 2013; Lonati et al., 2014). In humans, abuse of products containing MAM-2201 causes a psychotic state with agitation, aggression, and anxiety, and can cause serious harm to the user including death. These reports imply that MAM-2201 exerts potent pharmacological actions on brain functions and causes psychoactive and intoxicating effects. Nevertheless, it remains unknown whether MAM-2201 activates CB1Rs and how MAM-2201 affects neuronal functions such as synaptic transmission.

Endocannabinoids (eCBs) mediate various types of synaptic plasticity throughout the mammalian brain. eCBs are released from postsynaptic neurons in response to synaptic activity and act in a retrograde manner on presynaptic terminals, to suppress neurotransmitter release (Wilson and Nicoll, 2002; Kano et al., 2009; Regehr et al., 2009). The synaptic effects of eCBs are mediated by presynaptic CB1Rs. In presynaptic terminals, activation of CB1Rs mainly inhibits voltage-gated Ca^{2+} channels coupled to exocytosis, leading to a reduction of neurotransmitter release (Brown et al., 2004; Kushmerick et al., 2004).

Numerous neurophysiological and neuropharmacological studies of CB1Rs have been performed on the cerebellum of rodents, which have well-characterized neuronal circuits and play crucial roles in motor coordination and motor learning (Llinas et al., 2004; Kano et al., 2009). In the cerebellum, Purkinje cells (PCs) are the principal GABAergic neurons and provide the sole output from the cerebellar cortex. PCs receive two types of glutamatergic excitatory inputs, climbing fibers (CFs) and parallel fibers (PFs). CFs arise from the inferior olivary complex. Activation of CF-PC synapses induces strong postsynaptic depolarization, which evokes a dendritic Ca^{2+} transient and complex spikes consisting of a burst of several action potentials (spikelets). PFs are the axons of the granule cells located in the deep layers of the cerebellum and form numerous *en passant* synapses on the spines of distal dendrites of PCs (Llinas et al., 2004). PCs also receive feed-forward inhibition from GABAergic interneurons in the molecular layer of the cerebellar cortex (Mittmann et al., 2005). Neurotransmitter release at CF-PC, PF-PC, and interneuron-PC synapses is suppressed via activation of presynaptic CB1Rs (Kreitzer and Regehr, 2001; Diana et al., 2002; Szabo et al., 2004; Kawamura et al., 2006; Safo et al., 2006). *In vivo* administration of synthetic CB1R agonists in mice impairs cerebellum-dependent motor coordination (DeSanty and Dar, 2001; Patel and Hillard, 2001). Thus, the effects of CB1R agonists on cerebellar functions are well understood. Therefore, the cerebellum is the ideal neuronal circuit to examine the potency of synthetic cannabinoids, whose actions on neuronal functions have not been determined.

Here, using whole-cell patch-clamp recordings, we investigated activity of MAM-2201 in human CB1R (hCB1R)-expressing AtT-20 cells, and then the effects of MAM-2201 on synaptic transmission in slice preparations of the mouse cerebellum. We found that MAM-2201 acted as an agonist of hCB1Rs and inhibited excitatory transmitter release at PF-PC synapses via activation of presynaptic CB1Rs. MAM-2201 decreased the synaptic transmission more strongly than Δ^9-THC within the range of 0.1–30 μM and naphthalen-1-yl-(1-pentylindol-3-yl)methanone [JWH-018, Fig. 1*B*, one of the most popular and potent synthetic cannabinoids detected in the herbal products (Atwood et al., 2010)], within the range of 0.03–3 μM. Furthermore, MAM-2201 induced presynaptic suppression of CF-PC synapses, leading to a reduction in the number of spikelets in complex spikes and to attenuated dendritic Ca^{2+} transients in PCs.

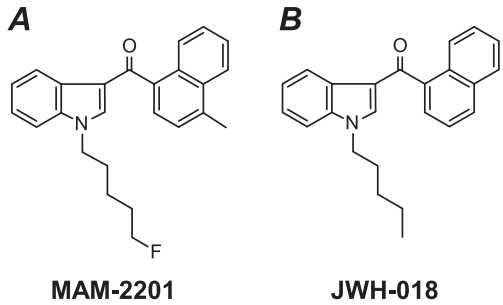

Fig. 1. The chemical structures of [1-(5-fluoropentyl)-1*H*-indol-3-yl](4-methyl-1-naphthalenyl)-methanone (MAM-2201, *A*) and naphthalen-1-yl-(1-pentylindol-3-yl) methanone (JWH-018, B).

2. Materials and methods

2.1. Cannabinoid-related compounds

MAM-2201 (Fig. 1*A*) and JWH-018 (Fig. 1*B*) were purchased from Cayman Chemical (Ann Arbor, MI, USA). (*R*)-(+)-[2,3-Dihydro-5-methyl-3-(4-morpholinylmethyl)pyrrolo[1,2,3-de]-1,4-benzoxazin-6-yl]-1-naphthalenylmethanone mesylate [WIN55,212-2 (WIN), a CB1R and CB2R agonist] and *N*-(Piperidin-1-yl)-5-(4-iodophenyl)-1-(2,4-dichlorophenyl)-4-methyl-1*H*-pyrazole-3-carboxamide (AM251, a CB1R antagonist) were purchased from Wako Pure Chemical Industries (Osaka, Japan) and Tocris Bioscience (Bristol, UK), respectively. Δ^9-THC was purchased from Cerilliant (Round Rock, TX, USA). These compounds were dissolved in dimethylsulfoxide as stock solutions. In electrophysiological recordings from AtT-20 cells and from cerebellar PCs, the final concentrations of dimethylsulfoxide in extracellular solutions were maintained at 0.1 and 0.3% (v/v), respectively. WIN was used as a positive control, because WIN has been used in many studies to suppress neurotransmitter release at PF-, CF-, and interneuron-PC synapses via activation of presynaptic CB1Rs (Kreitzer and Regehr, 2001; Diana et al., 2002; Safo and Regehr, 2005; Kawamura et al., 2006).

2.2. Heterologous expression of CB1R in AtT-20 cells

AtT-20 cells were obtained from JCRB Cell Bank (Osaka, Japan) and were maintained in Ham's F-10 medium (GIBCO, Grand Island, NY) supplemented with 10% horse serum (GIBCO), 2.5% fetal bovine serum (GIBCO), and a mixture of penicillin and streptomycin solution (100 unit/mL and 100 mg/mL, respectively; GIBCO) in a 5% CO_2 incubator at 37 °C. The cells were plated onto grass coverslips coated with poly-D-lysine (Sigma–Aldrich, St Louis, MO) for gene transfection. hCB1R (SC111611; Origene, Rockville, MD; NCBI Reference Sequence: NM_016083.3) (Bruno et al., 2014) or mouse CB1R (mCB1R, MC206086; Origene; GenBank: BC079564.1) cDNAs, and green fluorescent protein (GFP) vector were cotransfected into the cells in a 9:1 M ratio using Lipofectamine LTX (Invitrogen, Carlsbad, CA) according to the manufacturer's instructions. Fluorescence of GFP was regarded as an indicator of transfected cells. Whole-cell patch-clamp recordings were made from the GFP-positive cells 20–48 h after transfection. The expression of CB1R proteins was confirmed by immunostaining with the combination of rabbit polyclonal anti-CB1R antibody (1:2000 dilution, CB1-Rb-Af380, Frontier Institute, Hokkaido, Japan) and AlexaFluor 568-conjugated goat anti-rabbit IgG secondary antibody (5 μg/mL, A-11011; Invitrogen) according to the methods described previously (Irie et al., 2014).

The immunofluorescence signal was observed under a confocal microscope (A1R; Nikon, Tokyo, Japan; Fig. 2*A*).

2.3. Electrophysiological recordings from AtT-20 cells

AtT-20 cells were transferred to a recording chamber and continuously perfused at 2 mL/min with high-K^+ extracellular solution containing (in mM): 87 NaCl, 60 KCl, 2 $CaCl_2$, 1 $MgCl_2$, 10 D-glucose, and 10 4-(2-hydroxyethyl)-1-piperazineethanesulfonic acid (HEPES) (pH adjusted to 7.4 with NaOH). The concentration of KCl was raised compared to normal extracellular solution to increase amplitudes of inwardly rectifier potassium currents (Mackie et al., 1995). All experiments were performed at 25 ± 1 °C. The cells were visualized by Nomarski optics and a near infrared-CCD camera (C3077-79; Hamamatsu Photonics, Hamamatsu, Japan) with a 40 × 0.8 NA numerical aperture water-immersion objective lens (Olympus, Tokyo, Japan) on an upright microscope (BX51WI; Olympus). GFP-positive cells were visualized and selected using epifluorescence optics (Olympus).

Patch pipettes were made from borosilicate glass capillaries (GC150F-100; Harvard Apparatus, Holliston, MA) and had a resistance of 3–5 MΩ when filled with a potassium gluconate-based internal solution containing (in mM): 125 K-gluconate, 10 KCl, 3 $MgCl_2$, 0.1 ethylene glycol tetraacetic acid (EGTA), 5 Na_2-ATP, 5 Na_2-phosphocreatine, 0.3 Na_2-GTP, and 10 HEPES (pH adjusted to 7.3 with KOH). Whole-cell patch-clamp recordings were performed from GFP-positive cells, and inward currents were evoked by applying voltage steps from a holding potential of −25 mV to −110 mV for 200 ms in voltage-clamp conditions. Membrane capacitance was calculated from the transient current evoked by applying a small voltage step (−5 mV, 20 ms duration) from a holding potential of −25 mV (Irie et al., 2006). Series resistance was compensated electronically by 70–90%, and the liquid junction potential (−5 mV) was corrected off-line.

Data were collected with Molecular Devices (Sunnyvale, CA) hardware and software (Multiclamp 700B, Digidata 1440A, Clampex 10.3) as described previously (Irie et al., 2014), and analyzed using Clampfit 10.3 software (Molecular Devices) and Igor Pro 6 software (Wavemetrics, Lake Oswego, OR) with the added import functionality provided by ReadPclamp XOP of the NeuroMatic software package (http://www.neuromatic.thinkrandom.com/). Representative current traces are shown after averaging four consecutive traces. To obtain inward current densities induced by MAM-2201 or WIN, the amplitudes of the current were normalized to membrane capacitances (picoamperes per picofarad, Fig. 2*C*). The densities were plotted as a function of the concentration and fit with the sigmoidal function, $Y = Bottom + (Top - Bottom)/(1 + 10^{\hat{}}[(LogEC50 - X)*Hillslope])$, using GraphPad Prism 5 (GraphPad Software, San Diego, CA).

2.4. Cerebellar slice preparation and electrophysiological recordings from PCs

ICR mice of either sex [postnatal day (P) 20–57 for Figs. 3–5 and Table 1; P14–20 for Figs. 6 and 7, and Table 2] were used according to the guidelines for animal use of the National Institute of Health Sciences. Cerebellar slices were prepared as described previously with some modifications (Shuvaev et al., 2011). Briefly, mice were anesthetized with halothane and decapitated. Parasagittal slices of the cerebellum (200-μm thick) were prepared using a microslicer (PRO7, Dosaka, Kyoto, Japan) in ice-cold, cutting solution containing (in mM): 234 sucrose, 2.5 KCl, 1.25 NaH_2PO_4, 10 $MgSO_4$, 0.5 $CaCl_2$, 26 $NaHCO_3$, 11 glucose, and bubbled with 5% CO_2/95% O_2. The slices were then allowed to recover for 1 h at room temperature in artificial cerebrospinal fluid (ACSF) solution containing (in mM): 120 NaCl, 2.5 KCl, 2 $CaCl_2$, 1 $MgCl_2$, 1.25 NaH_2PO_4, 26 $NaHCO_3$, 17 glucose, 0.4 ascorbic acid, 3 myo-inositol, 2 sodium pyruvate, and bubbled with 5% CO_2/95% O_2. In electrophysiological recordings, ascorbic acid, myo-inositol, and sodium pyruvate were omitted.

Cerebellar slices were transferred to a recording chamber, and continuously perfused at 2 mL/min with ACSF at 25 ± 1 °C (Figs. 3–6 and Table 1) or near physiological temperature (34 ± 1 °C; Fig. 7 and Table 2). Electrophysiological recordings were done using the same equipment described above. Excitatory and inhibitory postsynaptic currents (EPSCs and IPSCs) were recorded in the presence of 100 μM picrotoxin (a $GABA_A$ receptor antagonist, Tocris Bioscience) and 40 μM 6,7-dinitroquinoxaline-2,3-dione (DNQX, an AMPA/kainate receptor antagonist, Tocris Bioscience), respectively. Patch pipettes had a resistance of 2–3 MΩ when filled with pipette solutions. A CsCl-based and the K-gluconate-based internal solutions were used for voltage- (Figs. 3–6 and Table 1) and current-clamp recordings (Fig. 7 and Table 2), respectively. The CsCl-based solution contained (in mM): 120 CsCl, 20 K-gluconate, 15 tetraethylammonium-Cl, 3 $MgCl_2$, 5 EGTA, 5 Na_2-ATP, 5 Na_2-phosphocreatine, 0.3 Na_2-GTP, 5 QX-314, and 10 HEPES (pH adjusted to 7.3 with CsOH). The liquid junction potentials (CsCl-based, −4 mV; K-gluconate-based, −10 mV) were corrected off-line.

Somatic whole-cell patch-clamp recordings were performed from PCs in lobules IV to VIII. PF-PC EPSCs and IPSCs were evoked by electrical stimulation of the molecular layer and recorded at the holding potential of −80 mV. CF-PC EPSCs and complex spikes were evoked by the stimulation of the granule cell layer. CF-PC EPSCs were recorded at a holding potential of −10 mV to decrease the driving force for cations through ionotropic glutamate receptors. The stimuli (100- to 200-μs pulses, 20–80 V amplitude) were performed with an ACSF-filled patch pipette (tip diameter, 10–15 μm for molecular layer stimulation and 2–3 μm for the granule cell layer) and applied at 0.1 Hz. In some experiments, paired-pulse stimulation (50 ms inter-stimulus intervals) was done to calculate the paired-pulse ratio (PPR), which is an index of the change of neurotransmitter release from presynaptic terminals (Zucker and Regehr, 2002; Irie and Ohmori, 2008). When postsynaptic currents were recorded, series resistance was monitored by applying small voltage steps (−10 mV, 20-ms duration), and the records were discarded if the resistance varied more than 25%. Quantal EPSCs (qEPSCs) from PFs and CFs were elicited by electrical stimulation (0.1 Hz) with PCs held at −80 mV and with $CaCl_2$ in ACSF replaced with equimolar $SrCl_2$ (Xu-Friedman and Regehr, 1999). Miniature IPSCs (mIPSCs) were recorded at a holding potential of −80 mV in the presence of 40 μM DNQX and 1 μM tetrodotoxin (TTX; Wako Pure Chemical Industries). In the start of current-clamp recordings, resting membrane potentials of PCs were adjusted at −60 to −70 mV by current injection to prevent spontaneous firing, and series resistance was compensated for using bridge balance and capacitance neutralization. Intrinsic membrane properties were examined by square-wave current injection (500-ms duration, Table 2). Input resistance was measured from averaged voltage responses evoked by small hyperpolarizing currents (−20 pA). Threshold current and threshold potential were measured by depolarizing current injections (from 0 pA to 200 pA, 20 pA increment). The maximum rate of rise and maximum rate of fall of action potentials and spike height were calculated from the first action potential waveform evoked at the threshold current. Firing frequency was obtained from the number of spikes observed during the current injection.

qEPSCs and mIPSCs were detected off-line using the template search function in the Clampfit 10.3 software. To analyze qEPSCs, data from 200 to 1600 ms after the stimulus artifact were used. Average cumulative probability histograms were obtained as follows: first, qEPSCs or mIPSCs were recorded more than 300 events from each cell in the presence or absence of MAM-2201. Then, for each cell, the amplitudes and inter-event intervals were binned, and individual cumulative probability histograms were plotted. Finally, these histograms were averaged. Representative EPSC and IPSC traces are shown after averaging four to six consecutive traces, and stimulus artifacts are truncated. EPSC and IPSC amplitudes were obtained by averaging six consecutive records. The coefficient of variation (CV), which is another index of the change of neurotransmitter release from presynaptic terminals, was calculated from 18 consecutive EPSC or IPSC traces (Korn and Faber, 1991). The inhibitory concentration 50% (IC50) values of the cannabinoid-related compounds against neurotransmitter release at PF-PC synapses were calculated as follows: control PF-PC EPSC amplitude was obtained from the averaged EPSCs recorded for 3 min before application of the synthetic cannabinoids. PF-PC EPSC amplitude in the presence of the cannabinoids was done from the EPCSs recorded for 8 to 10 min after the application, normalized to the control values, and plotted as a function of the concentration. The data were fit with the sigmoidal function, $Y = 100/(1 + 10^{\hat{}}[(LogIC50 - X)*Hillslope])$ (Table 1). The reasons for using PF-PC synapses for measurement of IC50s were as follows: PF-PC synapses exhibit more stable synaptic transmission than interneuron-PC synapses (Vincent and Marty, 1996), they are more sensitive to CB1R agonists, and they express CB1R proteins more abundantly than CF-PC synapses (Kawamura et al., 2006).

2.5. Simultaneous recordings of Ca^{2+} transients and complex spikes

Current-clamp recordings were done from PCs using the K-gluconate-based intracellular solution in which EGTA was replaced with 100 μM Oregon Green 488 BAPTA-1 hexapotassium salt (OGB-1; Invitrogen, Carlsbad, CA) in the presence of picrotoxin. PC somata and dendrites were dialyzed with the pipette solution for 30 min to obtain a stable intracellular concentration of OGB-1. Confocal imaging was then performed with a Nipkow disk confocal scanner unit (CSU-10; Yokogawa Electric, Tokyo, Japan) attached to the Olympus BX51WI microscope with the 40× objective lens. A 488 nm beam from a diode laser (Yokogawa Electric) for excitation was coupled to the scanner unit through an optical fiber. Fluorescence was detected via a 520 nm long-path filter using an EMCCD camera (iXon3 DU897; Andor Technology, Belfast, Northern Ireland). The pixels were binned 2 × 2 on the chip, and images were acquired at 25.8 Hz. Complex spikes were evoked at 0.1 Hz, and the electrophysiological recordings were synchronized with the acquisition of time-lapse fluorescent images. The number of spikelets in complex spikes was obtained from average value of five to seven consecutive traces. The imaging experiments were controlled and analyzed using Andor iQ2 software (Andor Technology). Three to five consecutive time-lapse images were averaged and used for analysis. The regions of interests were set on primary dendrites (approximately between 20 and 100 μm from the center of the cell body, Fig. 7*Ca*). Fluorescence changes were background-corrected and expressed as $\Delta F/F_0$, where F_0 is the fluorescence intensity when the cells were at rest, and ΔF is the absolute values of fluorescence changes during activity. Integration of Ca^{2+} transients was performed over 2 s from the onset.

All data other than EC50s or IC50s are provided as the means ± standard deviation. EC50s and IC50s are expressed as the best-fit values with 95% confidence interval (CI; Table 1). *n* indicates the number of experiments. Statistical significance was tested using paired *t*-tests test unless otherwise stated (significance, $p < 0.05$).

3. Results

3.1. MAM-2201 acts as an agonist of hCB1Rs and mCB1Rs

To examine whether MAM-2201 activates CB1Rs, we expressed hCB1R or mCB1R cDNAs in murine tumor line AtT-20. Because

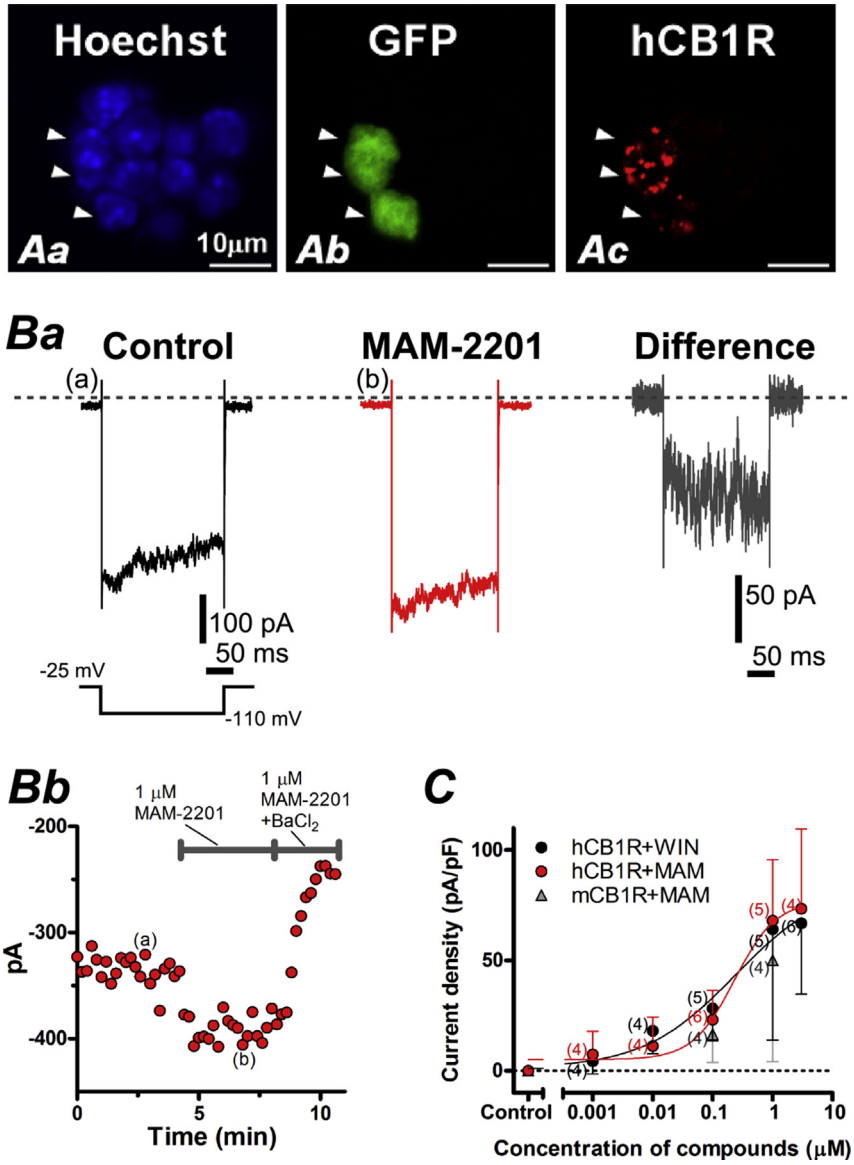

Fig. 2. Heterologous expression of cannabinoid receptor type 1 (CB1R) cDNAs in AtT-20 cells. A, Immunofluorescence images of AtT-20 cells transfected with human CB1R (hCB1R) and green fluorescent protein (GFP) cDNAs. Cell nuclei were stained with Hoechst 33342 (1 μg/mL, Dojindo, Kumamoto, Japan; Aa). Arrowheads indicate GFP and hCB1R double positive cells. Proteins of hCB1Rs were visualized by immunolabelling with rabbit anti-CB1R antibody and AlexaFluor 568-conjugated anti-rabbit secondary antibody (Ac). B, Representative data recorded from hCB1R-expressing cell. Ba, Inward currents were evoked by applying voltage steps from a holding potential of −25 mV to −110 mV for 200 ms. In trace (a) and (b), averages of four consecutive responses are shown. These traces correspond to the responses at time points marked (a) or (b) in Bb. The holding current level is shown by a dotted line. Bb, Time course of mean inward currents. Each point represents an averaged value obtained from four consecutive records. C, Concentration-dependent increases of inward current densities induced by MAM-2201 or (*R*)-(+)-[2,3-Dihydro-5-methyl-3-(4-morpholinylmethyl)pyrrolo[1,2,3-de]-1,4-benzoxazin-6-yl]-1-naphthalenylmethanone mesylate [WIN55,212-2 (WIN)]. To obtain current densities, amplitudes of inward current induced by MAM-2201 or WIN were normalized to membrane capacitances (picoamperes per picofarad). The densities were plotted as a function of the concentration and fit with the sigmoidal function, $Y = \text{Bottom} + (\text{Top} - \text{Bottom})/(1 + 〖10〗^{\wedge}((\text{LogEC50} - X)*\text{Hillslope}))$, where EC50 is effective concentration 50%. Here and in the following figures, error bars and the numbers in parentheses indicate standard deviation and the number of experiments, respectively.

application of CB1 agonists on AtT-20 cells expressing CB1Rs activates inward rectifier potassium currents, activities of compounds against CB1Rs can be determined using this heterologous expression system (Mackie et al., 1995; Felder et al., 1998). Whole-cell patch clamp recordings were done from hCB1R or mCB1R-expressing cells, and inward currents were evoked by applying hyperpolarizing voltage pulses (Fig. 2*B*). Bath application of MAM-2201(1 μM) increased the amplitude of inward current within 5 min (Fig. 2*Bb*). Subsequent application of low concentration of Ba^{2+} (200 μM $BaCl_2$), which blocks inward rectifier potassium currents (Hagiwara et al., 1976), markedly reduced the inward currents. This indicates that, in addition to MAM-2201-induced currents, MAM-2201-independent inward rectifier potassium currents were simultaneously blocked (Dousmanis and Pennefather, 1992). The time course of the induced current, obtained by subtracting the currents before from those after the application of MAM-2201, showed slow activation at the beginning of voltage pulse (Fig. 2*Ba*, Difference). This property is characteristic of activation of G-protein coupled potassium channels (Kubo et al., 1993). Fig. 2*C* shows the concentration-dependent increase of current

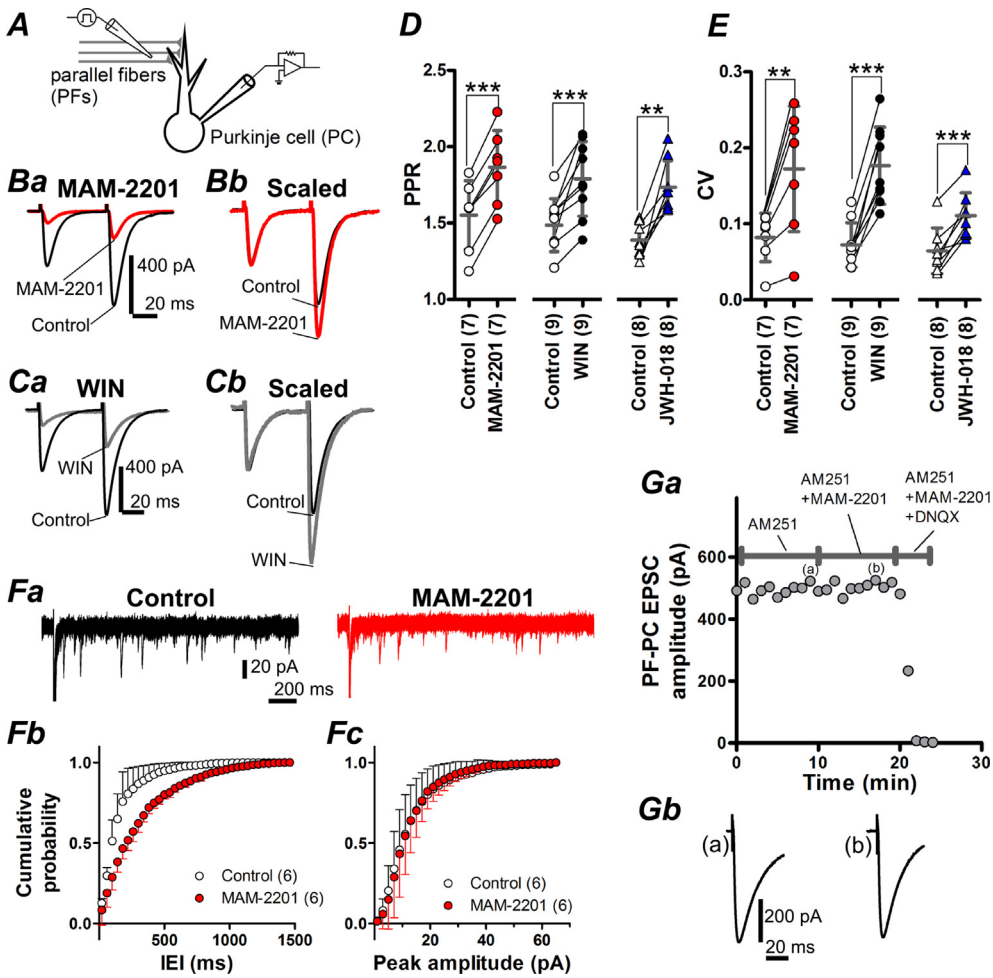

Fig. 3. MAM-2201 inhibits synaptic transmission at parallel fiber (PF)-Purkinje cell (PC) synapses presynaptically via activation of presynaptic CB1Rs. *A*, Experimental configuration for Fig. 3*B*–*G* and 4. *B*, PF-induced excitatory postsynaptic currents (EPSCs) were evoked with pairs of stimuli (50 ms interval) under control conditions (Control) or in the presence of 10 μM MAM-2201 (MAM-2201). The holding potential was −80 mV. Picrotoxin (100 μM) was added to the extracellular artificial cerebrospinal fluid (ACSF) to block $GABA_A$ receptor-mediated inhibitory postsynaptic currents (IPSCs). The first EPSC peak in MAM-2201 was reduced to 21.9% of control. In each trace, averages of six trials are shown. In the right panel, the EPSC evoked by the first stimulus in MAM-2201 is scaled to the amplitude of the first EPSC in Control. MAM-2201 increased paired-pulse facilitation (*Bb*). Stimulus artifacts are truncated. *C*, Same as in *A*, but in the presence of 10 μM WIN. In *Ca*, the first peak in WIN was reduced to 24.1% of control. In the right panel, the EPSC evoked by the first stimulus in WIN is scaled to the amplitude of the first EPSC in Control. *D* and *E*, Summary of paired-pulse ratio (PPR, *D*) and coefficient of variation (CV, *E*) of PF-PC EPSCs before and after application of MAM-2201, WIN, or JWH-018 (10 μM in all groups). Here and in the following figures, the statistical significance was tested using paired *t*-tests unless otherwise stated (significance, $p < 0.05$). $^{**}p < 0.01$ and $^{***}p < 0.001$. *F*, To isolate quantal EPSCs (qEPSCs) from PFs, asynchronous neurotransmitter release from PF terminals was evoked by stimulating PFs in the presence of Sr^{2+} (2 mM, see Materials and Methods). *Fa*, Five superimposed traces before (Control) and after application of MAM-2201. Asynchronously released quanta are seen as downward current deflections. Synchronous PF-PC EPSCs are truncated. *Fb* and *Fc*, Average cumulative probability histograms of inter-event interval (IEI, *Eb*, bin width: 40 ms) and peak amplitude (*Ec*, bin width: 2 pA) of PF-PC qEPSCs. *Ga*, Time course of peak PF-PC EPSC amplitudes in the presence of *N*-(Piperidin-1-yl)-5-(4-iodophenyl)-1-(2,4-dichlorophenyl)-4-methyl-1*H*-pyrazole-3-carboxamide (AM251, 5 μM). Each point represents an averaged value obtained from six consecutive records. MAM-2201 (10 μM) had no detectable effect on the amplitude. Additional application of 6,7-dinitroquinoxaline-2,3-dione (DNQX, 40 μM) abolished PF-PC EPSCs completely. *Gb*, Traces show normalized PF-PC EPSC responses at time points marked (a) and (b) in *Ga*.

densities induced by MAM-2201 or WIN in CB1R-expressing cells. Interestingly, in hCB1R-expressing cells, MAM-2201 increased current densities in a concentration-dependent manner (Fig. 2*C*, red circles) with an EC50 of 0.230 μM (95% CI, 0.0384–1.37 μM). Similar responses were obtained by application of WIN (Fig. 2*C*, black circles; EC50 = 0.234 μM; 95% CI, 0.410×10^{-3}-140 μM), which was consistent with previous report (Mackie et al., 1995). In the presence of AM251 (5 μM, a CB1R antagonist), MAM-2201 (1 μM) did not induce the inward currents (−2.38 ± 7.23 pA/pF, $n = 6$). In cells transfected with GFP alone, MAM-2201 (1 μM) did not elicit any changes (1.55 ± 6.78 pA/pF, $n = 5$). In mCB1R-expressing cells, MAM-2201 induced concentration-dependent increase in the current density (Fig. 2*C*, gray triangles). These results demonstrate that MAM-2201 activates hCB1Rs and mCB1Rs.

3.2. MAM-2201 inhibits synaptic transmission presynaptically via activation of presynaptic CB1Rs at PF-PC synapses in mouse cerebellum

We tested the effects of MAM-2201 on neurotransmitter release at PF-PC synapses and the involvement of CB1Rs (Fig. 3), and compared the potency of MAM-2201 with that of WIN, JWH-018, and Δ^9-THC (Fig. 4 and Table 1). Whole-cell patch-clamp recordings were performed from somata of PCs in mouse cerebellar slices under voltage-clamp conditions, and PF-PC EPSCs were evoked by electrical stimulation of PFs in the molecular layer in the presence of picrotoxin. The recording configuration is illustrated in Fig. 3*A*. As shown in Fig. 3*B*, bath application of MAM-2201 (10 μM, 8 min) significantly decreased the first EPSC amplitude

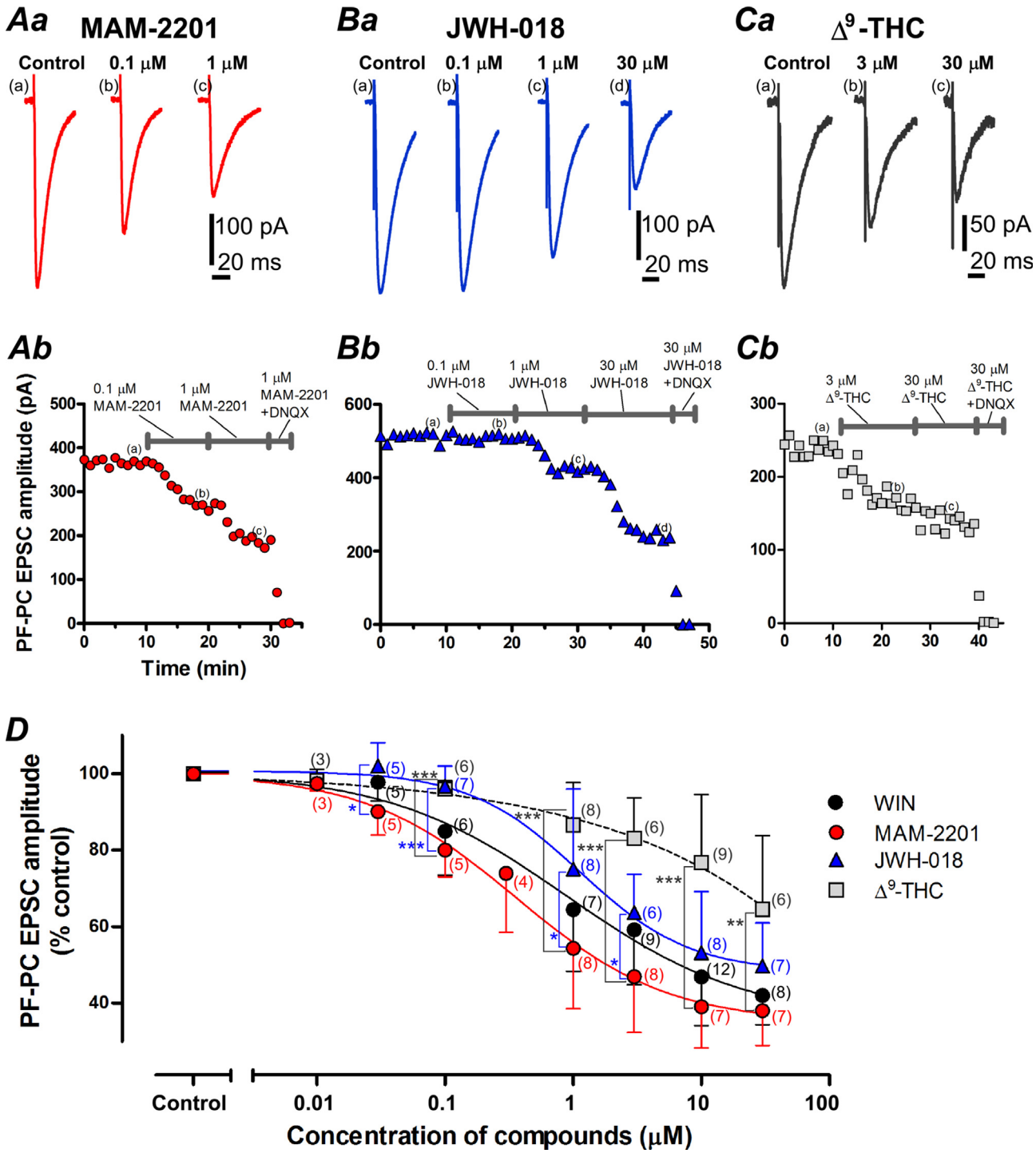

Fig. 4. MAM-2201 is a more potent inhibitor than Δ^9-tetrahydrocannabinol (Δ^9-THC) and JWH-018 at PF-PC synapses. *Aa*, Representative PF-PC EPSC traces recorded in control conditions, or in 0.1 or 1 μM MAM-2201. These traces show normalized PF-PC EPSC responses at time points marked (a), (b), or (c) in *Ab*. *Ab*, Time course of peak amplitudes of PF-PC EPSCs. Each point represents an averaged value obtained from six consecutive records. *Ba*, Representative PF-PC EPSC traces recorded in control conditions, or in 0.1, 1, or 30 μM JWH-018. These traces correspond to the responses at time points marked (a), (b), (c), or (d) in *Bb*. *Bb*, Time course of peak amplitudes of PF-PC EPSCs. *C*, Representative PF-PC EPSC traces recorded in control conditions, or in 3, or 30 μM Δ^9-THC. These traces correspond to the responses at time points marked (a), (b), or (c) in *Cb*. *Cb*, Time course of the peak amplitudes. In *Aa*, *Ba*, and *Ca*, stimulus artifacts are truncated. *D*, Concentration-dependent decreases of PF-PC EPSC amplitudes induced by cannabinoid-related compounds. Control PF-PC EPSC amplitude was obtained from averaged PF-PC EPSCs recorded for 3 min before the application of the compounds. PF-PC EPSC amplitudes in the presence of these compounds were recorded for 8–10 min after application, normalized to the control values, and plotted as a function of concentration (Fig. 4*C*). Each plot was fit with a sigmoidal function, $Y = 100/(1 + [10]^{[(LogIC50 - X)*Hillslope]})$, where IC50 is inhibitory concentration 50%. $^*p < 0.05$, $^{**}p < 0.01$, and $^{***}p < 0.001$ by unpaired *t*-tests test.

(39.0 ± 10.8% of control value, $n = 7$, $p < 0.001$). To investigate whether the effects of MAM-2201 on PF-PC EPSC amplitude were mediated by presynaptic mechanisms, PPR and CV analyses were performed. MAM-2201 (10 μM) significantly increased PPR (Fig. 3*Bb* and *D*) and CV (Fig. 3*E*), indicating a decrease in presynaptic neurotransmitter release. WIN (10 μM, 8-min application) induced a similar decrease in PF-PC EPSC amplitude and a parallel increase in the PPR and CV (Fig. 3*C*–*E*). MAM-2201 (10 μM) also

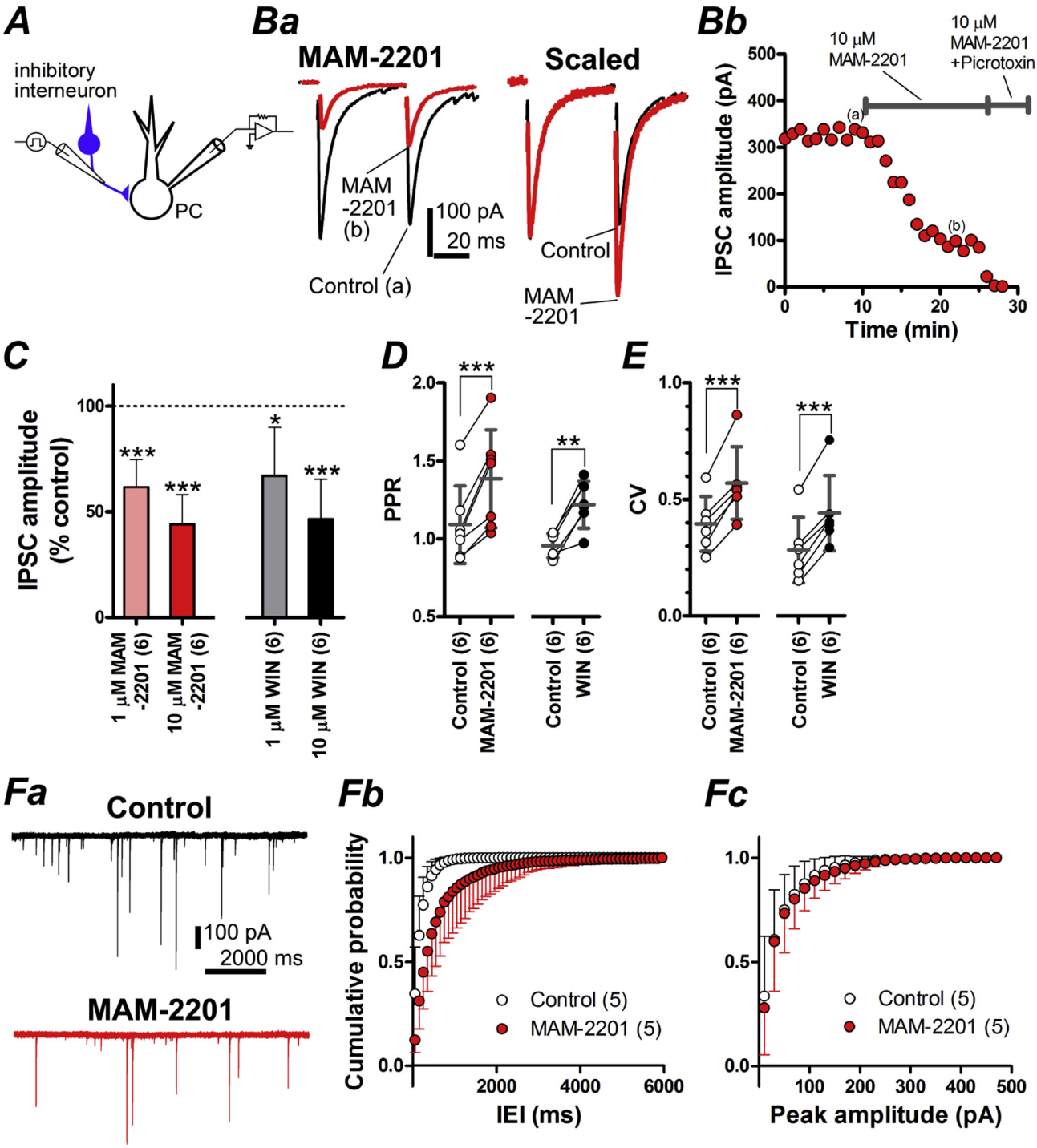

Fig. 5. MAM-2201 reduces GABAergic synaptic transmission at interneuron-PC synapses via presynaptic mechanisms. *A*, Experimental configuration for Fig. 5*B*–*E*. *Ba*, Averaged current traces of IPSCs in control conditions (Control) and 10 μM MAM-2201. These traces show normalized IPSC responses at time points marked (a) and (b) in *Bb*. IPSCs were evoked with pairs of stimuli (50 ms interval) in the presence of 40 μM DNQX and were recorded as inward currents because of the use of the CsCl-based internal solution. The holding potential was −80 mV, and stimulus artifacts were blanked for clarity. The first peak in MAM-2201 was reduced to 28.0% of control. In the right panel, the first IPSC in MAM-2201 is scaled to the amplitude of the first IPSC in Control (Scaled), showing a clear increase of PPR. *Bb*, Time course of peak amplitudes of the first IPSC. Each point represents an averaged value obtained from six consecutive records. *C*, Concentration-dependent decreases of peak amplitude of IPSC by MAM-2201 and WIN. IPSC amplitudes were normalized to the control value (=baseline responses) and expressed as a percentage of control. $*p < 0.05$ and $***p < 0.001$. *D* and *E*, Summary of PPR (*D*) and CV (*E*) of IPSCs before and after application of MAM-2201 and WIN (10 μM in both groups). $**p < 0.01$. *F*, Miniature IPSCs (mIPSCs) recorded in the presence of tetrodotoxin (TTX, 1 μM) and DNQX. *Fa*, Five superimposed traces before (Control) and after application of MAM-2201. mIPSCs appear as downward current deflections. *Fb* and *Fc*, Average cumulative probability histograms of IEI (*Fb*, bin width: 100 ms) and peak amplitude (*Fc*, bin width: 20 pA) of mIPSCs.

decreased PF-PC qEPSC frequency [Inter-event interval (IEI), Control: 194.0 ± 24.1 ms, MAM-2201: 288.7 ± 30.2 ms, $p < 0.001$, $n = 6$, Fig. 3*Fa* and *Fb*] without affecting PF-PC qEPSC amplitude (peak amplitude, Control: 18.9 ± 2.1 pA, MAM-2201: 18.6 ± 4.3 pA, $p = 0.860$, $n = 6$, Fig. 3*Fa* and *Fc*). In the absence of MAM-2201, amplitudes of PF-PC EPSCs did not show significant changes during 45-min recording under condition in which series resistance was stable (105.2 ± 10.5% of control, $n = 7$, $p = 0.271$).

Table 1
IC50s of synthetic cannabinoids against PF-PC EPSCs.

	WIN	MAM-2201	JWH-018
IC50 (μM) [95% CI (μM)][a]	0.890 [0.296-2.679]	0.363 [0.193-0.681]	1.121 [0.551-2.282]
Relative IC50	1.00	0.41	1.25

[a] Data are provided as the best-fit values with 95% confidence intervals (CI).

To examine whether MAM-2201 altered postsynaptic responses by activating presynaptic CB1Rs, MAM-2201 was bath-applied to the cerebellar slices in the presence of AM251 (5 μM). MAM-2201 did not induce any change of PF-PC EPSC amplitude in the presence of AM251 (Fig. 3*G*, 102.2 ± 6.0% of control, $n = 5$, $p = 0.443$). Subsequent application of DNQX (40 μM) abolished PF-PC EPSCs, demonstrating that glutamatergic synaptic transmission was indeed evoked, and bath application of these chemicals was successful (Fig. 3*Ga*). Taken together, these results indicate that the MAM-2201-induced changes are mediated by a decrease in presynaptic neurotransmitter release from PF terminals via activation of presynaptic CB1Rs.

3.3. MAM-2201 is a more potent inhibitor of PF-PC synapses than Δ^9-THC and JWH-018

Fig. 4*A–C* show representative traces of PF-PC EPSCs in the presence of MAM-2201 (Fig. 4*A*), JWH-018 (Fig. 4*B*), or Δ^9-THC (Fig. 4*C*), respectively. The inhibitory effect of MAM-2201 on PF-PC

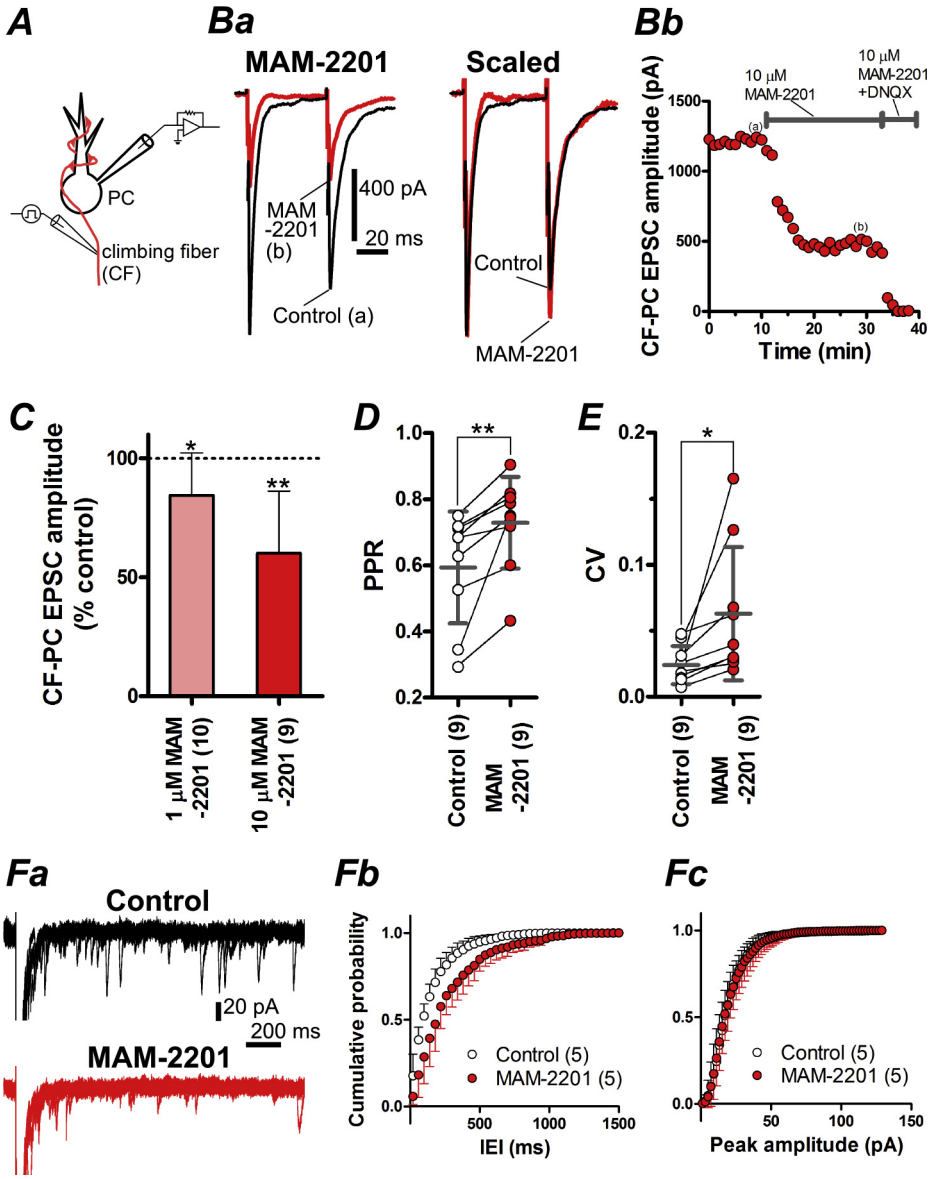

Fig. 6. MAM-2201-mediated presynaptic inhibition at climbing fiber (CF)-PC synapses. *A*, Experimental configuration for Fig. 6*B–F* and 7. *Ba*, Averaged current traces of CF-PC EPSCs in control (Control) and 10 μM MAM-2201. These traces show normalized CF-PC EPSC responses at time points marked (a) and (b) in *Bb*. CF-PC EPSCs were evoked with pairs of stimuli (50 ms interval) in the presence of 100 μM picrotoxin. PCs were held at −10 mV to reduce the driving force for AMPA receptor-mediated currents. Stimulus artifacts were truncated for clarity. The first peak in MAM-2201 was reduced to 38.4% of control. In the right panel, the first CF-PC EPSC in MAM-2201 is scaled to the amplitude of the first CF-PC EPSC of control (Scaled). *Bb*, Time course of peak amplitudes of first CF-PC EPSC. Each point represents an averaged value obtained from six consecutive records. *C*, Concentration-dependent decreases of the peak amplitudes of CF-PC EPSCs by MAM-2201. CF-PC EPSC amplitudes were expressed as a percentage of control. $*p < 0.05$ and $**p < 0.001$. *D* and *E*, Summary of PPR (*D*) and CV (*E*) of CF-PC EPSCs before and after application of MAM-2201 (10 μM). *F*, CF-PC qEPSCs in the presence of picrotoxin and Sr^{2+} (2 mM $SrCl_2$). The qEPSCs were recorded at a holding potential of −80 mV. *Fa*, Five superimposed traces before (Control) and after application of MAM-2201. Synchronous CF-PC EPSCs are truncated. *Fb* and *Fc*, Average cumulative probability histograms of IEI (*Fb*, bin width: 40 ms) and peak amplitude (*Fc*, bin width: 2 pA) of CF-PC qEPSCs.

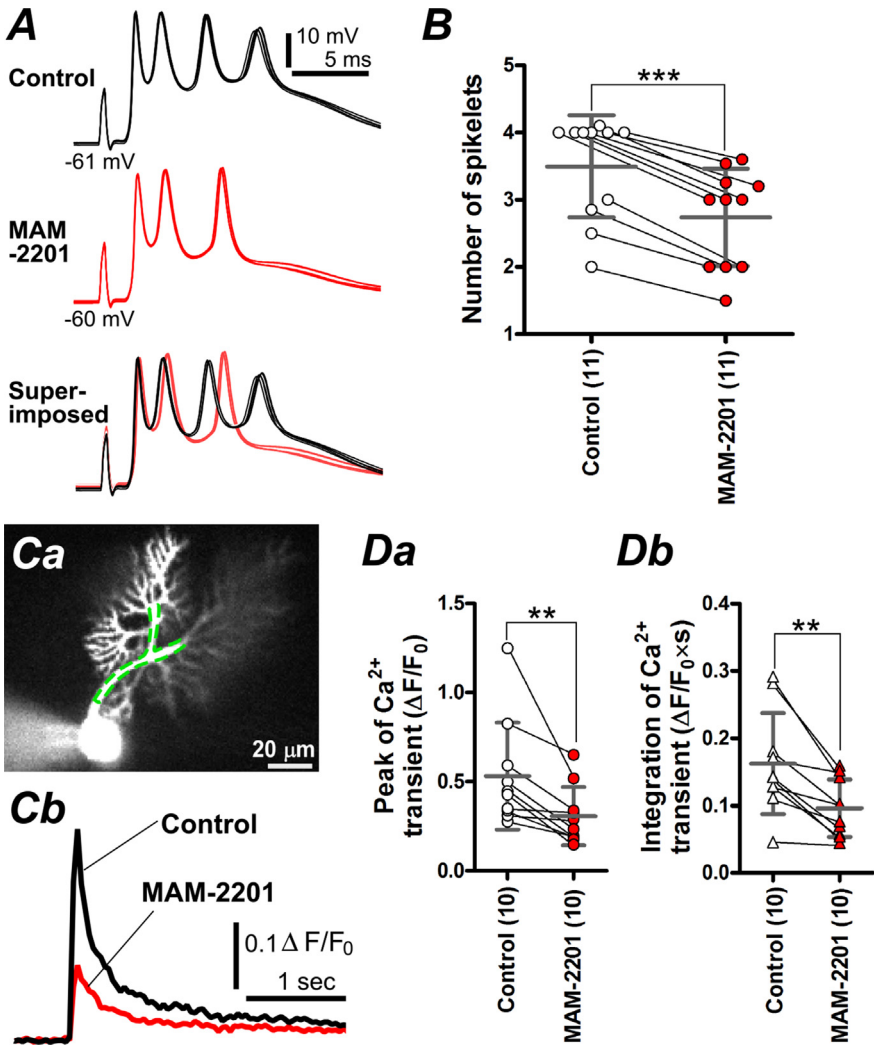

Fig. 7. MAM-2201 reduces the number of spikelets in complex spikes and dendritic Ca^{2+} transients evoked by CF stimulation. *A–D*, Simultaneous recordings of complex spikes and dendritic Ca^{2+} transients. *A*, Representative superimposed traces of complex spikes (5 traces) evoked by stimulation of CFs (0.1 Hz) in the presence of picrotoxin at near physiological temperature (34 ± 1 °C). The K-gluconate-based intracellular solution containing Oregon Green 488 BAPTA-1 hexapotassium salt (OGB-1, 100 μM) was used for current-clamp recordings. At the start of the recording, the resting membrane potential was adjusted around −60 to −70 mV by current injection to prevent spontaneous firing. MAM-2201 (10 μM, 10 min) reduced the number of spikelets (4 spikelets in Control; 3 spikelets in MAM-2201). Superimposed traces reveal delay and reduction of spikelets in MAM-2201. *B*, Summary of average number of spikelets before and after application of MAM-2201 (10 μM). ***$p < 0.001$. *C*, A dendritic Ca^{2+} transient induced by CF stimulation. Intracellular Ca^{2+} measurement in *C* was simultaneously performed while recording the complex spikes in *A*. *Ca*, Representative confocal image of PC loaded with OGB-1 via a patch pipette. Area indicated by dotted line represents region of interest used for the calculation of the dendritic Ca^{2+} transients. *Cb*, Representative Ca^{2+} transients in control and MAM-2201 (10 μM). F_0 is the fluorescence intensity when the cells were at rest, and ΔF is the absolute values of fluorescence changes during activity. *Da* and *Db*, Summary of Ca^{2+} transient peaks (*Da*) and integration of Ca^{2+} transients (*Db*). The integration was performed for 2 s from the onset. **$p < 0.01$.

EPSC amplitude was first detectable at 0.03 μM (Fig. 4*D*, 90.1 ± 6.1% of control, $n = 5$, $p < 0.05$), and became more apparent at higher concentrations. Application of 0.1 μM MAM-2201 was sufficient to induce a clear reduction [trace (b) in Fig. 4*Aa*, 71.9% of control], and subsequent administration of 1 μM MAM-2201 induced further decrease [trace (c) in Fig. 4*Aa*, 51.0% of control]. On the other hand, 0.1 μM JWH-018 did not have detectable effects on PF-PC EPSCs [trace (b) in Fig. 4*Ba*, 99.0% of control; 0.1 μM JWH-018 in Fig. 4*D*, $n = 7$, $p = 0.096$]. Higher concentrations of JWH-018 were required to reduce PF-PC EPSC amplitude [trace (c) in Fig. 4*Ba*, 1 μM, 81.0% of control; trace (d) in Fig. 4*Ba*, 30 μM, 44.2% of control]. Application of Δ^9-THC, which acts as a partial agonist of CB1Rs (Shen and Thayer, 1999; Luk et al., 2004), decreased amplitude of PF-EPSCs obviously at 3 μM [trace (b) in Fig. 4*C*, 68.6% of control], but subsequent administration of 30 μM Δ^9-THC did not induce a clear reduction [trace (c) in Fig. 4*C*, 57.0% of control]. Δ^9-THC (30 μM) significantly increased PPR and CV ($n = 6$, data not shown), indicating a decrease in presynaptic neurotransmitter release. Fig. 4*D* shows the concentration-dependent decreases of PF-PC EPSC amplitude induced by cannabinoid-related compounds. MAM-2201 decreased PF-PC EPSCs more potently than JWH-018 within the range of 0.03–3 μM (Fig. 4*D*, blue triangles (in the web version), $p < 0.05$ and $p < 0.01$ by unpaired *t*-tests test) and Δ^9-THC within the range of 0.1–30 μM (Fig. 4*D*, gray squares, $p < 0.001$ by unpaired *t*-tests test). Application of WIN decreased PF-PC EPSC amplitude to 64.5 ± 0.16% ($n = 7$) of the control value at a concentration of 1 μM and to 46.8 ± 0.13% ($n = 12$) at 10 μM (Fig. 4*D*, WIN). These results are comparable to the previous reports using cerebellar slice preparations from rodents (see Discussion) (Levenes et al., 1998; Takahashi and Linden, 2000; Kawamura et al., 2006). The IC50s of the synthetic cannabinoids against PF-PC EPSCs are summarized in Table 1, and indicate that the rank order of potency for inhibition is MAM-

Table 2
MAM-2201 did not affect intrinsic membrane properties of PCs.

	Control ($n = 10$)	10 μM MAM-2201 ($n = 10$)	p value
Resting membrane potential (mV)	−65.3 ± 3.2	−66.0 ± 3.5	0.43
input resistance (MΩ)	113 ± 51	101 ± 34	0.29
Threshold current (pA)	71.0 ± 39.5	77.8 ± 7.4	0.24
Threshold potential (mV)	−45.4 ± 5.6	−44.9 ± 6.4	0.50
Spike height (mV)	44.9 ± 6.4	45.4 ± 47.6	0.71
Maximum rate of rise (V/s)	114 ± 40	131 ± 37	0.20
Maximum rate of fall (V/s)	−93.0 ± 17	−89.2 ± 15.8	0.14
Firing frequency at 200 pA (Hz)	33.0 ± 18.4	34.4 ± 20.5	0.77
Firing frequency at 500 pA (Hz)	72.6 ± 29.8	77.8 ± 42.1	0.68

Young mice (P14–20) and the K-gluconate-based internal solution were used for the experiments. Current-clamp recordings were performed at near physiological temperature (34 ± 1 °C).
Data are provided as the means ± standard deviation, and n = number of experiments.

2201 > WIN > JWH-018. These findings are consistent with our unpublished data on the IC50s for these synthetic cannabinoids, measured by a binding assay for human recombinant CB1Rs (see Discussion). IC50 of Δ^9-THC was not able to be calculated due to ambiguous fitting. These results demonstrate that MAM-2201 is a more potent inhibitor of PF-PC synaptic transmission than JWH-018 and Δ^9-THC.

3.4. MAM-2201 inhibits GABAergic synaptic transmission at inhibitory interneuron-PC synapses via presynaptic mechanisms

PCs receive feed-forward inhibition from GABAergic inhibitory interneurons lying in the molecular layer of the cerebellar cortex (Llinas et al., 2004), and this inhibition shapes the spike output of PCs (Mittmann et al., 2005). To explore how MAM-2201 modulates this inhibitory synaptic input, we recorded GABAergic synaptic transmission at inhibitory interneuron-PC synapses and examined the effects of MAM-2201 on inhibitory transmission. As shown in Fig. 5*B*, 10 μM MAM-2201 decreased the first IPSC amplitude (MAM-2201 in Fig. 5*Ba* and *Bb*; Fig. 5*C*, $n = 6$, $p < 0.001$), and a similar reduction was observed by 1 μM MAM-2201, indicating the MAM-2201-induced decrease was concentration-dependent (Fig. 5*C*, MAM-2201). MAM-2201 (10 μM) significantly increased PPR and CV (Scaled in Fig. 5*Ba*, *D* and *E*, MAM-2201), and these increases were comparable to those obtained by WIN (10 μM, Fig. 5*D* and *E*, WIN). Moreover, MAM-2201 (10 μM) decreased mIPSC frequency (IEI, Control: 451.2 ± 464.1 ms, MAM-2201: 718.8 ± 542.9 ms, $p < 0.05$, $n = 5$, Fig. 5*Fa* and *Fb*) without affecting mIPSC amplitude (peak amplitude, Control: 45.3 ± 22.3 pA, MAM-2201: 48.3 ± 24.1 pA, $p = 0.53$, $n = 5$, Fig. 5*Fa* and *Fc*). These results demonstrate that MAM-2201 inhibits GABAergic synaptic transmission at interneuron-PC synapses via presynaptic mechanisms.

3.5. MAM-2201-mediated presynaptic inhibition at CF-PC synapses reduces the number of spikelets in complex spikes and dendritic Ca^{2+} transients in PCs

Activation of CFs produces AMPA receptor-mediated strong postsynaptic depolarization and evokes an all-or-none spike with multiple peaks (spikelets), called "complex spikes" in the soma (Llinas et al., 2004). Complex spikes are accompanied by a large, dendritic Ca^{2+} transient, which plays a crucial role in producing long-term depression (LTD) at PF-PC synapses (Konnerth et al., 1992). At CF terminals, activation of presynaptic CB1Rs by WIN reduces glutamate release (Maejima et al., 2001). To examine how presynaptic modulation by MAM-2201 at CF-PC synapses affects the waveforms of complex spikes and CF-induced dendritic Ca^{2+} transients, we first confirmed presynaptic inhibition by MAM-2201 at CF-PC synapses (Fig. 6), and then performed simultaneous recordings of complex spikes and intracellular Ca^{2+} transients (Fig. 7).

First, CF-PC EPSCs were recorded at the holding potential of −10 mV in the presence of picrotoxin (Fig. 6*B–E*). To improve the space clamp in dendrites, young mice (P14–20) were used for the following experiments. This was because CF innervation of PCs is almost matured at this age (Hashimoto and Kano, 2013), and their dendrites are compact compared with those of adult (~P57) mice (McKay and Turner, 2005). As shown in Fig. 6*B* and *C*, bath application of MAM-2201 (1 or 10 μM) reduced CF-PC EPSC amplitude in a concentration-dependent manner. This reduction was accompanied by significant increases in PPR and CV (10 μM MAM-2201; Scaled in Fig. 6*Ba*, *C* and *D*). Moreover, MAM-2201 (10 μM) decreased CF-PC qEPSC frequency (IEI, Control: 176.5 ± 40.3 ms, MAM-2201: 234.5 ± 51.1 ms, $p < 0.01$, $n = 5$, Fig. 6*Fa* and *Fb*) without affecting CF-PC qEPSC amplitude (peak amplitude, Control: 22.5 ± 2.7 pA, MAM-2201: 22.0 ± 4.0 pA, $p = 0.75$, $n = 5$, Fig. 6*Fa* and *Fc*). These results indicate that MAM-2201 presynaptically inhibits neurotransmitter release from CF terminals.

We then simultaneously recorded complex spikes in the somata and Ca^{2+} transients in the dendrites of PCs using the K-gluconate-based internal solution containing OGB-1 at near physiological temperature. Complex spikes were elicited under current-clamp conditions. As presented in Fig. 7*A*, electrical stimulation of CFs evoked all-or-none complex spikes consisting of spikelets (Control in Fig. 7*A*). MAM-2201 (10 μM, 10 min) significantly reduced the number of spikelets to 78% of the control (Fig. 7*B*, $n = 11$, $p < 0.001$). Because MAM-2201 modulated synaptic properties via activation of presynaptic CB1Rs (Fig. 3), and because PCs do not express CB1Rs (Kano et al., 2009), we would not expect MAM-2201 to affect the intrinsic membrane properties of PCs. As expected, we were able to confirm that MAM-2201 did not affect the resting membrane potential, input resistance, or action potential properties of PCs (Table 2). Accordingly, MAM-2201-induced changes in complex spike waveforms can be interpreted based on depression of CF-PC EPSCs. The complex spikes evoked by CF stimulation were accompanied by large Ca^{2+} transients in the dendrites (Fig. 7*Cb*, Control). MAM-2201 substantially decreased the peak amplitude of the Ca^{2+} transient (Fig. 7*Cb*, MAM-2201). Both the peak and the integral of the Ca^{2+} transients were significantly attenuated by 10 μM MAM-2201 (peak: $n = 10$, $p < 0.01$, Fig. 7*Da*; integration: $n = 10$, $p < 0.01$, Fig. 7*Db*). Taken together, these results indicate that MAM-2201 alters PC responses to CF activation by reducing the number of spikelets and the dendritic Ca^{2+} transients. This implies that MAM-2201 would decrease complex spike-mediated information propagation from PCs to the next nuclei and might affect induction of intracellular Ca^{2+}-dependent LTD at PF-PC synapses (see Discussion).

4. Discussion

This is the first study of the effects of MAM-2201 on neuronal functions. We found that MAM-2201 acted as an agonist of CB1Rs (Fig. 2). We also found that MAM-2201 inhibited glutamatergic synaptic transmission presynaptically via activation of presynaptic CB1Rs (Fig. 3). At the same concentrations, MAM-2201 decreased PF-PC EPSCs more potently than JWH-018 and Δ^9-THC (Fig. 4). Moreover, MAM-2201 also presynaptically suppressed GABAergic synaptic transmission at interneuron-PC synapses (Fig. 5) and glutamatergic synaptic transmission at CF-PC synapses (Fig. 6). In the case of smaller CF-PC EPSCs, MAM-2201 led to reduction of the number of action potentials in complex spikes and to reduced

dendritic intracellular Ca^{2+} transients (Fig. 7). Thus, it is likely that, in humans, the psychoactive effects caused by MAM-2201 are mainly due to inhibition of neurotransmitter release via activation of presynaptic CB1Rs.

4.1. The validity of our data on presynaptic inhibition at PF-PC synapses induced by synthetic cannabinoids

In our experiments, WIN reduced PF-PC EPSC amplitude to 64.5% (1 μM) and 46.8% (10 μM) of the control value using P20–57 mice (Fig. 4*D*). These reductions are comparable to previously published values obtained from acute cerebellar slice preparations: 55.6% of control in 1 μM WIN (P15–21 rats) (Levenes et al., 1998), 29.1 and 12.3% in 1 and 5 μM WIN, respectively (P15–19 rats) (Takahashi and Linden, 2000), and 23.5% in 5 μM WIN (P9–14 mice) (Kawamura et al., 2006). The latter two reports show somewhat smaller percentages compared with our data, but this can be attributed to the differences in the ages of the animals used: an immunohistochemical study revealed that the distribution patterns of CB1Rs in the molecular layer show developmental changes (Kawamura et al., 2006).

Atwood et al. reported that the IC50 of JWH-018 against synaptic transmission is 14.9 nM using autaptic hippocampal neuronal cultures (Atwood et al., 2010), whereas our IC50 value for JWH-018 was approximately 100 times larger than that of their report (Table 1). This discrepancy might be explained by the different neuronal preparations used: Atwood et al. utilized dissociated neuronal cultures, whose synapses would not be wrapped by cell structures such as glial membranes. These synapses would be more easily exposed to CB1R agonists compared with those in cerebellar slice preparations, and therefore synaptic transmission in the autaptic hippocampal cultures might be suppressed by a lower concentration of JWH-018.

Using a binding assay for human recombinant CB1Rs, we recently found that relative IC50s for WIN, MAM-2201, and JWH-018 against CB1Rs were 1.00, 0.70, and 5.30, respectively (Kikura-Hanajiri et al., manuscript in preparation). These data agree well with our observation of the relative IC50s against excitatory neurotransmitter release from PF terminals to PCs using cerebellar slice preparations (Table 1). Therefore, we consider our observations of IC50s in cerebellar preparations to be reasonable.

4.2. Adverse effects of MAM-2201 on targets of the cerebellar cortex and on cerebellum-dependent motor functions

PCs are the sole output GABAergic neurons from the cerebellar cortex and make direct synaptic contacts onto the deep cerebellar nuclear neurons and vestibular nuclear neurons (Voogd and Glickstein, 1998; Zheng and Raman, 2010). PCs receive two types of excitatory input from CFs and PFs. CFs arise from the inferior olivary complex located in the brainstem. CFs are activated during motor learning and induce complex spikes in PCs (Ito, 2001; Llinas et al., 2004). Spikelets in complex spike can propagate to the synaptic terminals of PCs (Khaliq and Raman, 2005). PFs are the axons of granule cells, which are excited by glutamatergic mossy fiber inputs. Mossy fibers originate from nuclei in the spinal cord and brain stem. The mossy fiber-PF pathway is the main operational input to the cerebellum and PCs, and carries afferent information both from the periphery and from other brain centers. PFs produce a brief excitatory postsynaptic potential in PCs that generates a single action potential called a “simple spike.” In addition, PCs receive feed-forward synaptic inhibition from GABAergic interneurons, and this inhibition increases the precision of PC spike outputs (Mittmann et al., 2005). Thus, all of these synaptic inputs to PCs can control the output of the cerebellar cortex. The absence of PC activity or genetic manipulation of synaptic transmission from PCs severely affects cerebellum-dependent motor functions: both in mutant mice and in spinocerebellar ataxia type 6 patients, selective degeneration of PCs induce motor dysfunction (Frontali, 2001; Porras-Garcia et al., 2013), and PC-specific vesicular GABA transporter knockout mice exhibit motor impairment (Kayakabe et al., 2013).

We demonstrate that MAM-2201 inhibits neurotransmitter release at PF-PC, interneuron-PC, and CF-PC synapses in a concentration-dependent manner (Figs. 3–6), and reduces the number of spikelets in CF-evoked complex spikes (Fig. 7*A* and *B*). Assuming that, in humans, MAM-2201 inhibits neurotransmitter release at these synapses, the inhibition at PF-PC synapses could cause failure of simple spike generation in PCs. The inhibition of interneuron-PC synapses may weaken the feed-forward inhibition, leading to decreased precision of PC spike outputs. MAM-2201-induced reduction of spikelets in complex spikes (Fig. 7*A* and *B*) could cause a decrease in the number of action potentials that propagate to the synaptic terminals of PCs. Consequently, MAM-2201 may interrupt normal GABAergic inhibition onto the deep cerebellar nuclear neurons and vestibular nuclear neurons, and thus could affect cerebellum-dependent motor coordination. This speculation could be supported by the report that consumption of drugs of abuse containing analogs of MAM-2201 can cause cerebellar dysfunction such as disturbance of finger-to-finger test (Musshoff et al., 2014).

4.3. Possible effects of MAM-2201 on cerebellar LTD initiated by dendritic Ca^{2+} transients and on motor learning functions

PF-PC LTD is thought to underlie cerebellar motor learning in mammals (Yuzaki, 2012). This learning is impaired in transgenic mice that exhibit a deficit in the expression of LTD *in vitro* (Kakegawa et al., 2008). Induction of LTD requires association of PF and CF activation both *in vivo* and *in vitro* (Ito, 2001). At the cellular level, CF synaptic inputs to PCs evoke dendritic Ca^{2+} transients, which play crucial roles in the expression of LTD (Konnerth et al., 1992). Interestingly, Carey and Regehr reported that presynaptic inhibition of CF-PC synapses by noradrenaline alters the complex spike waveform and decreases CF-evoked dendritic Ca^{2+} transients, leading to interference with the induction of LTD (Carey and Regehr, 2009). This noradrenergic modulation shares many features with our observations of MAM-2201-induced changes of CF-evoked responses in PCs (Figs. 6 and 7): depression of CF-PC EPSCs via presynaptic mechanisms, reduction of the number of spikelets in complex spikes, and attenuation of CF-induced Ca^{2+} transients in PC dendrites. Taken together, MAM-2201 may interfere with the induction of LTD *in vitro* and might result in an impairment of cerebellar motor learning *in vivo*. Further work will be needed to clarify whether MAM-2201 indeed blocks the induction of LTD.

4.4. Implications for adverse effects of MAM-2201 on other brain functions

In the brain, CB1Rs are widely and abundantly expressed, and numerous *in vitro* studies have revealed that activation of CB1Rs by agonists suppresses synaptic transmission in several regions such as the hippocampus, nucleus accumbens, striatum, and cerebellar cortex (Kano et al., 2009). Moreover, in rat hippocampal slice preparations, pharmacological activation of CB1Rs modulates long-term potentiation in the CA1 region (Navakkode and Korte, 2014), and *in vivo* administration of WIN impairs hippocampal-dependent short-term memory (Hampson and Deadwyler, 2000). WIN also activates the “reward circuitry” in the brain, including the ventral tegmental area-nucleus accumbens pathway, and alters reward-

related behaviors in a similar manner to other reward-enhancing addictive drugs (Gardner, 2005). In this study, we demonstrated that MAM-2201 suppresses synaptic transmission in the cerebellum and that this action parallels that induced by WIN (Figs. 3–5). Taken together, in humans, MAM-2201 could cause psychoactive effects that are similar to those observed in the laboratory animal experiments using WIN or other synthetic cannabinoids.

Acknowledgments

This work was supported by Health Labour Sciences Research Grants. We thank Dr. Nobutake Hosoi (Gunma University) for technical advice on intracellular Ca^{2+} imaging.

References

Atwood, B.K., Huffman, J., Straiker, A., Mackie, K., 2010. JWH018, a common constituent of 'Spice' herbal blends, is a potent and efficacious cannabinoid CB receptor agonist. Br. J. Pharmacol. 160, 585–593.
Auwarter, V., Dresen, S., Weinmann, W., Muller, M., Putz, M., Ferreiros, N., 2009. 'Spice' and other herbal blends: harmless incense or cannabinoid designer drugs? J. Mass Spectrom. 44, 832–837.
Brown, S.P., Safo, P.K., Regehr, W.G., 2004. Endocannabinoids inhibit transmission at granule cell to Purkinje cell synapses by modulating three types of presynaptic calcium channels. J. Neurosci. 24, 5623–5631.
Bruno, A., Lembo, F., Novellino, E., Stornaiuolo, M., Marinelli, L., 2014. Beyond radiodisplacement techniques for identification of CB1 ligands: the first application of a fluorescence-quenching assay. Sci. Rep. 4, 3757.
Carey, M.R., Regehr, W.G., 2009. Noradrenergic control of associative synaptic plasticity by selective modulation of instructive signals. Neuron 62, 112–122.
Derungs, A., Schwaninger, A.E., Mansella, G., Bingisser, R., Kraemer, T., Liechti, M.E., 2013. Symptoms, toxicities, and analytical results for a patient after smoking herbs containing the novel synthetic cannabinoid MAM-2201. Forensic Toxicol. 31, 164–171.
DeSanty, K.P., Dar, M.S., 2001. Cannabinoid-induced motor incoordination through the cerebellar CB(1) receptor in mice. Pharmacol. Biochem. Behav. 69, 251–259.
Diana, M.A., Levenes, C., Mackie, K., Marty, A., 2002. Short-term retrograde inhibition of GABAergic synaptic currents in rat Purkinje cells is mediated by endogenous cannabinoids. J. Neurosci. 22, 200–208.
Dousmanis, A.G., Pennefather, P.S., 1992. Inwardly rectifying potassium conductances in AtT-20 clonal pituitary cells. Pflugers Arch. 422, 98–104.
Felder, C.C., Joyce, K.E., Briley, E.M., Glass, M., Mackie, K.P., Fahey, K.J., Cullinan, G.J., Hunden, D.C., Johnson, D.W., Chaney, M.O., Koppel, G.A., Brownstein, M., 1998. LY320135, a novel cannabinoid CB1 receptor antagonist, unmasks coupling of the CB1 receptor to stimulation of cAMP accumulation. J. Pharmacol. Exp. Ther. 284, 291–297.
Frontali, M., 2001. Spinocerebellar ataxia type 6: channelopathy or glutamine repeat disorder? Brain Res. Bull. 56, 227–231.
Gardner, E.L., 2005. Endocannabinoid signaling system and brain reward: emphasis on dopamine. Pharmacol. Biochem. Behav. 81, 263–284.
Hagiwara, S., Miyazaki, S., Rosenthal, N.P., 1976. Potassium current and the effect of cesium on this current during anomalous rectification of the egg cell membrane of a starfish. J. Gen. Physiol. 67, 621–638.
Hampson, R.E., Deadwyler, S.A., 2000. Cannabinoids reveal the necessity of hippocampal neural encoding for short-term memory in rats. J. Neurosci. 20, 8932–8942.
Hashimoto, K., Kano, M., 2013. Synapse elimination in the developing cerebellum. Cell. Mol. Life Sci. 70, 4667–4680.
Huestis, M.A., Gorelick, D.A., Heishman, S.J., Preston, K.L., Nelson, R.A., Moolchan, E.T., Frank, R.A., 2001. Blockade of effects of smoked marijuana by the CB1-selective cannabinoid receptor antagonist SR141716. Arch. Gen. Psychiatry 58, 322–328.
Irie, T., Fukui, I., Ohmori, H., 2006. Activation of GIRK channels by muscarinic receptors and group II metabotropic glutamate receptors suppresses Golgi cell activity in the cochlear nucleus of mice. J. Neurophysiol. 96, 2633–2644.
Irie, T., Matsuzaki, Y., Sekino, Y., Hirai, H., 2014. Kv3.3 channels harbouring a mutation of spinocerebellar ataxia type 13 alter excitability and induce cell death in cultured cerebellar Purkinje cells. J. Physiol. 592, 229–247.
Irie, T., Ohmori, H., 2008. Presynaptic GABA(B) receptors modulate synaptic facilitation and depression at distinct synapses in fusiform cells of mouse dorsal cochlear nucleus. Biochem. Biophys. Res. Commun. 367, 503–508.
Ito, M., 2001. Cerebellar long-term depression: characterization, signal transduction, and functional roles. Physiol. Rev. 81, 1143–1195.
Kakegawa, W., Miyazaki, T., Emi, K., Matsuda, K., Kohda, K., Motohashi, J., Mishina, M., Kawahara, S., Watanabe, M., Yuzaki, M., 2008. Differential regulation of synaptic plasticity and cerebellar motor learning by the C-terminal PDZ-binding motif of GluRdelta2. J. Neurosci. 28, 1460–1468.
Kano, M., Ohno-Shosaku, T., Hashimotodani, Y., Uchigashima, M., Watanabe, M., 2009. Endocannabinoid-mediated control of synaptic transmission. Physiol. Rev. 89, 309–380.
Kawamura, Y., Fukaya, M., Maejima, T., Yoshida, T., Miura, E., Watanabe, M., Ohno-Shosaku, T., Kano, M., 2006. The CB1 cannabinoid receptor is the major cannabinoid receptor at excitatory presynaptic sites in the hippocampus and cerebellum. J. Neurosci. 26, 2991–3001.
Kayakabe, M., Kakizaki, T., Kaneko, R., Sasaki, A., Nakazato, Y., Shibasaki, K., Ishizaki, Y., Saito, H., Suzuki, N., Furuya, N., Yanagawa, Y., 2013. Motor dysfunction in cerebellar Purkinje cell-specific vesicular GABA transporter knockout mice. Front. Cell. Neurosci. 7, 286.
Khaliq, Z.M., Raman, I.M., 2005. Axonal propagation of simple and complex spikes in cerebellar Purkinje neurons. J. Neurosci. 25, 454–463.
Kikura-Hanajiri, R., Uchiyama, N., Kawamura, M., Goda, Y., 2013. Changes in the prevalence of new psychoactive substances before and after the introduction of the generic scheduling of synthetic cannabinoids in Japan. Drug Test. Anal..
Konnerth, A., Dreessen, J., Augustine, G.J., 1992. Brief dendritic calcium signals initiate long-lasting synaptic depression in cerebellar Purkinje cells. Proc. Natl. Acad. Sci. U. S. A. 89, 7051–7055.
Korn, H., Faber, D.S., 1991. Quantal analysis and synaptic efficacy in the CNS. Trends Neurosci. 14, 439–445.
Kreitzer, A.C., Regehr, W.G., 2001. Retrograde inhibition of presynaptic calcium influx by endogenous cannabinoids at excitatory synapses onto Purkinje cells. Neuron 29, 717–727.
Kubo, Y., Reuveny, E., Slesinger, P.A., Jan, Y.N., Jan, L.Y., 1993. Primary structure and functional expression of a rat G-protein-coupled muscarinic potassium channel. Nature 364, 802–806.
Kushmerick, C., Price, G.D., Taschenberger, H., Puente, N., Renden, R., Wadiche, J.I., Duvoisin, R.M., Grandes, P., von Gersdorff, H., 2004. Retroinhibition of presynaptic Ca^{2+} currents by endocannabinoids released via postsynaptic mGluR activation at a calyx synapse. J. Neurosci. 24, 5955–5965.
Levenes, C., Daniel, H., Soubrie, P., Crepel, F., 1998. Cannabinoids decrease excitatory synaptic transmission and impair long-term depression in rat cerebellar Purkinje cells. J. Physiol. 510 (Pt 3), 867–879.
Llinas, R., Walton, K.D., Lang, E.J., 2004. Cerebellum. In: Shepard, G.M. (Ed.), The Synaptic Organization of the Brain, fifth ed. Oxford University Press, New York, NY, US, pp. 271–309.
Lonati, D., Buscaglia, E., Papa, P., Valli, A., Coccini, T., Giampreti, A., Petrolini, V.M., Vecchio, S., Serpelloni, G., Locatelli, C.A., 2014. MAM-2201 (analytically confirmed) intoxication after "synthacaine" consumption. Ann. Emerg. Med..
Luk, T., Jin, W., Zvonok, A., Lu, D., Lin, X.Z., Chavkin, C., Makriyannis, A., Mackie, K., 2004. Identification of a potent and highly efficacious, yet slowly desensitizing CB1 cannabinoid receptor agonist. Br. J. Pharmacol. 142, 495–500.
Mackie, K., 2008. Signaling via CNS cannabinoid receptors. Mol. Cell. Endocrinol. 286, S60–S65.
Mackie, K., Lai, Y., Westenbroek, R., Mitchell, R., 1995. Cannabinoids activate an inwardly rectifying potassium conductance and inhibit Q-type calcium currents in AtT20 cells transfected with rat brain cannabinoid receptor. J. Neurosci. 15, 6552–6561.
Maejima, T., Hashimoto, K., Yoshida, T., Aiba, A., Kano, M., 2001. Presynaptic inhibition caused by retrograde signal from metabotropic glutamate to cannabinoid receptors. Neuron 31, 463–475.
McKay, B.E., Turner, R.W., 2005. Physiological and morphological development of the rat cerebellar Purkinje cell. J. Physiol. 567, 829–850.
Mittmann, W., Koch, U., Hausser, M., 2005. Feed-forward inhibition shapes the spike output of cerebellar Purkinje cells. J. Physiol. 563, 369–378.
Monory, K., Blaudzun, H., Massa, F., Kaiser, N., Lemberger, T., Schutz, G., Wotjak, C.T., Lutz, B., Marsicano, G., 2007. Genetic dissection of behavioural and autonomic effects of Delta(9)-tetrahydrocannabinol in mice. PLoS Biol. 5, e269.
Moosmann, B., Kneisel, S., Girreser, U., Brecht, V., Westphal, F., Auwarter, V., 2012. Separation and structural characterization of the synthetic cannabinoids JWH-412 and 1-[(5-fluoropentyl)-1H-indol-3yl]-(4-methylnaphthalen-1-yl)methanone using GC-MS, NMR analysis and a flash chromatography system. Forensic Sci. Int. 220, e17–22.
Musshoff, F., Madea, B., Kernbach-Wighton, G., Bicker, W., Kneisel, S., Hutter, M., Auwarter, V., 2014. Driving under the influence of synthetic cannabinoids ("Spice"): a case series. Int. J. Legal Med. 128, 59–64.
Navakkode, S., Korte, M., 2014. Pharmacological activation of CB1 receptor modulates long term potentiation by interfering with protein synthesis. Neuropharmacology 79, 525–533.
Patel, S., Hillard, C.J., 2001. Cannabinoid CB(1) receptor agonists produce cerebellar dysfunction in mice. J. Pharmacol. Exp. Ther. 297, 629–637.
Porras-Garcia, M.E., Ruiz, R., Perez-Villegas, E.M., Armengol, J.A., 2013. Motor learning of mice lacking cerebellar Purkinje cells. Front. Neuroanat. 7, 4.
Regehr, W.G., Carey, M.R., Best, A.R., 2009. Activity-dependent regulation of synapses by retrograde messengers. Neuron 63, 154–170.
Safo, P.K., Cravatt, B.F., Regehr, W.G., 2006. Retrograde endocannabinoid signaling in the cerebellar cortex. Cerebellum 5, 134–145.
Safo, P.K., Regehr, W.G., 2005. Endocannabinoids control the induction of cerebellar LTD. Neuron 48, 647–659.
Saito, T., Namera, A., Miura, N., Ohta, S., Miyazaki, S., Osawa, M., Inokuchi, S., 2013. A fatal case of MAM-2201 poisoning. Forensic Toxicol. 31, 333–337.
Seely, K.A., Lapoint, J., Moran, J.H., Fattore, L., 2012. Spice drugs are more than harmless herbal blends: a review of the pharmacology and toxicology of synthetic cannabinoids. Prog. Neuro Psychopharmacol. Biol. Psychiatry 39, 234–243.

Shen, M., Thayer, S.A., 1999. Delta9-tetrahydrocannabinol acts as a partial agonist to modulate glutamatergic synaptic transmission between rat hippocampal neurons in culture. Mol. Pharmacol. 55, 8–13.
Showalter, V.M., Compton, D.R., Martin, B.R., Abood, M.E., 1996. Evaluation of binding in a transfected cell line expressing a peripheral cannabinoid receptor (CB2): identification of cannabinoid receptor subtype selective ligands. J. Pharmacol. Exp. Ther. 278, 989–999.
Shuvaev, A.N., Horiuchi, H., Seki, T., Goenawan, H., Irie, T., Iizuka, A., Sakai, N., Hirai, H., 2011. Mutant PKC{gamma} in spinocerebellar ataxia type 14 disrupts synapse elimination and long-term depression in Purkinje cells in vivo. J. Neurosci. 31, 14324–14334.
Szabo, B., Than, M., Thorn, D., Wallmichrath, I., 2004. Analysis of the effects of cannabinoids on synaptic transmission between basket and Purkinje cells in the cerebellar cortex of the rat. J. Pharmacol. Exp. Ther. 310, 915–925.
Takahashi, K.A., Linden, D.J., 2000. Cannabinoid receptor modulation of synapses received by cerebellar Purkinje cells. J. Neurophysiol. 83, 1167–1180.
Taura, F., Sirikantaramas, S., Shoyama, Y., Shoyama, Y., Morimoto, S., 2007. Phytocannabinoids in Cannabis sativa: recent studies on biosynthetic enzymes. Chem. Biodivers. 4, 1649–1663.
Uchiyama, N., Kawamura, M., Kikura-Hanajiri, R., Goda, Y., 2013. URB-754: a new class of designer drug and 12 synthetic cannabinoids detected in illegal products. Forensic Sci. Int. 227, 21–32.
Vardakou, I., Pistos, C., Spiliopoulou, C., 2010. Spice drugs as a new trend: mode of action, identification and legislation. Toxicol. Lett. 197, 157–162.
Vincent, P., Marty, A., 1996. Fluctuations of inhibitory postsynaptic currents in Purkinje cells from rat cerebellar slices. J. Physiol. 494 (Pt 1), 183–199.
Voogd, J., Glickstein, M., 1998. The anatomy of the cerebellum. Trends Cogn. Sci. 2, 307–313.
Wilson, R.I., Nicoll, R.A., 2002. Endocannabinoid signaling in the brain. Science 296, 678–682.
Xu-Friedman, M.A., Regehr, W.G., 1999. Presynaptic strontium dynamics and synaptic transmission. Biophys. J. 76, 2029–2042.
Yuzaki, M., 2012. Cerebellar LTD vs. motor learning-lessons learned from studying GluD2. Neural Netw..
Zheng, N., Raman, I.M., 2010. Synaptic inhibition, excitation, and plasticity in neurons of the cerebellar nuclei. Cerebellum 9, 56–66.
Zucker, R.S., Regehr, W.G., 2002. Short-term synaptic plasticity. Annu Rev. Physiol. 64, 355–405.

ミクログリアの発生と分化

佐藤　薫

ミクログリアの発生と分化過程

脳の免疫機能担当細胞として長らく知られてきたミクログリアは脳細胞の5%を占める．Macrophage 1 antigen (Mac1)，major histocompatibility complex (MHC) class Ⅱ，CD68，F4/80やfragment，crystallizable(Fc)受容体，low density lipoprotein(LDL)受容体といった細胞表面抗原を発現していること，貪食能，サイトカイン分泌といった機能を有することなど，モノサイトやマクロファージに類似点が多いため，脳内炎症レベルの決定細胞として長らく炎症を伴う病態研究の対象となってきた．ミクログリアをモノサイトやマクロファージと決定的に区別できる細胞表面抗原がまだ見つかっていないため，その起源についてもモノサイトやマクロファージと共通であると長らく考えられてきた．しかし2010〜12年にかけて，ミクログリアが系統的に発生過程の早い時期にマクロファージと分かれていることが明らかにされた．ミクログリアは胎生7.5日齢に骨髄前駆細胞から分化し胎生8.5〜9.5日齢にはすでに脳内に移行している[1,2]．Ginhouxらは，造血幹細胞(モノサイトやマクロファージのもとになる幹細胞)の完成前である胎生7日齢に，ミクログリア前駆細胞がすでに卵黄嚢で発生しており，胎生9日齢までにこれらの細胞が脳に移行してミクログリアとなることを実験的に証明した[1]．これは神経幹細胞であるラジアルグリアが脳内に発生する(胎生10.5日齢)よりも早いタイミングの出来事である．このミクログリア前駆細胞はCsf1受容体を発現したMyb(−)，PU.1依存的であることも[2]，Myb(＋)な造血幹細胞とは異なる点である．一方，病態時には血液脳関門のバリア機能低下により血球系細胞の脳内浸潤が起こるが，これらの細胞がミクログリアにはならないことも示されている．モノサイトやマクロファージのみがgreen fluorescent protein(GFP)標識されたマウスに実験的脳脊髄炎(experimental allergic encephalomyelitis：EAE)を発症させると，EAE症状の重篤度に応じてモノサイトが脊髄に浸潤するが，炎症終息後にGFP陽性細胞は消失した[3]．以上のことから，脳内で生理的な機能を持つミクログリアのほとんどが胎生7.5日齢に脳内に移行したミクログリア前駆細胞の子孫たちであると考えられる．ところが，このように共通の先祖を持ちながらミクログリアは中枢神経系の発達，機能分化とともに，ミエリン，血管系，血液脳関門，周囲細胞の細胞外マトリックス，神経伝達物質，といった周囲環境との相互作用によって，その領域，その時期に特異的な形態，抗原発現パターン，増殖パターン，生理機能を獲得する[4,5]．さらに言えば，一領域中のミクログリア集団の中に感染や外傷に対して非常に劇的に反応する集団とそうでもない集団が含まれていることもあり[6]，ミクログリアと微細な周囲環境との相互作用が起こっていると考えられる．

ミクログリアは，正常脳でよくみられるような，細かく発達した多くの突起を持つ「静止型」と神経炎症等の病変部に集積しているアメボイド状の「活性化型」との間を環境の変化に応じて行き来する細胞である．しかし最近の研究で，静止型ミクログリアはその発達した突起により周囲環境を実に積極的に探索していることが明らかとなっている[5]．したがって「静止型」，「活性化型」はもはや言葉通りに捉えきれなくなっている．現在，ミクログリアの活性状態はM0，M1，M2ステージというカテゴリーで表現されるが，この概念はそもそもマクロファージ研究から導入された[7]．マクロファージは外部刺激に対する反応によってM1，M2a，M2b，M2cというカテゴリーに分けられるが[8]，ミクログリアと異なる点は，分類に有効な35種類の表面抗原が明らかになっている点である．M1ミクログリアは炎症誘発特性，M2ミクログリアが抗炎症特性を持つ，と言われるが，そのどちらにも入らないM0ミクログリアという集団も発見されている[4]．M1，M2の中間とも言えるミクログリアも存在する．生後初期マウスのミクログリアはM1遺伝子(iNOS，TNFα)とM2遺伝子(Arginase-1)の両者を高発現している．M0，M1，M2ステージの他に

さとう かおる　国立医薬品食品衛生研究所薬理部第一室長(中枢神経薬理)

0289-0585/20/￥90/頁/JCOPY

HoxB8というホメオボックスタンパク質の発現によってミクログリアを分類しているグループもいる[9]．HoxB8(＋)細胞はCD11b(＋)ミクログリアの15％を占め，卵黄嚢から分化するミクログリアとは異なる細胞集団であると報告されている．HoxB8を欠損したマウスは強迫性障害スペクトラムに伴う脱毛症と非常によく似た症状が現れるため，病態解明への応用が期待されている．

脳室下帯ミクログリアに関する最近の知見

脳室帯(ventricular zone：VZ)と脳室下帯(subventricular zone：SVZ)は一生を通じて神経新生やグリア新生が起こる領域であることが明らかとなって久しい．主要な投射神経は胎生期に，アストロサイトは胎生期から生後初期まで，オリゴデンドロサイトは胎生後期から生後初期にかけて，介在神経は胎生後期以降新生される[10]．一方，上で述べたように胎生8.5〜9.5日齢にはアメボイド型のミクログリアが脳内にすでに存在している[1,2]．ミクログリアは生後初期に爆発的に増加するが[11]，発達が進むにつれアメボイド型のミクログリアは減少し成体においてほとんど静止型になる[12]．しかし，胎生期の神経新生にミクログリアがどのように関わっているかについては2013年にCunninghamらが報告するまで，ほとんどわかっていなかった[13]．彼らは胎生期の大脳皮質神経細胞新生過程の後半において，ミクログリアが貪食作用によって神経前駆細胞プールの細胞数を調節していることを明らかにした．このとき，ミクログリアが貪食した細胞はアポトーシスを起こしていない点は興味深い．成体海馬歯状回顆粒細胞層(subgranular zone：SGZ)での神経新生の場合，ミクログリアはアポトーシスを起こした細胞を貪食しているからである[14]．発達期SVZと成体SGZでの神経新生とミクログリアの関連について，さらなる解明が待たれる．

生後SVZの神経新生におけるミクログリアの役割については胎生期に増してほとんど情報がなかったが，2006年に，SVZのように神経新生が活発な領域とそれ以外の領域とでミクログリアの活性化や機能に差があることが指摘された[15]．最近われわれは，生後初期に活性化型ミクログリアがSVZに一過的に集積しており，成熟に伴い，より突起の発達したミクログリアが白質まで分散するようになることを見出した．われわれは生後初期SVZでこのように特異な挙動を示すミクログリアが，SVZにおける神経新生およびオリゴデンドロサイト新生を促進することを明らかにした[16](図1)．SVZは一生を通じて神経新生が継続するものの，年を重ねるにつれ新生細胞数は激減する．われわれのデータでも，生後30日齢のSVZに活性化型ミクログリアはすでにほとんど存在せず，SVZ神経新生動態と相関がある．興味深いことに，SVZでの神経新生に対するミクログリアの作用はSVZ中の位置によって異なるようである．われわれも体軸の中間あたり，線条体と海馬が対面するあたりが最もミクログリア密度が高いことを見出している．この細胞分布の偏りは血管系が関与している可能性がある．血管は成体脳SVZにおいて神経新生ニッチとなることが知られているが[17,18]，SVZは血管叢と呼ばれるほど血管が発達しており[19,20]，特にSVZ中心部は腹側から大きな血管が来ている[20,21]．血管から多種の液性因子が放出されていることはよく知られているが[17]，大脳皮質にミクログリアが移行するのに重要なシグナルカスケードであるCXCL12/CXCR4シグナル[22]の関与などが考えられる．成体脳における脳室上衣下層(subependymal zone：SEZ)では吻側尾側方向，背側腹側方向に高度に領域化されており，各領域からは異なる神経細胞系列が新生してくることも知られている[23]．また，背側SEZではより多くのオリゴデンドロサイト新生が起こることも知られている[24]．今後，SVZ領域をさらに細分化してミクログリアの役割について検討する必要があろう．

成体脳SVZからとってきた神経幹細胞や神経前駆細胞の場合，Th2ヘルパーT細胞由来サイトカインによって刺激されたミクログリアが神経新生やオリゴデンドロサイト新生を促進する[25]．このとき，ミクログリアから放出されるIGF-1が作用に関与していることが示唆されている．しかし，生後初期SVZにおいてはIGF-1を発現しているミクログリアはわずかに確認されるが，IGF-1はミクログリアの神経新生促進作用の作用本体ではなかった[16]．われわれは，ミクログリアが神経新生，オリゴデンドロサイト新生を促進するメカニズムとして生後4〜9日齢のSVZにおいて一過的に濃度が上昇するサイトカイン群(IL-1β，IL-6，TNFα，IFNγ)が重要であることを明らかとした．興味深いのは，神経幹細胞塊(neurosphere)とミクログリアの共培養系を用いた実験で，上記4種のサイトカインのう

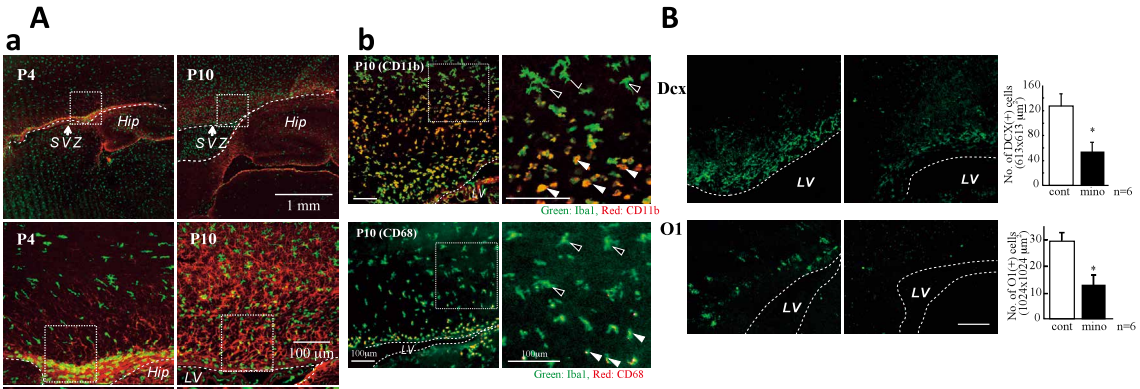

図 1　生後初期 SVZ ミクログリアの神経新生およびオリゴデンドロサイト新生における役割

A-a）生後初期 SVZ に活性化型ミクログリアが集積していることを見出した．

A-b）集積ミクログリアの活性化型マーカー（CD11b，CD68）の発現．白矢頭は Iba1（＋）marker（＋）細胞を表す．

B）ミノサイクリンを P1-4 で腹腔内投与すると，神経前駆細胞マーカー Dcx とオリゴデンドロサイト前駆細胞マーカー O1 を発現する細胞数が有意に減少した．＊$p<0.05$ vs. control group, student's *t* test（N＝6）．（Shigemoto-Mogami ら[16] より改変）

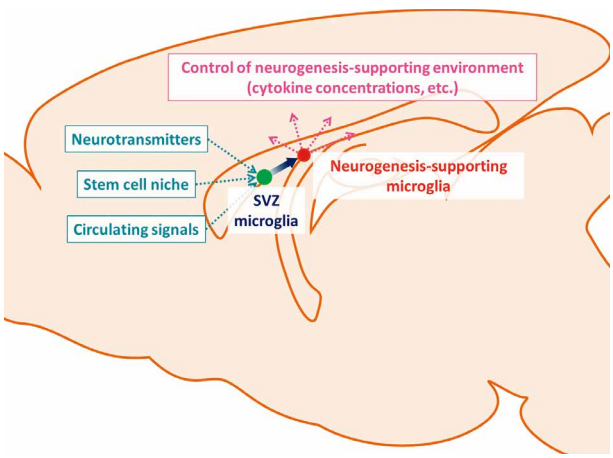

図 2

SVZ ミクログリアは脳内・脳外環境からの信号に応じてサイトカイン環境を調節する‘Hub’として機能しているのではないか．

ち 1 種のサイトカイン機能を機能中和抗体で阻害してもミクログリアの作用に何ら影響はなかったが，全てのサイトカインを同時に阻害するとミクログリアの作用が消失したことである．この結果は神経新生やオリゴデンドロサイト新生を複数のサイトカインが相補的に促進していることを示唆している．これまで，神経新生に関するサイトカインの作用としては，神経前駆細胞が IL-1β，IL-1R1，IL-1R2 を発現し，IL-1β は神経前駆細胞の増殖と分化を調節していること[26]，IL-6 が IL-6R を介して神経新生を促進すること[27] などが報告されていたが，複数サイトカインによる相補的な作用は報告がなかった．Li らは IFNγ の作用はミクログリア存在下では表現系が異なることを示しており，われわれが示した相補的作用を支持するものである[28]．そもそも，IL-1β，IL-6，TNFα，IFNγ は炎症性サイトカインとして，LPS（lipopolysaccharide）刺激[29]，EAE[30]，status epilepticus（SE）[31] といった病理的条件下では神経新生を抑制する本体として研究されてきた．しかし，より穏やかな実験条件では異なる作用が発揮される．炎症モデル作成のために使われる LPS は，適用条件（適用時間など）をわずかに調整することでミクログリアの神経新生への影響が変化する[32]．サイトカイン自身も濃度によって作用が変化する．TNFα は 1 ng/mL では神経幹細胞を増殖する一方，10 ng/mL 以上の濃度でアポトーシスを起こす[33]．われわれのデータでは，ミノサイクリンがミクログリアの活性化を抑制すると，神経前駆細胞の数は半分以下に減少するのに対し，それぞれのサイトカインレベルの減少は皆一様に穏やかであった．サイトカインはミクログリアだけでなく

アストロサイトなどの周囲細胞からも放出される．おそらく，ミクログリアからのサイトカイン放出が‘cytokine storm’[34]には遠く及ばない程度の，‘cytokine drizzling’とも言える連続的なサイトカイン放出トリガーとなっていることが予想される．

むすび

われわれにとって次の課題は，生後初期ミクログリアの活性化機構の解明である．重大なヒントとして胎生期から生後にかけてSVZでのミクログリア機能が大きく変化する点があげられる．体内を循環している種々のメディエーターは誕生の前後で質，量ともに大きく変化する[35]．われわれは，SVZミクログリアはこのような脳内・脳外環境からの信号に応じてサイトカイン環境を調節する‘Hub’として機能しているのではないかと考えている(図2)．このような脳外から脳内への情報デリバリー，それに伴うミクログリアによる神経新生の調節メカニズムの解明は，発達障害を含む神経障害治療にもブレークスルーをもたらすことが期待される．

文献

1) Ginhoux F, Greter M, Leboeuf M, et al. Fate mapping analysis reveals that adult microglia derive from primitive macrophages. Science. 2010；330：841-5.
2) Schulz C, Gomez Perdiguero E, Chorro L, et al. A lineage of myeloid cells independent of Myb and hematopoietic stem cells. Science. 2012；336：86-90.
3) Ajami B, Bennett JL, Krieger C, et al. Infiltrating monocytes trigger EAE progression, but do not contribute to the resident microglia pool. Nat Neurosci. 2011；14：1142-9.
4) Butovsky O, Jedrychowski MP, Moore CS, et al. Identification of a unique TGF-β-dependent molecular and functional signature in microglia. Nat Neurosci. 2014；17：131-43.
5) Kettenmann H, Hanisch UK, Noda M, Verkhratsky A. Physiology of microglia. Physiol Rev. 2011；91：461-553.
6) Scheffel J, Regen T, Van Rossum D, et al. Toll-like receptor activation reveals developmental reorganization and unmasks responder subsets of microglia. Glia. 2012；60：1930-43.
7) Sica A, Mantovani A. Macrophage plasticity and polarization：in vivo veritas. J Clin Invest. 2012；122：787-95.
8) Geissmann F, Gordon S, Hume DA, et al. Unravelling mononuclear phagocyte heterogeneity. Nat Rev Immunol. 2010；10：453-60.
9) Chen SK, Tvrdik P, Peden E, et al. Hematopoietic origin of pathological grooming in Hoxb8 mutant mice. Cell. 2010；141：775-85.
10) Wang DD, Bordey A. The astrocyte odyssey. Prog Neurobiol. 2008；86：342-67.
11) Sminia T, de Groot CJ, Dijkstra CD, et al. Macrophages in the central nervous system of the rat. Immunobiology. 1987；174：43-50.
12) Zusso M, Methot L, Lo R, et al. Regulation of postnatal forebrain amoeboid microglial cell proliferation and development by the transcription factor Runx1. J Neurosci. 2012；32：11285-98.
13) Cunningham CL, Martínez-Cerdeño V, Noctor SC. Microglia regulate the number of neural precursor cells in the developing cerebral cortex. J Neurosci. 2013；33：4216-33.
14) Sierra A, Encinas JM, Deudero JJ, et al. Microglia shape adult hippocampal neurogenesis through apoptosis-coupled phagocytosis. Cell Stem Cell. 2010；7：483-95.
15) Goings GE, Kozlowski DA, Szele FG. Differential activation of microglia in neurogenic versus non-neurogenic regions of the forebrain. Glia. 2006；54：329-42.
16) Shigemoto-Mogami Y, Hoshikawa K, Goldman JE, et al. Microglia enhance neurogenesis and oligodendrogenesis in the early postnatal subventricular zone. J Neurosci. 2014；34：2231-43.
17) Goldberg JS, Hirschi KK. Diverse roles of the vasculature within the neural stem cell niche. Regen Med. 2009；4：879-97.
18) Quaegebeur A, Lange C, Carmeliet P. The neurovascular link in health and disease：molecular mechanisms and therapeutic implications. Neuron. 2011；71：406-24.
19) Ihrie RA, Alvarez-Buylla A. Lake-front property：a unique germinal niche by the lateral ventricles of the adult brain. Neuron. 2011；70：674-86.
20) Shen Q, Wang Y, Kokovay E, et al. Adult SVZ stem cells lie in a vascular niche：a quantitative analysis of niche cell-cell interactions. Cell Stem Cell. 2008；3：289-300.
21) Dorr A, Sled JG, Kabani N. Three-dimensional cerebral vasculature of the CBA mouse brain：a magnetic resonance imaging and micro computed tomography study. Neuroimage. 2007；35：1409-23.
22) Arnò B, Grassivaro F, Rossi C, et al. Neural progenitor cells orchestrate microglia migration and positioning into the developing cortex. Nat Commun. 2014；5：5611.
23) Merkle FT, Mirzadeh Z, Alvarez-Buylla A. Mosaic organization of neural stem cells in the adult brain. Science. 2007；317：381-4.
24) Ortega F, Gascon S, Masserdotti G, et al. Oligodendrogliogenic and neurogenic adult subependymal zone neural stem cells constitute distinct lineages and exhibit differential responsiveness to Wnt signalling. Nat Cell Biol. 2013；15：602-13.
25) Butovsky O, Ziv Y, Schwartz A, et al. Microglia activated by IL-4 or IFN-gamma differentially induce neurogenesis and oligodendrogenesis from adult stem/progenitor cells. Mol Cell Neurosci. 2006；31：149-60.
26) Wang X, Fu S, Wang Y, et al. Interleukin-1beta mediates proliferation and differentiation of multipotent neural precursor cells through the activation of SAPK/JNK pathway. Mol Cell Neurosci. 2007；36：343-54.
27) Islam O, Gong X, Rose-John S, Heese K. Interleukin-6 and neural stem cells：more than gliogenesis. Mol Biol Cell. 2009；20：188-99.
28) Li L, Walker TL, Zhang Y, et al. Endogenous interferon gamma directly regulates neural precursors in the non-inflammatory brain. J Neurosci. 2010；30：9038-50.
29) Monje ML, Toda H, Palmer TD. Inflammatory blockade restores adult hippocampal neurogenesis. Science. 2003；302：1760-5.
30) Ben-Hur T, Ben-Menachem O, Furer V, et al. Effects of proinflammatory cytokines on the growth, fate, and motility of multipotential neural precursor cells. Mol Cell Neurosci. 2003；24：623-31.
31) Iosif RE, Ekdahl CT, Ahlenius H, et al. Tumor necrosis factor receptor 1 is a negative regulator of progenitor proliferation in adult hippocampal neurogenesis. J Neurosci. 2006；26：9703-12.
32) Cacci E, Ajmone-Cat MA, Anelli T, et al. In vitro neuronal and glial differentiation from embryonic or adult neural precursor cells are differently affected by chronic or acute activation of microglia. Glia. 2008；56：412-25.
33) Bernardino L, Agasse F, Silva B, et al. Tumor necrosis factor-alpha modulates survival, proliferation, and neuronal differentiation in neonatal subventricular zone cell cultures. Stem Cells. 2008；26：2361-71.
34) Clark IA. The advent of the cytokine storm. Immunol Cell Biol. 2007；85：271-3.
35) Spencer SJ, Mouihate A, Galic MA, Pittman QJ. Central and peripheral neuroimmune responses：hyporesponsiveness during pregnancy. J Physiol. 2008；586：399-406.

Sensors and Materials, Vol. 27, No. 10 (2015) 1035–1044
MYU Tokyo

S & M 1140

Improvements in Enzyme-Linked Photoassay Systems for Spatiotemporal Observation of Neurotransmitter Release

Kazunori Watanabe, Nobuto Takahashi, Naohiro Hozumi[1] and Sachiko Yoshida*

Department of Environmental and Life Sciences,
Toyohashi University of Technology, 1-1 Hibarigaoka, Tempaku-cho, Toyohashi 441-8580, Japan
[1]Int'l Cooperation Center for Engineering Education Development/
Department of Electrical & Electronic Information Engineering,
Toyohashi University of Technology, 1-1 Hibarigaoka, Tempaku-cho, Toyohashi 441-8580, Japan

(Received February 23, 2015; accepted September 25, 2015)

Key words: neurotransmitter, glutamate, GABA, enzyme immobilization, UV LED

Neurotransmitters and neuronal releasing molecules are not only the regulators of neuronal function but also the indicators of neuronal conditions. Glutamate and γ-amino butyric acid (GABA) play important roles in cerebellar differentiation and function. In the mature cortex, they are released from synapses and taken up by transporter molecules. We have developed enzyme-linked photoassay systems for glutamate, GABA, and adenosine triphosphate (ATP), and reported their release in the developing cerebellar cortex. Our systems showed slow transmitter release in the immature cerebellum, whereas it was hard to detect the fast synaptic release from mature neurons, because there were some limitations in time resolution and data depth derived from a charge-coupled device (CCD), and the enzyme-linked photodevice was sometimes unstable. In this study, we report the dynamic observation of neurotransmitter release in the developing cerebellar slices using improved photodevices and a high-speed 16-bit CCD. With this new system, the rapid measurement of transmitter release in a young-adult cerebellar cortex is possible. We suggest that these photoassay systems are useful for observing synaptic release in several diseases.

1. Introduction

Neurotransmitter molecules released from neurons are not only the regulators of neuronal transduction but also the indicators of neuronal conditions.(1–3) Glutamate and γ-aminobutyric acid (GABA) are known as typical transmitters in the brain's cortex, and they play important roles as stimulators and suppressors, respectively. Lack of balance in the release of glutamate and GABA may lead to autism, epilepsy, or Parkinson's disease.(4)

*Corresponding author: e-mail: syoshida@ens.tut.ac.jp

ISSN 0914-4935

To observe spatiotemporal neurotransmitter release in the cerebellar cortex, we have recently developed an enzyme-linked photoassay system, which is a device with an immobilized enzyme on a quartz glass surface. Using this system, we observed glutamate or GABA release in developing cerebellar slices using either new or authorized methods.(5) Enzyme-linked photoassay is sensitive and selective, and it can discriminate the substrates from their pharmacological analogues. Our system can detect transmitter release in the cerebral cortex,(6) hippocampus, retina, and cultured cells,(7) and made it possible to detect the release of adenosine triphosphate (ATP),(8) glucose, sucrose, and fructose. On the other hand, enzymes tend to denature and separate from the quartz. For the detection of transmitter release in mature neuronal circuits, increasing the sensitivity and stability of the device is required.

In this paper, we propose new immobilizing methods and discuss the optimization of the enzyme-linked photoassay.

2. Materials and Methods

2.1 *Substrate and enzyme reaction*

Imaging neurotransmitter release was monitored for the reaction in which oxidoreductases generate reduced nicotinamide adenine dinucleotide (NAD^+) or diphosphonucleotide ($NADP^+$). For glutamate, GABA, or adenosine triphosphate (ATP) imaging, we used glutamate dehydrogenase, GABA disassembly enzyme [GABase, Fig. 1(a)] or glyceraldehyde 3-phosphate dehydrogenase, respectively.(9–11) The NADH or NADPH, the reductants of NAD^+ or $NADP^+$, respectively, which is generated stoichiometrically, emits 480 nm fluorescence after excitation at 340–365 nm.

2.2 *Surface photoexcitation*

For UV excitation, a quartz glass plate illuminated with an ultraviolet light-emitting diode (UV-LED, Nichia, Tokushima, Japan) was used. Leaking UV light onto the glass surface excited fluorescent NADH or NADPH [Fig. 1(b)].

2.3 *Imaging apparatus*

All fluorescence images through the inverted microscope (IX73, Olympus Co., Ltd., Tokyo, Japan) were observed by a cooled charge-coupled device (CCD) (ORCA-ER CCD) or a high-speed complimentary metal-oxide semiconductor (CMOS) (ORCA-Flash 4.0) camera, supplied by Hamamatsu Photonics Co., Ltd., Hamamatsu, Japan. Imaging data were analyzed by iVision software (BD Biosciences, San Jose, CA, USA).

2.4 *Enzyme immobilization and sample preparation*

Enzymes were typically covalently immobilized on the quartz glass surface using a silane coupling agent and a crosslinking agent, 3-aminopropyltriethoxy silane (3-APTS) and glutaraldehyde, respectively [Fig. 2(a)].(12) These surface modifications determine both the stability of the enzyme reaction and the distance between the sample and the glass surface.

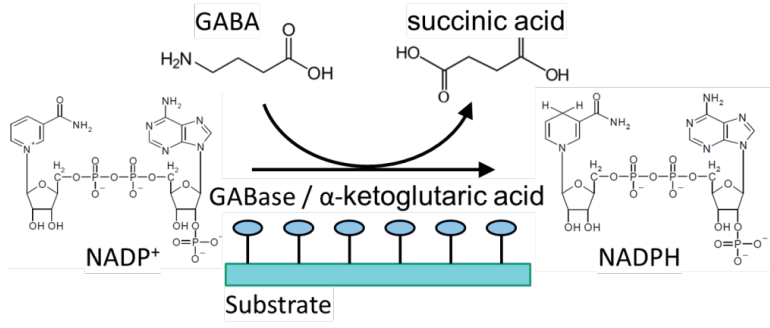

(a)

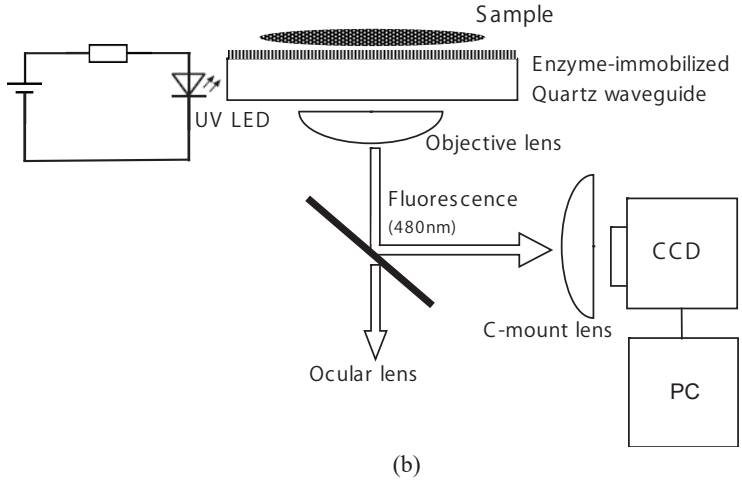

(b)

Fig. 1. (Color online) (a) Released neurotransmitters are oxidized by the oxidoreductase, and NAD(P)H is formed stoichiometrically. In GABA oxidization, released GABA is converted to succinic acid with NADPH formation by GABase. (b) Schematic diagram of the enzyme-linked photoassay system. The oxidoreductases are immobilized on the quartz glass surface, and the excitation light radiating from UV-LED passes through the quartz waveguide. Fluorescent images are obtained by CCD or CMOS, and analyzed using a computer system.

In some cases, glass surfaces were treated with either aromatic crosslinkers, 1,4-phenylene diisothiocyanate (1,4-DIC), or 1,3-phenylene diisothiocyanate [1,3-DIC, Fig. 2(b)], and glutaraldehyde (GA).[13] Others were treated with a phosphonic acid, 11-aminoundecylphosphonic acid [11-AUPA, Fig. 2(c)], as a replacement for 3-APTS.[14]

Cerebellar acute slices were treated from postnatal day 3 (P3) to P15 in rats, sliced sagittally to a thickness of 400 μm with a rotor slicer (Dohan EM, Kyoto, Japan),

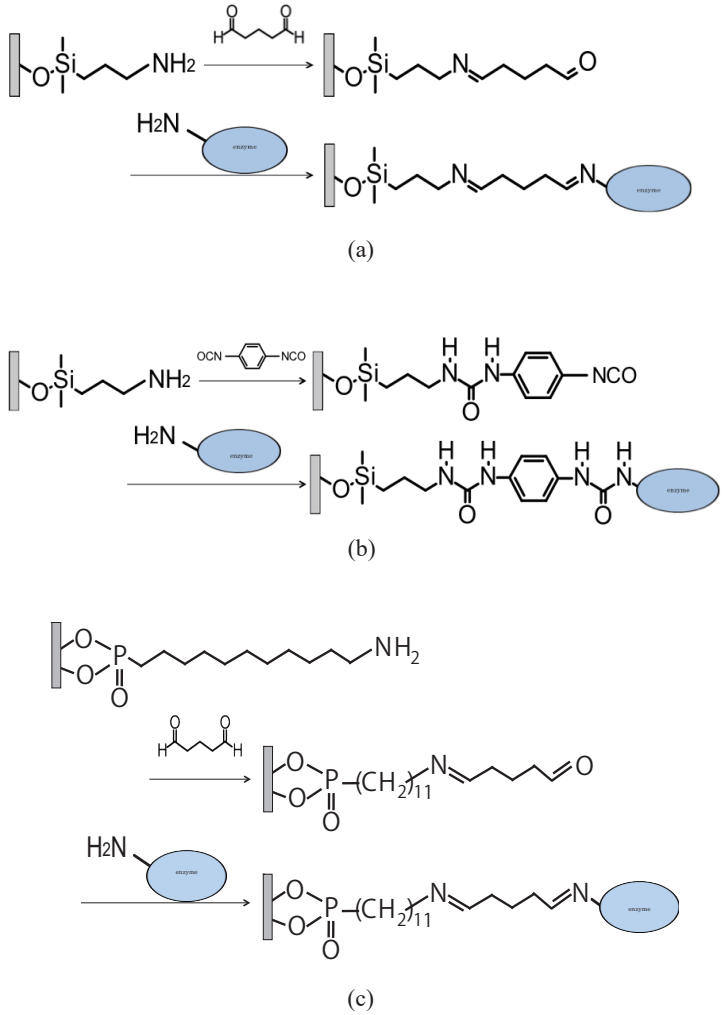

Fig. 2. (Color online) (a) Method of enzyme immobilization using 3-APTS and glutaraldehyde. Surface treatment and crosslinking between waveguide quartz and enzyme. (b) Crosslinking using 1,3-DIC. (c) Surface treatment with 11-AUPA.

and incubated in oxygen-aerated PBS for 45 min. All experimental procedures were approved by the committee for the use of animals at Toyohashi University of Technology and by the guidelines of the Ministry of Education, Culture, Sports, Science and Technology, Japan.

3. Results

3.1 *Spatiotemporal observation of glutamate release*

Figure 3(a) shows an illustration of rat cerebellar development. In the developing cerebellum, neuronal arrangement and circuit formation progress after birth. Granule cells, small input neurons, proliferate and migrate down from the external granular layer (EGL) to the internal granular layer (IGL). Purkinje cells, major output neurons, develop their dendrites and associate neuronal connections between granule cells and other interneurons. The layer of Purkinje cell somas is identified to be the Purkinje layer (PL). A neuronal circuit layer forms the molecular layer (ML).[15,16] To understand the roles of neurotransmitters in the cerebellar development, we have developed a new visualizing device and, with it, we have observed spatiotemporal molecular dynamics.

Using the enzyme-linked photoassay system, we have observed many kinds of transmitter release in several developmental stages and organs. Our system has visualized both spontaneous and responsive transmitter release processes with 0.5 s time resolution. Figures 3(b)–3(k) show the transitions in glutamate release in response to 100 μM GABA application in developing cerebellar slices.[17] Glutamate was released in both the EGL and the IGL, whereas the PL was indicated by a negative line. In the developing cerebellum, the granule cells that distributed in the EGL and IGL are the only neurons that release glutamate, so both layers showed fluorescence activities. Glutamate release in P3 cerebellar slices appeared in both layers slowly but continuously, whereas it started rapidly in the lower EGL and then spread to the IGL within a short time in P7 celebellar slices.[18] Granule cells in the P3 cerebellum did not develop sufficiently to react to GABA stimulation nor release the transmitter actively, but they still proliferated. On the other hand, the granule cells in the P7 cerebellum developed sufficiently to react to GABA stimulation, so they released glutamate rapidly.

Although spatiotemporal observation could give us dynamic information about neuronal reaction, our system needs to be improved in terms of stability, sensitivity and time resolution for us to observe fast synaptic transmissions. The targets of our improvements were the (1) sensing CCD, (2) excitation waveguide, and (3) manner of enzyme immobilization shown in Fig. 2.

3.2 *Effects of new crosslinkers and surface treatment*

Two types of glass devices with either aromatic crosslinkers, 1,3-DIC or 1,4-DIC, and GA were examined to observe spontaneous GABA release with 500 ms time resolution using ORCA ER CCD. The device formed using 1,3-DIC and GA gave images with a better contrast of GABA release than the GA crosslinked device in the P10 cerebellar slice [Fig. 4(a)], whereas it showed no difference in the P6 cerebellar slice. The 1,4-DIC crosslinked device yielded no good images.

The aromatic crosslinkers make the glass surface hydrophobic. Because mature brain tissues become hydrophobic as the myelin structure develops, 1,3-DIC crosslinking should increase the affinity of the enzyme for the tissues.

The binding between the glass and the acceptor molecules has been weak, because the silane coupling agents tend to undergo hydrolysis under biological conditions. The

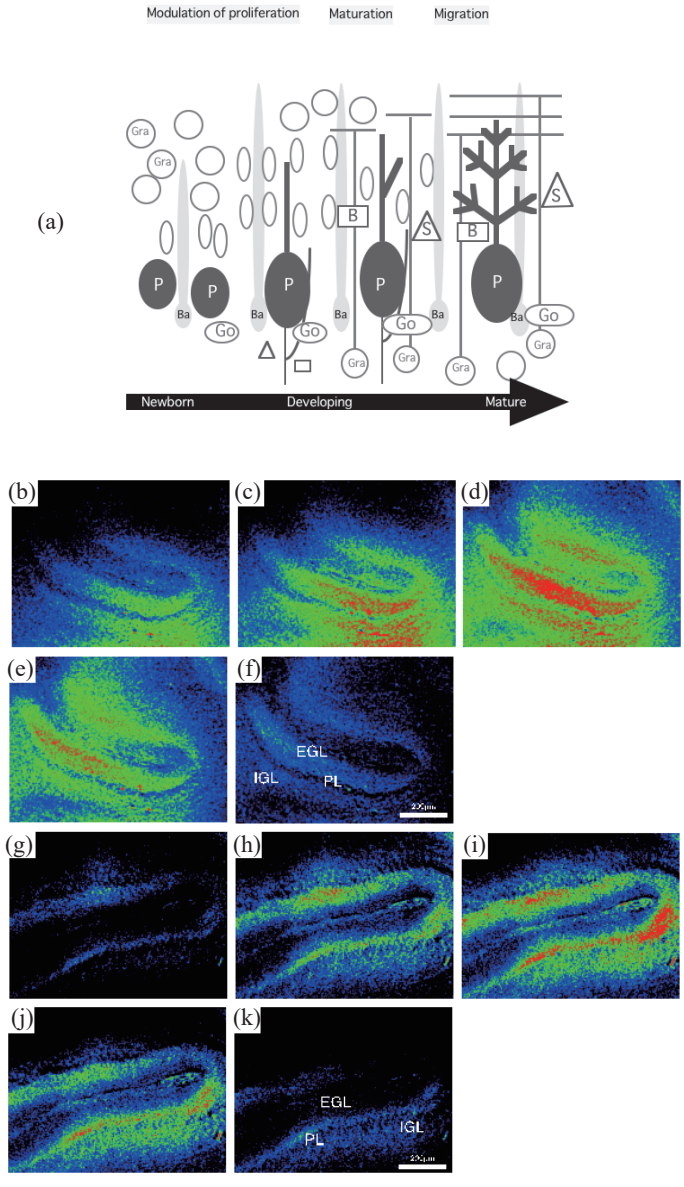

Fig. 3. (a) Diagram of cerebellar development. In the newborn cerebellum (1 to 3 days after birth), granule cell progenitors (Gra) proliferate in the EGL, while immature Purkinje cells (P) form the PL with Golgi cells (Go) and some Bergmann glia (Ba). During the developement, 5 to 7 days after birth, Gra-cells elongate their axon and migrate inside, and P-cells spread their dendrites and connect to other neurons within two weeks. B denotes basket cells, and S, satellite cells. Evoked glutamate wave with GABA application in developing cerebellar cortex. (b)–(f): 2.0, 4.5, 7.0, 12.5, and 23.5 s after stimulation in P3 cerebellar cortex, respectively. (g)–(k): 0.5, 2.5, 4.0, 11.0, and 16.0 s after stimulation in P7 cerebellar cortex, respectively.

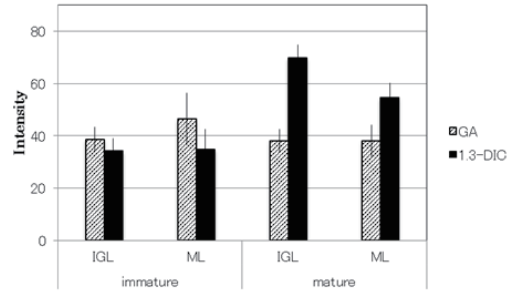

(a)

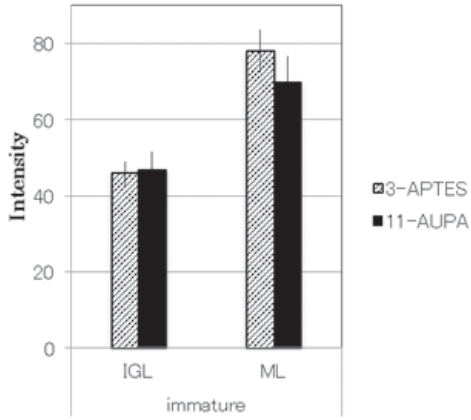

(b)

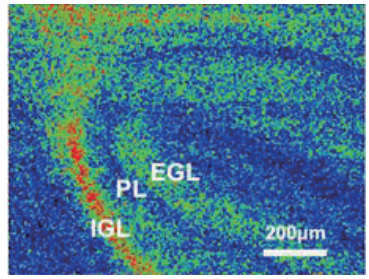

(c)

Fig. 4. (Color online) (a) New crosslinker, 1,3-DIC, gave us better contrast images than GA in mature cerebellar observation, while it made little difference from GA in immature organ. (b) The 11-AUPA-GA treatment showed the same result as the APTS-GA treatment in the immature organ. (c) Spontaneous GABA release image in P12 cerebellar slice using 1,3-DIC crosslinking glass device.

surface treatment by 11-AUPA, as a replacement for 3-APTS, was expected to inhibit hydrolysis, but it had low affinity for the glass. We constituted a new glass device with 11-AUPA-coupling enzymes and examined its sensitivity and stability. Figure 4(b) shows that the new device performed with the same sensitivity and stability as the device with APTS.

3.3 *Observation using high-speed CMOS camera*

The fluorescence intensity of NADH is very low and is only a few thousands of the intensity of typical artificial fluorescence. To collect data with sufficient time resolution, a highly sensitive and rapid data transferring camera is required. The time resolution

shown in Fig. 3 is 0.5 s for the 12-bit ORCA CCD, which is too low to detect the synaptic transmitter reaction.

A 16-bit CMOS camera, Flash 4.0, could detect weak light and transfer data in less than a microsecond. Using this camera, transient glutamate release could be detected with a 20 ms time resolution (Fig. 5). In developing the P7 cerebellum, glutamate release was increased in the EGL by applying a glutamate receptor-stimulating agent, α-amino-3-hydroxy-5-methyl-4-isoxazolepropionic acid (AMPA). Even in the premature P14 cerebellum, the increment in the rate of glutamate release was observed. It was not strong and noiseless, but the AMPA stimulation-induced glutamate release was observed in the ML and IGL where the glutamatergic neurons are distributed.

4. Discussion

The detection of neurotransmitter release gives us important information about developmental conditions and diseases. Parkinson's disease, a degenerative disorder of the central nervous system, is caused by the alteration of the release of neurotransmitters. The detection of the spatial or temporal alteration of the release would require early diagnosis and treatment of Parkinson's disease. In immature or lesioned neuronal organs, transmitters are released and taken up slowly, so the time resolution required is from 0.5 to 1 s. In young-adult stages, the release speed becomes higher than that in the immature stage within 20 ms.

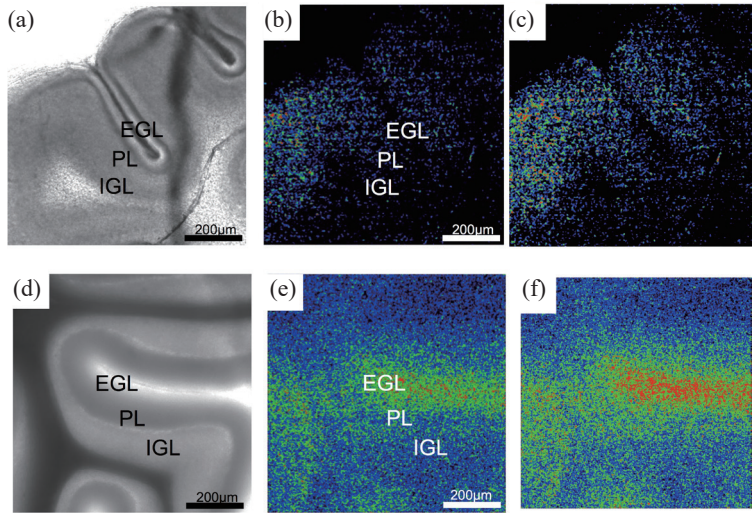

Fig. 5 (Color online) Evoked glutamate release images to AMPA stimulation for 20 ms time resolution using Flash 4.0 CMOS system. (a)–(c) P7 cerebellar slice; (d)–(f) P14 cerebellar slice. (a) and (d) Phase contrast light images. (b) and (e) Fluorescence images before stimulation and (c) and (f) just after AMPA stimulation.

Enzyme-linked assays were applied previously for chemical detection because of their specificity. In spatial observations, however, their fluorescence intensity is too weak to detect. Our enzyme-linked photodevice was developed to detect spatiotemporal neurotransmitter release, and it was improved to observe rapid synaptic release. New crosslinkers could contribute to a more sensitive detection, and the phosphonic surface treatment would expand the range of applications. In order to detect a high-speed transmitter release, both the light accumulation system for weak fluorescence and the close contact between the specimen and the enzyme are required. At present, our photodetection system detects several ms releases from neuronal synapses in the presence of noise, and in the future, it could give us more noiseless observations using an optimal image processing system.

5. Conclusions

The newly developed enzyme-linked photoassay is useful for the visualization of neurotransmitter release in brain slices. In the immature cerebellum, the granule cells release glutamate slowly or rapidly at their stage of neuronal development and synaptogenesis.

Using a fast new system, the rapid measurement of transmitter release in a young-adult cerebellar cortex became possible. Crosslinkers and other device techniques are required for stable observations. We suggest that the photoassay systems have advantages for the observation of synaptic release in several diseases.

Acknowledgements

This study was supported by grants from Scientific Research (C) 23500516 and 26350498, and Health Labor Sciences Research.

References

1 J. Moran and M. Rivera-Gaxiola: J. Neurosci. Res. **33** (1992) 239.
2 P. Varju, Z. Katarova, E. Madarasz and G. Szabo: Cell Tissue Res. **305** (2001) 239.
3 D. Casel, J. Brockhaus and J. W. Deitmer: J. Physiol. **568** (2005) 111.
4 M. Ochi, S. Shiozaki and H. Kase: Neuroscience **127** (2004) 223.
5 T. Morishima, M. Uematsu, T. Furukawa, Y. Yanagawa, A. Fukuda and S. Yoshida: Neurosci. Res. **67** (2010) 347.
6 T. Wang, T. Kumada, T. Morishima, S. Iwata, T. Kaneko, Y. Yanagawa, S. Yoshida and A. Fukuda: Cereb Cortex **24** (2014) 1088.
7 S. Yoshida and N. Hozumi: JNNS **20** (2013) 14.
8 H. Muramoto, Y. Sekino, N. Hozumi, A. Fukuda and S. Yoshida: 42th Neuroscience Meeting (2012) (CD-ROM).
9 B. Innocenti, V. Parpura and P. G. Haydon: J. Neurosci. **20** (2000) 1800.
10 M. Israel and B. Lesbats: J. Neurochem. **67** (1996) 2624.
11 S. Yoshida: Japanese Patent No. 4480952 (2010).
12 L. Blasi, L. Longo, PP. Pompa, L. Manna, G. Ciccarella, G. Vasapollo, R. Cingolani, R. Rinaldi, A. Rizzello, R. Acierno, C. Storelli and M. Maffia: Biosens. Bioelectron. **21** (2005) 30.

13 N. Aissaoui, J. Landoulsi, L. Bergaoui, S. Boujday and J. F. Lambert: Enzyme Microb. Technol. **52** (2013) 336.
14 M. Bariana, M. S. Aw, M. Kurkuri and D. Losic: Int. J. Pharm. **443** (2013) 230.
15 M. Yamada, M. Terao, T. Terashima, T. Fujiyama, Y. Kawaguchi, Y. Nabeshima and M. Hoshino: J. Neurosci. **27** (2007) 10924.
16 M. Ito: The Cerebellum and Neural Control (Raven Press, New York, 1984) Chap. 1.
17 M. L. Fiszman and A. Schousboe: J. Neurosci. Res. **76** (2004) 435.
18 K. Okochi, S. Hirano, K. Maruya, T. Morishima, C. Takayama, A. Fukuda and S. Yoshida: Neurosci. Res. **61** (2008) S114.

About the Authors

Kazunori Watanabe was born in Hokkaido, Japan, on February 3, 1992. He is a 2nd-year student in the Graduate School of Toyohashi University of Technology. His research focuses on the optimization of surface modifications for biosensors and the detection of neurotransmitters. He is a member of the Japan Neuroscience Society.

Nobuto Takahashi was born in Tokyo, Japan, on December 9, 1992. He is a 1st-year student in the Graduate School of Toyohashi University of Technology. His research focuses on bioengineering photoanalysis of cells and the developmental mechanism of cultured neurons. He is a member of the Japan Neuroscience Society.

Naohiro Hozumi was born in Kyoto, Japan, on April 2, 1957. He received his B.S., M.S., and Ph.D. degrees in 1981, 1983, and 1990, respectively, from Waseda University. He was at the Central Research Institute of Electric Power Industry (CRIEPI) from 1983 to 1999. He was an associate professor at Toyohashi University of Technology from 1999 to 2006, and a professor at Aichi Institute of Technology from 2006 to 2011. Since 2011, he has been a professor at Toyohashi University of Technology. He has been engaged mostly in research on insulating materials and diagnosis of high-voltage equipment and acoustic measurement for biological and medical applications. In 1990 and 1999, he received awards from IEE of Japan for his outstanding research papers. He is a member of IEEE, IEE of Japan, and the Acoustic Society of Japan.

Sachiko Yoshida was born in Toyama, Japan, on January 24, 1961. She received her B.S., M.S., and Ph.D. degrees in 1983, 1986, and 1990, respectively, from the University of Tokyo. She was a JSPS Postdoctoral Researcher from 1990 to 1992, a JST PRESTO Researcher from 1992 to 1994, and a research associate at Toyohashi University of Technology from 1995 to 1996. Since 1996, she has been a lecturer at Toyohashi University of Technology. Her research interests focus on physiological interaction and morphological transformation through brain differentiation, and their detection. She is a member of IEEE, International Brain Research Organization, the Society for Neuroscience, and the Japan Neuroscience Society.

電気学会論文誌 A（基礎・材料・共通部門誌）
IEEJ Transactions on Fundamentals and Materials
Vol.136 No.2 pp.99-104 DOI: 10.1541/ieejfms.136.99

Paper

Visualization of Spatially Distributed Bioactive Molecules using Enzyme-Linked Photo Assay

Hikaru Mabuchi* Student Member, HongYao Ong* Associate
Kazunori Watanabe* Non-member, Sachiko Yoshida* Non-member
Naohiro Hozumi*a) Senior Member

(Manuscript received March 18, 2015, revised Oct. 4, 2015)

In this paper, we propose a new simple device for visualizing bioactive molecules with a fine spatial resolution by using a membrane in which a specific enzyme is immobilized. The layer produces fluorescence after association with a specific substance. The layer, on which a biological tissue is to be mounted, is deposited on a quartz substrate that is used as a light guide to introduce UV light to the layer. Substance release is observed by a CCD camera from the opposite side of the substrate. In order to shorten the experiment time, we had automated the optical device. The paper also describes the reduction of background fluorescence by means of image processing technique. Images were acquired by employing two UV-LEDs with slightly different angle. Image processing was performed to separate background and target fluorescence by means of independent component analysis. Finally the release of GABA(γ-aminobutyric acid) and glutamate from specific layers in rat cerebellum was successfully observed. It is expected that, using this method, both real-time transmitter release and its response to medicine can be observed.

Keywords : bioactive molecules, enzyme-linked photo assay, independent component analysis

1. Introduction

Light guide is composed of a dielectric material that can enclose the light propagation. In addition to being applied to communication, it is useful for sensing as well. In chemical sensing the surface of the light guide has to be coated with some specific chemical that may change its optical property depending on chemical reactions. Such a function can be applied to chemical imaging, if the light guide has a flat surface. This study proposes an application of two-dimensional light guide, of which surface is chemically modified, to biochemical imaging.

Neurotransmitter molecules released from neurons are not only regulators of neuronal transduction but also indicators of neuronal conditions. Glutamate and γ-aminobutyric acid (GABA) are known as typical transmitters in brain cortex that play important roles as stimulator and suppresser, respectively. Lack of balance in the release of glutamate and GABA may lead to autism, epilepsy or Parkinson's disease[(1)(2)].

In order to observe the spatio-temporal release in cerebellar cortex, we have newly proposed the enzyme-linked photo assay system, which is realized even using normal CCD camera, and observed GABA release in developing cerebellar slice using either new or authorized methods[(3)].

In this paper, we propose a new simple device for this purpose by using a reactive layer in which a specific enzyme is immobilized, and produces fluorescence after association with a specific substance released from mounted slice. This layer is bound a quartz substrate that is used as a light guide for UV light excitation. Fluorescence derived from a substance is observed by a CCD camera from the opposite side of the substrate.

The paper describes the reduction of background fluorescence by means of image processing technique. Finally it will be shown that the release of transmitters from specific layers in rat cerebellum was successfully observed.

2. Specimen Preparation and Photo Excitation System

Imaging of neurotransmitter release was monitored the reaction of oxidoreductases generating reduced nicotinamide adenine dinucleotide (NAD^+) or diphosphonucleotide ($NADP^+$). For glutamate and GABA, we used glutamate dehydrogenase and GABA disassembly enzyme (GABase), respectively.

Enzymes were covalently immobilized on the quartz glass substrate using a silane coupling agent and a crosslink agent. The substrate was as thick as 1 mm. Stoichiometrically generated NADH or NADPH emits 480 nm fluorescence after excitation at 340-365 nm.

Existence of glutamate and GABA lead to fluorescence when co-existing with specific enzyme and co-enzyme. A glass substrate on which specific enzyme is coated is in contact with the biological specimen. A chamber space is created around the specimen. The space is filled with buffer liquid and co-enzyme. On the glass substrate therefore, the specimen is in contact with both enzyme and co-enzyme.

Consequently glutamate or GABA, that is released from the tissue spontaneously by stimulation, makes an oxidation-reduction reaction on the substrate. Although both glutamate and GABA do not produce fluorescence by themselves, NAD(P)H that is created as the result of the above chemical reaction makes fluorescence. As the ratio of glutamate or GABA and NAD(P)H is 1:1, the

a) Correspondence to: Naohiro Hozumi. E-mail: hozumi@icceed.tut.ac.jp
* Toyohashi University of Technology
1-1, Hibarigaoka, Tenpaku, Toyohashi 441-8580, Japan

fluorescence can be correlated to the amount of released glutamate or GABA.

In the experiment, rat cerebellum was sliced sagittally at 400 μm thick and incubated in oxygen-aerated HEPES-Na^+ buffer for 40 min. The slice was placed on the quartz glass substrate with both $NADP^+$ and α-ketoglutarate. Figure 1 shows the schematic diagram of the observation system including the device. The enzyme was immobilized covalently on the glass as shown in Fig. 2. Figure 3 shows chemical reactions taking place on the substrate. $NADP^+$ (nicotinamide adenine dinucleotide phosphate) changes into NADPH (reduced nicotinamide adenine dinucleotide phosphate) just as glutamate and GABA degeneration. Synthesized NADPH was illuminated by 360 nm surface UV-LED, and emitted the 480 nm fluorescent light observed by cooled CCD (ORCA ER, Hamamatsu Photonics). The quartz substrate can be recognized as a light guide to illuminate the surface of the substrate.

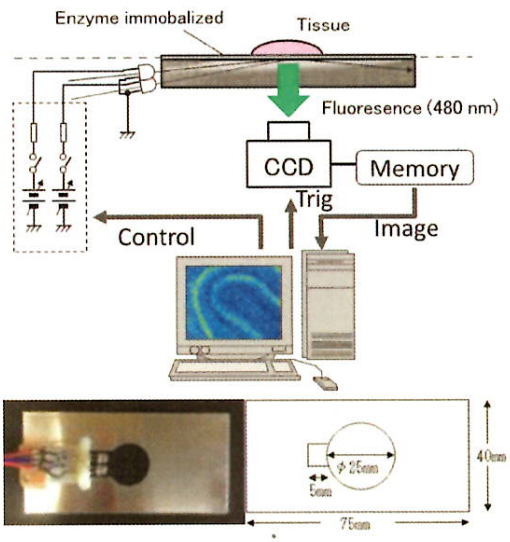

Fig. 1. Schematic diagram of the observation system including the device and its outlook

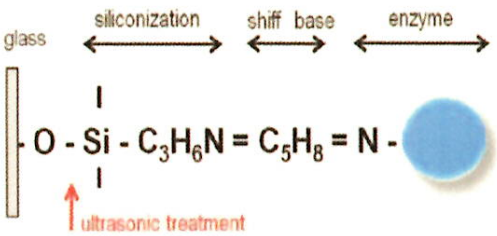

Fig. 2. Immobilized enzyme

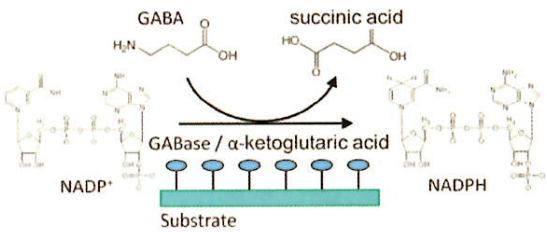

Fig. 3. Chemical reaction on the substrate

3. Image Processing

The fluorescent light detected by the CCD camera is divided into target light and background light. As significant intensity of background light is detected, it is assumed that fluorescence is excited by the light that is refracted on the interface between the substrate and tissue system including the layer. The light, being generated by LEDs and propagates though the substrate, can be decomposed into plane waves with different angles of propagation. Each plane wave transfers across the enzyme layer and comes into the tissue. We assume that both target and background light were predominantly excited by normal light. As the background light significantly damage the quality of the image, it should be reduced as much as possible. Making use of the evanescent light may be a solution, however, it may make the system complicated, and the target light may be not as significant as this case. Therefore we tried to reduce the background by means of a simple image processing.

Assuming that the light is a plane wave and scatter can be neglected, wave propagation and detected fluorescence can be illustrated as Fig. 4. In the figure, fluorescence, attributed to the layer where the enzyme is fixed, is represented as I_0. This is

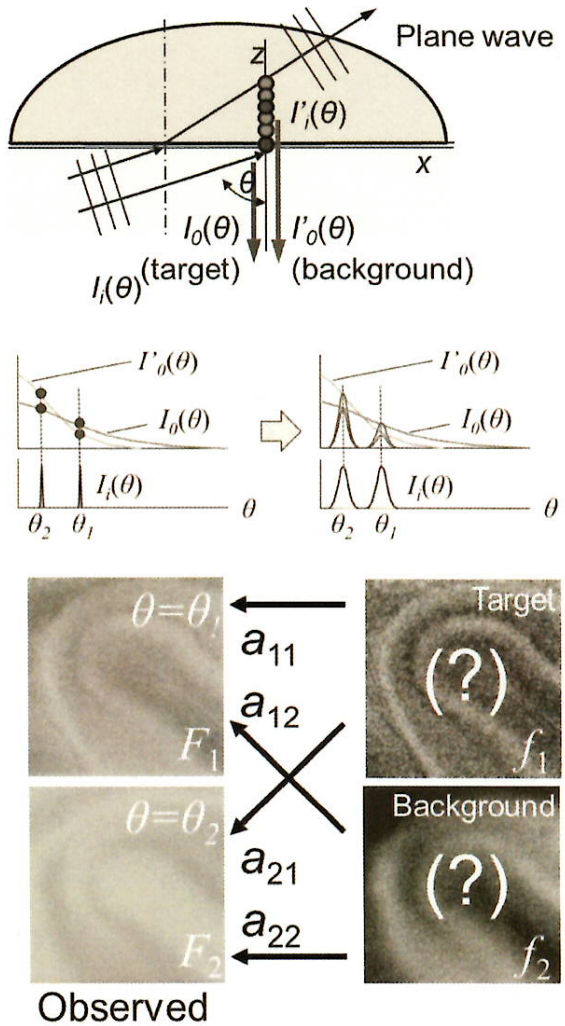

Fig. 4. Fluorescence detected by CCD camera

defined as to be the target. The fluorescence attributed to the tissue is represented as I'_0. This is defined as to be the background. Both I_0 and I'_0 depends on the incident angle θ. The thickness of the quartz plate, which is used as a light guide, is as thick as 1 mm. As it is much thicker than the diameter of normal optical fiber it is relatively easy to introduce two kinds of lights of which angles of center axes are significantly different. In addition, in practice, they depend differently on the incident angle. As the result, the proportion (I_0/I'_0) is not the same along θ. This is true even if the incident angle has distributed.

As the result, the captured fluorescence with different angle of optical axis is composed of target and background fluorescence with different mixture ratios. This can be represented as:

$$\begin{pmatrix} F_1 \\ F_2 \end{pmatrix} = \begin{pmatrix} a_{11} & a_{12} \\ a_{21} & a_{22} \end{pmatrix} \begin{pmatrix} f_1 \\ f_2 \end{pmatrix} \quad \cdots\cdots (1)$$

where $F_1(x,y)$ and $F_2(x,y)$ are captured fluorescence image, $f_1(x,y)$ and $f_2(x,y)$ are spatial distributions of fluorescence as the target and background, a_{11}, a_{12}, a_{21}, a_{22} are constants. Although the image acquisition is sequential, ICA is performed by assuming that two images, $F_1(x,y)$ and $F_2(x,y)$ are acquired with a negligible time lag. Reproduced images $f'_1(x,y)$ and $f'_2(x,y)$ are calculated from F_1 and F_2. As the result of periodical acquisitions of F_1 and F_2, time dependent images of f'_1 and f'_2 are calculated. Eq. (1) can also be described using a matrix expression as:

$$\mathbf{F} = \mathbf{A} \cdot \mathbf{f} \quad \cdots\cdots (2)$$

The target and background fluorescence distribution can be calculated by applying $\mathbf{A}^{-1}$ to $\mathbf{F}$. In practice, only contrast of the image would be enough to recognize the distribution. In such a case $\mathbf{A}^{-1}$ can be represented as:

$$\begin{pmatrix} 1 & \alpha \\ \beta & 1 \end{pmatrix} \quad \cdots\cdots (3)$$

After capturing two images $\mathbf{F}_1$ and $\mathbf{F}_2$ by changing the angle of optical axis, the target and background images can be separated by finding appropriate numbers for α and β. α and β can be tuned manually by monitoring the quality of reproduced image, however, the theory of independent component analysis (ICA) may be powerful for solving such a problem[4].

Stochastic distribution of pixel intensity in images f'_1 and f'_2 are represented as $p(y_{1i})$ and $p(y_{2j})$, where y_{1i} and y_{2j} represent the intensity.

$$\left.\begin{aligned} p(y_1) &\equiv \{p(y_{11}),\cdots,p(y_{1i}),\cdots p(y_{1n})\} \\ p(y_2) &\equiv \{p(y_{21}),\cdots,p(y_{2j}),\cdots p(y_{2n})\} \end{aligned}\right\} \quad \cdots\cdots (4)$$

$p(y_{1i},y_{2j})$ represents the probability that the intensity of a pixel in image f'_1 is y_{1i} and that of the corresponding point in image f'_2 is y_{2j}. In other words $p(y_1)$ and $p(y_2)$ are probabilities that cases y_1 and y_2 take place, respectively, and $p(y_1,y_2)$ is the probability that cases y_1 and y_2 takes place simultaneously. Variables y_1 and y_2 are considered to be independent when

$$p(y_1,y_2) = p(y_1)p(y_2) \quad \cdots\cdots (5)$$

is established. Kullback-Leibler(K-L) parameter is often employed to indicate the independency of variables:

$$KL \equiv \sum_{i,j} p(y_{1i},y_{2j}) \log \frac{p(y_{1i},y_{2j})}{p(y_{1i})p(y_{2j})} \quad \cdots\cdots (6)$$

The K-L parameter is zero when two sets of variables y_1 and y_2 are completely independent together. In practice, α and β in Eq. (3), which determine the probabilities $p(y_1)$, $p(y_2)$ and $p(y_1,y_2)$, can be tuned so that the K-L parameter indicates the minimum.

The process of ICA is illustrated in Fig. 5. The equation described in the form of matrix indicates that two images, F_1 and F_2, derive from linear combination of unknown original images f_1 and f_2. If an appropriate inverse matrix can be found then the original images can be reproduced. However as the matrix to describe the linear combination is unknown as well, ICA algorithm is applied to find the most appropriate matrix (as the inverse matrix). In the

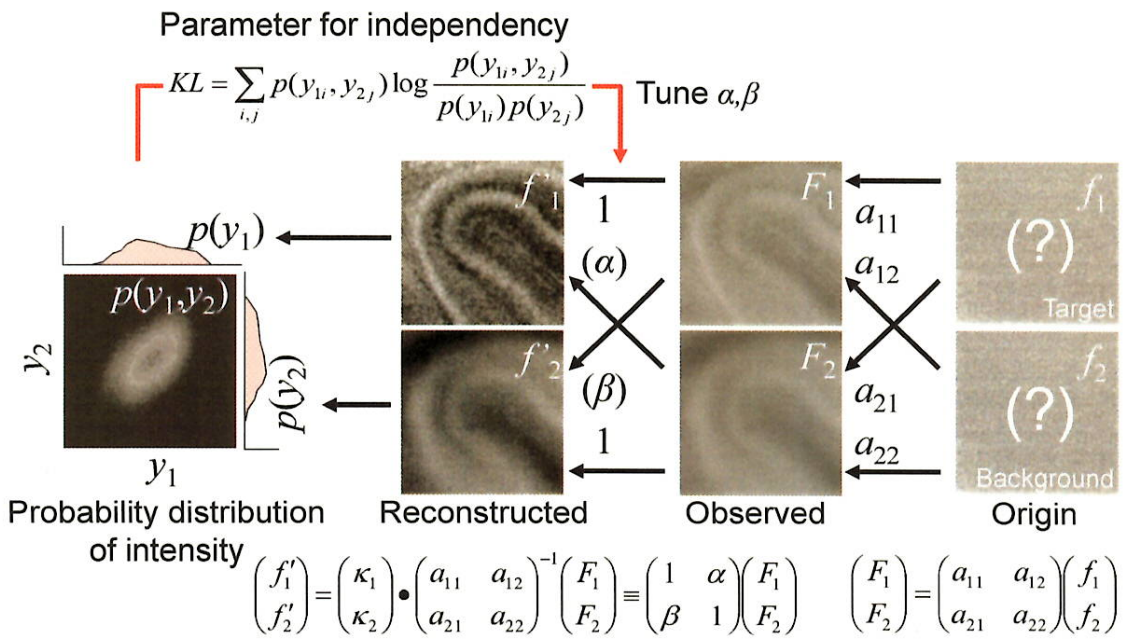

Fig. 5. Illustration for image processing based on independent component analysis

ICA process K-L parameter is calculated in order to evaluate the probabilistic independency of images f'_1 and f'_2. It can be considered that in the reproduction algorithm the core process is the calculation of the K-L parameter. In this preliminary study K-L parameter is successively calculated by manually changing the inverse matrix, and images are assumed to be reproduced when the K-L parameter indicates the minimum.

4. Results and Discussion

4.1 Image Processing using the ICA Figure 6 (a) shows visible light image of the cerebellum with postnatal 21 days. In developing cerebellum, granule cells, small input neurons, proliferate and migrate down from the external granular layer (EGL) to the internal granular layer (IGL). As the development proceeds, EGL turns into molecular layer (ML) whereas IGL remains. Purkinje cells, big output neurons, develop their dendrites and associate neuronal connections between granule cells and other interneurons. Neuronal circuit layer forms the ML. As the cerebellum shown in Fig. 6 (a) is mature, ML, PL, IGL are clearly visible. Note that ML is on the outer side of the cerebellum, and a wrinkle surrounded by the ML is seen in Fig. 6 (a).

As for fluorescence observation, three different images were acquired. Two were with different inclination of the excitation light source, and one was with no excitation light. Each of the two images with excitation light was subtracted with the image with no excitation light, in order to reduce the background light from the outside. These two images after the subtraction were defined as images A and B.

Figure 6 (b) shows these images for a rat cerebellum. Both images are very unclear, because of the background fluorescence. Figure 6 (c) shows the result of image processing. It is clearly shown in the image entitled as "target" that the fluorescence intensity is high in two layers, whereas that entitled as "background" is not clear. By morphological inspection these layers are recognized as ML and IGL. These layers are known that GABAergic neurons distribute in mature cerebellum. Studies using HPLC and electrophysiological method have shown that GABA is released from the postnatal cerebellar cortex even before synaptogenesis, and that GABA receptors act on the developing cerebellar Purkinje cells[(4)(5)]. However, dynamic GABA release could not be observed unless the enzyme-linked photo assay is used. In addition, because cytoplasmic autofluorescence becomes noisy background light, it is useful that the image processing system extracted the image of GABA release from the autofluorescence-contained image. Using this method, both real-time transmitter release and its response to medicine can be observed.

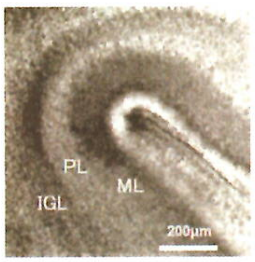

(a) Visible light image

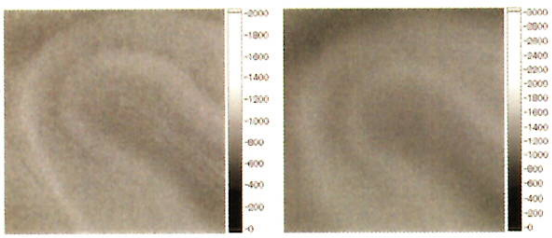

Small angle (image A). Large angle (image B).

(b) Fluorecence images before image processing

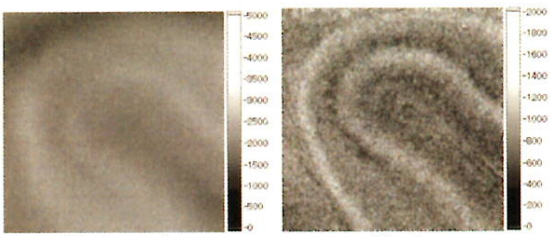

Background Target

(c) Fluorecence images after image processing

Fig. 6. Cross sectional mages of cerebellar cortex: (a) Visible light image, (b) original fluorescent images with different angle of optical axes, and (c) fluorescent images after the image processing. Scales are indicated in arbitrary unit. Specimen: rat cerebellum (postnatal 21 days), target: GABA

4.2 Transition after Chemical Stimulation In relatively developed cerebellum, cells distributed in the ML and IGL are only the neurons of glutamate release, so that both layers showed fluorescent activities. Figure 7 indicates release distribution of glutamate in comparison with normal optical image illuminated with visible light. The fluorescent image, indicating glutamate release, is after the ICA processing. Figure 7 (c) indicates the regions of interest for analysis. Regions highlighted as ML and IGL have relatively strong intensity in fluorescence. They have a contrast to the region highlighted as PL. Release from white matter (WM), which is mostly composed of fatty materials, is much less significant.

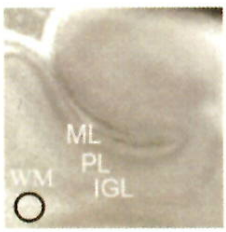

(a) Visible light image

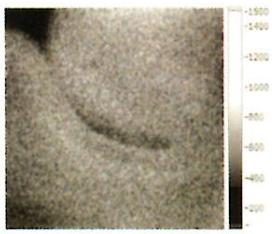

(b) Fluorescent image

(c) Regions of interest for analysis

Fig. 7. Cerebellum with postnatal 7 days observed with visible light and fluorescent light indicating glutamate release. 0.9 mm × 0.9 mm. Gray scale is arbitrary. ML: molecular layer, PL: Purkinje layer, IGL: internal granular layer, WM: white matter. Specimen: rat cerebellum (postnatal 7 days)

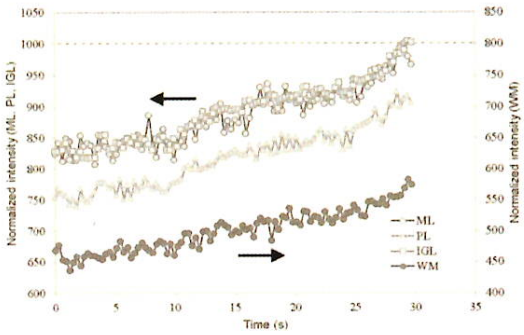

Fig. 8. Transition in fluorescence intensity in each layer (normalized by the intensity of ML 30 s after stimulation that is indicated as 1000). Specimen: rat cerebellum (postnatal 7 days), target: glutaminate

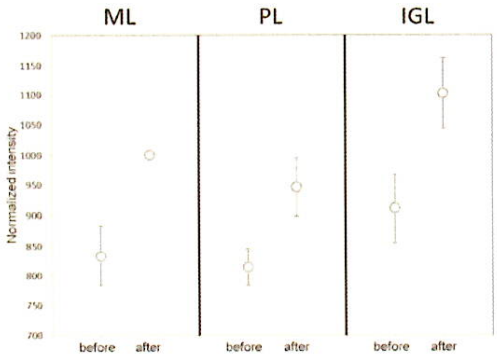

Fig. 9. Change in fluorescence intensity before and after AMPA stimulation (normalized by the intensity of ML 30 s after stimulation that is indicated as 1000). Specimen: rat cerebellum (postnatal 7 days), target: glutaminate

Our system can visualize both spontaneous and responsive transmitter release with about 0.2 s time resolution. Figure 8 shows the transition of glutamate release in response to 100 μmol/ℓ (S)-alpha-Amino-3-hydroxy- 5 methylisoxazole-4-propionic acid (AMPA) application in cerebellar slices. All values are normalized by the intensity of ML 30 s after stimulation that is indicated as 1000. Fluorescence, as indication glutamate release, was intense in both the IGL and ML, whereas the PL was indicated with lower intensity. As shown in Fig. 8, a clear increase in fluorescence was observed after stimulation. Transition in fluorescence was similar for ML and IGL, suggesting that these layers are activated. However PL, which was not expected to release glutamate, showed fluorescence as well although it was less intense than ML and IGL. As this specimen was taken from relatively young rat (postnatal 7 days), the cerebellar development was not totally completed, and the layers were not separated enough. It is hence considered that diffusion from ML and IGL to PL would take place, leading to an increase in fluorescence in this layer. The increase in fluorescence in WM suggests that glutamate might have been diffused into WM as well, although the absolute value was much lower than ML and IGL.

Figure 9 compares the fluorescence in each layer before and after stimulation. Four different specimens were used for the observation, in order to confirm reproducibility. It is clear that the AMPA stimulation brought a significant glutamate release from ML and IGL, although the increase is also seen with PL.

5. Conclusions

A new method for visualization of spatially distributed bioactive molecules using enzyme-linked photo assay has been proposed. It is based on fluorescent reaction assisted by an enzyme immobilized on the substrate, however, background fluorescence disturbs the observation. In order to reduce the background fluorescence, two images were acquired by changing the optical axis of UV illumination. Image processing based on independent component analysis made the target image clear. Observation of rat cerebellum was successfully performed and GABA and glutamate release from two specific layers was clearly indicated.

Acknowledgement

The study was partially supported by grants from Scientific Research (C) 23500516, 26350498 and Health Labor Sciences Research.

References

(1) N. C. Danbolt : "Glutamate Uptake", *Neurobiology*, Vol.65, pp.1-105 (2001)
(2) N. Kasai, Y. Jimbo, O. Niwa, T. Matsue, and K. Torimitsu : "Rea-time Multisite Observation of Glutamate Release in Rat Hippocampal Slices", *Neurosdence Lett.*, Vol.304, pp.112-116 (2001)
(3) T. Morishima, M. Uematsu, T. Furukawa, Y. Yanagawa, A. Fukuda, and S. Yoshida : "GABA Imaging in Brain Slices Using Enzyme-linked Photo Analysis", *Neurosci. Res.*, Vol.67, pp.347-353 (2001)
(4) V. Calhoun, G. Pearlson, and T. Adali : "Independent Component Analysis to fMRI Data, A Generative Model for Validating Results", VLSI Signal Processing, Vol.37, pp.281-291 (2004)
(5) F. F. Trigo, M. Chat, and A. Marty : "Enhancement of GABA Release through Endogenous Activation of Axonal GABA(A) Receptors in Juvenile Cerebellum", *J. Neurosci.*, Vol.27, No.46, pp.12452-63 (2007)
(6) K. Obata : "Excitatory and Trophic Action of GABA and Related Substances in Newborn Mice and Organotypic Cerebellar Culture", *Dev Neurosci*, Vol.19, No.1, pp.117-119 (1997)

Hikaru Mabuchi

(Student Member) was born in Hokkaido, Japan on July 25, 1992. He is 1st-year student in Graduate School of Toyohashi University of Technology. His major is electric and electronic information. He has been engaged in research on bio-sensing by means of optical measurement. He is a student member of IEEJ.

HongYao Ong

(Associate) was born in Malaysia on June 30, 1990. He received his B.S degree in 2014 from Toyohashi University of Technology, Japan. His major is electric and electronic information. He is currently engaged in GS Reality Sdn. Bhd., Malaysia. His major is electric and electronic information. He is an associate member of IEEJ.

Kazunori Watanabe

(Non-member) was born in Asahikawa, Japan on February 3, 1992. He is 2nd-year student in Graduate School of Toyohashi University of Technology. His research focuses both the optimization of surface modification for biosensor, and detection of neurotransmitters. He is a member of Japan neuroscience Society.

Sachiko Yoshida

(Non-member) was born in Toyama, Japan on January 24, 1961. She received her B.S., M.S. and Ph.D. degrees in 1983, 1986 and 1990 from University of Tokyo. She was engaged in JSPS Postdoctoral Researcher from 1990 to 1992, JST PRESTO Researcher from 1992 to 1994, and Research Associate at Toyohashi University of Technology from 1995 to 1996. Since 1996, she has been a lecturer of Toyohashi University of Technology. Her research interests focus the physiological interaction and morphological transformation through brain differentiation, and these detections. She is a member of a member of IEEE, International Brain Research Organization, Society for neuroscience, Japan neuroscience Society, and the Physiological Society of Japan.

Naohiro Hozumi

(Senior Member) was born in Kyoto, Japan on April 2, 1957. He received his B.S., M.S. and Ph.D. degrees in 1981, 1983 and 1990 from Waseda University. He was engaged in Central Research Institute of Electric Power Industry (CRIEPI) from 1983 to 1999. He was an associate professor of Toyohashi University of Technology from 1999 to 2006, and a professor of Aichi Institute of Technology from 2006 to 2011. Since 2011, he has been a professor of Toyohashi University of Technology. He has been engaged in the research in insulating materials and diagnosis for high voltage equipment, acoustic measurement for biological and medical applications, etc. He was awarded in 1990 and 1999 from IEE of Japan for his outstanding research papers. He is a member of IEEE, IEE of Japan and the Acoustic Society of Japan.

A cross-fostering analysis of bromine ion concentration in rats that inhaled 1-bromopropane vapor

Toru ISHIDAO[1], Yukiko FUETA[1], Susumu UENO[2], Yasuhiro YOSHIDA[3], and Hajime HORI[1]

[1] Department of Environmental Management, School of Health Sciences, University of Occupational and Environmental Health, Japan.

[2] Department of Occupational Toxicology, Institute of Industrial Ecological Sciences, University of Occupational and Environmental Health, Japan.

[3] Department of Immunology and Parasitology, School of Medicine, University of Occupational and Environmental Health, Japan.

Correspondence to: Toru Ishidao, Department of Environmental Management, School of Health Sciences, University of Occupational and Environmental Health, Japan. Iseigaoka 1-1, Yahatanishi-ku, Kitakyushu 807-8555, Japan

(*e-mail: ishidao@health.uoeh-u.ac.jp*)

Running title: **A cross-fostering analysis of bromine ion concentration**

The number of words in the abstract: **238**; text: **2087**, and the number of tables: **2**; figures: **3**

Field: ***Toxicology***

1

Abstract: Objective: Inhaled 1-bromopropane decomposes easily and releases bromine ion. However, the kinetics and transfer of bromine ion into the next generation have not been clarified. In this work, the kinetics of bromine ion transfer to the next generation was investigated by using cross-fostering analysis and a one-compartment model. **Methods:** Pregnant Wistar rats were exposed to 700 ppm of 1-bromopropane vapor for 6 h per day during gestation days (GDs) 1–20. After birth, cross-fostering was performed between mother exposure groups and mother control groups, and the pups were subdivided into the following four groups: exposure group, postnatal exposure group, gestation exposure group, and control group. Bromine ion concentrations in the brain were measured temporally. **Results:** Bromine ion concentrations in mother rats were lower than those in virgin rats, and the concentrations in fetuses were higher than those in mothers on GD20. In the postnatal period, the concentrations in the gestation exposure group decreased with time, and the biological half-life was 3.1 days. Conversely, bromine ion concentration in the postnatal exposure group increased until postnatal day 4 and then decreased. This tendency was also observed in the exposure group. A one-compartment model was applied to analyze the behavior of bromine ion concentration in the brain. By taking into account the increase of body weight and change in the bromine ion uptake rate in pups, the bromine ion concentrations in the brains of the rats could be estimated with acceptable precision.

Key words: 1-Bromopropane inhalation, Cross-fostering, Bromine ion concentration, One-compartment model, Animal experiment

1-Bromopropane (1-BP, CAS no. 106-94-5) is widely used as a substitute for chlorofluorocarbons, which destroy the ozone layer. The toxicity of 1-BP has been

reviewed[1)], and the Japan Society for Occupational Health recommends an occupation exposure limit of 0.5 ppm[2)]. Previously, we studied the effects of inhaled 1-BP vapor in male rats on the nervous[3-8)] and immune systems[9, 10)].

We also studied the effects of inhaled 1-BP vapor on metabolism in male rats and reported that 1-BP rapidly decomposes and releases bromine ion in the blood[11)], indicating that bromine ion is a major index of 1-BP exposure. Recently, because of the health effects reported in female workers exposed to 1-BP[12-14)], there is concern regarding the health effects of 1-BP exposure on the next generation. Some researchers have reported results of experiments in female animals[15-17)]; however, the kinetics of bromine ion distribution to the next generation has not been elucidated. In this study, pregnant rats were exposed to 700 ppm of 1-BP vapor, and the concentration of bromine ion in the rat brain was measured. The distribution of bromine in fetuses and cross-fostered pups was investigated. A one-compartment model was employed to analyze the behavior of bromine ion in rats.

Methods

Animals

Female (9-week-old) and male (10-week-old) Wistar rats were purchased from Kyudo Co., Ltd. (Saga, Japan). After acclimation in polycarbonate cages with dry chips, they were housed in pairs in animal rooms under 12-h light–dark cycle conditions at 22 ± 1°C and 55 ± 5% relative humidity, with free access to food and water. The presence of sperm in the vaginal smear was defined as day 0 of gestation (GD0; female rats were 11 weeks old). In the inhalation study, the female rats were divided into three groups: 1-BP-exposed virgin female group (n = 5), 1-BP-exposed mother group (n = 11), and the control mother group (n = 5). After the final exposure of mother rats on GD20, they

were housed in an animal room for the onset of birth. Postnatal day (PND) i.e., the day after birth, was defined as day 0 (PND0 = GD21). On PND1, a litter size of eight pups was assembled and cross-fostering[17, 18] of pups was performed between mother exposure groups (n = 3) and mother control groups (n = 3). The pups were subdivided into four groups: (1) exposure group (1-BP-exposed pups were raised by their birth mother exposed to 1-BP), (2) postnatal exposure group (control pups were raised by 1-BP-exposed mother), (3) gestation exposure group (1-BP-exposed pups were raised by control mother), and (4) control group (control pups were raised by their control mother). The experimental groups are summarized in Table 1. Body weight was measured periodically. The experiments were conducted per the guidance of the Ethics Committee of Animal Care and Experimentation in accordance with The Guiding Principle for Animal Care Experimentation, University of Occupational and Environmental Health, Japan (AE03-065), which conforms to the National Institutes of Health Guide for the Care and Use of Laboratory Animals and the Japanese Law for Animal Welfare and Care.

Exposure

Reagent-grade 1-BP was obtained from Kanto Chemical Co., Ltd. (Tokyo, Japan). 1-BP vapor was introduced into a 400-*l* stainless-steel exposure chamber. Details of this apparatus and procedure have been given elsewhere[11]. In order to study change in bromine ion in blood and brain when the condition of dysfunction of feedback inhibition (i.e., disinhibition) was confirmed, exposure concentration was designed to be 700 ppm, which was higher than LOAEL (400 ppm) for disinhibition[7]. The actual concentration of 1-BP vapor in the chamber was 701.3 ± 5.2 ppm. In the control group, only clean air was introduced into the chamber. The exposure period was 6 h per day

between 9 a.m. and 3 p.m. throughout gestation or GD1-20 (virgin female group was exposed until GD21). Table 1 displays the age of the rats on sampling day. They were deeply anesthetized with diethyl ether and then decapitated. The brains and the stomachs with milk from only the exposure group on PND1 were gently removed and stored in a freezer.

Measurement of bromine ion concentration

The brains (cerebrum and diencephalon) and stomachs (0.25 g) were homogenized with water (1.5 m*l*) at 0°C. The sample (1 m*l*) was dispensed into a vial, and 0.1 m*l* of dimethyl sulfate was added to convert bromine ion to methyl bromide. Then, 0.1 m*l* of an aqueous solution of isopropyl alcohol (0.5 volume percent) was added as an internal standard. The vial was heated at 50°C for 1 h. The bromine ion concentration was determined by measuring peak area of methyl bromide vapor in the headspace by using a gas chromatograph mass spectrometer (GC/MS, QP-5050; Shimadzu, Kyoto, Japan)[11)].

Estimation method of bromine ion concentration

As previously described, inhaled 1-BP was metabolized and bromine ions were released. In this study, the behavior of released bromine ion concentration in the brain was analyzed by using a one-compartment model[19)]. We assumed the bromine ion uptake rate, i.e., the generation rate of bromine ion, is equal to the 1-BP uptake rate because 1-BP is decomposed quickly[11)] and releases bromine ion. Under this assumption, mass balance equations of bromine ion during exposure and clearance periods respectively were as follows:

$$\frac{dx}{dt} = R - kx \tag{1}$$

$$\frac{dx}{dt} = -kx \tag{2}$$

where x is the amount of bromine ion (μg); t is time (h); R is the generation rate of bromine ion (μg/h), which corresponds to the 1-BP uptake rate; and k is the excretion rate constant (1/h). From equations (1) and (2), the bromine ion concentrations C (μg/g) during exposure and clearance respectively were obtained as follows:

$$C = \frac{R}{\rho V k}\left(1 - e^{-kt}\right) \tag{3}$$

$$C = C_0 e^{-kt} \tag{4}$$

where V is the volume of the compartment (ml), ρ is the density of the compartment (g/ml), and C_0 is the initial concentration during clearance (μg/g). The excretion rate constant k is given by the biological half-life, $t_{1/2}$ (h) or $T_{1/2}$ (days).

$$k = \frac{\ln 2}{t_{1/2}(\mathrm{h})} = \frac{0.693}{T_{1/2}(\mathrm{days}) \times 24} \tag{5}$$

Experimental Results

Fig. 1 shows the change in the average body weight of mother rats exposed to 700 ppm of 1-BP up to GD20 and that of the pups after the exposure. The time, T (on the

horizontal axis), includes the GDs and PNDs. Litter sizes of exposed mothers and control mothers were 15.0 ± 2.8 and 14.9 ± 2.5 pups, respectively. The body weight of both mothers and pups increased rapidly. This tendency was also observed in the control group, and there was no significant difference between the exposure group and the control group. For the virgin female group, body weight did not change significantly (271.1 ± 17.0 g) during GD1-20.

Bromine ion concentration in the rat brain (μg/g-brain) exposed to 700 ppm of 1-BP on GDs is presented as symbols in Fig. 2. The bromine ion concentration in mother rats was lower than that in virgin rats, and the concentration in fetuses was higher than that in mothers. Fig. 3 shows changes in bromine ion concentration in pup brain for PNDs. The concentration in the gestation exposure group decreased between PND4 and PND8, whereas that in the postnatal exposure group increased from PND2 to PND4 and then decreased. This tendency was also observed in the exposure group, although the concentration on PND1 was lower than that on GD20 (fetus in Fig. 2). Specifically, the concentration in the exposure group was the highest just after birth, but decreased at PND1. The concentration then increased from PND1 to PND3, but decreased again with time. In the control pups, the bromine ion concentration was 11.2 ± 7.7 μg/g-brain on PND3.

The bromine ion concentration in pup stomachs with milk from the exposure group on PND1 was 830.6 ± 188.8 μg/g-stomach, which was about twice as much as that in the mother brain at GD20 (Fig. 2).

Discussion

The one-compartment model was applied to analyze the bromine ion concentration in the brains of virgin females, mothers, fetuses, and pups. Equations (3) and (4) have

two parameters, the excretion rate constant k and the 1-BP uptake rate R. The excretion rate constant, k, can be easily calculated from equation (5) by using the biological half-life $T_{1/2}$ (days). In our previous work[11], $T_{1/2}$ for male rats was 4.7–15.0 days in blood and 5.0–7.5 days in urine. Therefore, $T_{1/2}$ = 7.0 days was used for mothers and virgin females in this study. $T_{1/2}$ in pups was 3.1 days, obtained by experimental data. Equation (4) was applied to the data from PND1 for the exposure group and from PND4 and PND8 for the gestation exposure group as shown in Fig. 3. $T_{1/2}$ = 3.1 days was also used for fetuses. The half-lives of between GD20 for fetuses and PND1 for the exposure group were excluded from the calculation because of the time lag due to birth.

As shown in Fig. 2, the bromine ion concentration in the brains of mothers was lower than that in the brains of virgin females. A reason for this might be that the bromine ion concentration was diluted because of increasing body weight. The average body weight of pups, w (g), was expressed using the following equation (Fig. 1):

$$w = 0.00028T^{3.31} \tag{6}$$

The average body weight of mothers, W (g), was calculated as the sum of that of virgin females (ρV = 271.1 g) and of pups, w, (interpolated value for GDs):

$$W = 271.1 + 27w \tag{7}$$

where 27 is the constant, which was determined to give the best fit for the experimental data as shown in Fig. 1.

For virgin females, the uptake rate, R, of 2853 μg/h was obtained to give the best fit

of equations (3) and (4) for the experimental data on GD21 in Fig. 2. Therefore, $R/\rho V = R/W = 2853/271.1 = 10.5$ μg/(h·g) for virgin females, and $R/\rho V = 2853/(271.1 + 27w)$ for mother rats was used in equation (3). For fetuses, R (bromine ion uptake rate from mothers) was assumed to be proportional to body weight, and $R/\rho V = R/w = 22.0$ μg/(h·g) was applied, which was obtained to give the best fit for the experimental data on GD20 in Fig. 2. On PNDs, suckling (exposure to bromine ion from milk) was assumed to occur at 2-h intervals. As shown in Fig. 3, the curve of bromine ion concentration in the brains of the postnatal exposure group is convex. In addition, on PND1, the concentration in pup stomachs with milk was high, and the level was higher than that in the mother brain, as calculated using the one-compartment model (486.2 μg/g-brain). Therefore, we assume that the uptake rate R of pups is high at first and then decreases. In this work, R in the postnatal exposure group can be expressed by the following equation:

$$R = 388e^{-0.126(t-32)} \tag{8}$$

where 32 is the initial suckling (h) and 388 and 0.126 are the constants determined experimentally. The bromine ion concentration in the exposure group was calculated as the sum of the concentrations in the gestation exposure and postnatal exposure groups. Conditions of the one-compartment model and the values of parameters obtained are listed in Table 2. Solid, broken, and dotted lines in Fig. 2 indicate calculated lines for fetuses, mothers, and virgin females, respectively. In Fig. 3, solid, broken, and dotted lines indicate calculated lines of exposure, postnatal exposure, and gestation exposure groups, respectively. The lines calculated using the proposed model could be estimated from the experimental data with acceptable precision as shown in both figures.

The calculated bromine ion uptake rates per weight, $R/\rho V$, for adults and fetuses were 10.5 and 22 μg/(h·g), respectively. This result suggests that the bromine ion easily transfers from mothers to fetuses, and the concentration in fetuses was higher than that in mothers. R in postnatal exposure group was expressed as an exponential function, and $R/\rho V$ of 55 μg/(h·g) was obtained at initial suckling time. This value was large compared to 22 μg/(h·g), the calculated value at GD20, before birth. This suggests that uptake rate of bromine ion via milk was higher than that via the placenta, and the bromine ion concentration in the exposure group could be explained as the sum of that in the gestation and postnatal exposure groups, which is shown in Fig. 3.

In summary, the results of this study suggest (1) the concentration of bromine ion in mother rats was lower than that in virgin female rats, (2) bromine ion easily transferred from mothers to fetuses and accumulated before birth, (3) bromine ion was concentrated more in milk than in the brains of the mothers, and (4) bromine ion uptake rate in pups was high immediately after birth.

Acknowledgments:

The authors thank Ms. Tomoko Tanaka, Kana Hayashi, Erika Ito, and Ai Kanemaru for technical help and Dr. Sumiyo Ishimatsu for her critical comments on our experiments.

References

1) Ichihara G. Neuro-reproductive toxicities of 1-bromopropane and 2-bromopropane. Int Arch Occup Environ Health 2005; 78; 79-96.
2) The Japan Society for Occupational Health. Recommendation of occupational exposure limits (2013-14). J Occup Health 2013; 55; 422-41.
3) Ohnishi A, Ishidao T, Kasai T, Arashidani K, Hori H. Neurotoxicity of 1-bromopropane in rats. J UOEH 1999; 21; 23-8.
4) Fueta Y, Ishidao T, Kasai T, Hori H, Arashidani K. Decreased paired-pulse inhibition in the dentate gyrus of the brain in rats exposed to 1-bromopropane vapor. J Occup Health 2000; 42; 149-51.
5) Fueta Y, Ishidao T, Arashidani K, Endo Y, Hori H. Hyperexcitability of the hippocampal CA1 and the dentate gyrus in rats subchronically exposed to a substitute for chlorofluorocarbons, 1-bromopropane vapor. J Occup Health 2002; 44; 156-65.
6) Fueta Y, Fukuda T, Ishidao T, Hori H. Electrophysiology and immunohistochemistry in the hippocampal CA1 and the dentate gyrus of rats chronically exposed to 1-bromopropane, a substitute for specific chlorofluorocarbons. Neuroscience 2004; 124; 593-603.
7) Fueta Y, Ishidao T, Ueno S, Yoshida Y, Kunugita N, Hori H. New approach to risk assessment of central neurotoxicity induced by 1-bromopropane using animal models. Neurotoxicology 2007; 28; 270-3.
8) Ueno S, Yoshida Y, Fueta Y, Ishidao T, Liu JQ, Kunugita N, Yanagihara N, Hori H. Changes in the function of the inhibitory neurotransmitter system in the rat brain following subchronic inhalation exposure to 1-bromopropane. Neurotoxicology 2007; 28; 415-20.

9) Yoshida Y, Liu JQ, Nakano Y, Ueno S, Fueta Y, Ishidao T, Kunugita N, Yamashita U, Hori H. 1-BP inhibits NF-kB activity and Bcl-xL expression in astrocytes in vitro and reduces Bcl-xL expression in the brains of rats in vivo. Neurotoxicology 2007; 28; 381-6.

10) Yoshida Y, Nakano Y, Ueno S, Liu JQ, Fueta Y, Ishidao T, Kunugita N, Yanagihara N, Sugiura T, Yamashita U, Hori H. Effects of 1-bromopropane, a substitute for chlorofluorocarbons, on brain-derived neurotrophic factor (BDNF) expression. Int Immunopharmacol 2009; 9; 433-8.

11) Ishidao T, Kunugita N, Fueta Y, Arashidani K, Hori H. Effects of inhaled 1-bromopropane vapor on rat metabolism. Toxicol Lett 2002; 134; 237-43.

12) Ichihara G, Miller JK, Ziolkowska A, Itohara S, Takeuchi Y. Neurological disorders in three workers exposed to 1-bromopropane. J Occup Health 2002; 44; 1-7.

13) Ichihara G, Li W, Ding X, Peng S, Yu X, Shibata E, Yamada T, Wang H, Itohara S, Kanno S, Sakai K, Ito H, Kanefusa K, Takeuchi Y. A survey on exposure level, health status, and biomarkers in workers exposed to 1-bromopropane. Am J Ind Med 2004; 45; 63-75.

14) Li W, Shibata E, Zhou Z, Ichihara S, Wang H, Wang Q, Li J, Zhang L, Wakai K, Takeuchi Y, Ding X, Ichihara G. Dose-dependent neurologic abnormalities in workers exposed to 1-bromopropane. J Occup Environ Med 2010; 52; 769-77.

15) Sekiguchi S, Suda M, Zhai YL, Honma T. Effects of 1-bromopropane, 2-bromopropane, and 1,2-dichloropropane on the estrous cycle and ovulation in F344 rats. Toxicol Lett 2002; 126; 41-9.

16) Yamada T, Ichihara G, Wang H, Yu X, Maeda K, Tsukamura H, Kamijima M, Nakajima T, Takeuchi Y. Exposure to 1-bromopropane causes ovarian dysfunction in rats. Toxicol Sci 2003; 71; 96-103.

17) Furuhashi K, Kitoh J, Tsukamura H, Maeda K, Wang H, Li W, Ichihara S, Nakajima T, Ichihara G. Effects of exposure of rat dams to 1-bromopropane during pregnancy and lactation on growth and sexual maturation of their offspring. Toxicology 2006; 224; 219-28.

18) Lau C, Thibodeaux JR, Hanson RG, Rogers JM, Grey BE, Stanton ME, Butenhoff JL, Stevenson LA. Exposure to perfluorooctane sulfonate during pregnancy in rat and mouse. II: postnatal evaluation. Toxicological Sci 2003; 74; 382-92.

19) Hori H, Hyakudo T, Oyabu T, Ishimatsu S, Yamato H, Tanaka I. Effects of inhaled methyl bromide gas on the metabolic system and kinetics of bromine ion in rats. J UOEH 2002; 24; 151-60.

Table 1. Experimental groups and ages of adult and fetal rats exposed to 700 ppm of 1-BP and of pups on sampling day

Groups (n)		Age (n) on sampling day
Virgin female	Exposure (5)	GD21 (2)
Mother	Exposure (11) Control (5)	GD20 (3)
Fetus	Exposure	GD20 (13)
Pup†	Exposure	PND1 (10), PND3 (10), PND5 (5), PND7 (5)
	Postnatal exposure	PND2 (5), PND4 (5), PND8 (5)
	Gestation exposure	PND4 (5), PND8 (5)
	Control	PND3 (5)

1-BP: 1-bromopropane, GD: gestation day, PND: postnatal day, †: Exposure = 1-BP exposed pups were raised by their birth mother exposed to 1-BP, Postnatal exposure = control pups were raised by 1-BP exposed mother, Gestation exposure = 1-BP exposed pups were raised by control mother, Control = control pups were raised by control mother

Table 2. Parameters of the one-compartment model

Groups		$T_{1/2}$ (days)	ρV (g)	R (μg/h)	Results
GD	Virgin female	7.0	271.1	2853	Fig. 2
	Mother	7.0	271.1+27w	2853	Fig. 2
	Fetus	3.1	w	22w	Fig. 2
PND	Gestation exposure	3.1			Fig. 3
	Postnatal exposure	3.1	w	$388e^{-0.126(t-32)}$	Fig. 3
	Exposure	Gestation exposure + Postnatal exposure			Fig. 3
	Mother	7.0			Text†

†: the concentration in mother brain corresponding to PND1 (486.2 μg/g-brain), $w=0.00028T^{3.31}$ by equation (6)

Figure Captions

Fig. 1. The average body weight of mothers (*W*) exposed to 700 ppm of 1-BP up to GD20 and that of pups (*w*) after exposure. 1-BP: 1-bromopropane; GD: gestation day; PND: postnatal day

Fig. 2. Change in bromine ion concentration in rat brain exposed to 700 ppm of 1-BP on GDs. Symbols represent experimental data: ●, fetus; ▲, mother; △, virgin female. Solid, broken, and dotted lines indicate calculated lines for fetuses, mothers, and virgin females, respectively. 1-BP: 1-bromopropane; GD: gestation day

Fig. 3. Change in bromine ion concentration in pup brain during PNDs. Symbols represent experimental data: ●, exposure group (1-BP exposed pups were raised by their birth mother exposed to 1-BP); ◇, postnatal group (control pups were raised by 1-BP exposed mother); □, gestation exposure (1-BP exposed pups were raised by control mother). Solid, broken, and dotted lines indicate calculated lines for exposure, postnatal exposure, and gestation exposure groups, respectively. 1-BP: 1-bromopropane; PND: postnatal day

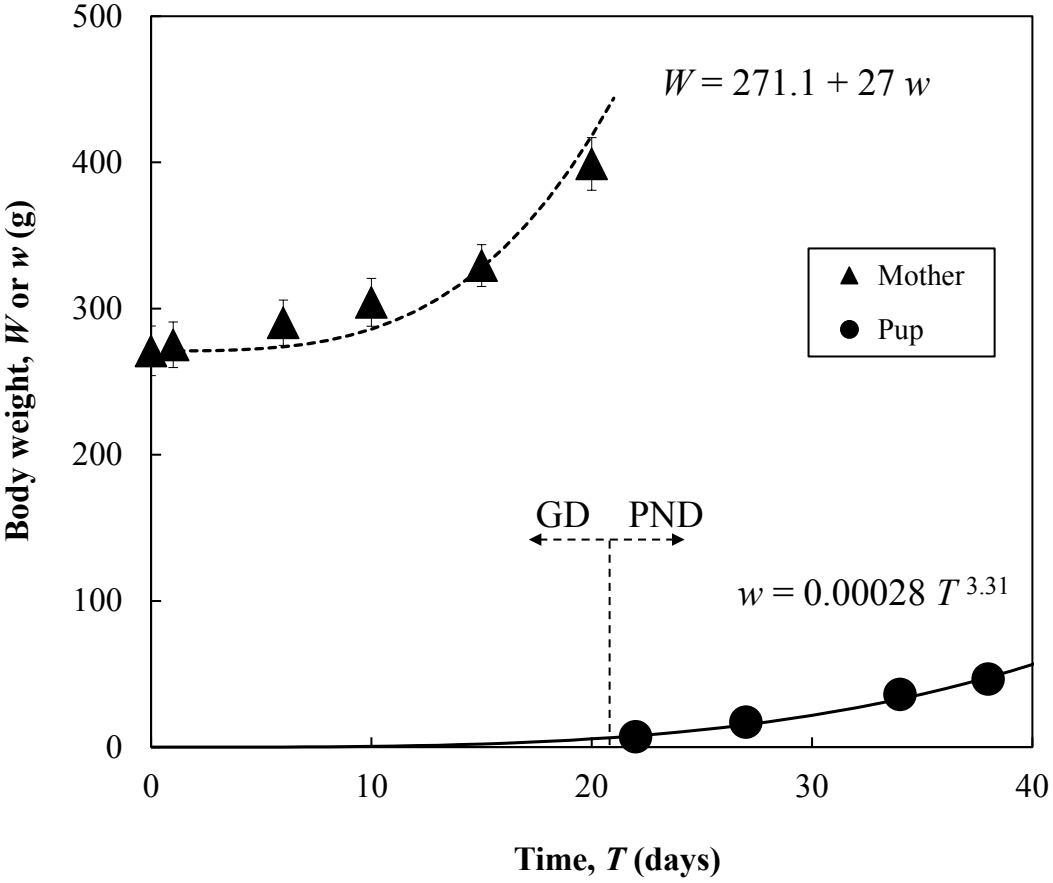
500
400
300
200
100
0
0
10
20
30
40
Body weight, W or w (g)
Time, T (days)
W = 271.1 + 27 w
Mother
Pup
GD
PND
w = 0.00028 T 3.31

Fig. 1.

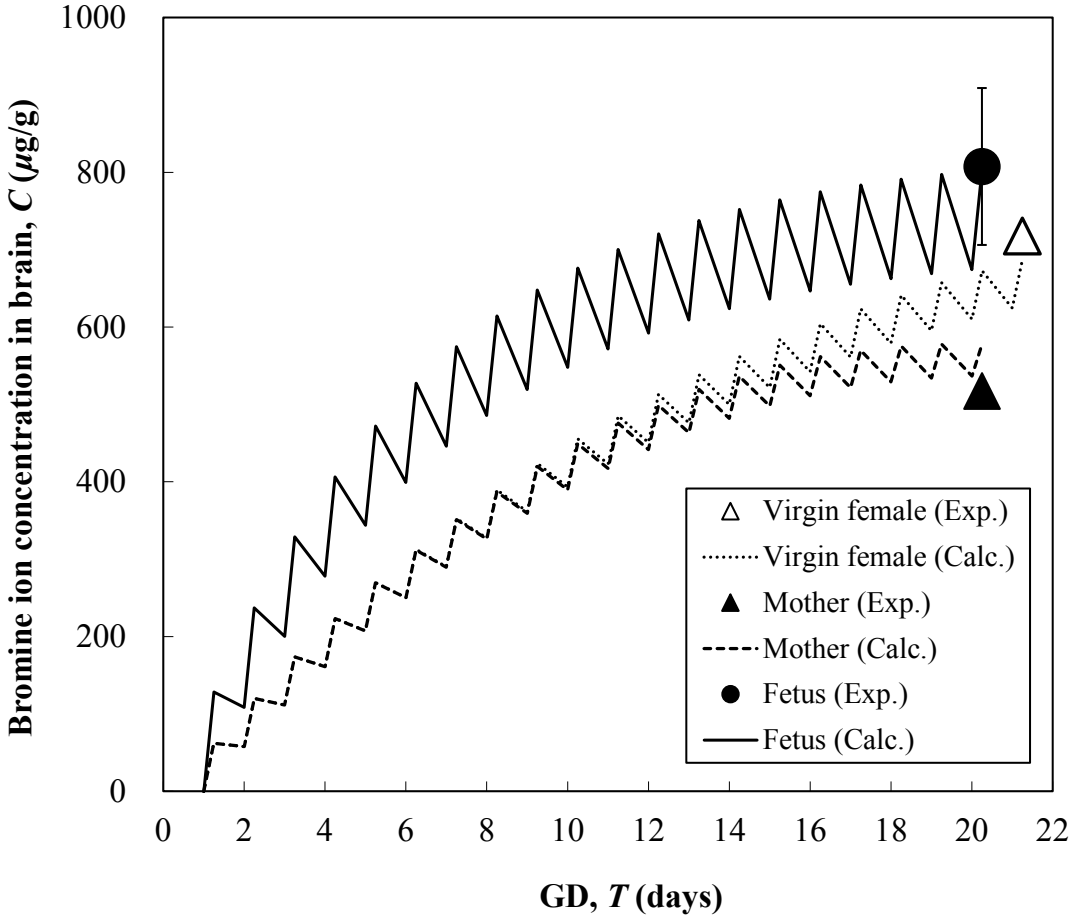
1000
800
600
400
200
0
0
2
4
6
8
10
12
14
16
18
20
22
Bromine ion concentration in brain, C (μg/g)
GD, T (days)
Virgin female (Exp.)
Virgin female (Calc.)
Mother (Exp.)
Mother (Calc.)
Fetus (Exp.)
Fetus (Calc.)

Fig. 2.

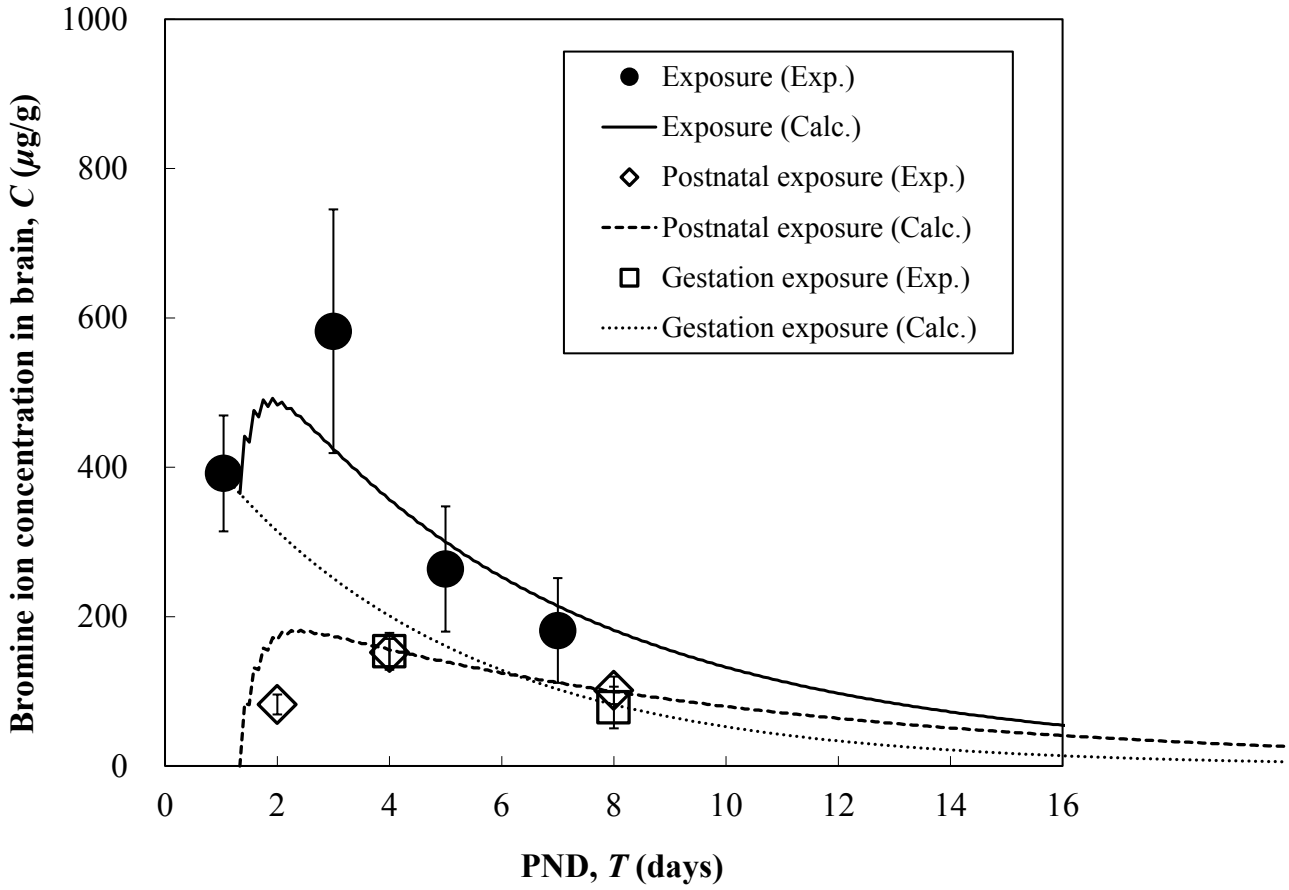
1000
800
600
400
200
0
0
2
4
6
8
10
12
14
16
Bromine ion concentration in brain, C (μg/g)
PND, T (days)
Exposure (Exp.)
Exposure (Calc.)
Postnatal exposure (Exp.)
Postnatal exposure (Calc.)
Gestation exposure (Exp.)
Gestation exposure (Calc.)

Fig. 3.

[Research Note]

Prenatal Exposure to 1-Bromopropane Suppresses Kainate-Induced Wet Dog Shakes in Immature Rats

Yukiko FUETA[1*], Masanari KANEMITSU[1], Sumie EGAWA[1], Toru ISHIDAO[1], Susumu UENO[2] and Hajime HORI[1]

[1] *Department of Environmental Management, School of Health Sciences, University of Occupational and Environmental Health, Japan. Yahatanishi-ku, Kitakyushu 807-8555, Japan*

[2] *Department of Occupational Toxicology, Institute of Industrial Ecological Sciences, University of Occupational and Environmental Health, Japan. Yahatanishi-ku, Kitakyushu 807-8555, Japan*

Abstract : 1-Bromopropane (1-BP) is used in degreasing solvents and spray adhesives. The adverse effects of 1-BP have been reported in human cases and adult animal models, and its developmental toxicity has also been reported, but its effects on developmental neurotoxicity have not been investigated in detail. We evaluated the effects in rat pups of prenatal exposure to 1-BP on behaviors such as scratching and wet dog shakes (WDS), which were induced by injection of kainate (KA). Pregnant Wistar rats were exposed to vaporized 1-BP with 700 ppm from gestation day 1 to day 20 (6 h/day). KA at doses of 0.1, 0.5, and 2.0 mg/kg were intraperitoneally injected into a control group and a 1-BP-exposed group of pups on postnatal day 14. There was no significant difference in scratching between the control and the prenatally 1-BP-exposed groups, while suppression of the occurrence ratio of WDS was observed at the low dose of 0.1 mg/kg of KA in the prenatally 1-BP-exposed pups. Our results suggest that prenatal exposure to 1-BP affects neurobehavioral responses in the juvenile period.

Keywords : 1-bromopropane, prenatal exposure, developmental neurotoxicity, wet dog shake, rats.

(Received June 26, 2015, accepted November 9, 2015)

Introduction

The volatile organic compound 1-bromopropane (CH_3-CH_2-CH_2Br; 1-BP), a substitute for specific chlorofluorocarbons, is mainly used in degreasing solvents and spray adhesives. It has been reported that occupational exposure to 1-BP causes neurotoxicity, such as numbness, gait disturbance, prolongation of distal latency and memory dysfunction [1].

Animal models exposed to 1-BP have also shown central neurotoxicity, including ataxic gait, prolongation of distal latency, alteration of mRNA levels of neurotransmitter receptors [1], and hippocampal disinhibition [2]. *In vitro* studies have revealed that the direct application of 1-BP enhanced the currents mediated by the activation of A type γ-aminobutyric acid ($GABA_A$) receptors, suppressed the currents mediated by neuronal nicotinic acetylcholine receptors, and potentiated feedback inhibition in the cornu ammonis 1 (CA1) subfield of hippocampal slices [3]. The gene expression of the B-cell lymphoma-extra large molecule (Bcl-xl), and the activity of nuclear factor-kappa B (NF-κB), were suppressed in *in vitro* and *in vivo* studies [4]. The developmental effects of 1-BP have also been investigated [5], but little is known about the developmental neurotoxicity in offspring.

*Corresponding Author: Yukiko FUETA, Department of Environmental Management, School of Health Sciences, University of Occupational and Environmental Health, Japan. Yahatanishi-ku, Kitakyushu 807-8555, Japan, Tel: +81-93-603-1611, Fax: +81-93-691-2694, E-mail: yukiko@med.uoeh-u.ac.jp

In our previous study of the developmental neurotoxicity of 1-BP, prenatal exposure to 1-BP altered hippocampal excitability and the gene expression of the Na^+ channel [6] and glutamate receptor subunits on postnatal day (PND) 14 [7]. These results raised the possibility that prenatal exposure to 1-BP affects brain development and its related behaviors. However, conventional behavioral tests for rodents are difficult to apply to pups. Thus, we focused on the particular behaviors of scratching and wet dog shakes (WDS), which can be observed in pups.

Scratching is defined as repetitive and quick flexion-extension movements of the hind limbs toward the neck or the head region. This behavior has been shown to be spontaneously induced in normal as well as pathological conditions and is used as an itch model in rodents [8], although the behavior in pups remains to be analyzed. WDS is characterized as brief and fierce shaking of the head, neck, and trunk, appearing when rodents are wet, as the name suggests [9]. Interestingly, it has been reported that both scratching and WDS can be induced by electrical stimulation of limbic structures [10], and by several pharmacological interventions, such as kainate (KA) [9, 11] and pentylenetetrazole. KA is the agonist of ionotropic glutamate receptors, which mediate excitatory neurotransmission and are predominantly distributed in the hippocampus, inner lamina of the neocortex, and ventral thalamus [12]. Thus, scratching and WDS induced by KA could be useful indices of changes in the excitatory neurotransmission of neuronal networks in pup brains. In this study, we examined the effect of prenatal exposure to 1-BP on behaviors in pups by evaluating the incidences of scratching and WDS induced by KA.

Materials and Methods

Animals and 1-BP inhalation

Thirty-two female and 16 male Wistar rats (designated the parental (P) generation) purchased from Kyudo *Co.* (Tosu, Japan) at 11 weeks of age were housed in plastic cages with paper-made chips (ALPHA-dri, Shepherd Specialty Papers, Milford, USA) on a 12 h light/dark cycle (light period: 07:00-19:00). The room temperature was kept at 23 ± 1°C. The relative humidity was about 70%. The animals had free access to food and water. Proestrus stage was verified with an impedance checker (MK-10B, Muromachi Kikai *Co., Ltd.*, Tokyo, Japan). When the impedance was over three kΩ, the F0 female rats were mated with male rats. In the morning of the following day, the existence of sperm in the vaginal smear or vaginal plug was verified as the gestation day (GD) 0. Fourteen dams from the colony were used in the experiment. The pregnant rats of the P generation were randomly divided into two groups (7 rats in each): one group as the control and the other for exposure to 1-BP.

1-BP was purchased from Kanto Chemical *Co., Ltd.* (Tokyo, Japan). Seven dams were exposed to 1-BP vapor at a concentration of 700 ppm (6 h/day) for 20 days from GDs 1 to 20 in an exposure chamber [13], whereas the other seven dams were provided fresh air in the same type of chamber. Both P generation groups were not allowed access to food and water during the inhalation period. Four weeks of 1-BP inhalation (700 ppm) resulted in apparent effects on the hippocampus in the adult rats [2]. Therefore, we first chose the concentration of 700 ppm to study the possible underlying mechanism of developmental neurotoxicity in prenatally 1-BP-exposed rats. The concentration of 1-BP was monitored with a gas chromatograph (GC353B FSL, GL Sciences *Inc.*, Japan) equipped with a flame ionization detector.

All the pregnant rats gave birth to offspring (termed the first filial (F1) generation) on GD 21. The day of birth was defined as PND 0. We randomly gathered 26 F1 rats from the 7 control litters and 22 F1 rats from the 7 1-BP-exposed litters. All the F1 pups were bred with their mother rats during the lactation period. In this study, 24 female and 3 male F1 rats were obtained from the 7 dams in the control group, and 18 female and 4 male F1 rats were obtained from the 7 dams in the 1-BP-exposed group, respectively. We examined the F1 rats for the general toxicity of 1-BP inhalation exposure, such as litter size, sex ratio, testicular descent, vaginal opening, ear opening, and survival rate. The body weight of the F1 rats was measured on PND 14.

KA administration and behavioral observation

KA was obtained from Wako Pure Chemical Industries, *Ltd.* (Osaka, Japan). KA (0.1, 0.5, and 2.0 mg/kg) was dissolved in phosphate buffered saline (PBS).

PBS or KA was intraperitoneally injected to the F1 rats at PND 14, after which the F1 rats were placed in a clear plastic cage, and the scratching and WDS were observed by video-recording for 180 min in a room for the behavioral observation. The room temperature was kept at about 25°C. The behavioral observation was conducted for 180 min between 09:30 and 15:30. The number of F1 rats that showed the scratching and the WDS behavior was counted and then the occurrence ratio was calculated. The duration and frequency of scratching and WDS were also measured. This experiment was approved by the Ethics Committee for Animal Care and Experimentation in accordance with the University of Occupational and Environmental Health, Japan.

All the chemicals used in this study were a reagent grade and purchased from commercial sources.

Statistical analysis

The difference in bodyweight between the F1 control and F1 1-BP-exposed groups was analyzed by Student *t*-test. The Mantel-Haeinzel procedure was utilized to see the whole effect of the prenatal inhalation of 1-BP on the occurrence ratio of scratching and WDS. When appropriate, Fisher's exact test determined significant differences. A two-way analysis of variance (ANOVA) was performed to clarify the effects of prenatal exposure to 1-BP and/or a dose of KA on the frequency and the duration of scratching and WDS. When appropriate, *post hoc* analysis by Scheffe's test determined significant differences, respectively. The criteria of significant difference was $P < 0.05$ in all the statistical analyses. Data represent mean ± standard error of the mean (SEM).

Results and Discussion

General toxicity of 1-BP inhalation exposure in F0 and F1 generations

There were no outward pathological signs related to 1-BP in the F0 rats. The body weights of the P generation dams treated with 1-BP were not significantly different from those in the control (fresh air) group (data not shown). None of the F1 rats died during the experimental period, indicating that the exposure seemed to cause little stress on the dams in this study. There was no difference in the sex ratio, survival rate, or other clinical signs between the F1 control and F1 1-BP-exposed groups, with the exception of body weight. The body weight in the female F1 1-BP-exposed group (32.5 ± 0.5 g) was significantly lower ($P < 0.01$, Student *t*-test) than that in the female F1 control group (35.0 ± 0.4 g). The 1-BP-exposed male F1 rats also had a lower body weight (33.5 ± 0.3 g) compared to the male F1 control group (37.0 ± 0.8 g) ($P < 0.01$, Student *t*-test). Our results were consistent with previous studies showing that prenatal exposure to 1-BP has no effects on postnatal survival rate, excluding the body weight [5].

Effect of prenatal exposure to 1-BP on behavioral responses

KA administration elicits immobilization, followed by scratching, WDS, forelimb clonus, and status epilepticus (continuous chronic-tonic posturing of all 4 limbs) [11]. It is also known that a low dose less than 3 mg/kg of KA elicits scratching and WDS but hardly ever elicits epileptic convulsions. Our preliminary study also showed that doses of KA higher than 4 mg/kg induced convulsive behaviors as well as scratching and WDS, thus we chose doses of 0.1, 0.5, and 2.0 mg/kg of KA.

Behavioral data obtained from both genders is combined in Tables 1 and 2, because it has been reported that there are no sex differences in KA induced-behaviors in pups [14].

In the F1 control group, all of the tested pups showed scratching during the 180 min after injection of PBS or KA. The frequency and duration of the scratching was significantly higher only at the dose of 2.0 mg/kg (Table 1). WDS were observed in 80% of the PBS-injected control pups and in all of the KA-injected control pups. A significantly higher frequency of WDS was observed at the dose of 2.0 mg/kg (Table 2). The behavioral changes induced by the KA doses of 0.1 and 0.5 mg/kg were similar to those of PBS, thus it can be said that these two doses are subclinical.

Spontaneous scratching and WDS were also observed in the F1 1-BP-exposed group. The occurrence ratio of scratching was 100% at all doses of KA (Table 1), whereas that of WDS was 40 to 60% in 0 to 0.5 mg/kg and 100% in 2.0 mg/kg of KA (Tables 2). The effect of prenatal exposure to 1-BP was observed

in the occurrence ratio of WDS ($P < 0.01$; Mantel-Haenszel test). The occurrence ratio in the F1 1-BP-exposed group at 0.1 mg/kg KA was lower than that in the F1 control group ($P < 0.05$ by Fisher's exact test). The dose of 0.5 mg/kg KA tended to decrease the occurrence ratio in the F1 1-BP-exposed group, but did not reach a significant level. Taken together with the results of the 0.1 and 0.5 mg/kg KA (subclinical doses), the occurrence ratio (6 out of 12 rat pups) in the F1 1-BP-exposed group exhibited a lower value than that in the F1 control group (16 out of 16 rat pups, $P < 0.005$ by Fisher's exact test). This indicates that the effects of prenatal 1-BP exposure can be observed only at the subclinical doses of KA. The duration and the frequency of the scratching and the WDS increased at the dose of 2.0 mg/kg ($P < 0.01$), but we did not find any significant effect of prenatal 1-BP exposure on the duration and frequency of WDS at any of the doses of KA. Our results suggest that prenatal exposure to 1-BP suppresses the occurrence of WDS only at a low dose of KA, possibly due to an effect on mechanisms underlying the generation of WDS.

WDS can be induced by electrical stimulation of limbic structures and by the administration of several chemicals, such as serotonergic compounds [15] and an opioid receptor agonist [16], as well as KA. KA-induced-WDS is depressed by μ-opioid receptor antagonists [16]. An antagonist of α-amino-3-hydroxy-5-methyl-4-isoxazolepropionic acid/KA receptors suppresses WDS induced by serotonin receptor agonists [15]. The mechanisms of WDS induction by these chemicals are assumed to be related to each other. Besides those receptors, nitric oxide has also been demonstrated to play a regulatory role in KA- and getting-wet-induced-WDS [9]. These receptors and nitric oxide might be the target of prenatal exposure to 1-BP.

Table 1. The occurrence ratio, duration and frequency of scratching in F1 control and 1-BP-exposed groups

	F1 control			F1 1-BP-exposed		
KA (mg/kg)	S/N	duration (s)	frequency (counts)	S/N	duration (s)	frequency (counts)
PBS	5/5	1.9 ± 0.3	21 ± 6	5/5	2.3 ± 0.3	17 ± 5
0.1	11/11	2.0 ± 0.1	14 ± 2	7/7	2.0 ± 0.1	26 ± 10
0.5	5/5	1.7 ± 0.3	25 ± 4	5/5	2.1 ± 0.5	20 ± 8
2.0	5/5	2.9* ± 0.4	557* ± 164	5/5	3.6* ± 0.2	517* ± 41

F1: first filial generation, 1-BP: 1-bromopropane, KA: kainate, PBS: phosphate buffered saline, S: the number of rats in which scratching was observed, N: the total number of rats used in the experiment, S/N: the occurrence ratio, *: significant effects of KA on the duration or the frequency by two-way ANOVA followed by Scheffe's test ($P < 0.01$), mean ± SEM: mean ± standard error of the mean

Table 2. The occurrence ratio, duration and frequency of WDS in F1 control and 1-BP-exposed groups

	F1 control			F1 1-BP-exposed		
KA (mg/kg)	S/N	duration (s)	frequency (counts)	S/N	duration (s)	frequency (counts)
PBS	4/5	0.3 ± 0.02	1.8 ± 0.6	3/5	0.2 ± 0.03	0.8 ± 0.4
0.1	11/11	0.3 ± 0.03	3.4 ± 0.6	4/7[a]	0.3 ± 0.09	1.0 ± 0.4
0.5	5/5	0.3 ± 0.02	2.6 ± 0.9	2/5	0.2, 0.3	0.8 ± 0.6
2.0	5/5	0.3 ± 0.05	29.2* ± 10.0	5/5	0.4 ± 0.02	54.4* ± 21.1

WDS: wet dog shakes, F1: first filial generation, 1-BP: 1-bromopropane, KA: kainate, PBS: phosphate buffered saline, S: the number of rats in which WDS were observed, N: the total number of rats used in the experiment, S/N: the occurrence ratio, a: a significant difference between F1 control and F1 1-BP-exposed groups at the dose of 0.1 mg/kg in the Fisher's exact test ($P < 0.05$), *: significant effects of KA ($P < 0.01$) on the two-way ANOVA followed by Scheffe's test, mean ± SEM: mean ± standard error of the mean. The data of durations in the F1 1-BP-exposed group administered 0.5 mg/kg of KA are shown in the duration(s) column

There are studies suggesting that the hippocampus is the target of KA. KA receptors have been found in the hippocampus in rat pups [12], and epileptic discharges have been observed when KA-induced seizures occur [17]. Moreover, KA-induced WDS was accompanied by robust electrographic seizures recorded from the hippocampus [18]. On the other hand, Fueta *et al.* have reported that prenatal 1-BP exposure decreases the paired-pulse ratio of population spikes in the CA1 subfield of the dorsal hippocampus in PND14 rats [19]. A decrease in the paired-pulse ratio of the population spike is generally interpreted as an increase in an inhibition [2]. Thus, prenatal 1-BP exposure may disturb the propagation of hyperactivity in the hippocampus, such as electrographic discharges associated with KA-induced WDS. This may account for the suppression of WDS by prenatal exposure to 1-BP. However, it should also be considered that the dentate gyrus (DG) in the ventral hippocampus is thought to be necessary for chemical interventions such as KA-, μ-opioid-, and electrical stimulation-induced WDSs in adult rats [16, 20, 21]. Therefore, further studies are needed to investigate the excitability of the DG in the ventral hippocampus in prenatally 1-BP-exposed rats.

In conclusion, we demonstrate here that prenatal exposure to 1-BP suppresses WDS induced by the administration of a low dose of KA. Our results indicate that prenatal 1-BP exposure may disturb the susceptibility to KA or the functions of neural networks related to the WDS. We also show that it may be advantageous to use pharmacological interventions with convulsants in investigations of the effects of environmental chemicals on behavioral responses in immature rats.

Conflict of Interest

No conflicts of interest to declare.

Acknowledgments

We gratefully acknowledge the animal care of K. Egashira. This study was partly supported by the Grants-in-Aid program of Japan Society for the Promotion of Science (No. 20591237, No. 23510084, and No.18510064), and a University of Occupational and Environmental Health (UOEH) Research Grant for Promotion of Occupational Health.

References

1. Ichihara G, Kitoh J, Li W, Ding X, Ichihara S & Takeuchi Y (2012): Neurotoxicity of 1-bromopropane: Evidence from animal experiments and human studies. J Adv Res 3: 91–98
2. Fueta Y, Ishidao T, Ueno S, Yoshida Y, Kunugita N & Hori H (2007): New approach to risk assessment of central neurotoxicity induced by 1-bromopropane using animal models. Neurotoxicology 28: 270–273
3. Ueno S, Fueta Y, Ishidao T, Yoshida Y, Tsutsui M, Toyohira Y, Hori H & Yanagihara N (2006): The central neurotoxicity of 1-bromopropane (1-BP), a substitute for chlorofluorocarbons: Studies on the effects caused by direct and subchronic exposure to 1-BP on hippocampal function. J Pharmacol Sci 100 (Suppl 1): 140
4. Yoshida Y, Liu JQ, Nakano Y, Ueno S, Ohmori S, Fueta Y, Ishidao T, Kunugita N, Yamashita U & Hori H (2007): 1-BP inhibits NF-κB activity and Bcl-xL expression in astrocytes in vitro and reduces Bcl-xL expression in the brains of rats *in vivo*. Neurotoxicology 28: 381–386
5. Huntingdon Life Sciences (2001): A developmental toxicity study in rat via whole body inhalation exposure. Study Number 98-4141. Ducument ID Title OAR-2002-0064: Document available in public dockets A-2001-07, OAR-2002-0064, and A-91-42. US EPA, Washington, DC
6. Ueno S, Fueta Y, Ishidao T, Yuhi T,Yoshida Y, Hori H & Yanagihara N (2008): Changes in the excitability and Na^+ channel gene expression in the hippocampus of postnatal 14 days-aged rats prenatally exposed to 1-bromopropane. Neurosci Res 61(1 Suppl): S269
7. Fueta Y, Ueno S, Ishidao T, Yoshida Y & Hori H (2009): Effects of prenatally exposed to 1-bromopropane on the brain of the young offspring. Neurosci Res 65 (Suppl 1): S250
8. Nojima H & Carstens E (2003): Quantitative assessment of directed hind limb scratching behavior as a rodent itch model. J Neurosci Methods 126: 137–143
9. Koylu EO, Uz T, Manev H & Pogun S (2002): Nitric oxide synthase inhibition suppresses wet dog shakes and augments convulsions in rats. Int J Neurosci 112: 291–300

10. Frush DP & McNamara JO (1986): Evidence implicating dentate granule cells in wet dog shakes produced by kindling stimulations of entorhinal cortex. Exp Neurol 92: 102–113
11. Albala BJ, Moshé SL & Okada R (1984): Kainic-acid-induced seizures: a developmental study. Brain Res 315: 139–148
12. Miller LP, Johnson AE, Gelhard RE & Insel TR (1990): The ontogeny of excitatory amino acid receptors in the rat forebrain–II. Kainic acid receptors. Neuroscience 35: 45–51
13. Ishidao T, Kunugita N, Fueta Y, Arashidani K & Hori H (2002): Effects of inhaled 1-bromopropane vapor on rat metabolism. Toxicol Lett 134 (1–3): 237–243
14. Doucette TA, Strain SM, Allen GV, Ryan CL & Tasker RA (2000): Comparative behavioral toxicity of domoic acid and kainic acid in neonatal rats. Neurotoxicol Teratol 22: 863–869
15. Gorzalka BB, Hill MN & Sun JC (2005): Functional role of the endocannabinoid system and AMPA/kainate receptors in 5-HT2A receptor-mediated wet dog shakes. Eur J Pharmacol 516: 28–33
16. Hong JS, Grimes L, Kanamatsu T & McGinty JF (1987): Kainic acid as a tool to study the regulation and function of opioid peptides in the hippocampus. Toxicology 46: 141–157
17. Ben-Ari Y, Tremblay E, Berger M & Nitecka L (1984): Kainic acid seizure syndrome and binding sites in developing rats. Brain Res 316: 284–288
18. Cherubini E, De Feo MR, Mecarelli O & Ricci GF (1983): Behavioral and electrographic patterns induced by systemic administration of kainic acid in developing rats. Brain Res 285: 69–77
19. Fueta Y, Ueno S, Ishidao T & Hori H (2010): Long-lasting effects on hippocampal excitability of the offspring prenatally exposed to 1-bromopropane, a substitute for specific chlorofluorocarbons. Neurosci Res 68 (Suppl 1): e417
20. Grimes LM, Earnhardt TS, Mitchell CL, Tilson HA & Hong JS (1990): Granule cells in the ventral, but not dorsal, dentate gyrus are essential for kainic acid-induced wet dog shakes. Brain Res 514: 167–170
21. Barnes MI & Mitchell CL (1990): Differential effects of colchicine lesions of dentate granule cells on wet dog shakes and seizures elicited by direct hippocampal stimulation. Physiol Behav 48: 131–138

1-ブロモプロパンへの胎生期曝露は発達期ラットにおいてカイニン酸で誘導されるWet Dog Shakesを抑制する

笛田　由紀子[1]，金光　雅成[1]，江川　純恵[1]，石田尾　徹[1]，上野　晋[2]，保利　一[1]

[1]産業医科大学　産業保健学部　作業環境計測制御学
[2]産業医科大学　産業生態科学研究所　職業性中毒学

要　　旨：1-ブロモプロパン(1-BP)は洗浄やスプレー接着剤の溶剤として用いられている．1-BPの有害性はヒトの事例や成獣を用いた動物で報告されてきた．発達毒性も報告されてはいるが，発達神経毒性についての詳細はわかっていない．我々は，1-BPの胎生期曝露が，発達期ラットへのカイニン酸投与により誘導される行動，すなわちscratching行動やwet dog shake様行動に及ぼす影響を調べた．ウィスター系妊娠ラットの妊娠1日目から20日目まで(6時間/日)，濃度700 ppmの1-BP蒸気を曝露した．生後14日目の対照群と1-BP曝露群にカイニン酸を0.1, 0.5, 2.0 mg/kgで腹腔内投与した．Scratching行動に関しては対照群と1-BP曝露群に違いは見られなかったが，wet dog shake様行動に関しては，低濃度である0.1 mg/kgにおいて発生率の低下が1-BP曝露群で見られた．1-BP胎生期曝露が発達期の神経行動に影響することが示唆された．

キーワード：1-ブロモプロパン，胎生期曝露，発達神経毒性，wet dog shake，ラット．

J UOEH(産業医大誌) 37(4)：255 − 261 (2015)

Naunyn-Schmiedeberg's Arch Pharmacol (2015) 388:1259–1269
DOI 10.1007/s00210-015-1161-y

ORIGINAL ARTICLE

Ikarisoside A inhibits acetylcholine-induced catecholamine secretion and synthesis by suppressing nicotinic acetylcholine receptor-ion channels in cultured bovine adrenal medullary cells

Xiaojia Li[1] · Yumiko Toyohira[1] · Takafumi Horisita[2] · Noriaki Satoh[3] · Keita Takahashi[1] · Han Zhang[4] · Munekazu Iinuma[5] · Yukari Yoshinaga[1] · Susumu Ueno[6] · Masato Tsutsui[7] · Takeyoshi Sata[2] · Nobuyuki Yanagihara[1]

Received: 20 April 2015 / Accepted: 27 July 2015 / Published online: 11 August 2015

Abstract Ikarisoside A is a natural flavonol glycoside derived from plants of the genus *Epimedium*, which have been used in Traditional Chinese Medicine as tonics, antirheumatics, and aphrodisiacs. Here, we report the effects of ikarisoside A and three other flavonol glycosides on catecholamine secretion and synthesis in cultured bovine adrenal medullary cells. We found that ikarisoside A (1–100 μM), but not icariin, epimedin C, or epimedoside A, concentration-dependently inhibited the secretion of catecholamines induced by acetylcholine, a physiological secretagogue and agonist of nicotinic acetylcholine receptors. Ikarisoside A had little effect on catecholamine secretion induced by veratridine and 56 mM K^+. Ikarisoside A (1–100 μM) also inhibited $^{22}Na^+$ influx and $^{45}Ca^{2+}$ influx induced by acetylcholine in a concentration-dependent manner similar to that of catecholamine secretion. In *Xenopus* oocytes expressing α3β4 nicotinic acetylcholine receptors, ikarisoside A (0.1–100 μM) directly inhibited the current evoked by acetylcholine. It also suppressed ^{14}C-catecholamine synthesis and tyrosine hydroxylase activity induced by acetylcholine at 1–100 μM and 10–100 μM, respectively. The present findings suggest that ikarisoside A inhibits acetylcholine-induced catecholamine secretion and synthesis by suppression of nicotinic acetylcholine receptor-ion channels in bovine adrenal medullary cells.

Keywords Adrenal medulla · Catecholamine secretion · *Epimedium* · Flavonoids · Ikarisoside A · Nicotinic acetylcholine receptor

✉ Nobuyuki Yanagihara
yanagin@med.uoeh-u.ac.jp

1 Department of Pharmacology, University of Occupational and Environmental Health, School of Medicine, 1-1, Iseigaoka, Yahatanishi-ku, Kitakyushu 807-8555, Japan

2 Department of Anesthesiology, University of Occupational and Environmental Health, School of Medicine, Yahatanishi-ku, Kitakyushu, Japan

3 Shared-Use Research Center, University of Occupational and Environmental Health, Yahatanishi-ku, Kitakyushu, Japan

4 Research Center of Traditional Chinese Medicine, Tianjin University of Traditional Chinese Medicine, Tianjin, China

5 Department of Pharmacognosy, Gifu Pharmaceutical University, Daigakunishi, Gifu, Japan

6 Department of Occupational Toxicology, Institute of Industrial Ecological Sciences, University of Occupational and Environmental Health, Yahatanishi-ku, Kitakyushu, Japan

7 Department of Pharmacology, Faculty of Medicine, University of The Ryukyus, Nishihara, Okinawa, Japan

Introduction

Flavonoids, a group of secondary metabolites with variable phenolic structure, which exist widely in plants (Nijveldt et al. 2001; Ren and Zuo 2012), may exert potential benefits associated with reduced risks of age- and life style-related diseases such as cardiovascular diseases, diabetes, and some cancers (Lu et al. 2013; Yanagihara et al. 2014). Ikarisoside A is one of the flavonol derivatives derived from plants of the genus *Epimedium*, which have been used in Traditional Chinese Medicine as tonics, antirheumatics, and aphrodisiacs (Dou et al. 2006). Previous studies reported that the total flavonoid fraction of *Epimedium* extract suppresses urinary calcium excretion and improves bone properties in ovariectomized mice (Chen et al. 2011), and that other extracts with structures similar to that of ikarisoside A, such as icariin, can stimulate osteogenic activities (Zhou et al. 2013) and have

anti-inflammatory effects (Lai et al. 2013). Furthermore, ikarisoside A also has pharmacological effects such as antioxidant and anti-inflammatory effects (Choi et al. 2008) as well as anti-osteoporosis effects (Choi et al. 2010).

In the human body, the most abundant catecholamines are adrenaline, noradrenaline, and dopamine, all of which are produced from phenylalanine and/or tyrosine. Catecholamines are produced mainly in the chromaffin cells of the adrenal medulla, the postganglionic fibers of the sympathetic nervous system, and the central nervous system. Catecholamines play very important roles in heart rate, blood pressure, blood glucose levels, and the general reactions of the sympathetic nervous system.

Adrenal medullary cells derived from embryonic neural crests are functionally homologous to sympathetic postganglionic neurons. In bovine adrenal medullary cells, catecholamine secretion is associated with the activation of three types of ionic channels: nicotinic acetylcholine receptor (nAChR)-ion channels, voltage-dependent Na^+ channels, and voltage-dependent Ca^{2+} channels (Wada et al. 1985b). ACh induces Na^+ influx via nAChR-ion channels, then, it induces Ca^{2+} influx and subsequent catecholamine secretion (Wada et al. 1985b). On the other hand, stimulation of catecholamine synthesis induced by ACh is associated with the activation of tyrosine hydroxylase in cultured bovine adrenal medullary cells (Yanagihara et al. 1987; Tsutsui et al. 1994). The conversion of tyrosine to L-3,4-dihydroxyphenylalanine (DOPA) is the rate-limiting step of catecholamine biosynthesis (Nagatsu et al. 1964). Adrenal medullary cells have provided a good model for the detailed analysis of a drug's actions on catecholamine secretion and synthesis (Kajiwara et al. 2002; Toyohira et al. 2005; Shinohara et al. 2007).

In our previous study, we isolated 20 flavonol glycosides from *Epimedium* species, including ikarisoside A, icariin, epimedoside A, and epimedin C (Mizuno et al. 1988). Ikarisoside A showed neurite outgrowth activity in cultured PC12h cells (Kuroda et al. 2000). There is, however, little evidence regarding ikarisoside A's effects on sympathetic nervous system activity. In the present study, we investigated the effects of four flavonol glycosides on bovine adrenal medullary cell functions and found that ikarisoside A, but not the other three flavonol glycosides, inhibited ACh-induced catecholamine secretion and synthesis by suppression of nAChR-ion channels in the cells.

Materials and methods

Materials

Oxygenated Krebs-Ringer phosphate (KRP) buffer was used throughout unless stated otherwise. Its composition is as follows (in mM): 154 NaCl, 5.6 KCl, 1.1 $MgSO_4$, 2.2 $CaCl_2$, 0.85 NaH_2PO_4, 2.15 Na_2HPO_4, and 10 glucose, adjusted to pH 7.4. Drugs and reagents were obtained from the following sources: Eagle's minimum essential medium (Eagle's MEM) (Nissui Pharmaceutical, Tokyo, Japan); collagenase (Nitta Zerachin, Osaka, Japan); calf serum (Cell Culture Technologies, Gravesano, Switzerland). ACh and veratridine were from Sigma (St. Louis, MO, USA). L-[U-^{14}C]tyrosine was from American Radiolabeled Chemicals Inc. (St. Louis, MO, USA); $^{45}CaCl_2$, $^{22}NaCl$, and L-[1-^{14}C]tyrosine from Perkin-Elmer Life Sciences (Boston, MA, USA).

Isolation of flavonol glycosides from the leaves of *Epimedium* species

The leaves of *Epimedium diphyllum* were collected at Miyazaki Prefecture, Japan. Ikarisoside A and other flavonol glycosides were purified by high performance liquid chromatography, as reported previously (Mizuno et al. 1988). Ikarisoside A and other flavonol glycosides were dissolved in 100 % dimethyl sulfoxide (DMSO) and then diluted in a reaction medium before use at a final DMSO concentration not exceeding 0.5 %, unless otherwise specified. DMSO (0.5 %) did not influence the basal and ACh-induced catecholamine secretion in the present study (data not shown).

Primary culture of bovine adrenal medullary cells

Bovine adrenal medullary cells were isolated by collagenase digestion of adrenal medullary slices according to the method as reported previously (Yanagihara et al. 1979, 1996). Cells were suspended in Eagle's MEM containing 10 % calf serum, 3 μM cytosine arabinoside, and several antibiotics, and maintained in monolayer culture at a density of 4×10^6 cells/dish (35 mm dish; Falcon, Becton Dickinson Labware, Franklin Lakes, NJ, USA) or 10^6 cells/well (24-well plate; Corning Life Sciences, Lowell, MA, USA) at 37 °C under a humidified atmosphere of 5 % CO_2 and 95 % air. The cells were used for experiments between 2 and 5 days of culture.

Catecholamine secretion from cultured bovine adrenal medullary cells

The secretion of catecholamines was measured as described previously (Yanagihara et al. 1979). Cells (10^6/well) were washed three times with oxygenated KRP buffer, then firstly preincubated with or without ikarisoside A (0.3–100 μM) or other flavonol glycosides (10 μM) at 37 °C for 10 min, and incubated with or without ikarisoside A (0.3–100 μM) or other flavonol glycosides (10 μM) in the presence or absence of various secretagogues (300 μM ACh, 100 μM veratridine or 56 mM K^+) at 37 °C for another 10 min. After the reaction, the incubation medium was transferred immediately to a test tube containing perchloric acid (final concentration, 0.4 M) for the

full stop of the reaction. Catecholamines (noradrenaline and adrenaline) secreted into the medium were adsorbed onto aluminum hydroxide and estimated by the ethylenediamine condensation method (Weil-Malherbe and Bone 1952) using a fluorescence spectrophotometer (F-2500; Hitachi, Tokyo, Japan) with excitation and emission wavelengths of 420 and 540 nm, respectively.

$^{22}Na^+$ and $^{45}Ca^{2+}$ influx

The influx of $^{22}Na^+$ and $^{45}Ca^{2+}$ was measured as reported previously (Wada et al. 1985a, b). After preincubation with or without ikarisoside A (0.3–100 μM) at 37 °C for 10 min, cells (4×10^6/dish) were incubated with 1.5 μCi of $^{22}NaCl$ or 1.5 μCi of $^{45}CaCl_2$ at 37 °C for 5 min with or without 300 μM ACh and ikarisoside A (0.3–100 μM) in KRP buffer. After incubation, the cells were washed three times with ice-cold KRP buffer, solubilized in 10 % Triton X-100, and counted for radioactivity of $^{22}Na^+$ and $^{45}Ca^{2+}$ by a gamma counter (ARC-2005, Aloka, Tokyo, Japan) and a liquid scintillation counter (TRI-CARB 2900TR, PACKARD INSTRUMENT CO., Meriden, CT, USA), respectively.

^{14}C-Catecholamine synthesis from [^{14}C]tyrosine in the cells

After preincubation for 10 min, cells (4×10^6/dish) were incubated with 20 μM L-[U-^{14}C]tyrosine (1.0 μCi) KRP buffer in the presence or absence of various concentrations of ikarisoside A (0.3–100 μM) and 300 μM ACh at 37 °C for 20 min. After removing the incubation medium by aspiration, cells were harvested in 0.4 M perchloric acid and centrifuged at 1600×*g* for 10 min. ^{14}C-Catecholamines were separated further by ion exchange chromatography on Duolite C-25 columns (H^+-type, 0.4 × 7.0 cm) (Yanagihara et al. 1987) and counted for the radioactivity by a liquid scintillation counter (TRI-CARB 2900TR, PACKARD INSTRUMENT CO., Meriden, CT, USA). ^{14}C-Catecholamine synthesis was expressed as the sum of the ^{14}C-catecholamines (adrenaline, noradrenaline, and dopamine).

Tyrosine hydroxylase activity in situ

After preincubation with or without ikarisoside A (0.3–100 μM) for 10 min, cells (10^6/well) were exposed to 200 μl of KRP buffer with or without ikarisoside A (0.3–100 μM) and 300 μM ACh, supplemented with 18 μM L-[1-^{14}C]tyrosine (0.2 μCi) for 10 min at 37 °C. Upon addition of the labeled tyrosine, each well was sealed immediately with an acrylic tube capped with a rubber stopper and fitted with a small plastic cup containing 200 μl of NCS-II tissue solubilizer (GE Healthcare UK Ltd. Little Chalfont, Buckinghamshire, UK) to absorb the $^{14}CO_2$ released by the cells and counted for the radioactivity (Bobrovskaya et al. 1998).

Expression of α3β4 nAChRs in *Xenopus* oocytes and electrophysiological recordings

The complementary DNAs (cDNAs) encoding the α3 and β4 subunits of rat neuronal nAChR, subcloned into pcDNAI/Neo (Invitrogen, Carlsbad, CA) vector, were kindly provided from Dr. James W. Patrick (Division of Neuroscience, Baylor College of Medicine, TX, USA). After linearization of cDNA with *Not*I, complementary RNAs (cRNAs) were transcribed using T7 RNA polymerase from the mMESSAGE mMACHINE kit (Ambion, Austin, TX, USA). Adult female *Xenopus laevis* frogs were obtained from Kyudo Co., Ltd. (Saga, Japan). *Xenopus* oocytes and cRNA microinjection were prepared as described previously (Ueno et al. 2004; Horishita and Harris 2008). cRNAs of α3 and β4 subunits were co-injected at a same ratio (10–20 ng/50 nL) into *Xenopus* oocytes, and electrophysiological recordings were performed 2–6 days after injection. Oocytes were placed in a 100 μl recording chamber and perfused at 2 ml/min with extracellular Ringer solution (110 mM NaCl, 2.5 mM KCl, 10 mM HEPES, 1.8 mM $BaCl_2$, pH 7.5) containing 1.0 μM atropine sulfate. Ca^{2+} in the solution was replaced with Ba^{2+} to minimize the effects of secondarily activated Ca^{2+}-dependent Cl^- channels. Recording electrodes (1–3 MΩ) were filled with 3 M KCl, and the whole-cell voltage clamp was achieved through these two electrodes using a Warner Instruments model OC-725C (Warner, Hamden, CT, USA) at −70 mV. We measured the peak of the transient inward current in response to ACh that was applied for 30 s and examined the effects of ikarisoside A on a concentration of ACh that produced 50 % of the maximal effect (EC_{50}) of ACh. The EC_{50} was determined for each oocyte by 1 mM ACh that produces a maximal current. Ikarisoside A stocks were prepared in 100 % DMSO and diluted in bath solution to a final DMSO concentration not exceeding 0.1 %. Ikarisoside A was preapplied for 2 min to allow an equilibration with its site of interaction before ACh was added and its effect on the cation currents was determined. In all cases, between two currents, there was 10 min interval under washing with normal Ringer solution.

Statistical analysis

All experiments were performed in duplicate or triplicate, and each experiment was repeated at least three times. All values are given as means ± SEM. The significance of differences between means was evaluated using one-way analysis of variance (ANOVA). When a significant F value was found by ANOVA, Dunnett's or Scheffe's test for multiple comparisons was used to identify differences among the groups. Values were considered statistically different when P was less than

0.05. Statistical analyses were performed using PRISM for Windows version 5.0J software (Abacus Concept, Berkeley, CA, USA).

Results

The structures of four flavonol glycosides isolated from *Epimedium*

The four flavonol glycosides ikarisoside A, icariin, epimedin C, and epimedoside A were isolated from the leaves of *E. diphyllum* as reported previously (Mizuno et al. 1988). The structures of these four flavonol glycosides are shown in Fig. 1.

Effects of the flavonol glycosides on catecholamine secretion induced by various secretagogues in adrenal medullary cells

None of the four flavonol glycosides (ikarisoside A, icariin, epimedin C, and epimedoside A) at 10 μM significantly affected the basal secretion of catecholamines (Fig. 2a). ACh (300 μM), an agonist of nAChRs, caused catecholamine secretion corresponding to 18.90 ± 0.38 % of the total catecholamines in the cells. When the cells were treated with the same four flavonol glycosides at 10 μM for 10 min, ikarisoside A strongly reduced catecholamine secretion induced by ACh, to 6.83 ± 0.51 % of the total, whereas the other three had little effect (Fig. 2a). Veratridine (100 μM), an activator of voltage-dependent Na^+ channels, and 56 mM K^+, which depolarizes cell membranes and then activates voltage-dependent Ca^{2+} channels, also caused catecholamine secretion corresponding to 26.52 ± 0.88 % (Fig. 2b) and 20.51 ± 0.70 % (Fig. 2c) of the total catecholamines, respectively. Treatment of cells with these flavonol glycosides at 10 μM did not affect catecholamine secretion induced by veratridine (Fig. 2b) and 56 mM K^+ (Fig. 2c).

Concentration-inhibition curves for the effects of ikarisoside A on catecholamine secretion, $^{45}Ca^{2+}$ influx, and $^{22}Na^+$ influx induced by ACh

We examined the effects of ikarisoside A on catecholamine secretion, $^{45}Ca^{2+}$ influx, and $^{22}Na^+$ influx induced by ACh. Treatment of cells with ikarisoside A at 1, 3, 10, 30, and 100 μM significantly inhibited ACh-induced secretion of catecholamines (18.22 ± 0.16 % of the total catecholamines in the cells) to 15.36 ± 0.38 %, 12.27 ± 0.40 %, 7.68 ± 0.30 %, 5.33 ± 0.47 %, and 4.95 ± 0.25 % of the total catecholamines in the cells, respectively (Fig. 3a). Ikarisoside A also inhibited ACh-induced $^{45}Ca^{2+}$ influx and $^{22}Na^+$ influx in a concentration-dependent manner (Fig. 3b, c). The half-maximal inhibitory concentration (IC_{50}) of ikarisoside A in catecholamine secretion, $^{45}Ca^{2+}$ influx, and $^{22}Na^+$ influx are 4.00, 9.90, and 2.96 μM, respectively.

Inhibitory mode of ikarisoside A on ACh-induced catecholamine secretion in adrenal medullary cells

To investigate the mechanism by which ikarisoside A inhibits ACh-induced catecholamine secretion, we examined whether or not the inhibitory effect of ikarisoside A on catecholamine secretion is overcome when the ACh concentration is

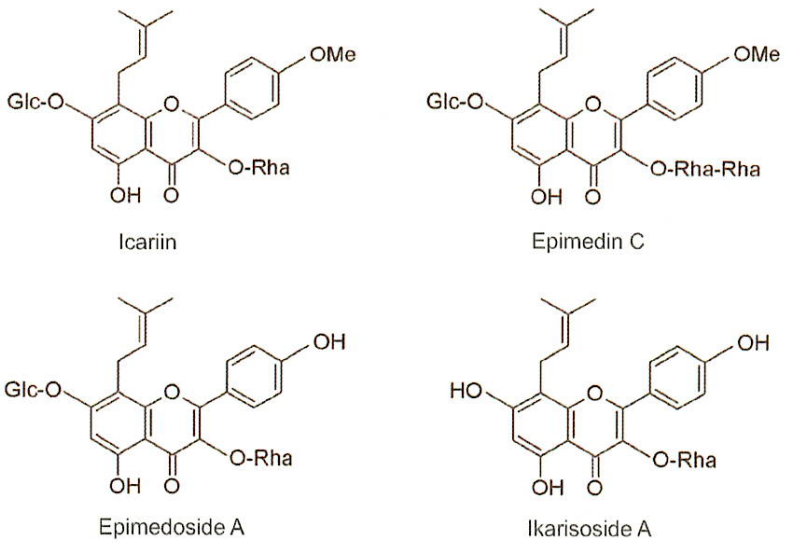

Fig. 1 Chemical structures of icariin, epimedin C, epimedoside A, ikarisoside A. The abbreviations Glc and Rha in the structures are glucose and rhamnose, respectively

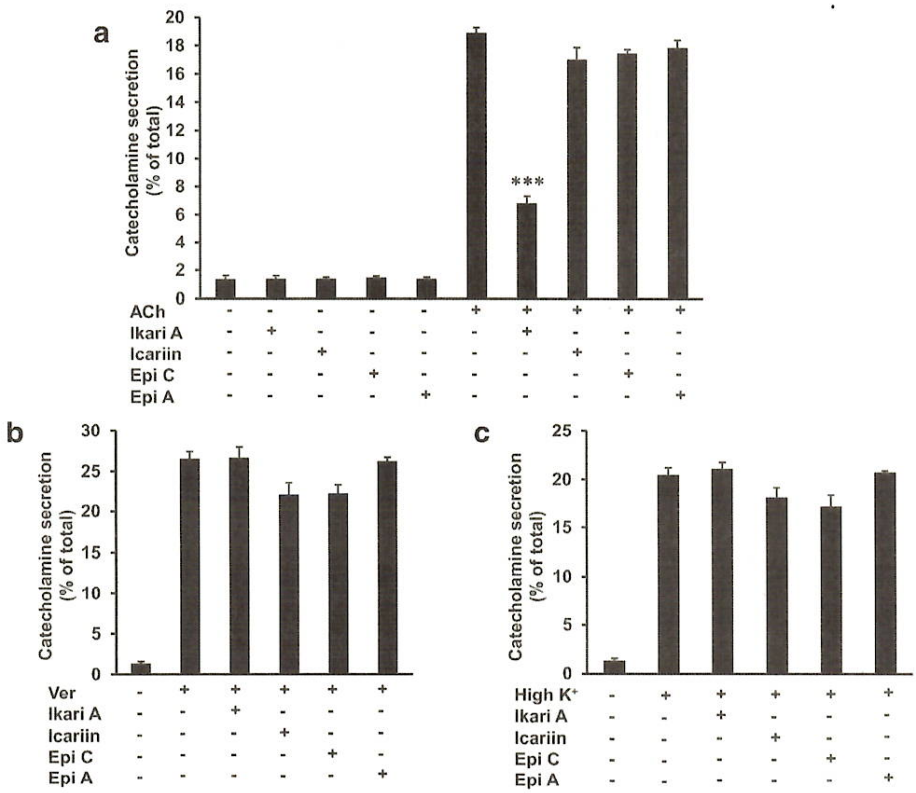

Fig. 2 Effects of ikarisoside A, icariin, epimedin C, or epimedoside A on catecholamine secretion induced by various secretagogues in cultured bovine adrenal medullary cells. After preincubation with cells with or without ikarisoside A (Ikari A) (10 μM), icariin (10 μM), epimedin C (Epi C) (10 μM), and epimedoside A (Epi A) (10 μM) for 10 min, the cells (10^6/well) were incubated with or without these four flavonol glycosides (10 μM), ACh (300 μM) (**a**), veratridine (100 μM) (**b**), or 56 mM K^+ (**c**) for another 10 min at 37 °C. Catecholamines secreted into the medium were expressed as a percentage of the total catecholamines in the cells. Data are means ± SEM from three separate experiments carried out in triplicate. ***$P < 0.001$, compared with ACh alone (analyzed by one-way ANOVA with Dunnett's multiple comparison post hoc test)

increased. Even when the ACh concentrations in the incubation medium increased from 3 to 300 μM, they did not overcome the inhibitory effect of ikarisoside A (Fig. 4a). Double-reciprocal plot analysis revealed that ikarisoside A exerts a noncompetitive type of inhibition on ACh-induced secretion of catecholamines (Fig. 4b).

Effects of ikarisoside A on ACh-induced inward current in *Xenopus* oocytes expressing α3β4 nAChRs

We examined the direct effects of ikarisoside A on ACh responses in *Xenopus* oocytes expressing rat α3β4 nAChRs. As shown in Fig. 5a, ikarisoside A reversibly inhibited ACh (0.2 mM)-induced currents. Ikarisoside A inhibited ACh-induced currents concentration dependently. It suppressed those currents to 80 ± 3 %, 69 ± 6 %, 43 ± 6 %, 32 ± 8 %, and 22 ± 5 % of the control at 0.1, 0.3, 1, 3, and 10 μM, respectively, and the inhibitory effects were significant from 0.10 μM onward; the IC_{50} was 0.48 μM (Fig. 5b).

Effect of aglycon of ikarisoside A on ACh-induced secretion of catecholamines

Ikarisoside A is a flavonol glycoside having one rhamnose at the 3 position in the chemical structure. 3,5,7-Trihydroxy-2-(4-hydroxyphenyl)-8-(3-methylbut-2-enyl)-4*H*-chromen-4-one is the aglycon of ikarisoside A. We examined the effect of this aglycon on ACh-induced secretion of catecholamines. As shown in Fig. 6, the aglycon of ikarisoside A did not affect basal or ACh-induced secretion of catecholamines.

Effect of ikarisoside A on ^{14}C-catecholamine synthesis from [^{14}C]tyrosine and tyrosine hydroxylase activity

As shown in Fig. 7a, ACh (300 μM) increased the synthesis of ^{14}C-catecholamines from [^{14}C]tyrosine about 3-fold in bovine adrenal medullary cells. The concurrent treatment of cells with ikarisoside A inhibited the stimulatory effect of 300 μM ACh on ^{14}C-catecholamine synthesis in a concentration (1–

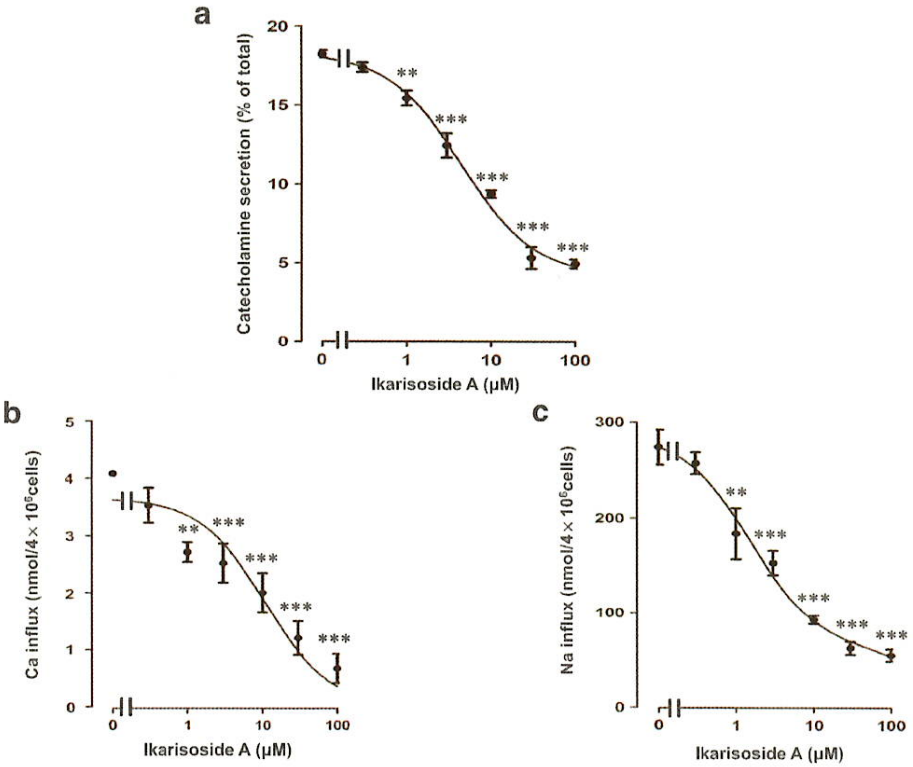

Fig. 3 Effects of ikarisoside A on catecholamine secretion (**a**), $^{45}Ca^{2+}$ influx (**b**), and $^{22}Na^{+}$ influx (**c**) induced by ACh. (**a**) After preincubation for 10 min with or without ikarisoside A (0.3–100 μM), cells were stimulated with ACh (300 μM) in the presence or absence of ikarisoside A (0.3–100 μM) for another 10 min at 37 °C. Catecholamines secreted into the medium were expressed as a percentage of the total catecholamines in the cells. **b**, **c** After preincubation for 10 min, cells were stimulated with ACh (300 μM) and 1.5 μCi of $^{45}CaCl_2$ (**b**) or $^{22}NaCl$ (**c**) in the presence or absence of ikarisoside A (0.3–100 μM) for another 5 min at 37 °C. $^{45}Ca^{2+}$ influx and $^{22}Na^{+}$ influx were measured and were expressed as nmol/4 × 10^6 cells. Data are means ± SEM from three separate experiments carried out in triplicate. $^{**}P < 0.01$ and $^{***}P < 0.001$, compared with ACh alone (analyzed by one-way ANOVA with Dunnett's multiple comparison post hoc test)

100 μM)-dependent manner (Fig. 7a), yielding an IC_{50} value of 2.85 μM. Ikarisoside A (1–100 μM) had little effect on the basal synthesis of ^{14}C-catecholamines.

We next examined the effect of ikarisoside A on tyrosine hydroxylase activity in the cells. After preincubation with or without ikarisoside A (0.1–100 μM) for 10 min, cells were incubated with 300 μM ACh in the absence or presence of ikarisoside A (0.1–100 μM) for another 10 min at 37 °C. Ikarisoside A (10–100 μM) inhibited the tyrosine hydroxylase activity induced by ACh and tended to inhibit the basal enzyme activity (Fig. 7b). The IC_{50} value of ikarisoside A for its inhibitory effect on the ACh-induced tyrosine hydroxylase activity was 9.13 μM (derived from the curve representing the difference between stimulated and basal tyrosine hydroxylase; not shown).

Discussion

In present study, we investigated the effects of four flavonol glycosides derived from the leaves of the genus *Epimedium*. We demonstrated that ikarisoside A, but not the other three, inhibited the secretion and synthesis of catecholamines induced by ACh in cultured bovine adrenal medullary cells. To our knowledge, this is the first direct evidence of an inhibitory effect of ikarisoside A on catecholamine secretion and synthesis in cultured bovine adrenal medullary cells.

Inhibitory effect of ikarisoside A on catecholamine secretion induced by ACh

The present study demonstrated that ikarisoside A significantly inhibits catecholamine secretion induced by ACh, but not by veratridine or 56 mM K^+ in adrenal medullary cells. We previously reported that ACh activates nAChR-ion channels, and induces Na^+ influx, subsequent Ca^{2+} influx, and finally catecholamine secretion. On the other hand, veratridine activates voltage-dependent Na^+ channels and 56 mM K^+ depolarizes cell membranes to activate voltage-dependent Ca^{2+} channels (Wada et al. 1984, 1985b). In the present study, ikarisoside A did not inhibit the stimulatory effects of veratridine and 56 mM K^+ on catecholamine secretion. Therefore,

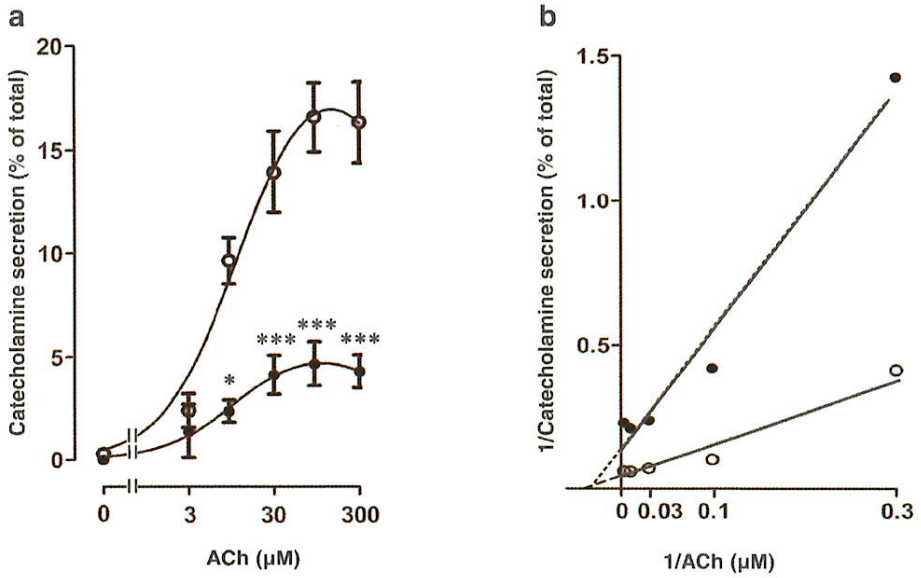

Fig. 4 Inhibitory mode of ikarisoside A on catecholamine secretion induced by ACh. **a** After preincubation for 10 min, cells were stimulated with (*black circle*) or without (*white circle*) ikarisoside A (10 μM) in the presence or absence of ACh (1–300 μM) for another 10 min at 37 °C. Catecholamines secreted into the medium were expressed as a percentage of the total catecholamines in the cells. Data are means + SEM from three separate experiments carried out in triplicate. The data of ACh plus ikarisoside A are shown by subtracting basal secretion obtained in the presence of ikarisoside A. $^{*}P < 0.05$ and $^{***}P < 0.001$, compared with ACh alone (analyzed by one-way ANOVA with Dunnett's multiple comparison post hoc test). **b** Double-reciprocal plot analysis of the data in (**a**)

ikarisoside A seems to inhibit nAChR-ion channels but not voltage-dependent Na^+ channels or voltage-dependent Ca^{2+} channels. Ikarisoside A inhibited Ca^{2+} influx and Na^+ influx induced by ACh in a concentration-dependent manner similar

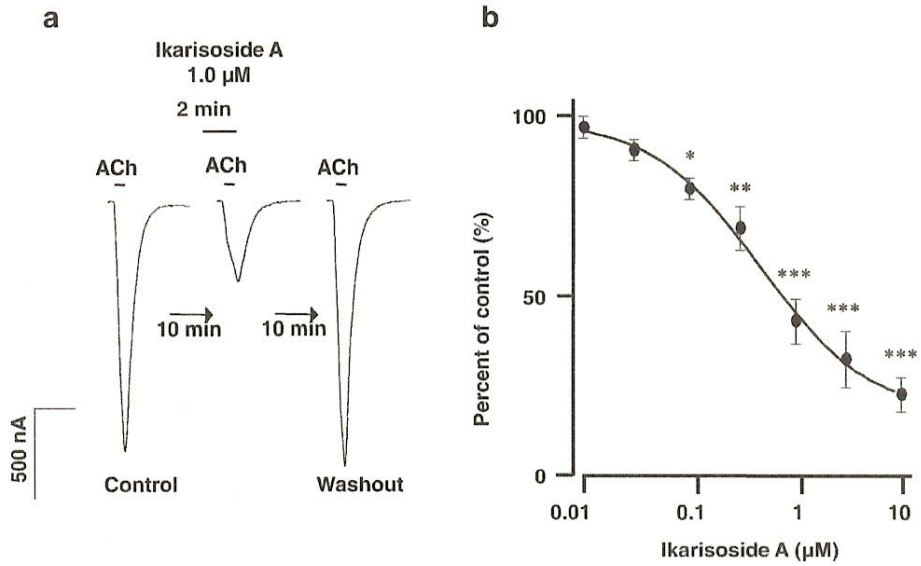

Fig. 5 Effects of ikarisoside A on peak ACh-induced inward currents in *Xenopus* oocytes expressing rat α3β4 nAChRs. **a** Representative traces from a single *Xenopus* oocyte are shown. The currents of ikarisoside A-treated oocytes were recorded 10 min after recording of the control currents, and the washout currents were obtained 10 min after ikarisoside A treatment. Ikarisoside A (1 μM) suppressed the currents induced by the EC_{50} (0.2 mM) of ACh, and the inhibitory effects were reversible. **b** Concentration-response curve for the inhibitory effects of ikarisoside A on ACh-induced currents. The peak current amplitude in the presence of ikarisoside A was normalized to that of the control and the effects are expressed as percentages of the control. Data are presented as means ± SEM from four separate experiments carried out in triplicate. $^{*}P < 0.05$, $^{**}P < 0.01$, and $^{***}P < 0.001$, compared to the control (based on one-way ANOVA with Dunnett's multiple comparison post hoc test). Nonlinear regression analysis was performed and the mean value of IC_{50} for ikarisoside A is 0.48 μM

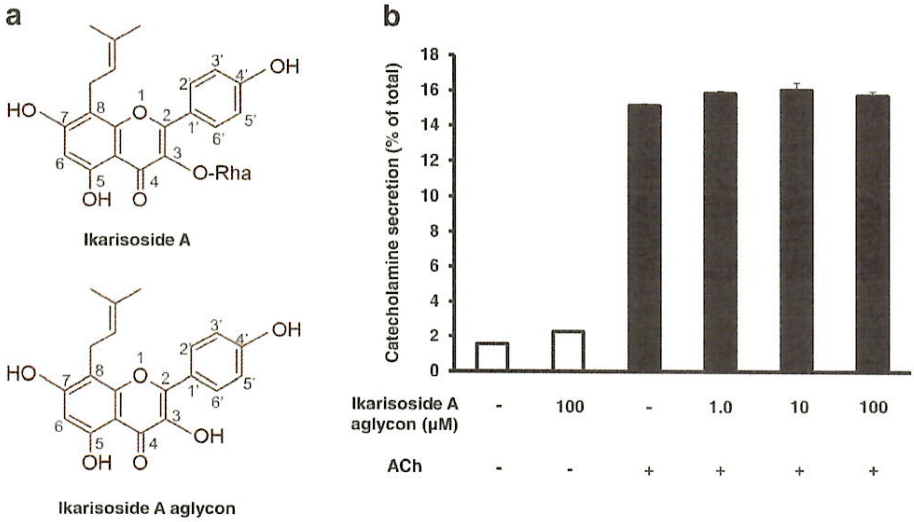

Fig. 6 Structure of ikarisoside A and its aglycon (**a**) and effect of aglycon of ikarisoside A on ACh-induced catecholamine secretion (**b**). **a** Structure of ikarisoside A and its aglycon (3,5,7-trihydroxy-2-(4-hydroxyphenyl)-8-(3-methylbut-2-enyl)-4*H*-chromen-4-one). **b** After preincubation with cells with or without aglycon of ikarisoside A (1–100 μM) for 10 min, the cells (10^6/well) were incubated with or without aglycon of ikarisoside A (1–100 μM) and ACh (300 μM) for another 10 min at 37 °C. Catecholamines secreted into the medium were expressed as a percentage of the total catecholamines in the cells. Data are means ± SEM from three separate experiments carried out in triplicate

to that of catecholamine secretion. In the exocytotic secretion of catecholamines, Ca^{2+} plays an indispensable role as the coupler in the stimulus-secretion coupling (Douglas and Rubin 1961, 1963). From these findings, it is likely that ikarisoside A inhibits ACh-induced catecholamine secretion by suppressing nAChR-ion channels. We investigated the inhibitory mode of ikarisoside A on nAChR-ion channels. Even when the concentration of ACh was increased, the inhibitory

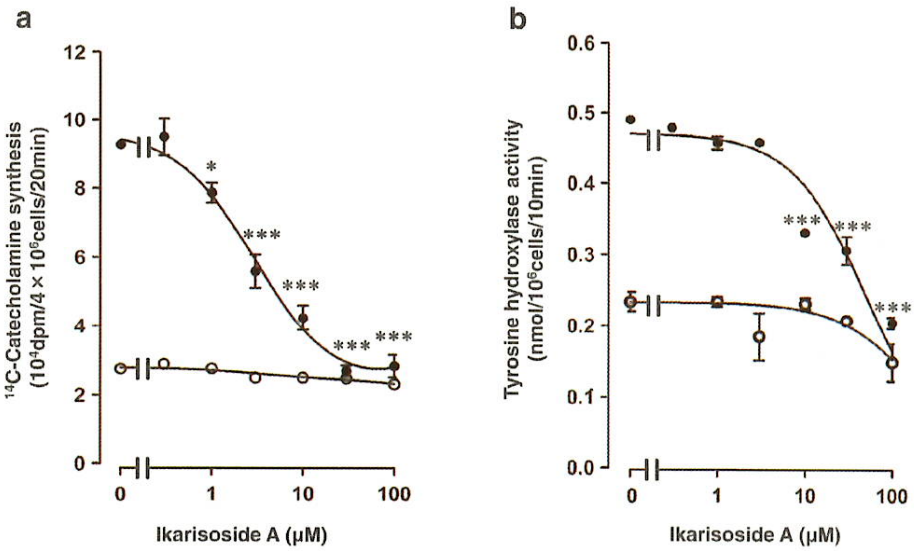

Fig. 7 Effects of ikarisoside A on ^{14}C-catecholamine synthesis from [^{14}C]tyrosine (**a**) and tyrosine hydroxylase activity (**b**) in the cells. **a** After preincubation for 10 min with or without ikarisoside A (0.1–100 μM), cells (4 × 10^6/dish) were incubated with L-[U-^{14}C] tyrosine (20 μM, 1 μCi) in the presence or absence of ikarisoside A (0.1–100 μM) and with (*black circle*) or without (*white circle*) 300 μM ACh at 37 °C for 20 min. The ^{14}C-catecholamines formed were measured. **b** After preincubation with or without ikarisoside A (0.1–100 μM) for 10 min, cells (10^6/well) were incubated with L-[1-^{14}C] tyrosine (18 μM, 0.2 μCi) in the presence or absence of ikarisoside A (0.1–100 μM) and with (*black circle*) or without (*white circle*) 300 μM ACh at 37 °C for 10 min, and tyrosine hydroxylase activity was measured. Data are means ± SEM from three separate experiments carried out in triplicate. $^*P < 0.05$ and $^{***}P < 0.001$, compared with ACh alone (analyzed by one-way ANOVA with Dunnett's multiple comparison post hoc test)

effect of ikarisoside A on ACh-induced secretion of catecholamines was not overcome, suggesting a noncompetitive inhibition and that ikarisoside A acts at a site different from that for ACh binding. A previous review (Lena and Changeux 1993) reported that the site at which noncompetitive blockers act lies at the interface between the nicotinic receptor protein and the membrane lipids.

In the *Xenopus* oocytes expressed with α3β4 nAChRs, ikarisoside A directly inhibited ACh-induced current. The IC_{50} values of ikarisoside A for $^{22}Na^+$ influx in adrenal medullary cells and for Na^+ current in the oocytes were 2.96 and 0.48 μM, respectively. The IC_{50} in the bovine adrenal medullary cells is 6.2-fold bigger than that of the drug in the oocyte system. Although the reason for the discrepancy of the IC_{50} between the two systems is not yet clear, the discrepancy may be explained in the following way. (1) A maximally effective concentration of ACh was used for the $^{22}Na^+$ influx experiments in bovine adrenal medullary cells but the half-maximal concentration was used for the Na^+ current in the oocyte system. (2) In the oocyte expression system, there may be some changes in the test compound potency compared to that of the method using mammalian cells, i.e., a decrease (Lambert et al. 2001; Akk et al. 2008) or an increase (Pintado et al. 2000) in the sensitivity of test compounds. (3) Bovine adrenal medullary cells express multiple nAChR subtypes such as α3β4 (Criado et al. 1992; Garcia-Guzman et al. 1995), α3β4α5 (Campos-Caro et al. 1997), and α7 (Lopez et al. 1998). We should study above possibilities and examine the effect of ikarisoside A on the function of nAChRs in other mammalian cells.

Structure-activity relationship of ikarisoside A for inhibition of nAChR-ion channels

In the present study, we used four flavonol glycosides derived from the *Epimedium* species. Ikarisoside A, but not the other three flavonols, inhibited the functioning of nAChR-ion channels. Judging from the differences in their structures, ikarisoside A has a hydroxyl group at the 7 position in the structure whereas other three have a glucose moiety at this position, suggesting that a glucose moiety at the 7 position may induce stereo-specific interference when flavonol glycosides interact with nAChRs. Furthermore, the inhibition of ACh-induced secretion by ikarisoside A disappeared by the removal of the rhamnose moiety at the 3 position from ikarisoside A. These findings suggest that the rhamnose moiety at the 3 position of ikarisoside A is essential to inhibit the function of nAChR-ion channels.

Inhibitory effect of ikarisoside A on catecholamine synthesis

Ikarisoside A inhibited not only catecholamine secretion but also reduced catecholamine synthesis in ACh-stimulated cells. In the regulation of catecholamine synthesis, Ca^{2+} plays an important role as the coupler in the stimulus-synthesis coupling (Yanagihara et al. 1987) as well as in the stimulus-secretion coupling (Douglas and Rubin 1961, 1963). In the present study, we observed that ikarisoside A suppressed the $^{22}Na^+$ influx and the subsequent $^{45}Ca^{2+}$ influx by inhibiting nAChR-ion channels. Therefore, it is likely that ikarisoside A inhibits catecholamine synthesis and tyrosine hydroxylase activity induced by ACh via the suppression of Ca^{2+} influx in cultured bovine adrenal medulla cells. In harmony with this view, the IC_{50} values of ikarisoside A for inhibition of $^{22}Na^+$ and $^{45}Ca^{2+}$ influx and for inhibition of catecholamine synthesis and tyrosine hydroxylase are very similar.

Pharmacological significance of the inhibitory effects of ikarisoside A on adrenal medullary functions

The human serum concentration of ikarisoside A has not been reported yet. Several previous in vitro studies reported that ikarisoside A at 5.0–20 μM inhibits osteoclastogenic differentiation and nitric oxide synthase in murine monocyte/macrophage cell line RAW264.7 cells (Choi et al. 2008, 2010) and induces neurite outgrowth activity in PC12h cells at 10 μM (Kuroda et al. 2000). In the present study, we observed a significant inhibition of ikarisoside A at 0.1 and 1.0 μM in ACh-induced current in *Xenopus* oocytes and ACh-induced synthesis and secretion of catecholamines, respectively.

It is well known that adrenaline and noradrenaline have an important role in the regulation of normal function in the central and peripheral sympathetic nervous systems. Under strong and prolonged stress, an increased catecholamine release may occur, which possibly induces cardiovascular diseases such as hypertension, atherosclerosis, coronary heart disease, and heart failure (Yanagihara et al. 2014). Chronic heart failure is reported to be associated with the activation of the sympathetic nervous system as manifested by increased circulating catecholamines (Westfall and Westfall 2011). Furthermore, Hara et al. (2011) reported that the stress hormone adrenaline stimulates β_2-adrenoceptors, which activates the Gs protein/cyclic AMP-dependent protein kinase and the β-arrestin-mediated signaling pathway, reduces the p53 level, and induces DNA damage.

Our previous studies reported that daidzein, a soy isoflavone, (Liu et al. 2007) and nobiletin, a citrus polymethoxy flavone, (Zhang et al. 2010) suppress the secretion and synthesis of catecholamines induced by ACh in cultured bovine adrenal medullary cells. In addition to these flavonoids, ikarisoside A also may protect the hyperactive catecholamine system induced by strong stress or emotional excitation which evokes the secretion of ACh from the splanchnic nerves. Further in vivo experiments will provide more conclusive information on ikarisoside A and promote the development of a

therapeutic drug for stress-induced disorders associated with mental or cardiovascular diseases.

Acknowledgments This work was supported, in part, by Grant-in-Aid (23617035, 23617036, 23590159, and 26350170) for Scientific Research (C) from the Japan Society for the Promotion of Science.

Conflict of interest The authors declare that they have no competing interests.

References

Akk G, Li P, Bracamontes J, Reichert DE, Covey DF, Steinbach JH (2008) Mutations of the $GABA_A$ receptor α1 subunit M1 domain reveal unexpected complexity for modulation by neuroactive steroids. Mol Pharmacol 74:614–627

Bobrovskaya L, Cheah TB, Bunn SJ, Dunkley PR (1998) Tyrosine hydroxylase in bovine adrenal chromaffin cells: angiotensin II-stimulated activity and phosphorylation of Ser^{19}, Ser^{31}, and Ser^{40}. J Neurochem 70:2565–2573

Campos-Caro A, Smillie FI, Dominguez del Toro E, Rovira JC, Vicente-Agullo F, Chapuli J, Juiz JM, Sala S, Sala F, Ballesta JJ, Criado M (1997) Neuronal nicotinic acetylcholine receptors on bovine chromaffin cells: cloning, expression, and genomic organization of receptor subunits. J Neurochem 68:488–497

Chen WF, Mok SK, Wang XL, Lai KH, Lai WP, Luk HK, Leung PC, Yao XS, Wong MS (2011) Total flavonoid fraction of the herba epimedii extract suppresses urinary calcium excretion and improves bone properties in ovariectomised mice. Br J Nutr 105:180–189

Choi HJ, Eun JS, Park YR, Kim DK, Li R, Moon WS, Park JM, Kim HS, Cho NP, Cho SD, Soh Y (2008) Ikarisoside A inhibits inducible nitric oxide synthase in lipopolysaccharide-stimulated RAW 264.7 cells via p38 kinase and nuclear factor-κB signaling pathways. Eur J Pharmacol 601:171–178

Choi HJ, Park YR, Nepal M, Choi BY, Cho NP, Choi SH, Heo SR, Kim HS, Yang MS, Soh Y (2010) Inhibition of osteoclastogenic differentiation by Ikarisoside A in RAW 264.7 cells via JNK and NF-κB signaling pathways. Eur J Pharmacol 636:28–35

Criado M, Alamo L, Navarro A (1992) Primary structure of an agonist binding subunit of the nicotinic acetylcholine receptor from bovine adrenal chromaffin cells. Neurochem Res 17:281–287

Dou J, Liu Z, Liu S (2006) Structure identification of a prenylflavonol glycoside from epimedium koreanum by electrospray ionization tandem mass spectrometry. Anal Sci 22:449–452

Douglas WW, Rubin RP (1961) Mechanism of nicotinic action at the adrenal medulla: calcium as a link in stimulus-secretion coupling. Nature 192:1087–1089

Douglas WW, Rubin RP (1963) The mechanism of catecholamine release from the adrenal medulla and the role of calcium in stimulus-secretion coupling. J Physiol 167:288–310

Garcia-Guzman M, Sala F, Sala S, Campos-Caro A, Stuhmer W, Gutierrez LM, Criado M (1995) α-Bungarotoxin-sensitive nicotinic receptors on bovine chromaffin cells: molecular cloning, functional expression and alternative splicing of the α7 subunit. Eur J Neurosci 7:647–655

Hara MR, Kovacs JJ, Whalen EJ, Rajagopal S, Strachan RT, Grant W, Towers AJ, Williams B, Lam CM, Xiao K, Shenoy SK, Gregory SG, Ahn S, Duckett DR, Lefkowitz RJ (2011) A stress response pathway regulates DNA damage through β_2-adrenoreceptors and β-arrestin-1. Nature 477:349–353

Horishita T, Harris RA (2008) n-Alcohols inhibit voltage-gated Na^+ channels expressed in Xenopus oocytes. J Pharmacol Exp Ther 326:270–277

Kajiwara K, Yanagita T, Nakashima Y, Wada A, Izumi F, Yanagihara N (2002) Differential effects of short and prolonged exposure to carvedilol on voltage-dependent Na^+ channels in cultured bovine adrenal medullary cells. J Pharmacol Exp Ther 302:212–218

Kuroda M, Mimaki Y, Sashida Y, Umegaki E, Yamazaki M, Chiba K, Mohri T, Kitahara M, Yasuda A, Naoi N, Xu ZW, Li MR (2000) Flavonol glycosides from Epimedium sagittatum and their neurite outgrowth activity on PC12h cells. Planta Med 66:575–577

Lai X, Ye Y, Sun C, Huang X, Tang X, Zeng X, Yin P, Zeng Y (2013) Icaritin exhibits anti-inflammatory effects in the mouse peritoneal macrophages and peritonitis model. Int Immunopharmacol 16:41–49

Lambert JJ, Belelli D, Harney SC, Peters JA, Frenguelli BG (2001) Modulation of native and recombinant $GABA_A$ receptors by endogenous and synthetic neuroactive steroids. Brain Res Brain Res Rev 37:68–80

Lena C, Changeux JP (1993) Allosteric modulations of the nicotinic acetylcholine receptor. Trends Neurosci 16:181–186

Liu M, Yanagihara N, Toyohira Y, Tsutsui M, Ueno S, Shinohara Y (2007) Dual effects of daidzein, a soy isoflavone, on catecholamine synthesis and secretion in cultured bovine adrenal medullary cells. Endocrinology 148:5348–5354

Lopez MG, Montiel C, Herrero CJ, Garcia-Palomero E, Mayorgas I, Hernandez-Guijo JM, Villarroya M, Olivares R, Gandia L, McIntosh JM, Olivera BM, Garcia AG (1998) Unmasking the functions of the chromaffin cell α7 nicotinic receptor by using short pulses of acetylcholine and selective blockers. Proc Natl Acad Sci U S A 95:14184–14189

Lu MF, Xiao ZT, Zhang HY (2013) Where do health benefits of flavonoids come from? Insights from flavonoid targets and their evolutionary history. Biochem Biophys Res Commun 434:701–704

Mizuno M, Iinuma M, Tanaka T, Sakakibara N, Hanioka S (1988) Flavonol glycosides in Epimedium species. Chem Pharm Bull 36(9):3487–3490

Nagatsu T, Levitt M, Udenfriend S (1964) Tyrosine hydroxylase. The initial step in norepinephrine biosynthesis. J Biol Chem 239:2910–2917

Nijveldt RJ, van Nood E, van Hoorn DE, Boelens PG, van Norren K, van Leeuwen PA (2001) Flavonoids: a review of probable mechanisms of action and potential applications. Am J Clin Nutr 74:418–425

Pintado AJ, Herrero CJ, Garcia AG, Montiel C (2000) The novel Na^+/Ca^{2+} exchange inhibitor KB-R7943 also blocks native and expressed neuronal nicotinic receptors. Br J Pharmacol 130:1893–1902

Ren ZL, Zuo PP (2012) Neural regeneration: role of traditional Chinese medicine in neurological diseases treatment. J Pharmacol Sci 120:139–145

Shinohara Y, Toyohira Y, Ueno S, Liu M, Tsutsui M, Yanagihara N (2007) Effects of resveratrol, a grape polyphenol, on catecholamine secretion and synthesis in cultured bovine adrenal medullary cells. Biochem Pharmacol 74:1608–1618

Toyohira Y, Kubo T, Watanabe M, Uezono Y, Ueno S, Shinkai K, Tsutsui M, Izumi F, Yanagihara N (2005) Selective blockade of nicotinic acetylcholine receptors by pimobendan, a drug for the treatment of heart failure: reduction of catecholamine secretion and synthesis in adrenal medullary cells. Naunyn Schmiedeberg's Arch Pharmacol 371:107–113

Tsutsui M, Yanagihara N, Miyamoto E, Kuroiwa A, Izumi F (1994) Correlation of activation of Ca^{2+}/calmodulin-dependent protein kinase II with catecholamine secretion and tyrosine hydroxylase activation in cultured bovine adrenal medullary cells. Mol Pharmacol 46:1041–1047

Ueno S, Tsutsui M, Toyohira Y, Minami K, Yanagihara N (2004) Sites of positive allosteric modulation by neurosteroids on ionotropic γ-aminobutyric acid receptor subunits. FEBS Lett 566:213–217

Wada A, Izumi F, Yanagihara N, Kobayashi H (1985a) Modulation by ouabain and diphenylhydantoin of veratridine-induced ^{22}Na influx and its relation to ^{45}Ca influx and the secretion of catecholamines in cultured bovine adrenal medullary cells. Naunyn Schmiedeberg's Arch Pharmacol 328:273–278

Wada A, Takara H, Izumi F, Kobayashi H, Yanagihara N (1985b) Influx of ^{22}Na through acetylcholine receptor-associated Na channels: relationship between ^{22}Na influx, ^{45}Ca influx and secretion of catecholamines in cultured bovine adrenal medulla cells. Neuroscience 15:283–292

Wada A, Yashima N, Izumi F, Kobayashi H, Yanagihara N (1984) Involvement of Na influx in acetylcholine receptor mediated secretion of catecholamines from cultured bovine adrenal medulla cells. Neurosci Lett 47:75–80

Weil-Malherbe H, Bone AD (1952) The chemical estimation of adrenaline-like substances in blood. Biochem J 51:311–318

Westfall TC and Westfall DP (2011) Adrenergic agonists and antagonists, in Goodman & Gilman's the pharmacological basis of therapeutics, 12th edn (Brunton LL, Chabner BC, and Knollmann BC, eds), pp. 277-330. McGraw-Hill, NY

Yanagihara N, Isosaki M, Ohuchi T, Oka M (1979) Muscarinic receptor-mediated increase in cyclic GMP level in isolated bovine adrenal medullary cells. FEBS Lett 105:296–298

Yanagihara N, Oishi Y, Yamamoto H, Tsutsui M, Kondoh J, Sugiura T, Miyamoto E, Izumi F (1996) Phosphorylation of chromogranin A and catecholamine secretion stimulated by elevation of intracellular Ca^{2+} in cultured bovine adrenal medullary cells. J Biol Chem 271: 17463–17468

Yanagihara N, Wada A, Izumi F (1987) Effects of α_2-adrenergic agonists on carbachol-stimulated catecholamine synthesis in cultured bovine adrenal medullary cells. Biochem Pharmacol 36:3823–3828

Yanagihara N, Zhang H, Toyohira Y, Takahashi K, Ueno S, Tsutsui M (2014) New insights into the pharmacological potential of plant flavonoids in the catecholamine system. J Pharmacol Sci 124:123–128

Zhang H, Toyohira Y, Ueno S, Shinohara Y, Itoh H, Furuno Y, Yamakuni T, Tsutsui M, Takahashi K, Yanagihara N (2010) Dual effects of nobiletin, a citrus polymethoxy flavone, on catecholamine secretion in cultured bovine adrenal medullary cells. J Neurochem 114:1030–1038

Zhou J, Chen KM, Ge BF, Ma XN, Guo XY, Cheng K, Gao YH, Yan LJ, Shi WG (2013) Comparison between icariin and genistein in osteogenic activity of marrow stromal cells. Zhongguo Zhong Yao Za Zhi 38:1783–1788